GLUCOSINOLATES: REGULATION OF BIOSYNTHESIS AND HYDROLYSIS

EDITED BY: Ralph Kissen, Tamara Gigolashvili and Naveen C. Bisht

PUBLISHED IN: Frontiers in Plant Science

frontiers Research Topics

frontiers

ISSN 1664-8714
ISBN 978-2-88966-372-9
DOI 10.3389/978-2-88966-372-9

About Frontiers

Frontiers is more than just an open-access publisher of scholarly articles: it is a pioneering approach to the world of academia, radically improving the way scholarly research is managed. The grand vision of Frontiers is a world where all people have an equal opportunity to seek, share and generate knowledge. Frontiers provides immediate and permanent online open access to all its publications, but this alone is not enough to realize our grand goals.

Frontiers Journal Series

The Frontiers Journal Series is a multi-tier and interdisciplinary set of open-access, online journals, promising a paradigm shift from the current review, selection and dissemination processes in academic publishing. All Frontiers journals are driven by researchers for researchers; therefore, they constitute a service to the scholarly community. At the same time, the Frontiers Journal Series operates on a revolutionary invention, the tiered publishing system, initially addressing specific communities of scholars, and gradually climbing up to broader public understanding, thus serving the interests of the lay society, too.

Dedication to Quality

Each Frontiers article is a landmark of the highest quality, thanks to genuinely collaborative interactions between authors and review editors, who include some of the world's best academicians. Research must be certified by peers before entering a stream of knowledge that may eventually reach the public - and shape society; therefore, Frontiers only applies the most rigorous and unbiased reviews.
Frontiers revolutionizes research publishing by freely delivering the most outstanding research, evaluated with no bias from both the academic and social point of view. By applying the most advanced information technologies, Frontiers is catapulting scholarly publishing into a new generation.

What are Frontiers Research Topics?

Frontiers Research Topics are very popular trademarks of the Frontiers Journals Series: they are collections of at least ten articles, all centered on a particular subject. With their unique mix of varied contributions from Original Research to Review Articles, Frontiers Research Topics unify the most influential researchers, the latest key findings and historical advances in a hot research area! Find out more on how to host your own Frontiers Research Topic or contribute to one as an author by contacting the Frontiers Editorial Office: researchtopics@frontiersin.org

GLUCOSINOLATES: REGULATION OF BIOSYNTHESIS AND HYDROLYSIS

Topic Editors:
Ralph Kissen, Norwegian University of Science and Technology, Norway
Tamara Gigolashvili, University of Cologne, Germany
Naveen C. Bisht, National Institute of Plant Genome Research (NIPGR), India

Citation: Kissen, R., Gigolashvili, T., Bisht, N. C., eds. (2021). Glucosinolates: Regulation of Biosynthesis and Hydrolysis. Lausanne: Frontiers Media SA. doi: 10.3389/978-2-88966-372-9

Table of Contents

frontiers in Plant Science

EDITORIAL
published: 25 November 2020
doi: 10.3389/fpls.2020.620965

Editorial: Glucosinolates: Regulation of Biosynthesis and Hydrolysis

*Bhanu Malhotra and Naveen C. Bisht**

Brassica Nutrigenomics and Signaling lab, National Institute of Plant Genome Research, New Delhi, India

Keywords: glucosinolate, methylthioalkylmalate synthase, glucosinolate transporters, glucosinolate turnover, nitrile-specifier proteins, myrosinase, epithiospecifier proteins

Editorial on the Research Topic

Glucosinolates: Regulation of Biosynthesis and Hydrolysis

The members of the *Brassicaceae* family possess a class of sulfur and nitrogen containing specialized metabolites glucosinolates (GSLs), that are important for plant defense and animal nutrition. Glucosinolates are both constitutive and inducible, and their accumulation is controlled by environmental, molecular, and genetic levels. Much of the information about the glucosinolate biosynthesis, transport, hydrolysis, turnover, crosstalk amongst biosynthesis and hormonal pathways, and mechanisms controlling glucosinolate accumulation and metabolism during abiotic and biotic stresses has been derived from the model plant *Arabidopsis thaliana* (**Figure 1**). However, there are still lacunae in fully understanding these regulatory processes in crop species. Thus, the purpose of this Research Topic is to decipher several aspects under the glucosinolate regulatory mechanisms, in view of which a total of eight research articles have been published.

Plants possess huge structural diversity of glucosinolates and studies in the last two decades have highlighted the key role of *GSL-ELONG* locus, encoding methylthioalkylmalate synthase (MAM or MAMS), controlling glucosinolates side chain diversity (3C, 4C, 5C) across the *Brassicaceae* species. Understanding the molecular basis of *MAM* evolution and generation of glucosinolate natural diversity in polyploid *Brassica* crops is a challenge due to their complex genome architecture (Kumar et al., 2019). Abrahams et al. investigated diversification of *MAM* locus utilizing a micro-synteny network and phylogenetic inference across a broader species phylogeny with comparisons to their primary metabolic ancestor, *isopropylmalate synthase*, uncovering critical steps in the origin of *MAM* and identifying patterns of domain specific diversity. With examination of few of the evolutionary consequences of whole-genome duplication events, local duplications, gene transpositions, and gene fusions, various new hypotheses are created to test the nature of *MAM* diversification and glucosinolate diversity in plants. The understanding of *MAM* evolution will enable fine engineering of desirable glucosinolate profiles in plants.

The accumulation of glucosinolates is controlled by the complex interplay of biosynthesis, transport, storage, and feedback regulatory pathways (**Figure 1**) the complexity of which is not fully understood. Touw et al. found distinct glucosinolate accumulation and composition during root herbivory in *Brassica rapa* infested with specialist *Delia radicum*. The increase in the total glucosinolate in the taproot was majorly due to indole and benzyl glucosinolates. It was initially hypothesized that the expression of glucosinolate transporter genes in distal tissues led to glucosinolate accumulation in taproot and preceded the localized expression of *de-novo* biosynthetic gene expression in the taproot. However, it was found that local biosynthesis but not transport from above ground parts drives the accumulation of indole glucosinolates in the taproot to protect from root-herbivory. Future studies should involve the use of isotope labeled glucosinolate precursors and understanding their transport upon root herbivory, confirming the precise role of transporter proteins in tissue-specific glucosinolate accumulation. Another study by

OPEN ACCESS

Edited and reviewed by:
Heiko Rischer,
VTT Technical Research Centre of Finland Ltd, Finland

***Correspondence:**
Naveen C. Bisht
ncbisht@nipgr.ac.in

Specialty section:
This article was submitted to Plant Metabolism and Chemodiversity, a section of the journal Frontiers in Plant Science

Received: *24 October 2020*
Accepted: *30 October 2020*
Published: *25 November 2020*

Citation:
Malhotra B and Bisht NC (2020) Editorial: Glucosinolates: Regulation of Biosynthesis and Hydrolysis. Front. Plant Sci. 11:620965. doi: 10.3389/fpls.2020.620965

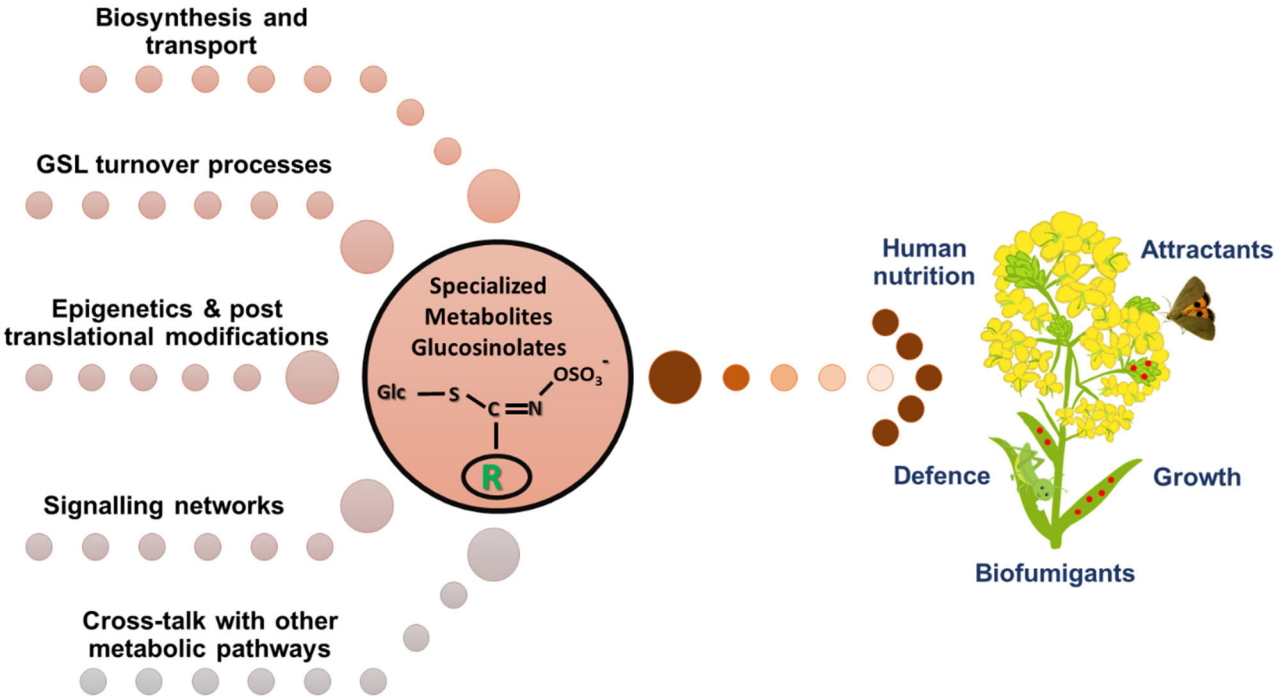

FIGURE 1 | Regulation of glucosinolate metabolism in plants is a complex interplay among various biological processes.

Sontowski et al. also investigated the effect of two specialist herbivores *D. radicum and D. floralis* on the expression pattern of genes involved in glucosinolate biosynthesis, transport, and hydrolysis during infestation of *B. rapa* varieties accumulating low and high root glucosinolate levels. Only minute response differences were observed in the contrasting glucosinolate varieties of *B. rapa* with no trade-offs occurring between the two in the roots compared to those reported in shoots (Rasmann et al., 2015). *B. rapa* low glucosinolate variety could not compensate for the improved defense responses even after attaining similar glucosinolate levels as high glucosinolate variety. Thus, glucosinolate based defenses can differ in plants and between different herbivores, depending upon their host specialization levels and feeding modes.

With the changing environmental conditions, plants modulate their metabolism toward carrying out a balanced resource investment to both the development and defense pathways. The levels of glucosinolates in the intact tissue are a result of interplay amongst their biosynthesis and however uncharacterized turnover processes in response to the changing environment. Jeschke et al. investigated glucosinolate turnover in the absence of tissue damage in *A. thaliana* seedlings under different nutrient availability conditions, stating that both biosynthesis and turnover processes coordinate to achieve glucosinolate levels. While limitation of sulfur and nitrogen negatively affected the *de-novo* accumulation of all classes of glucosinolates, the exogenous application of carbon sources had quantitative effects on aliphatic glucosinolates. Raphanusamic acid (RA), a breakdown metabolite formed potentially from all glucosinolate structures in-planta (Bednarek et al., 2009), was found to correlate with enhanced accumulation of endogenous glucosinolates only but not its turnover in *A. thaliana*. Thus, RA could represent a metabolic checkpoint to control the flux of the glucosinolate biosynthesis and turnover processes in response to both external and internal signals. Meier et al., with the use of T-DNA mutants of enzymes responsible for glucosinolate breakdown, provided clue toward involvement of β-glucosidases belonging to BGLU18-BGLU33 clade, nitrile-specifier proteins (NSPs) during different stages of seed maturation and germination processes as potential candidates involved in glucosinolate turnover processes. The turnover processes are subjected to different substrate specificities of the glucosinolate hydrolytic enzymes. In addition, to evaluate the components involved in the glucosinolate turnover pathways, ascertaining the tissue specific effects of turnover is important like for example, increased turnover in one tissue balanced by enhanced biosynthesis in the other, balancing the total glucosinolate levels. Therefore, the study by Meier et al. has opened various dimensions and involvement of numerous candidates for glucosinolate turnover in the seeds, which require an in-depth investigation in coming years.

The biological activities of glucosinolates are governed post hydrolysis by myrosinases (β-thioglucoside glucohydrolase, TGG), where some hydrolysis products have the capabilities to induce stomatal closure (Hossain et al., 2013). But the physiological processes which control the TGG-mediated stomatal activity remain elusive. For further insights into these

processes, Zhang et al. raised overexpression transgenics in *Arabidopsis* using *TGG1* homolog from broccoli and found enhanced resistant against the bacterial pathogen *Pseudomonas syringae*, by accelerating stomatal closure and inhibition of stomatal reopening upon challenge. This work provided a first indication that the TGG1-regulated stomatal defense response moves via multiple phytohormone signaling pathways. The *BoTGG1* overexpression lines also displayed delayed flowering phenotype by promoting the expression of the floral repressor, *FLOWERING LOCUS C (FLC)*- an indicative of the cross talk of the glucosinolate pathway to modulate flowering time regulation. This study opens a new avenue for manipulation of classical myrosinases for engineering pathogen resistance and control of flowering time, which are important breeding objectives for accumulating higher yields in the cultivated *Brassica* species.

Glucosinolates hydrolytic forms epithionitriles are triggered upon the presence of epithiospecifier proteins (ESPs) in the medium, and only glucosinolates which possess a terminal double bond in their side-chain structure can form epithionitriles. A single gene in the model plant *A. thaliana* governs epithionitrile formation, however our knowledge so far remains limited in the crops of the *Brassicaceae* family, as they underwent a lineage-specific whole genome triplication event after their split from *Arabidopsis*. Witzel et al. recently identified three *ESP* homologs using *in-silico* analysis in *B. oleracea*. The BoESPs possess differential transcript profiles across tissue types and exhibited distinct substrate specificities toward seven tested glucosinolate structures, to shape the glucosinolates hydrolysis product diversity in *B. oleracea* genotypes. The BoESP activities were examined using functional complementation studies in *A. thaliana* accession lacking functional ESP, suggesting isoform-specific roles of BoESPs in glucosinolate breakdown. The formation of nitriles and epithionitriles have several notified effects particularly higher susceptibility against herbivores, and reducing the attractiveness for oviposition of specialists by attracting their natural enemies. Epithionitriles in the *Brassica* vegetables have a lower impact on aroma and pungency as desired for human consumption, as opposed to ITCs which are the most comprehensively characterized GHP molecules so far. We still lack the full understanding of the biological significance of nitriles and epithionitriles toward their roles in biotic interactions. Ting et al. recently established the involvement of nitriles in disease resistance during pathogen challenge using 3-butenenitrile (3BN) treatment in *Arabidopsis*. Interestingly, plants treated with 3BN showed alleviated leaf lesion symptoms when challenged using *Pectobacterium carotovorum* and *Botrytis cinerea* consequently reducing pathogen growth on leaves. Therefore, 3BN molecule is proposed to act as a DAMP for the induction of broad immune responses in *Arabidopsis*, involving a crosstalk between signaling pathways for NO, ROS, JA, and SA production in plants. Future studies should focus to identify the precise target pathogen recognition receptors that might bind 3BN for its action. Therefore, such studies provide essential information to alter and reduce ESP activities in planta correlating with an optimal defense output.

In conclusion, we perceive the studies published within this Research Topic "*Glucosinolates: Regulation of Biosynthesis and Hydrolysis*" expand our current understanding of regulatory molecular mechanisms of glucosinolate biosynthesis, hydrolysis, turnover, and regulation in plants.

AUTHOR CONTRIBUTIONS

All authors listed have made a substantial, direct and intellectual contribution to the work, and approved it for publication.

FUNDING

Glucosinolate research at NCB laboratory is supported by various research grants from Department of Biotechnology, India. BM acknowledges funding from CSIR, India.

ACKNOWLEDGMENTS

We sincerely thank Dr. Ralph Kissen and Dr. Tamara Gigolashvili for conceiving this Research Topic and editing research articles. Contribution from all scientists who published their work under this Research Topic are also acknowledged.

REFERENCES

Bednarek, P., Pislewska-Bednarek, M., Svatos, A., Schneider, B., Doubsky, J., Mansurova, M., et al. (2009). A glucosinolate metabolism pathway in living plant cells mediates broad-spectrum antifungal defense. *Science* 323, 101-106. doi: 10.1126/science.1163732

Hossain, M. S., Ye, W., Hossain, M. A., Okuma, E., Uraji, M., Nakamura, Y., et al. (2013). Glucosinolate degradation products, isothiocyanates, nitriles, and thiocyanates, induce stomatal closure accompanied by peroxidase-mediated reactive oxygen species production in Arabidopsis thaliana. *Biosci. Biotechnol. Biochem.* 77, 977-983. doi: 10.1271/bbb.120928

Kumar, R., Lee, S., Augustine, R., Reichelt, M., Vassão, D., Palavalli, M., et al. (2019). Molecular basis of the evolution of methylthioalkylmalate synthase and the diversity of methionine-derived glucosinolates. *Plant Cell* 31, 1633-1647. doi: 10.1105/tpc.19.00046

Rasmann, S., Chassin, E., Bilat, J., Glauser, G., and Reymond, P. (2015). Trade-off between constitutive and inducible resistance against herbivores is only partially explained by gene expression and glucosinolate production. *J. Exp. Bot.* 66, 2527-2534. doi: 10.1093/jxb/erv033

Conflict of Interest: The authors declare that the research was conducted in the absence of any commercial or financial relationships that could be construed as a potential conflict of interest.

frontiers in Plant Science

ORIGINAL RESEARCH
published: 04 October 2019
doi: 10.3389/fpls.2019.01230

Overexpressing the Myrosinase Gene *TGG1* Enhances Stomatal Defense Against *Pseudomonas syringae* and Delays Flowering in Arabidopsis

*Kaixin Zhang, Hongzhu Su, Jianxin Zhou, Wenjie Liang, Desheng Liu and Jing Li**

College of Life Sciences, Northeast Agricultural University, Harbin, China

Myrosinase enzymes and their substrate glucosinolates provide a specific defensive mechanism against biotic invaders in the Brassicaceae family. In these plants, myrosinase hydrolyzes glucosinolates into diverse products, which can have direct antibiotic activity or function as signaling molecules that initiate a variety of defense reactions. A myrosinase, β-thioglucoside glucohydrolase 1 (TGG1) was previously found to be strikingly abundant in guard cells, and it is required for the abscisic acid (ABA) response of stomata. However, it remains unknown which particular physiological processes actually involve stomatal activity as modulated by TGG1. In this experimental study, a homologous *TGG1* gene from broccoli (*Brassica oleracea* var. *italica*), *BoTGG1*, was overexpressed in *Arabidopsis*. The transgenic plants showed enhanced resistance against the bacterial pathogen *Pseudomonas syringae* pv. *tomato* (*Pst*) DC3000 *via* improved stomatal defense. Upon *Pst* DC3000 infection, overexpressing *BoTGG1* accelerated stomatal closure and inhibited the reopening of stomata. Compared with the wild type, *35S::BoTGG1* was more sensitive to ABA- and salicylic acid (SA)-induced stomatal closure but was less sensitive to indole-3-acetic acid (IAA)-inhibited stomatal closure, thus indicating these hormone signaling pathways were possibly involved in stomatal defense regulated by TGG1. Furthermore, overexpression of *BoTGG1* delayed flowering by promoting the expression of *FLOWERING LOCUS C* (*FLC*), which encodes a MADS-box transcription factor known as floral repressor. Taken together, our study's results suggest glucosinolate metabolism mediated by TGG1 plays a role in plant stomatal defense against *P. syringae* and also modulates flowering time by affecting the FLC pathway.

Keywords: *Arabidopsis*, flowering, myrosinase, *Pst* DC3000, stomatal defense

OPEN ACCESS

Edited by:
Tamara Gigolashvili, University of Cologne, Germany

Reviewed by:
Dayong Li, Zhejiang University, China
Fengming Song, Zhejiang University, China

****Correspondence:***
Jing Li
lijing@neau.edu.cn

Specialty section:
This article was submitted to Plant Metabolism and Chemodiversity, a section of the journal Frontiers in Plant Science

Received: *22 June 2019*
Accepted: *04 September 2019*
Published: *04 October 2019*

Citation:
Zhang K, Su H, Zhou J, Liang W, Liu D and Li J (2019) Overexpressing the Myrosinase Gene TGG1 Enhances Stomatal Defense Against Pseudomonas syringae and Delays Flowering in Arabidopsis. Front. Plant Sci. 10:1230. doi: 10.3389/fpls.2019.01230

INTRODUCTION

Glucosinolates are major secondary metabolites found in the Brassicales order, including the model plant *Arabidopsis* and many vegetables (Agerbirk and Olsen, 2012). Myrosinase (β-thioglucoside glucohydrolase, TGG) hydrolyzes glucosinolates by cleaving the thioglucosidic bond to release hydrolysis products that are toxic to insects and pathogens (Tierens et al., 2001; Hopkins et al., 2009; Calmes et al., 2015). Glucosinolates and myrosinase are normally harbored in separate compartments within plants (Andreasson et al., 2001; Koroleva et al., 2010). But they come into contact with each other upon tissue disruption from chewing by insects or damaged by pathogens

rapidly releasing large amounts of toxic hydrolysis products, typically isothiocyanates and nitriles and their derivatives (Halkier and Gershenzon, 2006).

Myrosinase activity has been detected in all glucosinolate-containing plants (Husebye et al., 2002). So far, six *TGG* genes encoding classical myrosinases have been found in the model plant *Arabidopsis* (Xu et al., 2004). The *TGG1* and *TGG2* genes are expressed aboveground, where the myrosinases encoded by each are considered to mainly break down aliphatic glucosinolates (Xue et al., 1995; Barth and Jander, 2006); *TGG3* and *TGG6* are pseudogenes having multiple frame-shift mutations in their coding regions, being specifically expressed in the plant's anthers (Husebye et al., 2002; Zhang et al., 2002); finally, *TGG4* and *TGG5* are specifically expressed in the roots and related to auxin synthesis and root-growth regulation (Fu et al., 2016). In addition to these six classical TGG myrosinases, two other β-glucosidases, PEN2 and PYK10, were identified as atypical myrosinases that primarily hydrolyze indole glucosinolates (Bednarek et al., 2009; Nakano et al., 2017).

Numerous studies have demonstrated that the glucosinolate–myrosinase defense system supports broad-spectrum immunity in *Arabidopsis*. Besides generating direct antimicrobial activity through toxic hydrolysis products, glucosinolate degradation can also form signaling molecules to initiate conserved defense responses. Clay et al. (2009) found that degradation of tryptophan-derived indole glucosinolate mediated by atypical myrosinase PEN2 is required for callose deposition in pathogen-associated molecular pattern (PAMP)-triggered immunity (PTI). Likewise, TGG1 and TGG2 are both presumed to be involved in conserved immune responses against pathogens. For example, the hydrolysis of methionine-derived aliphatic glucosinolates mediated by TGG1 and TGG2 is required for programmed cell death (PCD) upon inoculation with the bacterial pathogen *Pseudomonas syringae* pv. *tomato* (*Pst*) DC3000 and the downy mildew *Hyaloperonospora arabidopsidis* (Andersson et al., 2015). Interestingly, the indole glucosinolate degradation, as catalyzed by TGG1, attenuates mycotoxin fumonisin B1 (FB1)-induced PCD (Zhao et al., 2015); this suggests that glucosinolates' metabolism responds to different kinds of pathogens through various molecular mechanisms.

Apart from influencing PCD, TGG1 and TGG2 also contribute to stoma activity in *Arabidopsis*. As the most abundant stomatal protein, TGG1 comprises 40% to 50% of the total proteins found in guard cells; accordingly, the *tgg1* mutant has impaired wound-induced stomatal closure and is less sensitive to abscisic acid (ABA)-inhibited opening of its stomata (Zhao et al., 2008), while the *tgg1/tgg2* double mutant is defective in both ABA and methyl jasmonate (MeJA)-induced stomatal closure (Islam et al., 2009). Consistent with those findings, some glucosinolate-derived isothiocyanates were found capable of inducing stomatal closure (Hossain et al., 2013; Sobahan et al., 2015). Taken together, these studies indicate that myrosinase activity and corresponding hydrolysis products play a critical role in the regulation of stomatal closure. Yet it remains elusive which particular physiological processes TGG-modulated stomatal activity is involved in.

Glucosinolate metabolism contributes to not only defense against biotic stress but also plant development. Several reports have suggested that glucosinolates and their metabolites are involved in the modulation of flowering time in *Arabidopsis* (Naur et al., 2003; Kerwin et al., 2011; Jensen et al., 2015; Kong et al., 2015; Xu et al., 2018). Both *AOP2* and *AOP3* are genes in the aliphatic glucosinolate biosynthesis pathway, encoding two 2-oxoglutarate-dependent dioxygenases that modify glucosinolate side chains (Kliebenstein et al., 2001). These two paralogous genes possess the ability to affect glucosinolate accumulation and flowering time; however, they differ in their ability to modulate flowering time, so the two genes may affect the flowering phenology *via* separate mechanisms (Jensen et al., 2015). In particular, *AOP2* can alter the circadian clock pathway, but whether this contributes to regulated flowering time is questionable (Kerwin et al., 2011). Although cross talk does occur between glucosinolate metabolism and flowering control, many unknown processes await further exploration.

In this study, transgenic *Arabidopsis* plants overexpressing a homologous *TGG1* gene from broccoli (designated here as *BoTGG1*) were investigated, from which several interesting phenotypes were observed. We also performed the same analysis in plants overexpressing endogenous *AtTGG1*; similar phenotypes were observed but none as significant as *35S::BoTGG1*. To more clearly expound on the function of myrosinase TGG1, only data concerning *35S::BoTGG1* are presented here.

We found that *35S::BoTGG1* plants were more resistant against the bacterial pathogen *Pst* DC3000. Given that TGG1 participates in stomatal activity, we hypothesized that this enhanced pathogen resistance present in 35S::BoTGG1 arose from an altered stomatal defense. Stomata are natural openings on the surface of leaves, which not only enable the gas exchange but also facilitate the entry of bacteria. Hence, stomatal closure is considered among the conservative immune mechanisms plants employ against bacterial pathogens (Melotto et al., 2006; Zeng et al., 2010; Sawinski et al., 2013). When bacteria attack, the plant first recognizes PAMP and responds by closing its stomata. To circumvent this immune response, bacteria may release a specific virulence factor to effectively cause stomata to reopen (Melotto et al., 2006). In our study, we discovered that overexpression of *BoTGG1* accelerated stomatal closure and inhibited stomatal reopening upon infection of *Pst* DC3000. Furthermore, *35S::BoTGG1* was more sensitive to ABA- and salicylic acid (SA)-induced stomatal closures while less sensitive to indole-3-acetic acid (IAA)-inhibited stomatal closure, indicating that TGG1-affected stomatal defense likely operates *via* the signaling pathway of these hormones. In addition to enhanced pathogenic resistance, *35S::BoTGG1* displayed another phenotype, that of delayed flowering, which led to significant increases in the biomass of both the aerial part and root system.

Considering that high biomass and pathogen resistance are important plant breeding goals, our study will prove useful for breeding economically valuable cruciferous vegetables with both traits by modifying their glucosinolate metabolism.

MATERIALS AND METHODS

Plant Material and Growth Conditions

Seeds of broccoli (*Brassica oleracea* var. *italica*) cultivar 'Qingxiu' were purchased from the JiaHe Seeds Company (Beijing, China)

and used for *BoTGG1* cloning. Seeds of *Arabidopsis* ecotype Columbia (Col-0) were obtained from the Arabidopsis Biological Resource Center and used for genetic transformation. All plants were grown under a 16-h photoperiod, with a photosynthetic photon flux density of 100 $\mu mol \cdot m^{-2} \cdot s^{-1}$, at a 23°C temperature and 60% relative humidity.

Molecular Cloning and Plant Transformation

Total RNA was extracted from 3-day-old broccoli seedlings using the EASYPure Plant RNA Kit (TransGen, Beijing, China). The cDNA was synthesized from total RNA with the PrimeScript RT-PCR Kit (Takara, Shiga, Japan). The coding sequence (CDS) of the *BoTGG1* gene was amplified by using the primers BoTGG1-F and BoTGG1-R (primer sequences are listed in **Table S1**). To construct the expression vector *35S::BoTGG1*, the obtained PCR product was cloned into the expression vector pCAMBIA330035Su according to a previously described method (Nour-Eldin et al., 2006).

The constructed expression vector was passed through the *Agrobacterium tumefaciens* strain *LBA4404* and transferred into *Arabidopsis via* inflorescence infection (Clough and Bent, 1998). To select the transformants, seeds were planted on the 1/2 Murashige and Skoog (MS) agar medium containing 50 mg L^{-1} of kanamycin. Two independent homozygous transgenic lines were used in the subsequent analyses.

Glucosinolate Extraction and Analysis

The *35S::BoTGG1* and wild-type plants were grown simultaneously for 4 weeks. For each plant, 100–150 mg of rosette leaves was harvested for the glucosinolate extraction according to a previously described method (Hansen et al., 2007). Glucosinolates were extracted with methanol, and the desulfoglucosinolates were obtained by filtration through a DEAE Sephadex column followed by sulfatase treatment. High-performance liquid chromatography (HPLC) analysis was carried out as previously described (Grosser and van Dam, 2017). Glucosinolates were identified as desulfoglucosinolates, with sinigrin used as the external standard.

Myrosinase Determination

Rosette leaves of 4-week-old wild-type plants and two independent transgenic lines of *35S::BoTGG1* were harvested for their myrosinase activity assay. These fresh leaves (150 mg) were frozen in liquid nitrogen and quickly ground into powder. This ground sample was solubilized in 1-ml extraction buffer (pH 7.2) containing 10 mM of K-phosphate, 1 mM of EDTA, 3 mM of dithiothreitol (DTT), and 5% glycerol and then vortexed and centrifuged at 12,000 × *g* for 15 min at 4°C. The supernatant was collected to measure myrosinase activity.

Myrosinase activity was quantified by calculating the rate of hydrolysis of sinigrin. For this, the reaction buffer consisted of 33.3 mM of K-phosphate (pH 6.5) and 0.2 mM of sinigrin; the reaction was initiated by adding 100-µl extracted enzyme into 2.9 ml of reaction buffer. The decline in absorbance at 227 nm and 37°C spanning a 5-min period was plotted. Myrosinase activity was evaluated as the amount of sinigrin degraded by the enzyme from 1 g of fresh leaf per minute.

Bacterial Growth Assay

The virulent pathogen *Pst* DC3000 was used, with bacteria cultured in King's B medium at 28°C. For the sprayed infection, 4-week-old plants were sprayed with a bacterial suspension of *Pst* DC3000 [10^8 colony-forming units (CFU) ml^{-1}] in 10 mM of $MgCl_2$ containing 0.04% Silwet L-77. For infection by injection, leaves were syringe-infiltrated with a bacterial suspension of *Pst* DC3000 (10^6 CFU ml^{-1}) in 10 mM of $MgCl_2$. Those plants sprayed or injected with only 10 mM of $MgCl_2$ served as the corresponding control. The inoculated plants were kept at high humidity for 3 days. The amount of bacterial growth in the infected leaves was determined as described (Katagiri et al., 2002).

Measurement of Stomatal Aperture

Four-week-old plants were used for the stomatal aperture bioassay. Peels of rosette leaves were first floated in an opening buffer containing 5 mM of KCl, 50 mM of $CaCl_2$, and 10 mM of MES-Tris (pH = 6.15) under light for 3 h to induce the maximum opening of the stomata. For the bacterial infection, leaf peels were transferred to a water suspension of *Pst* DC3000 (10^8 CFU ml^{-1}), while those moved to water alone served as the control. Stomatal aperture was observed every 15 min during a 3-h period. For the ABA, SA, and MeJA treatments, leaf peels were respectively transferred to the opening buffer with 10 µM of ABA, 500 µM of SA, and 10 µM of MeJA for 2 h. For the IAA treatment, two groups of leaf peels were transferred to a new opening buffer solution, with or without IAA addition, and then placed under darkness for 2 h. Leaf peels likewise transferred to the opening buffer without hormone additions served as the control. Width and length of each stoma were measured using ImageJ software, and stomatal apertures were expressed by their width-to-length ratio.

Quantitative Real-Time PCR Analysis

To detect transcript levels of genes involved in the glucosinolate biosynthesis pathway, rosette leaves from 4-week-old plants were harvested. To detect transcription levels of genes involved in stomatal defense, detached leaves from 4-week-old plants were incubated with a water suspension of *Pst* DC3000 (10^8 CFU ml^{-1}). Leaves incubated with water served as the corresponding control. The incubated leaves were collected every 15 min during a 1-h period. To detect transcript levels of genes involved in flowering, rosette leaves from 18-day-old plants were harvested. For all sets of leaves, their total RNA was isolated using the TRIzol reagent (Invitrogen, Carlsbad, CA). The first strand of cDNA was synthesized using the PrimeScript RT Reagent Kit (Takara, Shiga, Japan), and quantitative real-time PCR (qRT-PCR) analyses were performed using the Trans Start Top Green qPCR SuperMix (TransGen, Beijing, China) on an ABI 7500 sequence detection system. The detected genes and the primers used in qPCR are listed in **Table S1**. The *ACTIN2* gene in *Arabidopsis* served as the internal reference gene. The gene expression level was calculated according to the $2^{-\Delta\Delta Ct}$ method.

Biomass Determination

For biomass determination, mature plants that had completely developed and grown after they produced their terminal flowers were used. The aerial tissues and seeds were harvested respectively and dried at 70°C for 2 days. The dry weight of each plant was measured, and the relative weight of wild type and *35S::BoTGG1* was calculated.

Detection of Drought Resistance

Wild-type and *35S::BoTGG1* plants were grown under a long-day condition (16-h photoperiod) for 4 weeks. Detached rosette leaves from *35S::BoTGG1* and the wild type were placed on a piece of weighing paper, and the fresh weight of these leaves was measured every 20 min during a 3-h period. Water loss was defined as the percentage of initial weight reduced at each time point.

The same amount of soil (by weight) was placed into each pot, after which all pots were soaked on a tray to ensure equivalent soil and water conditions among them. Seeds of *35S::BoTGG1* and the wild type were planted and allowed to grow for 4 weeks, with water added to the tray twice a week. To emulate drought, water was withheld from plants for 2 weeks, and then all the plants were rewatered for 2 days. Plant growth under each water condition was photographed and observed.

RESULTS

Cloning of *BoTGG1* From Broccoli

According to our previous transcriptome analysis in broccoli (Gao et al., 2014), the CDS of a myrosinase gene was amplified from the broccoli (*B. oleracea* var. *italica*) cultivar 'Qingxiu', by using the unigene *TGG* as the reference sequence. The CDS of the obtained gene was 1,647 nucleotides long, encoding a protein of 548 amino acids; this revealed 98.4% nucleotide and 99.2% amino acid identity when compared to the predicted myrosinase gene in broccoli (*B. oleracea* var. *oleracea*). Compared to its homologous *TGG* genes in *Arabidopsis*, the obtained gene was most similar to *TGG1*, with which it shared 71.5% nucleotide and 79.5% amino acid identity. We therefore designated the obtained gene as *BoTGG1* (GenBank accession no. MG252789).

Overexpression of *BoTGG1* Increased Myrosinase Activity and Decreased Aliphatic Glucosinolate Content in *Arabidopsis*

To confirm whether *BoTGG1* possesses myrosinase activity as its homolog in *Arabidopsis*, *BoTGG1* was overexpressed in *Arabidopsis*, and this overexpression of *BoTGG1* was confirmed by RT-PCR (**Figure S1**).

Rosette leaves from 4-week-old *35S::BoTGG1* and wild-type plants were harvested, and the myrosinase activity assay was performed using sinigrin (2-propenyl glucosinolate) as the substrate. Compared with wild-type plants, myrosinase activity in *35S::BoTGG1* was significantly increased (**Figure 1**), demonstrating that *BoTGG1* is functional *in vitro*.

To further detect the effects of overexpressing *BoTGG1* on the glucosinolate profile *in vivo*, the glucosinolate content of rosette leaves from wild-type and *35S::BoTGG1* plants was measured. In *35S::BoTGG1*, the content of indole glucosinolates did not show any significant difference, but aliphatic glucosinolates were significantly reduced to approximately half that in the wild type (**Figures 2A**, **B**). This decrease of aliphatic glucosinolates in *35S::BoTGG1* was possibly due to increased myrosinase activity, but it could also have arisen from decreased biosynthesis of these compounds. To determine which, the expression levels of key genes involved in glucosinolate biosynthesis were assessed. Comparing with the wild type, in *35S::BoTGG1* plants, expression levels of the indole glucosinolate biosynthetic genes *MYB51* and *CYP83B1* were apparently not altered, while *CYP79B3* and *SUR1* were slightly changed (**Figure 2C**). For the genes related to aliphatic glucosinolate biosynthesis, the respective expressions of *MYB28*, *MYB29*, *CYP83A1*, *SUR1*, and $FMO_{GS\text{-}OX1}$ were all slightly increased, whereas *MAM1* and *CYP79F2* were not changed and *CYP79F1* slightly decreased (**Figure 2D**). Nevertheless, since the altered expression of each gene was less than twofold, we may infer that these genes' expression during both indole and aliphatic glucosinolate biosynthesis in *35S::BoTGG1* remained unchanged compared with the wild type. This suggested the lowered content of aliphatic glucosinolates in *35S::BoTGG1* ought to be due to enhanced myrosinase activity and corresponding degradation

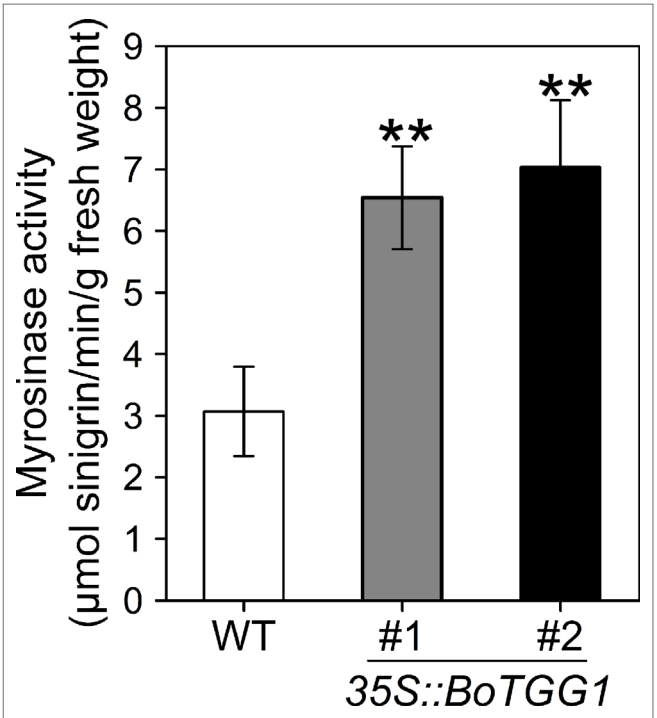

FIGURE 1 | Myrosinase activity of wild type (WT) and *35S::BoTGG1*. Rosette leaves of 4-week-old WT and two independent transgenic lines of *35S::BoTGG1* were harvested for myrosinase activity assay. Means (± SE) from three independent biological replicates and three technical repeats are shown. **, significantly different (Student's *t*-test; $P < 0.01$) from the WT.

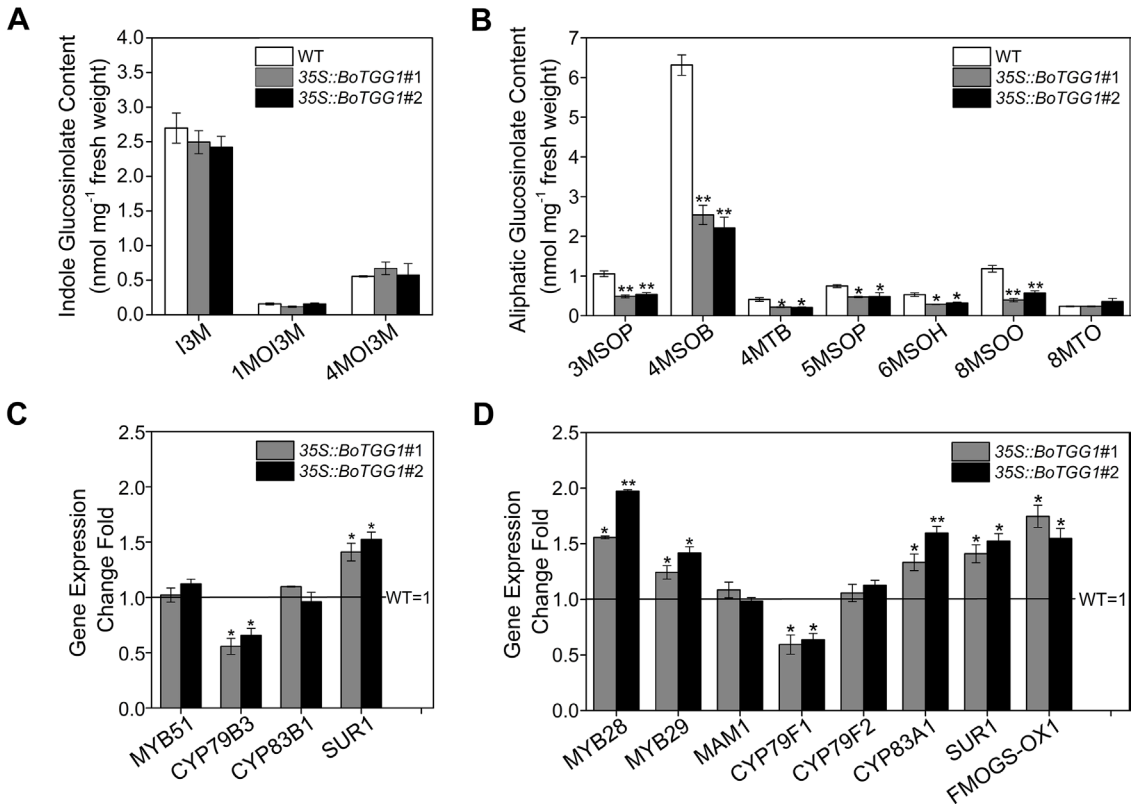

FIGURE 2 | Glucosinolate profiles and expression of genes in the glucosinolate biosynthetic pathway. **(A)** Content of indole glucosinolates. I3M, indol-3-ylmethyl-glucosinolate; 1MOI3M, 1-methoxyindol-3-ylmethyl-glucosinolate; 4MOI3M, 4-methoxyindol-3-ylmethyl-glucosinolate. **(B)** Content of aliphatic glucosinolates. 3MSOP, 3-methylsulfinylpropyl-glucosinolate; 4MSOB, 4-methylsulfinylbutyl-glucosinolate; 4MTB, 4-methylthiobutyl-glucosinolate; 5MSOP, 5-methylsulfinylpentyl-glucosinolate; 6MSOH, 6-methylsulfinylhexyl-glucosinolate; 8MSOO, 8-methylsulfinyloctyl-glucosinolate; 8MTO, 8-methylthiooctyl-glucosinolate. **(C)** Relative expression level of genes in the indolic glucosinolate biosynthetic pathway. **(D)** Relative expression level of genes in the aliphatic glucosinolate biosynthetic pathway. Rosette leaves of 4-week-old wild type (WT) and two independent transgenic lines were harvested for analysis of their glucosinolate contents and quantitative real-time PCR. Relative expression values are given in comparison with the WT (WT = 1). Means (± SE) from three independent biological replicates and three technical repeats are shown. * and **, significantly different (Student's *t*-test; $*0.01 < P < 0.05$, $**P < 0.01$) from the WT.

processes. In sum, these results indicated that under normal growing conditions, the overexpressed *BoTGG1* primarily broke down aliphatic glucosinolates in intact tissues of *Arabidopsis*.

Overexpression of *BoTGG1* Enhanced Resistance to *Pst* DC3000

To determine whether overexpression of *BoTGG1* could affect pathogenic resistance in *Arabidopsis*, virulent *Pst* DC3000 was used as a representative pathogen, and dip inoculation and syringe infiltration assays were performed. Leaves of *35S::BoTGG1* and wild-type plants were infected with *Pst* DC3000. Three days after infection, for both dip inoculation and syringe infiltration, wild-type plants displayed clear chlorotic symptoms. In contrast, *35S::BoTGG1* plants showed no significant signs of infection (**Figures 3A, B**). The growth of bacteria in leaves of the wild type was approximately 10-fold higher than that of *35S::BoTGG1* in the dip assay and likewise sixfold higher in the syringe assay (**Figures 3C, D**). These results suggested that overexpression of *BoTGG1* enhanced resistance to *Pst* DC3000 in *Arabidopsis*. The difference in bacterium growth between the wild type and *35S::BoTGG1* was larger when inoculated on the surface than when inoculated directly into the apoplast; hence, it may be more difficult for bacteria to enter through the epidermis in *35S::BoTGG1*.

Overexpression of *BoTGG1* Accelerated Stomatal Closure and Inhibited Stomatal Reopening Upon Infection of *Pst* DC3000

Previous work discovered that *Arabidopsis* responds to the PAMPs of bacteria by closing its stomata ~1 h after incubation with *Pst* DC3000, but this stomatal closure was transient, as bacteria subsequently produced a polyketide toxin, coronatine, which induced stomatal reopening ~3 h after incubation to let them enter the host plant (Melotto et al., 2006). It is of great interest to know whether overexpression of *BoTGG1* can affect the closing and reopening of stomata during the arms race between plants and pathogenic bacteria. Therefore, we observed the dynamic state of stomata during the first 3 h of *Pst* DC3000 incubation. Water incubation was performed as control, and no stomatal movement was observed (**Figure S2**). In the wild type, 90% of stomata had completely closed by ~60 min post inoculation, while in *35S::*

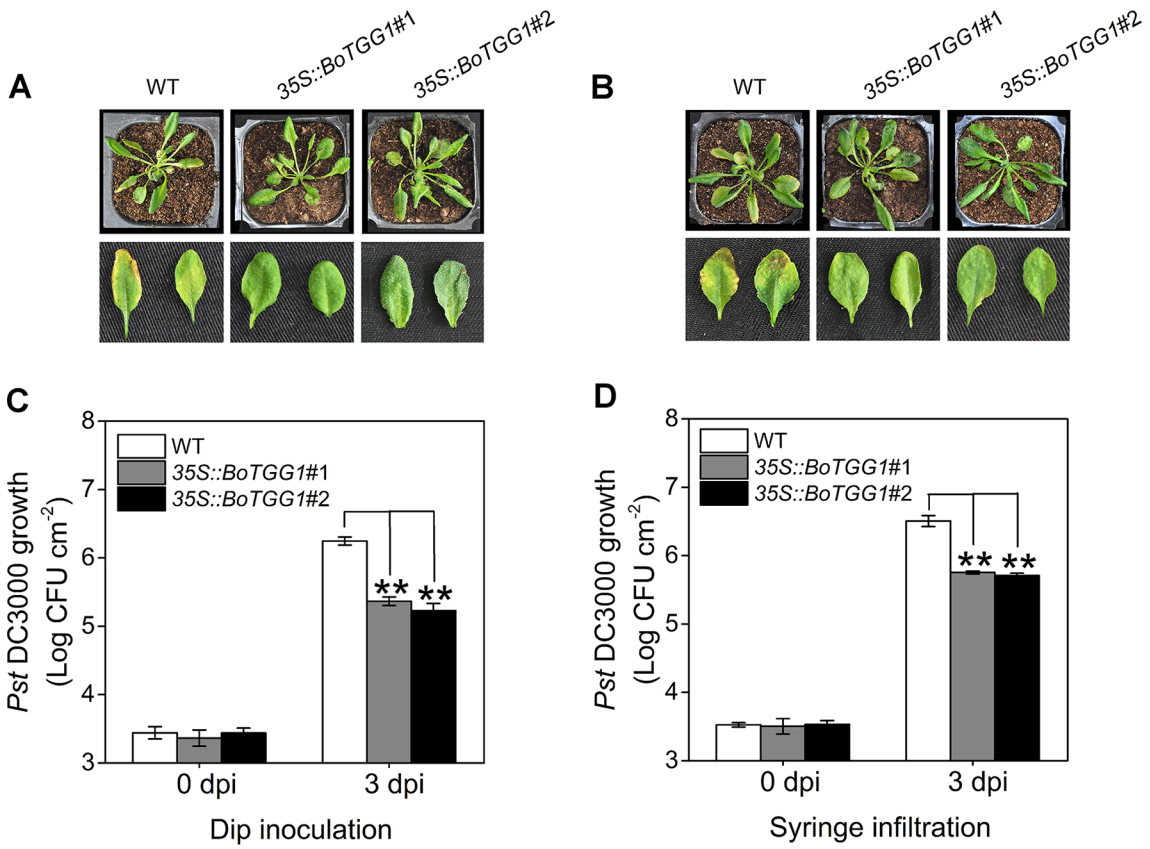

FIGURE 3 | Enhanced resistance of *35S::BoTGG1* infected with *Pseudomonas syringae* pv. *tomato* DC3000 (*Pst* DC3000). The wild type (WT) and *35S::BoTGG1* were dip-inoculated with a suspension of *Pst* DC3000 (10^8 CFU ml^{-1}) and syringe-infiltrated with a suspension of *Pst* DC3000 (10^6 CFU ml^{-1}), respectively. **(A)** Disease symptoms of plants infected with *Pst* DC3000 by dip inoculation. **(B)** Disease symptoms of plants infected with *Pst* DC3000 by syringe infiltration. The pictures were taken at 3 days after inoculation. **(C)** Bacterial growth on leaves infected with *Pst* DC3000 by dip inoculation. **(D)** Bacterial growth on leaves infected with *Pst* DC3000 by syringe infiltration. Means (± SE) from three independent biological replicates and three technical repeats are shown. **, significantly different (Student's *t*-test; $P < 0.01$) from the WT. dpi, days post inoculation.

BoTGG1 this extent of closure occurred earlier, at ~45 min post inoculation. Within 60–120 min after the inoculations, half of the stomata had reopened, but not to their maximum apertures, and they were subsequently closed again at 120 min post inoculation in both wild-type and transgenic plants. No significant differences between the two genotypes were observed within this period. During the last 60 min, however, 90% of the stomata had reopened gradually in the wild type while most of the stomata remained closed in *35S::BoTGG1* (**Figures 4A, B**). These results suggested that overexpression of *BoTGG*1 accelerated *Pst* DC3000-induced closing of the stomata and inhibited their later reopening.

35S::BoTGG1 Was More Sensitive in ABA- and SA-Induced Stomatal Closure and Less Sensitive in IAA-Inhibited Stomatal Closure

As shown in **Figures 5A**, **C**, ABA and SA effectively induced stomatal closure in both the wild type and *35S::BoTGG1*. Compared with wild-type plants, the stomatal aperture was significantly smaller in *35S::BoTGG1*, indicating the latter plant was more sensitive to ABA- and SA-induced closing of the stomata. Much like ABA and SA, JA was able to induce stomatal closure in both the wild type and 35S::*BoTGG1*, but no significant difference was observed between the two genotypes, suggesting that overexpression of *BoTGG1* did not affect stomatal closure induced by this hormone. IAA is another hormone that can positively regulate stomatal opening and is strongly induced by coronatine upon infection by pathogenic bacteria (Lohse and Hedrich, 1992; Kunkel and Harper, 2018). As **Figures 5B**, **D** show, in wild-type plants, stomata were largely closed under darkness in the absence of IAA but stayed open in its presence. In contrast, in *35S::BoTGG1*, the darkness led to stomatal closure irrespective of IAA being present or not. This result suggested that *35S::BoTGG1* was less sensitive to IAA-inhibited stomatal closure.

ABA-mediated stomatal closure is involved in bacterium-triggered stomatal defense (Melotto et al., 2017). To determine whether ABA-mediated stomatal closure is more sensitive in *35S::BoTGG1* in response to *P. syringae*, we analyzed the expression levels of several pathogen defense-related genes in the ABA-mediated stomatal closure. Since bacterium-triggered stomatal defense is a fast response (<1 h) (Melotto et al., 2017), the gene expression levels were detected at five time points within an hour

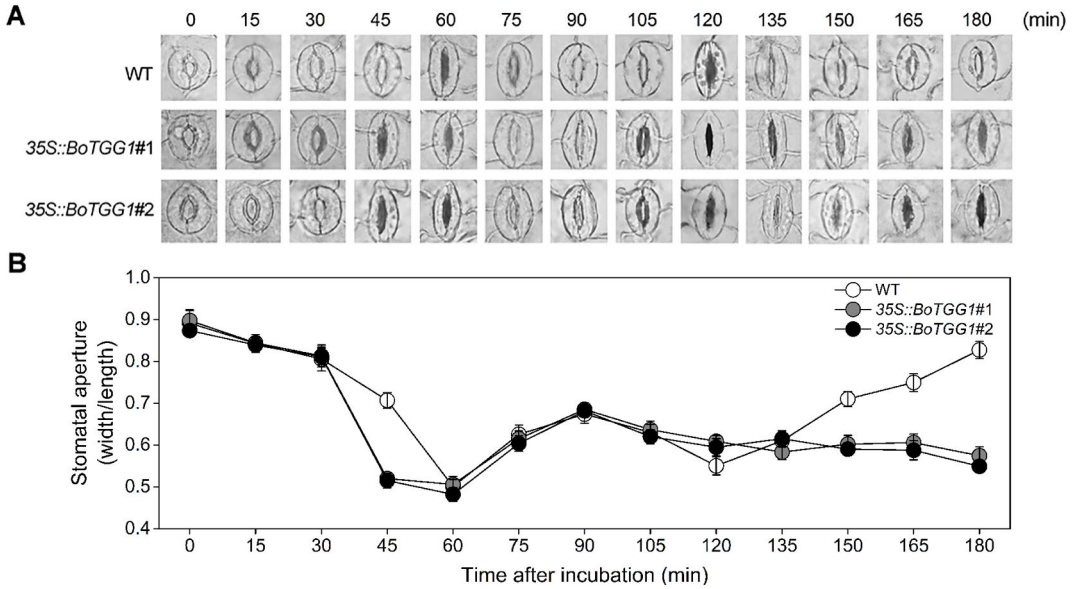

FIGURE 4 | Stomatal movement in wild type (WT) and *35S::BoTGG1* upon infection of *Pseudomonas syringae* pv. *tomato* DC3000 (*Pst* DC3000). Leaf peels of WT and *35S::BoTGG1* plants were incubated with a suspension of *Pst* DC3000 (10^8 CFU ml^{-1}) for 3 h, and their stomatal apertures were observed and measured every 15 min. **(A)** The images of representative stomata at each time point during the infection. **(B)** Stomatal apertures at each time point during the infection. Means (± SE) from three independent experiments, each with 100 stomata, are shown.

upon *Pst* DC3000 infection. ABI1, ABI2, and PP2CA are negative regulators of ABA signaling and play essential roles in pathogen resistance (Park et al., 2009; Rodrigues et al., 2013). The expression levels of the three genes were significantly higher in *35S::BoTGG1* than in the wild type before *Pst* DC3000 infection (**Figure 6A**). During the first hour of *Pst* DC3000 infection, the expression levels of *ABI1*, *ABI2*, and *PP2CA* in *35S::BoTGG1* decreased, while the expression levels of the three genes in the wild type did not change significantly. The decreased expression of these negative regulator genes indicated the activating of the ABA signaling pathway, and this might contribute to the faster stomatal closure in *35S::BoTGG1*.

The SA signaling pathway is also required for stomatal defense (Khokon et al., 2011). NPR1 is a major activator of SA-mediated responses and is essential for stomatal defense (Schellenberg et al., 2010). *LOX1*, a gene expressed in guard cells, encodes lipoxygenase, the catalytic product of which triggers SA-mediated stomatal closure (Montillet et al., 2013). As shown in **Figure 6B**, the expression of both *NPR1* and *LOX1* showed a rapid and transient increase during the first 30 min of *Pst* DC3000 infection. The expression level of the two genes in *35S::BoTGG1* increased much more than that in wild-type plants, which suggested SA-triggered stomatal response might be more sensitive in *35S::BoTGG1*.

SLAC1 encodes a guard cell-expressed anion channel, which is a major contributor of stomatal closure. OST1 and GHR1 are two kinases that activate SLAC1 in parallel during ABA-induced stomatal closure, and GHR1 is also involved in SA-mediated stomatal closure (Hua et al., 2012; Acharya et al., 2013). Similar to what has been observed in *LOX1* and *NPR1*, a rapid and transient increase in the expression of *OST1* and *GHR1* was observed in *35S::BoTGG1* during the early response to *Pst* DC3000, while the expression increases of the two genes in wild type were not significant (**Figure 6C**). These results further suggested that in response to *Pst* DC3000, stomatal closure mediated by ABA and SA might be more sensitive in *35S::BoTGG1*.

ANAC019, ANAC055 and ANAC072 are three homologous NAC family transcription factors that are required for coronatine-induced stomatal reopening through JA signaling pathway (Zheng et al., 2012). As shown in **Figure 6D**, the expression of these three genes showed a significant and transient increase, but no significant difference were observed between *35S::BoTGG1* and the wild type. So ANAC019, ANAC055 and ANAC072 might not (or at least not at transcription level) contribute to the insensitive stomatal reopening in *35S::BoTGG1*.

Stoma's movement is the most critical factor regulating water transpiration in plants, and is closely related to their drought resistance. Compared with the wild type, *35S::BoTGG1* exhibited no difference in the water loss of its detached rosette leaves and showed comparable growth under drought stress (i.e., withholding water for 2 weeks; **Figures S3A, B**). This result suggested that overexpressing *BoTGG1* enhanced stomatal closure in response to pathogen infection but not to drought stress, and thus it did not change the drought resistance of plants.

Overexpression of *BoTGG1* Delayed Flowering Time

The mechanism by which glucosinolates modulate flowering time and whether myrosinase is involved in the modulation remains unclear. We found that overexpressing *BoTGG1* in *Arabidopsis* significantly delayed flowering under a long-day condition (**Figures 7A–C**). Compared with the wild type, *35S::BoTGG1* plants flowered about 8-9 days later. Recently,

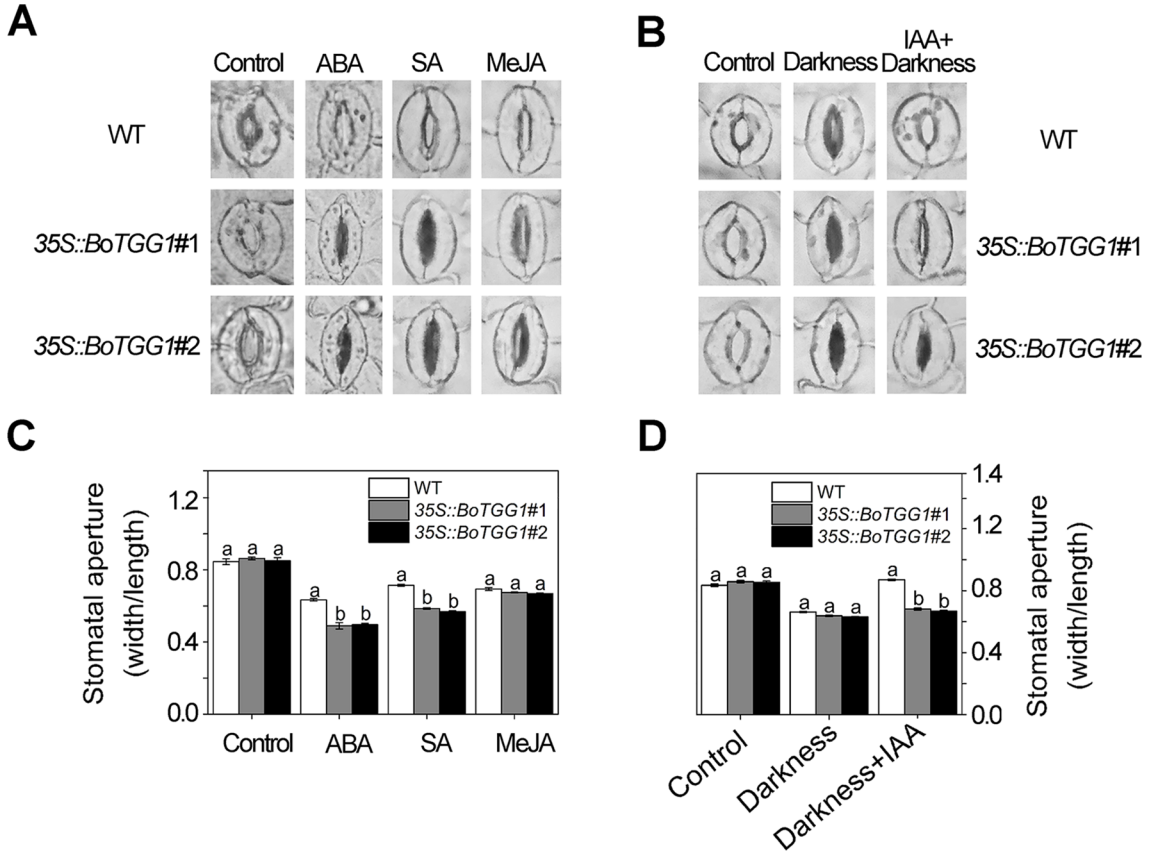

FIGURE 5 | Stomatal responses to different phytohormones in wild type (WT) and *35S::BoTGG1*. **(A)** Images of representative stomata treated with abscisic acid (ABA), salicylic acid (SA), and methyl jasmonate (MeJA) hormones. Leaf peels of WT and *35S::BoTGG1* were respectively incubated with a stomatal opening buffer with 10 μM of ABA, 500 μM of SA, or 10 μM of MeJA under lighted conditions for 2 h. Leaf peels transferred to the opening buffer were used as the control. **(B)** Images of representative stomata treated with indole-3-acetic acid (IAA). Two groups of leaf peels (with maximum opening of stomata) were transferred to new opening buffer with or without IAA addition and left under darkness for 2 h. Leaf peels transferred to the same opening buffer lacking hormone addition were used as the control. **(C)** Stomatal apertures under treatment with ABA, SA, and MeJA. **(D)** Stomatal apertures under treatment with IAA. For stomatal apertures, means (± SE) from three independent experiments, each with 100 stomata, are shown. Different letters indicate significant differences (ANOVA test; $P < 0.05$) between the WT and *35S::BoTGG1* under the same treatment.

by using two *Aethionema arabicum* accessions with distinct glucosinolate profile, Mohammadin et al. (2017) identified a single major quantitative trait locus controlling total glucosinolate content; they suggested that *FLC* is a potential major regulator of glucosinolate content, and that a plant's defense and its vegetative-to-reproductive stage transition can affect each other. To determine whether the delayed flowering in *35S::BoTGG1* was indeed related to a *FLC*-mediated flowering pathway, transcription levels of *FLC*, *FT*, and *SOC1* genes in rosette leaves of wild-type and *35S::BoTGG1* plants were detected. As **Figure 7D** shows, in *35S::BoTGG1* the expression of *FLC* significantly exceeded the wild type whereas that of *FT* and *SOC1* were significantly lower than in wild type. This indicated that an *FLC*-dependent flowering pathway might have contributed to the delayed flowering that characterized *35S::BoTGG1*.

Due to this delayed flowering, vegetative growth in *35S::BoTGG1* was prolonged by 9 days and its total growth phase prolonged ca. 28 days. Consequently, these transgenic plants appeared significantly larger in both their aerial and underground parts in the later stage of life cycle (**Figures 8A**, **B**). After terminal flower production, the final dry weight of aerial tissue and seeds of *35S::BoTGG1* respectively reached 2.4- and 1.9- fold that of wild-type counterparts (**Figures 8C**, **D**). However, an increased biomass in *35S::BoTGG1* before flowering could not be detected, indicating the improved biomass found before was due to a prolonged growth phase caused by delayed flowering.

DISCUSSION

Being the most common natural openings in plants, stomata are the first barriers bacterial pathogens must overcome to successfully colonize their host. Not surprisingly, plants have evolved ways to thwart such pathogen attack by closing their stomata rapidly upon detecting an infection in progress. To circumvent this plant immune response, bacteria have evolved a

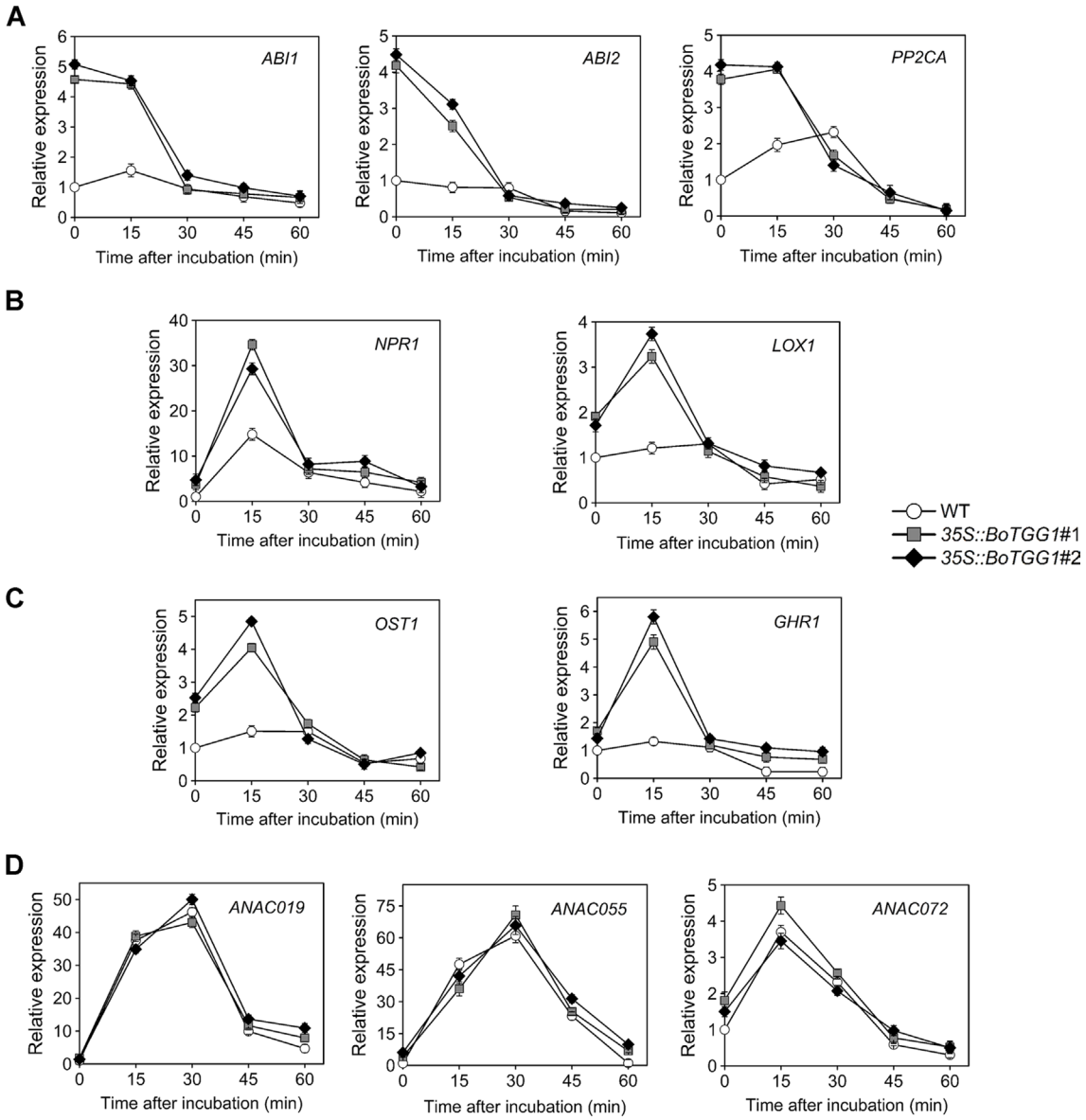

FIGURE 6 | Relative expression of several stomatal defense-related genes in response to *Pseudomonas syringae* pv. *tomato* DC3000 (*Pst* DC3000) in the wild type (WT) and *35S::BoTGG1*. **(A)** Relative expression of genes in ABA-mediated stomatal closure pathway. **(B)** Relative expression of genes in SA-mediated stomatal closure pathway. **(C)** Relative expression of *OST1* and *GHR1*. **(D)** Relative expression of genes inducing stomatal reopening. Detached leaves after dip inoculation with a suspension of *Pst* DC3000 (10^8 CFU ml^{-1}) at the given time points were used for quantitative real-time PCR analysis. Transcript levels in the WT at 0 min was set to 1. Means (± SE) from three independent biological replicates and three technical repeats are shown.

reciprocal strategy to effectively cause stomata to reopen, so they could penetrate the host (Melotto et al., 2006).

In this study, we found that enhanced myrosinase activity promoted plant resistance against a pathogenic bacterium (*Pst* DC3000) by accelerating the closure and inhibiting the reopening of stomata upon infection. Both ABA and SA play positive roles in stomatal closure and are thought to function in PAMP-induced stomatal closure (Melotto et al., 2017). In our study, *BoTGG1*-overexpressing plants were more sensitive to ABA-and SA-induced stomatal closure, thus indicating overexpression of *BoTGG1* promoted bacteria-induced stomatal closure possibly *via* the ABA and SA signaling pathways. The quantitative real time PCR analysis of the key genes in ABA- and SA- mediated stomatal closure pathways supported our speculation. In *Arabidopsis*, *TGG1* and *TGG2* are required in ABA- and MeJA-induced stomatal closure (Islam et al., 2009). We found that MeJA induced stomata to close in both wild-type and *35S::BoTGG1* plants, but no difference was detected between the two genotypes; this suggests altered TGG1 activity did not affect MeJA-mediated stomatal closure pathway as tested under our experimental conditions. Although MeJA-induced stomatal closure has

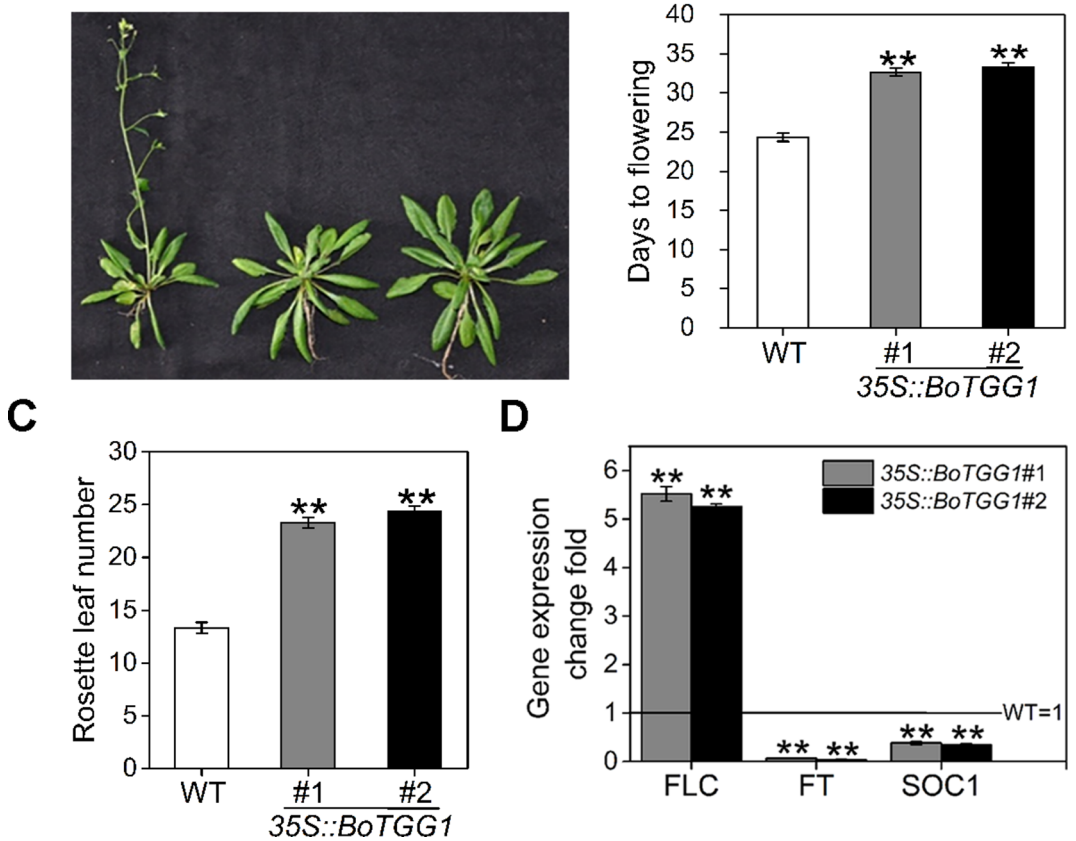

FIGURE 7 | Delayed flowering in *35S::BoTGG1* plants. **(A)** Flowering phenotype in *35S::BoTGG1*. **(B)** Average flowering time (days after germination). **(C)** The average number of rosette leaves at time of flowering. **(D)** Relative expression levels of flowering-related genes in the wild type (WT) and *35S::BoTGG1*. Rosette leaves from 18-day-old plants grown under a 16-h photoperiod were harvested for quantitative real-time PCR analysis. Change fold of gene expression in comparison with the WT is shown. Means (± SE) from three independent biological replicates and three technical repeats are shown. **, significantly different (Student's *t*-test; $^{**}P < 0.01$) from the WT.

been detected in some studies (Suhita et al., 2004; Munemasa et al., 2007; Arnaud et al., 2012; Hua et al., 2012; Yan et al., 2015), this could not always be verified by other research groups (Montillet et al., 2013; Savchenko et al., 2014). In fact, the role of JA-Ile as an inhibitor of stomatal closure is more strongly supported (Staswick and Tiryaki, 2004; Sellam et al., 2007; Panchal et al., 2016). In response to plant stomatal defenses, bacterium-produced coronatine mimics JA-Ile to induce stomatal reopening. This inconsistency is explained in that MeJA-induced stomatal closure might depend on reaching an endogenous ABA threshold (Hossain et al., 2011).

Generally, IAA plays a positive role in regulating the opening of stomata (Lohse and Hedrich, 1992). *Pst* was found to promote IAA production and enable the pathogen to colonize successfully host plants (Chen et al., 2007). In our study, darkness-induced stomatal closure was successfully inhibited by IAA in the wild type but not in *35S::BoTGG1*, indicating that *35S::BoTGG1* was insensitive to IAA-inhibited stomatal closure. Taken together, we speculate that IAA production triggered by *Pst* DC3000 perhaps promotes stomatal reopening and an insensitivity to IAA may contribute to enhanced stomatal defense in *35S::BoTGG1*.

In addition to improving stomatal defense, overexpression of *BoTGG1* should have activated other immune pathway(s), since *35S::BoTGG1* showed significantly higher resistance to *Pst* DC3000 than the wild type in the syringe assay which bypass the stomatal barrier. In *35S::BoTGG1*, aliphatic glucosinolates were significantly reduced due to increased TGG activity, indicating that aliphatic glucosinolate degradation possibly contributes to the enhanced pathogen resistance. Isothiocyanates derived from aliphatic glucosinolates were reported to limit pathogen growth by direct antimicrobial activity for a wide range of bacterial pathogens (Sellam et al., 2007). In addition, TGG mediated degradation of aliphatic glucosinolates is required in programmed cell death during hypersensitive responses upon bacterial inoculation (Andersson et al., 2015). Thus, we speculate that, in addition to stomatal defense, the improved immune response in *35S::BoTGG1* might be due to the increased antimicrobial activity and (or) the activated hypersensitive response.

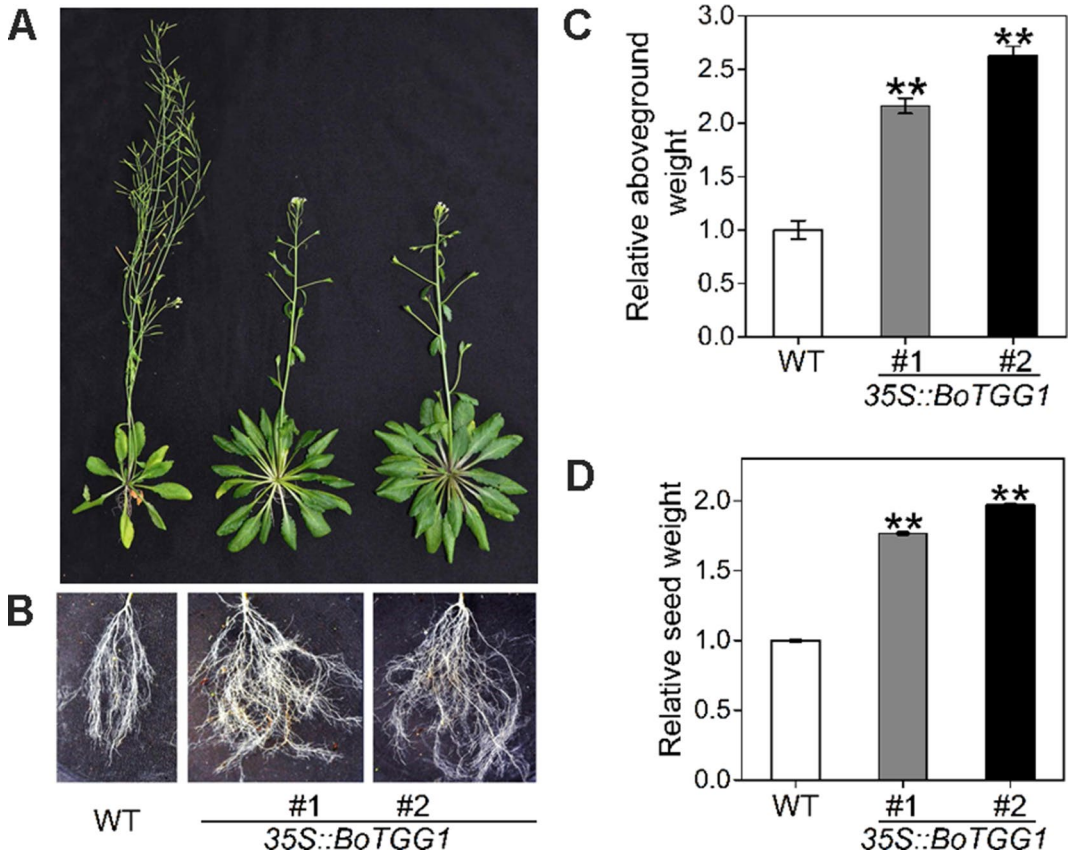

FIGURE 8 | Biomass of wild type (WT) and *35S::BoTGG1*. **(A)** Aboveground parts of WT and *35S::BoTGG1*. **(B)** Roots of WT and *35S::BoTGG1*. **(C)** Relative aboveground dry weight of WT and *35S::BoTGG1*. **(D)** Relative seed dry weight of WT and *35S::BoTGG1*. Means (± SE) from measurements of more than five plants per genotype are shown. Relative weight of WT and *35S::BoTGG1* were measured after the plants produced their terminal flowers; for WT, these are 43-day-old plants, and for *35S::BoTGG1*, these are 71-day-old plants. **, significantly different (Student's *t*-test; $P < 0.01$) from the WT.

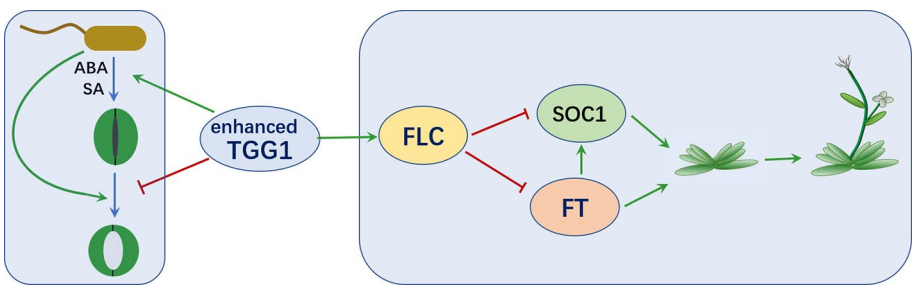

FIGURE 9 | TGG1 modulates stomatal defense and flowering time. Enhanced TGG1 activity improves plant stomatal defense against bacterial pathogens by accelerating stomatal closure and inhibiting the reopening of stomata. TGG1 may modulate flowering time *via* an interaction with the FLC pathway.

Overexpressing *BoTGG1* promoted stomatal resistance against bacteria by enhancing the ability of stomata to close. Nevertheless, the stomatal behavior in response to drought stress seemed unaffected, since in *35S::BoTGG1* transpirational water loss from its detached rosette leaves and whole-plant survival under drought stress were similar to wild-type plants. This finding indicates that enhanced stomatal closure behavior may specifically function in the plant defense response against bacterial pathogens, in a way that is distinguishable from other stomatal-related physiological activities responsive to abiotic stress.

Under adverse environmental conditions, plants do not only initiate defense reactions, but also need to coordinate their growth and defense to maximize plant fitness. As a potent defensive compound, glucosinolate and its metabolism play a vital role in biotic stress resistance while also profoundly impacting plant development. Previously, it was found that overexpressing *CYP83B1*, a glucosinolate

biosynthesis enzyme that catalyzes indole-3-acetaoxime to indole-3-acetonitrile oxide, causes the early onset of flowering (Naur et al., 2003; Xu et al., 2018). When Jensen et al. (2015) introduced *AOP2* (encoding a 2-oxoglutarate-dependent dioxygenase modifying glucosinolate side chains) into a naturally null Col-0 background, this led to delayed flowering under long-day condition. The double-mutant *myb28/myb29*, which lacks both MYB28 and MYB29, the main regulators of biosynthesis of aliphatic glucosinolates, presents delayed flowering under both short days and long days. Interestingly, under a constant lit condition, the plants with *AOP2* introduced to them were observed to flower earlier, yet *myb28/myb29* showed no alteration in its flowering time (Kerwin et al., 2011). Furthermore, Jensen et al. (2015) showed that the ability of *AOP2* to affect flowering time varies in different accessions due to different genetic backgrounds. Kerwin et al. (2011) study demonstrated that the glucosinolate pathway modulates the plant circadian clock, subsequently leading to complex physiological shifts; however, they also suggested that glucosinolate pathway's influence on circadian clock does not extend to flowering time. In our study, the expression of *FLC* was significantly higher in late-flowering *TGG1*-overexpressing plants, thus indicating glucosinolate metabolism may regulate flowering time through the *FLC* pathway. In short, the mechanism by which glucosinolates regulate flowering time is quite complex, requiring further study to reveal more about the cross talk between this secondary metabolite and flowering in plants.

In summary, as depicted in **Figure 9**, we have showed that overexpressing a myrosinase gene *TGG1* promoted stomatal defense against a bacterium pathogen in two complementary ways: (1) by accelerating stomatal closure and (2) by inhibiting the reopening of stomata, with former response possibly mediated by ABA and SA. Additionally, the transformation of TGG1 delayed flowering, possibly by promoting the *FLC* pathway.

Due to delayed flowering, the vegetative and total growth phases were prolonged by 9 and 28 days, respectively, which translated into a significant increase in plant biomass. In an applied breeding context, controlling flowering time would be helpful to produce high yields throughout the year. For many Brassicaceae vegetable crops, their late flowering is an important breeding goal; for example, premature bolting is a severe problem in *Brassica rapa* plants—including Chinese cabbage, pak choi, and turnip—as it largely reduces both quality and yield, so extremely late bolting is a major breeding goal in these crops (Kitamoto et al., 2017). Considering that the glucosinolate–myrosinase system is highly conserved between cruciferous crops and the model plant *Arabidopsis*, transformation of *TGG1* might offer a viable and valuable method for breeding late flower varieties to increase their biomass as well as their resistance to bacterial pathogens.

DATA AVAILABILITY STATEMENT

All datasets generated for this study are included in the manuscript/**Supplementary Files**.

AUTHOR CONTRIBUTIONS

JL designed the experiment and KZ conducted the experiment. HS, JZ, WL, and DL participated in various parts of the experiment. JL and KZ wrote the manuscript. All authors have read and approved the final manuscript.

FUNDING

This work was supported by the National Natural Science Foundation of China (NSFC) (31570298) and the Heilongjiang Natural Science Foundation (C2017031).

SUPPLEMENTARY MATERIAL

The Supplementary Material for this article can be found online at: https://www.frontiersin.org/articles/10.3389/fpls.2019.01230/full#supplementary-material

FIGURE S1 | Expression level of BoTGG1 in wild type (WT) and 35S::BoTGG1. Rosette leaves of 4-week-old WT and two independent transgenic lines were harvested for the RT-PCR analysis. ACTIN2 served as the internal control.

FIGURE S2 | Stomatal movement in wild type (WT) and 35S::BoTGG1 upon incubation of water. Leaf peels of WT and 35S::BoTGG1 plants were incubated in water for 3 h and their stomatal apertures were observed and measured every 15 min. (A) The images of representative stomata at each time point during the incubation. (B) Stomatal apertures at each time point during the incubation. Means (± SE) from three independent experiments, each with 100 stomata, are shown.

FIGURE S3 | Phenotypes of wild type (WT) and 35S::BoTGG1 under drought stress. (A) Water loss assay of WT and 35S::BoTGG1 plants. Rosette leaves of 4-week-old WT and 35S::BoTGG1 plants were removed, and detached rosette leaves were weighed at different time points. Means (± SE) from n = 10 individual plants per genotype are shown. (B) Drought resistance of WT and 35S::BoTGG1 plants. Four-week-old WT and 35S::BoTGG1 were treated by withholding water for 2 weeks followed by re-watering.

REFERENCES

Acharya, B. R., Jeon, B. W., Zhang, W., and Assmann, S. M. (2013). Open Sstomata 1 (OST1) is limiting in abscisic acid responses of Arabidopsis guard cells. *New Phytol.* 200 (4), 1049–1063. doi: 10.1111/nph.12469

Agerbirk, N., and Olsen, C. E. (2012). Glucosinolate structures in evolution. *Phytochemistry* 77, 16–45. doi: 10.1016/j.phytochem.2012.02.005

Andersson, M. X., Nilsson, A. K., Johansson, O. N., Boztas, G., Adolfsson, L. E., Pinosa, F., et al. (2015). Involvement of the electrophilic isothiocyanate sulforaphane in Arabidopsis local defense responses. *Plant Physiol.* 167 (1), 251–261. doi: 10.1104/pp.114.251892

Andreasson, E., Bolt Jorgensen, L., Hoglund, A. S., Rask, L., and Meijer, J. (2001). Different myrosinase and idioblast distribution in *Arabidopsis* and *Brassica napus*. *Plant Physiol.* 127 (4), 1750–1763. doi: 10.1104/pp.010334

Arnaud, D., Desclos-Theveniau, M., and Zimmerli, L. (2012). Disease resistance to *Pectobacterium carotovorum* is negatively modulated by the *Arabidopsis* lectin receptor kinase LecRK-V.5. *Plant Signal. Behav.* 7 (9), 1070–1072. doi: 10.4161/psb.21013

Barth, C., and Jander, G. (2006). *Arabidopsis* myrosinases TGG1 and TGG2 have redundant function in glucosinolate breakdown and insect defense. *Plant J.* 46 (4), 549–562. doi: 10.1111/j.1365-313X.2006.02716.x

Bednarek, P., Pislewska-Bednarek, M., Svatos, A., Schneider, B., Doubsky, J., Mansurova, M., et al. (2009). A glucosinolate metabolism pathway in living plant cells mediates broad-spectrum antifungal defense. *Science* 323 (5910), 101–106. doi: 10.1126/science.1163732

Calmes, B., N'Guyen, G., Dumur, J., Brisach, C. A., Campion, C., Iacomi, B., et al. (2015). Glucosinolate-derived isothiocyanates impact mitochondrial function in fungal cells and elicit an oxidative stress response necessary for growth recovery. *Front. Plant Sci.* 6, 414. doi: 10.3389/fpls.2015.00414

Chen, Z., Agnew, J. L., Cohen, J. D., He, P., Shan, L., Sheen, J., et al. (2007). *Pseudomonas syringae* type III effector AvrRpt2 alters *Arabidopsis thaliana* auxin physiology. *Proc. Natl. Acad. Sci. U. S. A.* 104 (50), 20131–20136. doi: 10.1073/pnas.0704901104

Clay, N. K., Adio, A. M., Denoux, C., Jander, G., and Ausubel, F. M. (2009). Glucosinolate metabolites required for an Arabidopsis innate immune response. *Science* 323(5910), 95–101. doi: 10.1126/science.1164627

Clough, S. J., and Bent, A. F. (1998). Floral dip: a simplified method for *Agrobacterium*-mediated transformation of *Arabidopsis thaliana*. *Plant J.* 16 (6), 735–743. doi: 10.1046/j.1365-313x.1998.00343.x

Fu, L., Wang, M., Han, B., Tan, D., Sun, X., and Zhang, J. (2016). *Arabidopsis* myrosinase genes *AtTGG4* and *AtTGG5* are root-tip specific and contribute to auxin biosynthesis and root-growth regulation. *Int. J. Mol. Sci.* 17 (6), 892. doi: 10.3390/ijms17060892

Gao, J., Yu, X., Ma, F., and Li, J. (2014). RNA-Seq analysis of transcriptome and glucosinolate metabolism in seeds and sprouts of broccoli (*Brassica oleracea* var. *italica*). *PLoS One* 9 (2), e88804. doi: 10.1371/journal.pone.0088804

Grosser, K., and van Dam, N. M. (2017). A straightforward method for glucosinolate extraction and analysis with high-pressure liquid chromatography (HPLC). *J. Vis. Exp.* (121), e55425. doi: 10.3791/55425

Halkier, B. A., and Gershenzon, J. (2006). Biology and biochemistry of glucosinolates. *Annu. Rev. Plant Biol.* 57, 303–333. doi: 10.1146/annurev.arplant.57.032905.105228

Hansen, B. G., Kliebenstein, D. J., and Halkier, B. A. (2007). Identification of a flavin-monooxygenase as the S-oxygenating enzyme in aliphatic glucosinolate biosynthesis in *Arabidopsis*. *Plant J.* 50 (5), 902–910. doi: 10.1111/j.1365-313X.2007.03101.x

Hopkins, R. J., van Dam, N. M., and van Loon, J. J. (2009). Role of glucosinolates in insect–plant relationships and multitrophic interactions. *Annu. Rev. Entomol.* 54, 57–83. doi: 10.1146/annurev.ento.54.110807.090623

Hossain, M. A., Munemasa, S., Uraji, M., Nakamura, Y., Mori, I. C., and Murata, Y. (2011). Involvement of endogenous abscisic acid in methyl jasmonate-induced stomatal closure in *Arabidopsis*. *Plant Physiol.* 156 (1), 430–438. doi: 10.1104/pp.111.172254

Hossain, M. S., Ye, W., Hossain, M. A., Okuma, E., Uraji, M., Nakamura, Y., et al. (2013). Glucosinolate degradation products, isothiocyanates, nitriles, and thiocyanates, induce stomatal closure accompanied by peroxidase-mediated reactive oxygen species production in *Arabidopsis thaliana*. *Biosci. Biotechnol. Biochem.* 77 (5), 977–983. doi: 10.1271/bbb.120928

Hua, D., Wang, C., He, J., Liao, H., Duan, Y., Zhu, Z., et al. (2012). A plasma membrane receptor kinase, GHR1, mediates abscisic acid- and hydrogen peroxide-regulated stomatal movement in *Arabidopsis*. *Plant Cell* 24 (6), 2546–2561. doi: 10.1105/tpc.112.100107

Husebye, H., Chadchawan, S., Winge, P., Thangstad, O. P., and Bones, A. M. (2002). Guard cell- and phloem idioblast-specific expression of thioglucoside glucohydrolase 1 (myrosinase) in *Arabidopsis*. *Plant Physiol.* 128 (4), 1180–1188. doi: 10.1104/pp.010925

Islam, M. M., Tani, C., Watanabe-Sugimoto, M., Uraji, M., Jahan, M. S., Masuda, C., et al. (2009). Myrosinases, TGG1 and TGG2, redundantly function in ABA and MeJA signaling in *Arabidopsis* guard cells. *Plant Cell Physiol.* 50 (6), 1171–1175. doi: 10.1093/pcp/pcp066

Jensen, L. M., Jepsen, H. S., Halkier, B. A., Kliebenstein, D. J., and Burow, M. (2015). Natural variation in cross-talk between glucosinolates and onset of flowering in *Arabidopsis*. *Front. Plant Sci.* 6, 697. doi: 10.3389/fpls.2015.00697

Katagiri, F., Thilmony, R., and He, S. Y. (2002). The *Arabidopsis thaliana–Pseudomonas syringae* interaction. *Arabidopsis Book* 1, e0039. doi: 10.1199/tab.0039

Kerwin, R. E., Jimenez-Gomez, J. M., Fulop, D., Harmer, S. L., Maloof, J. N., and Kliebenstein, D. J. (2011). Network quantitative trait loci mapping of circadian clock outputs identifies metabolic pathway-to-clock linkages in *Arabidopsis*. *Plant Cell* 23 (2), 471–485. doi: 10.1105/tpc.110.082065

Khokon, A. R., Okuma, E., Hossain, M. A., Munemasa, S., Uraji, M., Nakamura, Y., et al. (2011). Involvement of extracellular oxidative burst in salicylic acid-induced stomatal closure in *Arabidopsis*. *Plant Cell Environ.* 34 (3), 434–443. doi: 10.1111/j.1365-3040.2010.02253.x

Kitamoto, N., Nishikawa, K., Tanimura, Y., Urushibara, S., Matsuura, T., Yokoi, S., et al. (2017). Correction to: development of late-bolting F1 hybrids of Chinese cabbage (*Brassica rapa* L.) allowing early spring cultivation without heating. *Euphytica* 213 (12), 292. doi: 10.1007/s10681-017-2079-x

Kliebenstein, D. J., Lambrix, V. M., Reichelt, M., Gershenzon, J., and Mitchell-Olds, T. (2001). Gene duplication in the diversification of secondary metabolism: tandem 2-oxoglutarate-dependent dioxygenases control glucosinolate biosynthesis in *Arabidopsis*. *Plant Cell* 13 (3), 681-693. doi: 10.1105/tpc.13.3.681

Kong, W., Li, Y., Zhang, M., Jin, F., and Li, J. (2015). A novel *Arabidopsis* microRNA promotes IAA biosynthesis via the indole-3-acetaldoxime pathway by suppressing superroot1. *Plant Cell Physiol.* 56 (4), 715–726. doi: 10.1093/pcp/pcu216

Koroleva, O. A., Gibson, T. M., Cramer, R., and Stain, C. (2010). Glucosinolate-accumulating S-cells in *Arabidopsis* leaves and flower stalks undergo programmed cell death at early stages of differentiation. *Plant J.* 64 (3), 456–469. doi: 10.1111/j.1365-313X.2010.04339.x

Kunkel, B. N., and Harper, C. P. (2018). The roles of auxin during interactions between bacterial plant pathogens and their hosts. *J. Exp. Bot.* 69 (2), 245–254. doi: 10.1093/jxb/erx447

Lohse, G., and Hedrich, R. (1992). Characterization of the plasma-membrane H(+)-ATPase from *Vicia faba* guard cells : modulation by extracellular factors and seasonal changes. *Planta* 188 (2), 206–214. doi: 10.1007/BF00216815

Melotto, M., Underwood, W., Koczan, J., Nomura, K., and He, S. Y. (2006). Plant stomata function in innate immunity against bacterial invasion. *Cell* 126 (5), 969–980. doi: 10.1016/j.cell.2006.06.054

Melotto, M., Zhang, L., Oblessuc, P. R., and He, S. Y. (2017). Stomatal defense a decade later. *Plant Physiol.* 174 (2), 561–571. doi: 10.1104/pp.16.01853

Mohammadin, S., Nguyen, T. P., van Weij, M. S., Reichelt, M., and Schranz, M. E. (2017). *Flowering Locus C (FLC)* is a potential major regulator of glucosinolate content across developmental dtages of *Aethionema arabicum* (Brassicaceae). *Front. Plant. Sci.* 8, 876. doi: 10.3389/fpls.2017.00876

Montillet, J. L., Leonhardt, N., Mondy, S., Tranchimand, S., Rumeau, D., Boudsocq, M., et al. (2013). An abscisic acid-independent oxylipin pathway controls stomatal closure and immune defense in *Arabidopsis*. *PLoS Biol.* 11 (3), e1001513. doi: 10.1371/journal.pbio.1001513

Munemasa, S., Oda, K., Watanabe-Sugimoto, M., Nakamura, Y., Shimoishi, Y., and Murata, Y. (2007). The coronatine-insensitive 1 mutation reveals the hormonal signaling interaction between abscisic acid and methyl jasmonate in *Arabidopsis* guard cells. Specific impairment of ion channel activation and second messenger production. *Plant Physiol.* 143 (3), 1398–1407. doi: 10.1104/pp.106.091298

Nakano, R.T., Pislewska-Bednarek, M., and Yamada, K. (2017). PYK10 myrosinase reveals a functional coordination between endoplasmic reticulum bodies and glucosinolates in *Arabidopsis thaliana*. *Plant J.* 89 (2), 204–220. doi: 10.1111/tpj.13377

Naur, P., Petersen, B. L., Mikkelsen, M. D., Bak, S., Rasmussen, H., Olsen, C. E., et al. (2003). CYP83A1 and CYP83B1, two nonredundant cytochrome P450 enzymes metabolizing oximes in the biosynthesis of glucosinolates in *Arabidopsis*. *Plant Physiol.* 133 (1), 63–72. doi: 10.1104/pp.102.019240

Nour-Eldin, H. H., Hansen, B. G., Norholm, M. H., Jensen, J. K., and Halkier, B. A. (2006). Advancing uracil-excision based cloning towards an ideal technique for cloning PCR fragments. *Nucleic Acids Res.* 34 (18), e122. doi: 10.1093/nar/gkl635

Panchal, S., Roy, D., Chitrakar, R., Price, L., Breitbach, Z. S., Armstrong, D. W., et al. (2016). Coronatine facilitates *Pseudomonas syringae* infection of *Arabidopsis* leaves at night. *Front. Plant Sci.* 7, 880. doi: 10.3389/fpls.2016.00880

Park, S. Y., Fung, P., Nishimura, N., Jensen, D. R., Fujii, H., Zhao, Y., et al. (2009). Abscisic acid inhibits type 2C protein phosphatases via the PYR/PYL family of START proteins. *Science* 324 (5930), 1068–1071. doi: 10.1126/science.1173041

Rodrigues, A., Adamo, M., Crozet, P., Margalha, L., Confraria, A., Martinho, C., et al. (2013). ABI1 and PP2CA phosphatases are negative regulators of Snf1-related protein kinase1 signaling in *Arabidopsis*. *Plant Cell* 25 (10), 3871–3884. doi: 10.1105/tpc.113.114066

Savchenko, T., Kolla, V. A., Wang, C. Q., Nasafi, Z., Hicks, D. R., Phadungchob, B., et al. (2014). Functional convergence of oxylipin and abscisic acid pathways controls stomatal closure in response to drought. *Plant Physiol.* 164 (3), 1151–1160. doi: 10.1104/pp.113.234310

Sawinski, K., Mersmann, S., Robatzek, S., and Bohmer, M. (2013). Guarding the green: pathways to stomatal immunity. *Mol. Plant Microbe Interact.* 26 (6), 626–632. doi: 10.1094/MPMI-12-12-0288-CR

Schellenberg, B., Ramel, C., and Dudler, R. (2010). *Pseudomonas syringae* virulence factor syringolin A counteracts stomatal immunity by proteasome inhibition. *Mol. Plant Microbe Interact.* 23 (10), 1287–1293. doi: 10.1094/MPMI-04-10-0094

Sellam, A., Iacomi-Vasilescu, B., Hudhomme, P., and Simoneau, P. (2007). *In vitro* antifungal activity of brassinin, camalexin and two isothiocyanates against the crucifer pathogens *Alternaria brassicicola* and *Alternaria brassicae*. *Plant Pathol.* 56 (2), 296–301. doi: 10.1111/j.1365-3059.2006.01497.x

Sobahan, M. A., Akter, N., Okuma, E., Uraji, M., Ye, W., Mori, I. C., et al. (2015). Allyl isothiocyanate induces stomatal closure in *Vicia faba*. *Biosci. Biotechnol. Biochem.* 79 (10), 1737–1742. doi: 10.1080/09168451.2015.1045827

Staswick, P. E., and Tiryaki, I. (2004). The oxylipin signal jasmonic acid is activated by an enzyme that conjugates it to isoleucine in *Arabidopsis*. *Plant Cell* 16 (8), 2117–2127. doi: 10.1105/tpc.104.023549

Suhita, D., Raghavendra, A. S., Kwak, J. M., and Vavasseur, A. (2004). Cytoplasmic alkalization precedes reactive oxygen species production during methyl jasmonate- and abscisic acid-induced stomatal closure. *Plant Physiol.* 134 (4), 1536–1545. doi: 10.1104/pp.103.032250

Tierens, K.F., Thomma, B. P., Brouwer, M., Schmidt, J., Kistner, K., Porzel, A., et al. (2001). Study of the role of antimicrobial glucosinolate-derived isothiocyanates in resistance of *Arabidopsis* to microbial pathogens. *Plant Physiol.* 125 (4), 1688–1699. doi: 10.1104/pp.125.4.1688

Xu, R., Kong, W. W., Peng, Y. F., Zhang, K. X., Li, R., and Li, J. (2018). Identification and expression pattern analysis of the glucosinolate biosynthetic gene BoCYP83B1 from broccoli. *Biologia Plantarum* 62 (3), 1–13. doi: 10.1007/s10535-018-0797-0

Xu, Z., Escamilla-Trevino, L., Zeng, L., Lalgondar, M., Bevan, D., Winkel, B., et al. (2004). Functional genomic analysis of *Arabidopsis thaliana* glycoside hydrolase family 1. *Plant Mol. Biol.* 55 (3), 343–367. doi: 10.1007/s11103-004-0790-1

Xue, J., Jorgensen, M., Pihlgren, U., and Rask, L. (1995). The myrosinase gene family in *Arabidopsis thaliana*: gene organization, expression and evolution. *Plant Mol. Biol.* 27 (5), 911–922. doi: 10.1007/BF00037019

Yan, S., McLamore, E. S., Dong, S., Gao, H., Taguchi, M., Wang, N., et al. (2015). The role of plasma membrane H(+)-ATPase in jasmonate-induced ion fluxes and stomatal closure in *Arabidopsis thaliana*. *Plant J.* 83 (4), 638–649. doi: 10.1111/tpj.12915

Zeng, W., Melotto, M., and He, S. Y. (2010). Plant stomata: a checkpoint of host immunity and pathogen virulence. *Curr. Opin. Biotechnol.* 21 (5), 599–603. doi: 10.1016/j.copbio.2010.05.006

Zhang, J., Pontoppidan, B., Xue, J., Rask, L., and Meijer, J. (2002). The third myrosinase gene TGG3 in *Arabidopsis thaliana* is a pseudogene specifically expressed in stamen and petal. *Plant Physiol.* 115 (1), 25–34. doi: 10.1034/j.1399-3054.2002.1150103.x

Zhao, Y., Wang, J., Liu, Y., Miao, H., Cai, C., Shao, Z., et al. (2015). Classic myrosinase-dependent degradation of indole glucosinolate attenuates fumonisin B1-induced programmed cell death in *Arabidopsis*. *Plant J.* 81 (6), 920–933. doi: 10.1111/tpj.12778

Zhao, Z., Zhang, W., Stanley, B.A., and Assmann, S. M. (2008). Functional proteomics of *Arabidopsis thaliana* guard cells uncovers new stomatal signaling pathways. *Plant Cell* 20 (12), 3210–3226. doi: 10.1105/tpc.108.063263

Zheng, X. Y., Spivey, N. W., Zeng, W., Liu, P. P., Fu, Z. Q., Klessig, D. F., et al. (2012). Coronatine promotes *Pseudomonas syringae* virulence in plants by activating a signaling cascade that inhibits salicylic acid accumulation. *Cell Host Microbe* 11 (6), 587–596. doi: 10.1016/j.chom.2012.04.014

Conflict of Interest: The authors declare that the research was conducted in the absence of any commercial or financial relationships that could be construed as a potential conflict of interest.

frontiers in Plant Science

ORIGINAL RESEARCH
published: 13 November 2019
doi: 10.3389/fpls.2019.01451

Same Difference? Low and High Glucosinolate *Brassica rapa* Varieties Show Similar Responses Upon Feeding by Two Specialist Root Herbivores

Rebekka Sontowski[1,2†], Nicola J. Gorringe[1,3†], Stefanie Pencs[1,2], Andreas Schedl[1,2], Axel J. Touw[1,2] and Nicole M. van Dam[1,2]*

[1] Molecular Interaction Ecology, German Centre for Integrative Biodiversity Research Halle-Jena-Leipzig, Leipzig, Germany, [2] Institute for Biodiversity, Friedrich Schiller University, Jena, Germany, [3] School of Biosciences, Cardiff University, Cardiff, Wales, United Kingdom

OPEN ACCESS

Edited by:
Ralph Kissen, Norwegian University of Science and Technology, Norway

Reviewed by:
Tom Pope, Harper Adams University, United Kingdom; Pilar Soengas, Biological Mission of Galicia (MBG), Spain

***Correspondence:**
Rebekka Sontowski
rebekka.sontowski@idiv.de

†These authors share first authorship

Specialty section:
This article was submitted to Plant Metabolism and Chemodiversity, a section of the journal Frontiers in Plant Science

Received: *19 July 2019*
Accepted: *17 October 2019*
Published: *13 November 2019*

Citation:
Sontowski R, Gorringe NJ, Pencs S, Schedl A, Touw AJ and van Dam NM (2019) Same Difference? Low and High Glucosinolate Brassica rapa Varieties Show Similar Responses Upon Feeding by Two Specialist Root Herbivores. Front. Plant Sci. 10:1451. doi: 10.3389/fpls.2019.01451

Glucosinolates (GSLs) evolved in Brassicaceae as chemical defenses against herbivores. The GSL content in plants is affected by both abiotic and biotic factors, but also depends on the genetic background of the plant. Since the bitter taste of GSLs can be unfavorable for both livestock and human consumption, several plant varieties with low GSL seed or leaf content have been bred. Due to their lower GSL levels, such varieties can be more susceptible to herbivore pests. However, low GSL varieties may quickly increase GSL levels upon herbivore feeding by activating GSL biosynthesis, hydrolysis, or transporter genes. To analyze differences in herbivore-induced GSL responses in relation to constitutive GSL levels, we selected four *Brassica rapa* varieties, containing either low or high root GSL levels. Plants were infested either with *Delia radicum* or *Delia floralis* larvae. The larvae of both root flies are specialists on *Brassica* plants. Root samples were collected after 3, 5, and 7 days. We compared the effect of root herbivore damage on the expression of GSL biosynthesis (*CYP79A1*, *CYP83B2*), transporter (*GTR1A2*, *GTR2A2*), and GSL hydrolysis genes (*PEN2, TGG2*) in roots of low and high GSL varieties in conjugation with their GSL levels. We found that roots of high GSL varieties contained higher levels of aliphatic, indole, and benzyl GSLs than low GSL varieties. Infestation with *D. radicum* larvae led to upregulation of indole GSL synthesis genes in low and high GSL varieties. High GSL varieties showed no or later responses than low varieties to *D. floralis* herbivory. Low GSL varieties additionally upregulated the GSL transporter gene expression. Low GSL varieties did not show a stronger herbivore-induced response than high GSL varieties, which indicates that there is no trade-off between constitutive and induced GSLs.

Keywords: plant–insect interactions, belowground herbivory, glucosinolate transporters, herbivore-induced plant responses, insects

INTRODUCTION

The Brassicaceae family contains many economically important plant crops with more than 170 million tons of cultivated vegetables and oilseeds produced worldwide each year (Fao, 2017). One intensively cultivated species of this family is *Brassica rapa* L., which has a long history of domestication in Europe (Warwick, 2011). *B. rapa* is cultivated for livestock and human consumption and includes many well-known varieties, such as turnip, pak choi, Chinese cabbage, and field-mustard. Humans and livestock as well as insects and microbes exploit these plants as food source. To defend themselves against herbivores, plants in the Brassicaceae produce glucosinolates (GSLs), a group of plant secondary metabolites (Jeschke and Burow, 2018). These compounds are located in all parts of the plants including in the roots. More than 130 GSLs have been identified to date (Agerbirk and Olsen, 2012). GSLs are generally categorized as aliphatic, indole, or benzyl (also referred to as aromatic) GSLs, depending on their amino acid precursors (Fahey et al., 2001). When plant tissue is damaged, myrosinases hydrolyze GSLs to form isothiocyanates, nitriles, thiocyanates, and other biologically active compounds (Bones and Rossiter, 2006). Myrosinases are broad-spectrum ß-thioglucosidases with a high affinity for a wide range of GSLs. Up- and downregulation of myrosinase transcripts upon aboveground herbivory has been described for *Brassica napus* [reviewed in Textor and Gershenzon (2009)]. The atypical ß-thioglucosidase PEN2 specifically hydrolyzes indole GSLs after which unstable isothiocyanates are formed (Bednarek et al., 2009). The latter spontaneously form carbinols, or are conjugated to glutathione and then converted to amines and structurally related indole acids, depending on the presence of modifying enzymes in the plant (Wittstock and Burow, 2010). Many of these hydrolysis products have defensive properties against a range of arthropods, microbes, and nematodes (Potter et al., 1998; Kim and Jander, 2007; Clay et al., 2009). Aliphatic GSLs and their breakdown products negatively affect chewing insects and microbes (Li et al., 2000; Arany et al., 2008). Indole GSLs play a role in pathogen defense and provide resistance to phloem-feeding insects and microbes (Agerbirk et al., 2009), whereas benzyl GSLs provide resistance to nematodes (Potter et al., 1999; Kabouw et al., 2010). Although GSLs are produced constitutively, their biosynthesis and that of ß-thioglucosidases can be induced during interactions with pest and pathogens as well (Brader et al., 2006; van Geem et al., 2015; Zhang et al., 2016). Upon herbivory, GSL levels can increase both locally and systemically (Textor and Gershenzon, 2009). Local GSL accumulation can be achieved by local biosynthesis or transport from organ to organ by specific transporter proteins (Nour-Eldin and Halkier, 2009). However, induced GSLs can in turn be hydrolyzed and released upon herbivory based on the higher anti-herbivore function of the hydrolysis products (Li et al., 2000). This process may result in lower or absent GSL accumulation in local tissues.

Although many studies have investigated the interactions between Brassicaceae and aboveground insects, interactions with belowground insects are less well studied. Two common specialists on *Brassica* plants are the cabbage root fly (*Delia radicum* L.) and the turnip root fly (*Delia floralis* Fall. Diptera: Anthomyiidae). After hatching at the interface between the lower part of the stem and the roots, the larvae move into the soil where they mine into the taproot (Dosdall et al., 1994). Because of the extensive damage the larvae can cause to the root system, both species are considered important pests in agriculture (Finch and Collier, 2000; Bjorkman et al., 2010). Plants respond to *D. radicum* and *D. floralis* attacks with local and systemic induction of GSLs in roots and leaves (Birch et al., 1992; Pierre et al., 2011; Tsunoda et al., 2018). This GSL accumulation can be caused by both an increase in GSL biosynthesis, by GSL transport from systemic parts such as other root parts, leaves or the stem, or a combination of both (Andersen et al., 2013). However, it is not yet known how the activation of GSL biosynthesis and transport mechanisms are connected.

All Brassicaceae produce GSLs, but GSL concentration and composition can greatly vary among varieties depending on their genetic background (Giamoustaris and Mithen, 1995;Wurst et al., 2006; del Carmen Martínez-Ballesta et al., 2013). Breeders have selected for varieties with high or low GSL levels, depending on consumers preference and the presence of specific GSLs. For example, consumers prefer a strong and bitter taste in some crops, such as mustard, wasabi, or horseradish. Other GSLs, such as glucoraphanin, are selected for because their breakdown products enhancement of human health (Fahey et al., 1997). In contrast, in oil seed rape breeders have selected for low levels of the 2OH-glucosinolate progoitrin, because of its hazardous effect on human health (Hopkins et al., 2009). However, these low GSL varieties may be more susceptible to herbivory due to low levels of constitutive GSLs (Glen et al., 1990; Beekwilder et al., 2008; Baaij et al., 2018). To compensate, varieties with low constitutive GSL concentrations may respond more strongly to herbivory than varieties with high constitutive GSL concentrations. Such trade-offs between constitutive and inducible defenses to aboveground herbivores have been experimentally assessed in *Arabidopsis thaliana* L. accessions differing in shoot GSL levels (Rasmann et al., 2015). To address whether trade-offs may also occur for belowground GSLs, we compared induced responses to the belowground feeding specialists *D. radicum* and *D. floralis* larvae in low and high GSL *B. rapa* varieties. We postulated that low GSL varieties respond faster and more strongly to root herbivory than high GSL varieties. Moreover, we hypothesized that the response to both root fly species, which have comparable feeding strategies, would be similar. We tested these hypotheses by measuring the temporal expression dynamics of genes involved in GSL biosynthesis, transport, and hydrolysis. Furthermore, we measured root GSL profiles before and after herbivory. This allowed us to compare gene expression patterns to changes in the level of different GSL classes in roots, and compare these between high and low GSL varieties.

MATERIALS AND METHODS

Insect Cultures

D. radicum and *D. floralis* larvae originated from our lab culture; a starting culture of *D. radicum* was kindly provided by Anne-Marie Cortesero, University of Rennes, France in 2014. Pupae

for the *D. floralis* starting culture were provided by Maria Björkman, Bioforsk – Norwegian Institute for Agricultural and Environmental Research, Norway in 2015. Both species were reared for more than two years in our lab under the same conditions in a controlled environment cabinet (Percival Scientific, Perry, Iowa, USA) at a constant temperature of 20°C ± 2°C, 85% ± 8% relative humidity and under a 16/8 h day/night light cycle with a light intensity of 69 ± 18 μmol s^{-1} m^{-2}. Larvae were reared in small plastic containers (10 × 10 × 6 cm) filled with 2 cm autoclaved sand on commercially bought kohlrabi (*Brassica oleracea*). Sand was kept moist and fresh kohlrabi pieces were provided every other day. Old pieces of uneaten kohlrabi which were left by the larvae, were removed. After about 24 days, the larvae crawl into the sand to pupae. Three days later, the pupae were removed from the sand by flooding the sand with tap water and decanted the water including swimming pupae with a small sieve. After about 3 weeks, adult flies emerged and transferred to a net cage (40 × 40 × 90 cm), where they were mass reared on a honey–water mix on cotton and a milk powder (Peter Knoll GmbH & Co KGaA, Elmshorn, Germany) yeast flakes (Sanotact GmbH, Muenster, Germany) mixture (1:1) offered in an open petri dish (8 cm diameter). The fly diet was exchanged for fresh diet twice a week. A box (10 × 10× 6 cm) filled with 2 cm moistened sand and a piece of kohlrabi was placed in the cage for the flies to oviposit on. The oviposition box was exchanged for a new box twice a week. Boxes that were removed from the cage, were closed with clear plastic lid, with 5 × 5 cm square in the middle, covered with gauge for aeration. The boxes with the eggs were placed back into the rearing cabinet. Larvae used for the experiment were reared on a semi-artificial diet containing 4% yeast extract (Carl Roth GmbH & Co KG, Karlsruhe, Germany), 4% lactose (Carl Roth GmbH & Co KG, Karlsruhe, Germany), 2% agar–agar plant (Carl Roth GmbH & Co KG, Karlsruhe, Germany), and 4% freeze-dried kohlrabi (commercially bought) in distilled water. This was done to minimize food adaptation.

Selection of High and Low GSL Varieties

Experimental Set-Up—Plant Growth and Selection of Varieties

To select *B. rapa* varieties with low and high root GSL levels, we purchased seeds from nine randomly selected *B. rapa* varieties from the seedbank IPK Gatersleben, Germany. In addition we used one wild variety propagated in-house which originated from a natural population in Maarssen, The Netherlands (Baaij et al., 2018; **Table S1**). Seeds were germinated in vermiculite (1–2 mm, duengerexperte.de, Attenzell, Germany) at 20°C ± 2°C and 85% ± 8% relative humidity in a controlled environment cabinet (Percival Scientific, Perry, Iowa, USA). After 17 days, 10 seedlings from each variety (in total 100 seedlings) were transferred to a greenhouse, repotted in a sand-B pot clay medium mix (1:1, commercially bought by Gerhard Rösl GmbH, Jesewitz and Baywa AG, Laussig, Germany), and fertilized with Osmotcote® pro 3-4M (Hermann Meyer KG, Rellingen, Germany). Plants were grown in the greenhouse of the Botanical Gardens, Leipzig, Germany, at 24°C ± 3°C, a relative humidity from 6% to 52%, under artificial lights (metal halogen vapor lamp Master HPI-T plus 400W, Phillips, Hamburg, Germany) set to maintain day length of 16 h. The plants were watered when needed but at least twice a week. Temperature and relative humidity were recorded every 12 min. After 6 weeks, the third fully expanded leaf and the roots were harvested from plants at a similar growth stage which had developed three pairs of leaves (BBCH code 13). All leaves were harvested by cutting them at the base of the petiole with a sharp razor, after which they were flash-frozen in liquid nitrogen. Roots were removed from the pots, rinsed with cold tap water in a bucket to remove soil particles from the fine roots, dried with tissue to remove excess water, and flash-frozen in liquid nitrogen as a whole. The samples were kept at −80°C until they were freeze-dried to constant weight. The dried leaf and root samples were ground to fine powder using a ball mill (Retsch MM 400, Retsch GmbH, Haan, Germany). An aliquot of the dried and ground root and leaf samples was extracted and analyzed for GSLs as below. In total 10 replicates of roots and leaves per variety were extracted and analyzed. Based on the total GSL concentrations in roots (**Figure S1**), we selected two *B. rapa* varieties with a low (variety A and B) and two with a high total GSL concentration (variety D and E) for the main experiment.

GSL Extraction and Quantification

The GSLs were extracted from 100 ± 5 mg of ground leaf or root samples according to Grosser and van Dam (2017). Briefly, GSLs were extracted in 70% methanol and the supernatant was transferred to an ion-exchange column (DEAE-Sephadex, Merck KGaA, Darmstadt, Germany). GSLs were desulfated with aryl sulfatase (type H-1 from *Helix pomatia*, Merck, Darmstadt, Germany). Desulfated GSLs were analyzed on high-performance liquid chromatography (HPLC) system equipped with a photodiode array detector (PDA; Ultimate 3000 series system DAD-3000(RS), Thermo Fisher Scientific, Waltham, MA, USA). HPLC-grade solvents were used throughout the analysis. Injection volume was set to 10 μl. Desulfated GSLs were separated on a reverse phase C_{18} column (Acclaim™ 300 C18 column, 4.6 × 150 mm, 300 Å, 5 μm, Thermo Fisher Scientific, Waltham, MA, USA) plus a C_{18} precolumn (10 × 4.6 mm, 5 μm particle size) using an acetonitrile-water gradient (Grosser and van Dam, 2017) at a flow of 0.75 ml/min and a column temperature of 40°C. Desulfated GSLs were identified based on retention time and UV spectra compared to commercial available reference standards (Phytoplan Diehm & Neuberger GmbH, Heidelberg, Germany, summarized in **Table S2**). GSLs were quantified at 229 nm using sinigrin as an external standard and response factors as in Grosser and van Dam (2017). Data were processed using Thermo Sientific Chromeleon Chromatography Data System software [version 7.2 SR5 MUa (9624) Thermo Fisher Scientific, Waltham, MA, USA].

Root Fly Induced GSL Responses in High and Low GSL Varieties

Experimental Set-Up

In the main experiment, seeds of the four selected *B. rapa* varieties were germinated and grown as described earlier. The roots of 7- to 8-week-old plants were infested with five, second-instar larvae

of *D. radicum* or *D. floralis*. Plants were randomly assigned to control, *D. radicum*, or *D. floralis* treatments. To infest a plant, the soil was carefully removed from around the root–shoot interface, after which five individual *D. radicum* or *D. floralis* larvae were added directly to the root system using a soft paint brush. Control plants were not infested. Harvesting took place 3, 5, and 7 days after the larvae were placed on the plants. To prevent that seasonal effects would affect our results, plants were grown in four batches between December 2017 and May 2018. Each batch included at least 18 plants per variety, including 2 plants per time point and treatment group. For this experiment only roots were harvested using the same procedure as during the selection of high and low GSL varieties. All *D. radicum* and *D. floralis* infested roots showed a visible feeding damage on the outside of the roots. After rinsing, the roots were flash-frozen in liquid nitrogen, freeze-dried, and ground. All together, we harvested eight replicates per treatment and variety at each time point after the start of herbivory (in total 288 plants). The samples of the two plants harvested per treatment at each time point in one and the same batch were pooled and used for all following extractions (in total 144 samples). This resulted in four replicates per treatment, time point, and variety.

Gene Expression Analysis

To study the molecular mechanisms that underlie the accumulation of GSLs in high and low GSL varieties in response to specialist root herbivores, we analyzed the expression of selected genes involved in the GSL biosynthesis, transport, and hydrolysis using a quantitative PCR (qPCR) procedure. We selected *CYP83A1* as marker gene for the aliphatic GSL biosynthesis and *CYP79B2* for the indole GSL biosynthesis (Mathur et al., 2013). We selected *GTR1A2* and *GTR2A2* expression as markers for the GSL transport activity. Both transporters are involved in the transport of aliphatic and indole GSLs (Jørgensen et al., 2017). We selected *TGG2* and *PEN2* as marker genes for GSL hydrolysis. *TGG2* encodes for myrosinase, a general GSL hydrolase (Xue et al., 1995). *PEN2* is specific for indole GSL hydrolysis (Wittstock and Burow, 2010). Using Primer3web version 4.1.0 (Untergasser et al., 2012), we designed primers for *PEN2*, *TGG2*, *GTR1A2*, and *GTR2A2*. A list of genes and primers is presented in **Table S3**. RNA was extracted from each of the pooled samples of ground and freeze-dried root material using innuPREP Plant RNA Kit (Analytik Jena, Jena, Germany) according to the manufacturer's instructions. Qualitative and quantitative RNA identification was done by gel electrophoresis (1% agarose) and a NanoPhotometer® P330 (Implen, Munich, Germany). We treated 5 µg of the extracted RNA with 2 U DNAse I (Thermo Fisher Scientific, Schwerte, Germany) according to the manufacturer's instructions. We checked whether DNA was completely removed from each RNA extract with gel electrophoresis (1% agarose). cDNA was synthesized from 2 µg RNA by using 400 U Revert Aid H-Reverse transcriptase (Thermo Fisher Scientific, Schwerte, Germany) according to the manufacturer's instructions. Samples were incubated at 42°C for 60 min, 50°C for 15 min, and finally 70°C for 15 min in a Thermal cycler (Techne, Stone, United Kingdom).

Quantitative real-time PCR (qPCR) was performed on a CFX384 Real-time system (BioRad, Munich, Germany) using a 10 µl reaction volume containing 5 µl SYBR Green qPCR master mix (2X, Thermo Fisher Scientific, Schwerte, Germany), 0.25 µl forward and reverse primer (10 µM), 0.05 µg cDNA, and 3.5 µl H_2O. The qPCR run under following conditions: 2 min at 50°C, 5 min at 95°C and 40 cycles of 30 s at 95°C, 30 s at 58°C, and 45 s at 72°C. Thereafter, a melting curve analysis was performed to verify the amplification of a single gene transcript. Two technical replicates of each sample and no template controls were performed. All no template controls showed a Ct value larger than 39. Data were analyzed using BioRad CFX manager 3.1 software (BioRad, Munich, Germany). Expression levels were normalized to the reference gene *TIP41*.

GSL Analysis

To test GSL responses to root herbivore specialists, we analyzed the qualitative and quantitative composition of GSL profiles in low and high GSL varieties. GSLs were extracted from pooled samples of ground material and detected as described above. This time, we adjusted the HPLC elution gradient in order to improve the separation of the peaks for gluconasturtiin and 4-methoxyglucobrassicin. We used H_2O as solvent A and acetonitrile as solvent B. The gradient profile started with an equilibration at 98% A for 4.3 min, followed by a gradient to 35% B within 24.3 min, hold until 29 min at 35% B. Thereafter the gradient went back to the initial 98% of A within 1 min and held the initial conditions for 10 min at 0.6 ml/min flow. The injection volume was 10 µl.

Statistical Analyses

Analyses were performed using R version 3.2.0 (R Core Team, 2015). Data were log transformed to obtain normal distribution of the residuals. QQ- and residual plots were used to visually inspect whether residuals were normally distributed. A three-way ANOVA, with GSL varieties (low vs. high), herbivory (control, *D. radicum*, and *D. floralis*), and time point (3, 5, 7 days) as fixed factors was used to test effects on GLS biosynthesis, GSL transport, GSL hydrolysis, GSL classes, and total GSLs. Interactions of GSL varieties and treatments within time points were analyzed using a two-way ANOVA followed by a Tukey HSD post-hoc test.

RESULTS

Effect of *D. radicum and D. floralis* Herbivory on GSL Biosynthesis, Transport, and Hydrolysis Gene Expression

To test how low and high GSL varieties respond to *D. radicum* or *D. floralis* herbivory, we analyzed GSL biosynthesis, GSL transport, and hydrolysis gene expression in the roots of both high and low GLS varieties harvested after 3, 5, and 7 days of root herbivory. The indole biosynthesis gene *CYP79B2* was significantly upregulated in both high (variety D and E) and low (variety A and B) GSL

varieties after 3 days of herbivory by *D. radicum* and reduced to control levels after 7 days in all varieties. (**Figure 1** upper row, **Table 1**, herbivory × time effect, **Table S4**). The expression of *CYP79B2* was only upregulated in low GSL varieties in response to *D. floralis* feeding after 3 days, and in variety B also after 5 days (**Figure 1**, **Table 1**, variety × herbivore × time effect). The high GSL varieties responded less strongly, and if at all later (variety D, 5 days) to *D. floralis* compared to the low GSL varieties (**Figure 1**).

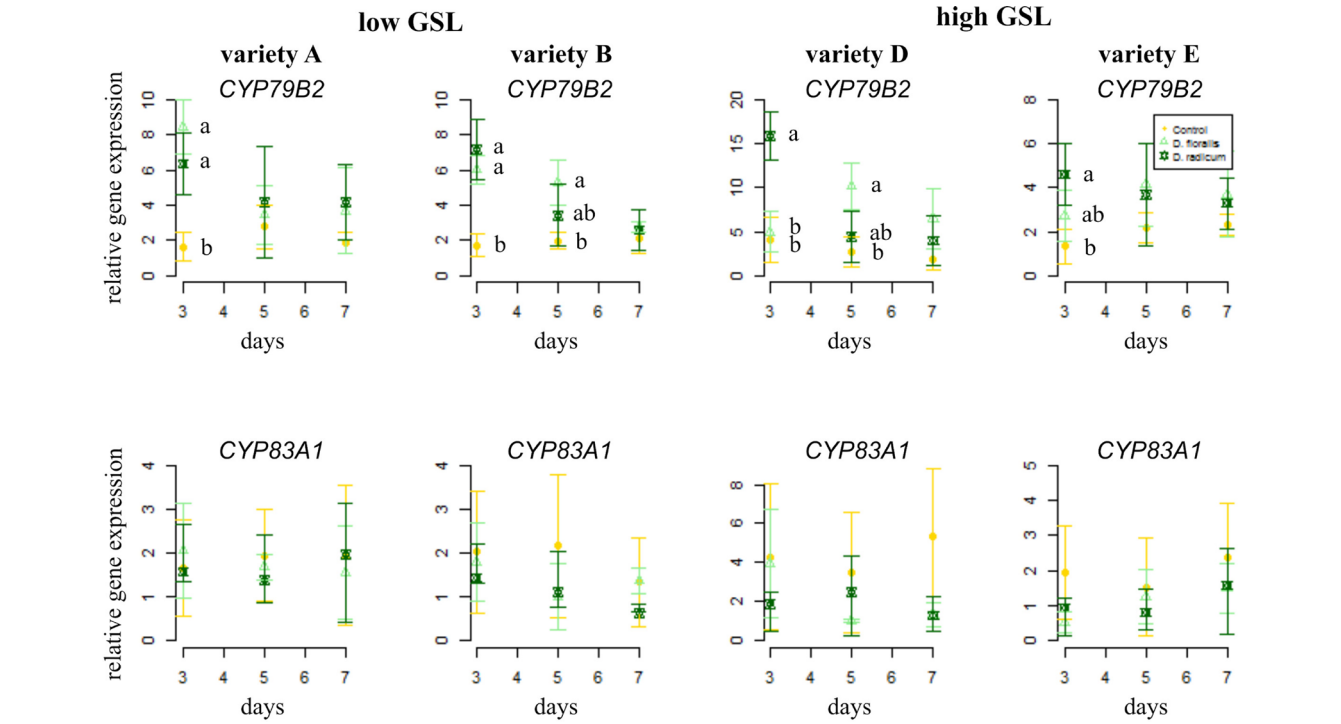

FIGURE 1 | Normalized gene expression (± standard deviation) of the indole *CYP79B2* (top) and aliphatic *CYP83A1* (bottom) glucosinolate (GSL) biosynthesis genes in roots of low (variety **A** and **B**, left) and high (variety **D** and **E**, right) GSL varieties of *Brassica rapa*. N = 4 per variety, time point, and treatment. Different letters indicate significant differences in gene expression within that time point ($p < 0.05$, Tukey HSD). Roots were infested with *Delia radicum* (dark green) or *D. floralis* (light green) larvae for 3, 5, or 7 days. Control plants (yellow) were not infested. Please note the different y-axis scaling of individual graphs.

TABLE 1 | Test values after three-way ANOVA on glucosinolate (GSL) biosynthesis (indole *CYP79B2,* aliphatic *CYP83A1*), GSL transporter (*GTR1A2*, *GTR2A2*), and GSL hydrolysis (myrosinase *TGG2*, indole hydrolysis *PEN2*) gene expression in *B. rapa* roots of low and high constitutive GSL varieties.

Factor	Df	GSL biosynthesis genes				GSL transporter genes			
		CYP79B2		*CYP83A1*		*GTR1A2*		*GTR2A2*	
		F value	P value	F value	P value	F value	P value	F value	P value
GSL variety (V)	1	0.60	0.44	0.55	0.46	56.86	<0.001 ***	1.72	0.19
Herbivory (H)	2	30.19	<0.001 ***	3.46	0.03 *	7.99	<0.001 ***	2.47	0.09
Time (T)	1	8.83	0.004 **	0.08	0.77	5.42	0.02 *	3.81	0.05
V:H	2	0.08	0.93	1.41	0.25	8.08	<0.001 ***	4.37	0.01 *
V:T	1	1.44	0.23	1.29	0.26	9.10	0.003 **	0.58	0.45
H:T	2	4.97	0.008 **	0.56	0.57	8.29	<0.001 ***	6.97	0.001 **
V:H:T	2	3.42	0.04 *	0.42	0.66	0.84	0.44	7.67	<0.001 ***
		GSL hydrolysis genes							
		TGG2							
GSL variety (V)	1	13.54	<0.001 ***	0.04	0.84				
Herbivory (H)	2	8.57	<0.001 ***	2.05	0.13				
Time (T)	1	6.00	0.02 *	14.38	<0.001 ***				
V:H	2	1.96	0.14	0.98	0.38				
V:T	1	5.70	0.02 *	0.05	0.82				
H:T	2	1.99	0.14	7.99	<0.001***				
V:H:T	2	0.94	0.39	0.06	0.94				

*Plants were either undamaged or induced with D. floralis or D. radicum larvae for 3, 5, or 7 days. * $p < 0.05$, ** $p < 0.01$, *** $p < 0.001$.*

D. radicum and *D. floralis* herbivory had no significant effect on the aliphatic biosynthesis gene expression (*CYP83A1*) in both high and low GSL varieties (**Figure 1**, lower row).

In general, the GSL transporter gene *GTR1A2* was expressed at higher levels in low than in high GSL varieties (**Figure 2**, note different y-axis values, **Table 1**). Herbivory by *D. radicum* affected the expression of *GTR1A2* (**Table 1**) differently in low and high GSL varieties. Whereas *GTR1A2* expression was upregulated in low GSL varieties in response to *D. radicum* feeding after 3 days, no response was observed in high GSL varieties (**Figure 2**, **Table 1**, variety × herbivore interaction). Herbivory by *D. floralis* led to upregulated *GTR1A2* expression in the low GSL variety A after 3 days. No effects of herbivory on *GTR1A2* expression were found in high GSL varieties. The herbivore response in low GSL varieties showed temporal dynamic; the expression of *GTR1A2* was upregulated after 3 days of herbivory and dropped to control levels after 7 days in low GSL varieties (**Table 1**, herbivore × treatment interaction). The gene expression of the other transporter, *GTR2A2*, showed the opposite effect. *D. radicum* feeding only affected expression of *GTR2A2* in high GSL varieties. In variety D, *D. radicum* feeding first upregulated expression after 3 days, after which *GTR2A2* expression was downregulated after 7 days, both in high GSL varieties D and E (**Figure 2**, lower row, **Table 1**, variety × herbivore × time effect).

The gene *TGG2*, encoding for myrosinase, showed higher base expression levels in high GSL varieties than in low GSL varieties (**Figure 3** and **Table 1**). *D. radicum* and *D. floralis* herbivory upregulated the *TGG2* expression in low GSL varieties at later time points (variety A after 5 days, variety B after 7 days). High GSL varieties did not alter *TGG2* expression upon root herbivory, through there was non-significant trend toward upregulation of *TGG2* at 7 days after *D. radicum* or *D. floralis* feeding in variety D and E (**Table 1**). *PEN 2,* a gene involved in indole GSL hydrolysis, was upregulated in response to 3 days of *D. radicum* and *D. floralis* feeding in low GSL variety A only (**Figure 3** lower row).

Effect on GSL Levels and Profiles

As expected, high GSL varieties had significantly higher total GSL concentrations in the roots than low GSL varieties at 3 days, except for the *D. floralis* and *D. radicum* infested plants of variety D (**Figure 4** and **Table 2**, variety effect, **Table S4**). Total GSL concentration was not significantly different at 5 and 7 days in low and high GSL varieties, except for variety A and D at 7 days (control and *D. floralis* treatment; **Figures 4** and **S2**). The high GSL concentration in the high GSL varieties were mainly due to high levels of indole GLSs in varieties D and E. Indole GSLs significantly differed in low and high GSL varieties at 3 and 7 days (**Figure 4** and **Table 2**). Aliphatic GSL levels were significantly lower in herbivore-infested roots of variety B (low GSL variety) than those of the high GSL varieties (variety D and E) at 5 days (**Figure S2** and **Table 2**). Benzyl GSLs showed a significant variety effect only at 3 days; the levels of benzyl GSLs were lowest in variety A (low GSL variety) and the highest in variety D (high GSL

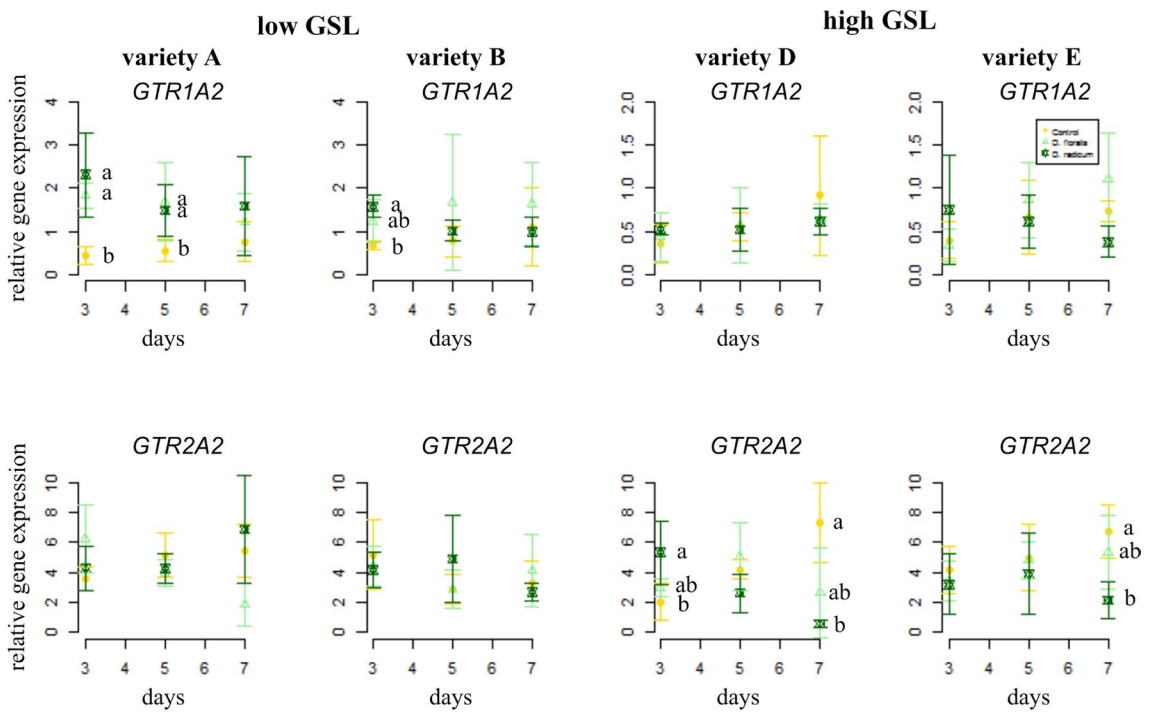

FIGURE 2 | Normalized gene expression (± standard deviation) of the GSL transporters *GTR1A2* (top) and *GTR2A2* (bottom) in *B. rapa* roots of low (variety **A** and **B**, left) and high (variety **D** and **E**, right) GSL varieties. N = 4 per variety, time point, and treatment. Different letters indicate significant differences in gene expression within that time point ($p < 0.05$, Tukey HSD). Roots were infested with *D. radicum* (dark green) or *D. floralis* (light green) for 3, 5, or 7 days. Control plants (yellow) were not infested. Please note the different y-axis scaling of individual graphs.

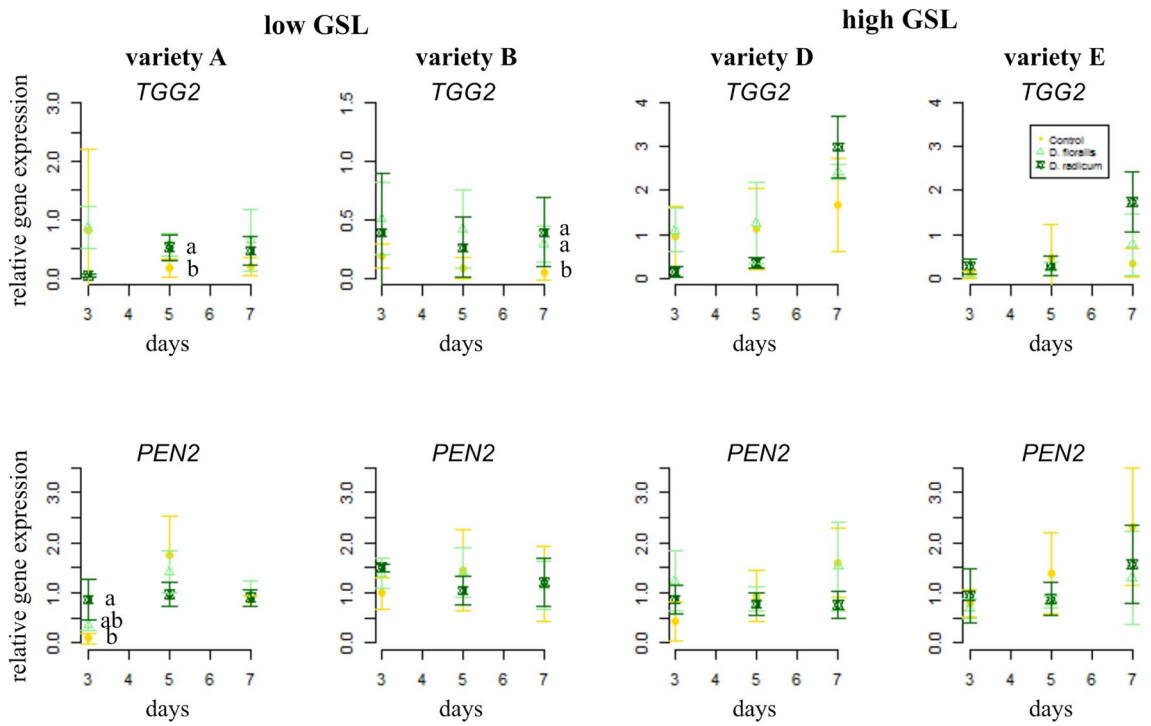

FIGURE 3 | Normalized gene expression (standard deviation) of the GLS hydrolysis pathways; myrosinase gene *TGG2* (top) and indole hydrolysis gene *PEN2* (bottom) in roots of low (variety **A** and **B**, left) and high (variety **D** and **E**, right) GSL varieties of *B. rapa*. N = 4 per variety, time point, and treatment. Different letters indicate significant differences in gene expression within that time point ($p < 0.05$, Tukey HSD). Roots were infested with *D. radicum* (dark green) or *D. floralis* (light green) for 3, 5, or 7 days. Control plants (yellow) were not infested. Please note the different y-axis scaling of individual graphs.

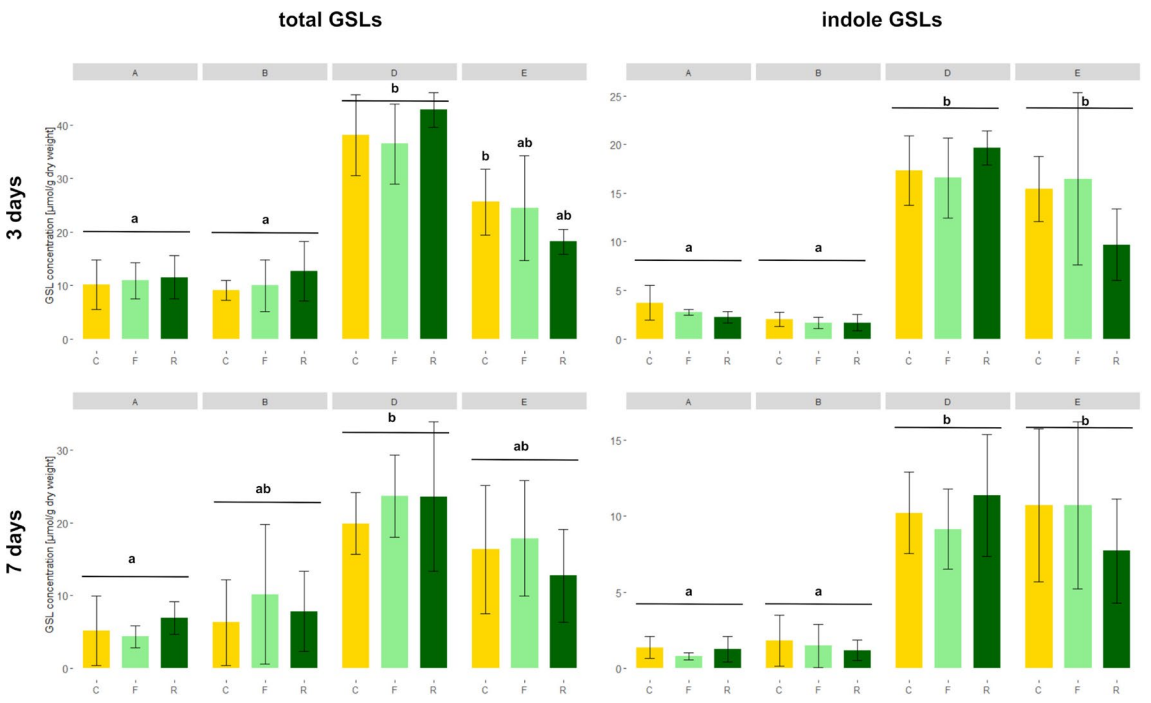

FIGURE 4 | Total (left) and indole (right) GSL concentrations (micromoles g−1 dry mass) in *B. rapa* roots of low (variety **A** and **B**) and high (variety **D** and **E**) GSL varieties. N = 4 per variety, time point, and treatment. Different letters indicate significant differences in GSL concentration within that time point ($p < 0.05$, Tukey HSD). Plants were infested with *D. radicum* (R, dark green) or *D. floralis* (F, light green) larvae. Control plants (C, yellow) were not infested. GSLs were measured after 3 (first column) and 7 days (second column) of herbivory. Please note the different scales on the y-axis for time points and GSL levels.

TABLE 2 | Test values after three-way ANOVA on total GSLs and GSL classes in *B. rapa* roots of low and high GSL varieties.

Factor	Df	Total GSLs		Indole GSLs		Aliphatic GSLs		Benzyl GSLs	
		F value	P value	F value	P value	F value	P value	F value	P value
GSL variety (V)	1	86.69	<0.001 ***	214.81	<0.001 ***	17.49	<0.001 ***	34.14	<0.001 ***
Herbivory (H)	2	0.59	0.56	0.25	0.78	4.58	0.01 *	0.39	0.68
Time (T)	1	28.71	<0.001 ***	19.83	<0.001 ***	3.98	0.05	46.55	<0.001 ***
V:H	2	1.01	0.37	0.04	0.96	0.27	0.76	1.03	0.36
V:T	1	0.40	0.53	1.13	0.29	0.27	0.60	1.28	0.26
H:T	2	0.30	0.74	0.24	0.79	0.93	0.40	0.01	0.99
V:H:T	2	0.21	0.81	0.15	0.86	0.78	0.46	0.37	0.69

*Plants were either undamaged or induced with D. floralis or D. radicum larvae for 3, 5, or 7 days. * $p < 0.05$, ** $p < 0.01$, *** $p < 0.001$.*

variety, **Figure S3**). Total, indole, and benzyl GSL concentrations fluctuated with time after harvest (**Table 2**, time effect). Herbivory by *D. radicum* or *D. floralis* larvae had no significant effect on total, indole, aliphatic, or benzyl GSL concentration when compared to their control plants (**Figures 4**, **S2** and **S3**).

DISCUSSION

We studied induced GSL defense responses in low and high GSL containing *B. rapa* varieties upon root herbivory by *D. radicum* and *D. floralis*. Our results show that roots of high and low GSL varieties both responded to *D. radicum* feeding by upregulating *CYP79B2*, a marker gene for indole GSL biosynthesis, after 3 days. Low GSL varieties showed a faster response to *D. floralis* herbivory than high GSL varieties. Expression of *CYP83A1*, a gene involved in aliphatic GSL biosynthesis, was not induced by root fly feeding. Root fly feeding also altered the expression of two GSL transporter genes; *GTR1A2* expression was upregulated particularly in low GSL varieties after 3 days of feeding, whereas, *GTR2A2* was downregulated in high GSL varieties after 7 days. *TGG2*, the gene coding for the enzyme myrosinase, was induced by herbivory only in low GSL varieties after 5 or 7 days, whereas *PEN2* expression was only upregulated three days of *D. radicum* herbivory in variety A. In contrast to the gene expression patterns, *D. radicum* and *D. floralis* herbivory had no effect on GSL profiles in either low or high GSL varieties. Combined, our results show that biosynthesis, hydrolysis, and transporter genes are all affected by root herbivory with only minor differences in responses between high and low GSL-containing varieties.

On the gene level, we found that the indole biosynthesis gene *CYP79B2* was upregulated in response to *D. radicum* feeding in all varieties after 3 days, whereas only low GSL varieties responded to *D. floralis* feeding after 3 days. The late or lack of responses to *D. floralis* in high GSL varieties may indicate a trade-off between constitutive and induced GSL levels, although this potential trade-off seems to be herbivore-specific. In contrast to the indole biosynthesis upregulation, herbivory did not lead to significant accumulation of indole GSLs in either low or high GSL varieties. Because of the lack of indole GSLs accumulations upon *D. radicum* or *D. floralis* feeding, we found no trade-offs between constitutive and induced indole GSLs. Our findings contrast with earlier studies in *B. oleracea*, *B. nigra*, and *B. napus*, reporting that upon *D. radicum* and *D. floralis* infestations, both indole and aliphatic GSLs can increase (Birch et al., 1990; Hopkins et al., 1998; van Dam and Raaijmakers, 2006; Tsunoda et al., 2018).

Discrepancies between GSL accumulation and GSL biosynthesis gene expression are not uncommon, as similar observations were reported for *A. thaliana* shoots damaged by aboveground herbivores (Rasmann et al., 2015). Inconsistencies between gene transcription and final product may be caused by disruptions in downstream processes, including modifications in RNA processing and post-translational protein modifications (Mazzucotelli et al., 2008). A second explanation may be that we did not sample the roots on a fine enough scale, as we harvested whole root systems. This may have diluted the induced GSL signature, in particular of indole GSLs which are rather minor constituents of the total GSL profile. Previous studies showed that only taproots, and not lateral and fine roots respond to root fly feeding by increasing GSL levels (van Dam and Raaijmakers, 2006). Fine roots, on the other hand, do not respond to root fly feeding, but contain relatively high levels of indole GSLs (Tsunoda et al., 2018). By analyzing the entire root, we pooled organ-specific GSL profiles, which may have obscured local responses in the taproot. Moreover, indole GSL levels varied considerably among replicates. By pooling the two replicates from one batch, we may have reduced our statistical power. Lastly, other processes than biosynthesis, such as GSL transport and hydrolysis, may have affected local indole GSL levels. This mismatch between biosynthesis pathway activation and GSL production in our experiment shows that analyzing the biosynthesis pathway, but not the resulting GSLs may result in misleading conclusions. We therefore recommend combining both approaches to obtain ecologically relevant results.

The expression of *GTR1A2* and *GTR2A2*, both transporters with affinity to indole and aliphatic GSLs, responded differently to root fly feeding in low and high GSL varieties (Jørgensen et al., 2017). Expression of *GTR1A2* was upregulated after three days of root fly feeding in low GSL varieties, whereas expression of *GTR2A2* was downregulated in high GSL varieties after seven days. This observation supports the hypothesis that low GSL varieties show an early and strong defense response potentially to compensate for low constitutive GSL levels. Varieties with high constitutive GSL levels are already well defended and may not need additional GSL transport to the site of herbivore attack (Madsen et al., 2014). However, the direction in which GSL transporters work, or in other words whether the upregulation of *GTR* genes results in enhanced export or import of GSL to the organ in which the transcriptional changes are observed, is as yet unclear (Touw et al., submitted to same issue).

Enhanced GSL breakdown might also contribute to the observed discrepancy between the enhanced expression of GSL biosynthesis genes and GSL accumulation in herbivore-induced roots. Upon herbivory, GSLs can be hydrolyzed to more effective breakdown products such as isothiocyanates and nitriles (Agrawal and Kurashige, 2003; Bones and Rossiter, 2006). We found that expression of the myrosinase gene *TGG2* which hydrolyzes a broad range of GSLs, is only upregulated in low GSL varieties in response to root fly feeding. However, *TGG2* upregulation occurred later than the activation of GSL synthesis genes. *PEN2*, which specifically hydrolyzes indole GSLs, showed hardly any response to root fly feeding. *D. radicum* feeding enhances (iso) thiocyanate emissions from *B. rapa* roots (Crespo et al., 2012). Our findings suggest that mainly *TGG2* is involved in the hydrolysis of root GSLs in *D. radicum* and *D. floralis* infested plants.

GSL defense responses in plants can differ between different herbivore species, depending on host specialization levels (generalist, specialist), and feeding mode (sucking, chewing) (Arany et al., 2008; Bidart-Bouzat and Kliebenstein, 2011; Danner et al., 2018). In our experiment, both herbivores used (*D. radicum* and *D. floralis)* are from the same family, specialized on the same host plants, and both mine in the roots (McDonald and Sears, 1992). *D. floralis* has a larger body size and weight and thus may causes more damage than *D. radicum,* which potentially can affect plant defense responses. Our results showed that in general, *B. rapa* varieties responded similar to both *Delia* species. Species-specific responses were detected only in high GSL varieties: the expression of *CYP79B2* was upregulated earlier, whereas *GTR2A2* was downregulated mainly upon *D. radicum* feeding. This suggests that the GSL defense pathways responded partly herbivore-specific.

GSLs play an important role in plant–herbivore interactions. Negative correlations between GSL concentration and aboveground herbivore performance have been found mainly for aboveground generalists (Giamoustaris and Mithen, 1995; Arany et al., 2008). Other studies showed that aboveground generalists and specialists performed similarly on high and low GSL containing plants (Poelman et al., 2008). The production of GSLs may be costly for plants, and plants with high constitutive GSL levels may grow less well than those with low GSLs (Bekaert et al., 2012). Inducing defenses upon herbivore attack is considered a viable strategy to reduce such costs (Backmann et al., 2019). However, to invest in production upon herbivory by well-adapted specialists such as *D. radicum* or *D. floralis* larvae, which are able to detoxify GLS and their breakdown products (Welte et al., 2016), may be a waste of resources. A further reason for the lack of GSL induction in our experiment may be that GSLs and their breakdown products also act as oviposition attractants to specialists (de Vos et al., 2008; Pierre et al., 2013). Infestation by *D. radicum* increased the attractiveness of broccoli plants to ovipositing female flies (Pierre et al., 2013). We suggest that plants recognized the belowground specialist and prevented GSL accumulations that attract more and/or other above- and belowground specialists.

To conclude, low and high GSL varieties of *B. rapa* responded similarly to *D. radicum* infestation in terms of activation of indole biosynthesis genes. However, both varieties responded differently to *D. floralis* infestations in terms of GSL transporter and indole biosynthesis gene expression. Our hypothesis that there might be a trade-off between constitutive and induced GLS defenses in roots, similar to what has been found in shoots (Rasmann et al., 2015), is thus not supported by our experiments. In other words, low GSL varieties did not compensate for lower constitutive GSL concentrations with a higher accumulation of induced GSLs upon *D. radicum* or *D. floralis* infestation to attain similar GSL levels as high GSL varieties. Finally, we found that the variation in root GSL levels among *B. rapa* varieties is larger than that for shoots. Several cultivated *B. rapa* varieties which are used for human and livestock consumption are selected for low seed or leaf GSL levels. Low GSL levels in the roots are likely non-target side effects of the breeding process, which may result in varieties that are more susceptible to root herbivores and pathogens (Potter et al., 1999; Kabouw et al., 2010). Therefore it is recommended that root GSL levels as well as their induced responses to generalist and specialist root herbivores should be considered when breeding GSL containing crops.

DATA AVAILABILITY STATEMENT

All datasets generated for this study are included in the article/ **Supplementary Material**.

AUTHOR CONTRIBUTIONS

ND and RS designed the project. RS and NG performed the experiment, extraction, and data analysis. AS developed the HPLC method. SP provided plants, designed, and tested primers. ND, AT, and RS interpreted the data. All authors contributed to the writing of the manuscript.

FUNDING

Financial support by Friedrich Schiller University Jena/German Research Foundation (DFG) Collaborative Research Center 1127 ChemBioSys and DFG funding to the German Centre for Integrative Biodiversity Research (iDiv) Halle-Jena-Leipzig (FZT 118) is gratefully acknowledged. We thank the "Thüringer Universitäts- und Landesbibliothek Jena" (THULB) for their contribution to the publication fee.

ACKNOWLEDGMENTS

We thank Harry Brown from Cardiff University for his help in extraction, Christian Ristok from iDiv for his advises on statistical analyses and Paul Moritz List from the University of Leipzig for his help in developing the HPLC method. We thank the editor and two reviewers for providing helpful comments on an earlier version of this manuscript.

SUPPLEMENTARY MATERIAL

The Supplementary Material for this article can be found online at: https://www.frontiersin.org/articles/10.3389/fpls.2019.01451/full#supplementary-material

REFERENCES

Agerbirk, N., De Vos, M., Kim, J. H., and Jander, G. (2009). Indole glucosinolate breakdown and its biological effects. *Phytochem. Rev.* 8, 101. doi: 10.1007/s11101-008-9098-0

Agerbirk, N., and Olsen, C. E. (2012). Glucosinolate structures in evolution. *Phytochemistry* 77, 16–45. doi: 10.1016/j.phytochem.2012.02.005

Agrawal, A. A., and Kurashige, N. S. (2003). A role for isothiocyanates in plant resistance against the specialist herbivore Pieris rapae. *J. Chem. Ecol.* 29, 1403–1415. doi: 10.1023/A:1024265420375

Andersen, T. G., Nour-Eldin, H. H., Fuller, V. L., Olsen, C. E., Burow, M., and Halkier, B. A. (2013). Integration of biosynthesis and long-distance transport establish organ-specific glucosinolate profiles in vegetative Arabidopsis. *Plant Cell* 25, 3133–3145. doi: 10.1105/tpc.113.110890

Arany, A. M., De Jong, T., Kim, H., van Dam, N. M., Choi, Y., Verpoorte, R., et al. (2008). Glucosinolates and other metabolites in the leaves of Arabidopsis thaliana from natural populations and their effects on a generalist and a specialist herbivore. *Chemoecology* 18, 65–71. doi: 10.1007/s00049-007-0394-8

Baaij, B. M., Kim, H. K., Grosser, K., Worrich, A., and De Jong, T. J. (2018). Slug herbivory on hybrids of the crop Brassica napus and its wild relative B. rapa. *Basic Appl. Ecol.* 31, 52–60. doi: 10.1016/j.baae.2018.06.001

Backmann, P., Grimm, V., Jetschke, G., Lin, Y., Vos, M., Baldwin, I. T., et al. (2019). Delayed chemical defense: timely expulsion of herbivores can reduce competition with neighboring plants. *Am. Nat.* 193, 125–139. doi: 10.1086/700577

Bednarek, P., Piślewska-Bednarek, M., Svatoš, A., Schneider, B., Doubský, J., Mansurova, M., et al. (2009). A glucosinolate metabolism pathway in living plant cells mediates broad-spectrum antifungal defense. *Science* 323, 101–106. doi: 10.1126/science.1163732

Beekwilder, J., van Leeuwen, W., van Dam, N. M., Bertossi, M., Grandi, V., Mizzi, L., et al. (2008). The impact of the absence of aliphatic glucosinolates on insect herbivory in Arabidopsis. *PloS One* 3, e2068. doi: 10.1371/journal.pone.0002068

Bekaert, M., Edger, P. P., Hudson, C. M., Pires, J. C., and Conant, G. C. (2012). Metabolic and evolutionary costs of herbivory defense: systems biology of glucosinolate synthesis. *New Phytol.* 196, 596–605. doi: 10.1111/j.1469-8137.2012.04302.x

Bidart-Bouzat, M. G., and Kliebenstein, D. (2011). An ecological genomic approach challenging the paradigm of differential plant responses to specialist versus generalist insect herbivores. *Oecologia* 167, 677. doi: 10.1007/s00442-011-2015-z

Birch, A. N. E., Griffiths, D. W., and Smith, W. H. M. (1990). Changes in forage and oilseed rape (Brassica napus) root glucosinolates in response to attack by turnip root fly (Delia floralis). *J. Sci. Food Agric.* 51, 309–320. doi: 10.1002/jsfa.2740510304

Birch, A. N. E., Wynne Griffiths, D., Hopkins, R. J., Macfarlane Smith, W. H., and Mckinlay, R. G. (1992). Glucosinolate responses of swede, kale, forage and oilseed rape to root damage by turnip root fly (Delia floralis) larvae. *J. Sci. Food Agric.* 60, 1–9. doi: 10.1002/jsfa.2740600102

Bjorkman, M., Hamback, P. A., Hopkins, R. J., and Ramert, B. (2010). Evaluating the enemies hypothesis in a clover-cabbage intercrop: effects of generalist and specialist natural enemies on the turnip root fly (Delia floralis). *Agric. For. Entomology* 12, 123–132. doi: 10.1111/j.1461-9563.2009.00452.x

Bones, A. M., and Rossiter, J. T. (2006). The enzymic and chemically induced decomposition of glucosinolates. *Phytochemistry* 67, 1053–1067. doi: 10.1016/j.phytochem.2006.02.024

Brader, G., Mikkelsen, M. D., Halkier, B. A., and Tapio Palva, E. (2006). Altering glucosinolate profiles modulates disease resistance in plants. *Plant J.* 46, 758–767. doi: 10.1111/j.1365-313X.2006.02743.x

Clay, N. K., Adio, A. M., Denoux, C., Jander, G., and Ausubel, F. M. (2009). Glucosinolate metabolites required for an Arabidopsis innate immune response. *Science* 323, 95–101. doi: 10.1126/science.1164627

Crespo, E., Hordijk, C. A., De Graaf, R. M., Samudrala, D., Cristescu, S. M., Harren, F. J., et al. (2012). On-line detection of root-induced volatiles in Brassica nigra plants infested with Delia radicum L. root fly larvae. *Phytochemistry* 84, 68–77. doi: 10.1016/j.phytochem.2012.08.013

Danner, H., Desurmont, G. A., Cristescu, S. M., and van Dam, N. M. (2018). Herbivore-induced plant volatiles accurately predict history of coexistence, diet breadth, and feeding mode of herbivores. *New Phytol.* 220, 726–738. doi: 10.1111/nph.14428

de Vos, M., Kriksunov, K. L., and Jander, G. (2008). Indole-3-acetonitrile production from indole glucosinolates deters oviposition by Pieris rapae. *Plant Physiol.* 146, 916–926. doi: 10.1104/pp.107.112185

del Carmen Martínez-Ballesta, M., Moreno, D., and Carvajal, M. (2013). The physiological importance of glucosinolates on plant response to abiotic stress in Brassica. *Int. J. Mol. Sci.* 14, 11607–11625. doi: 10.3390/ijms140611607

Dosdall, L., Herbut, M., and Cowle, N. (1994). Susceptibilities of species and cultivars of canola and mustard to infestation by root maggots (Delia spp.)(Diptera: Anthomyiidae). *Can. Entomologist* 126, 251–260. doi: 10.4039/Ent126251-2

Fahey, J. W., Zalcmann, A. T., and Talalay, P. (2001). The chemical diversity and distribution of glucosinolates and isothiocyanates among plants. *Phytochemistry* 56, 5–51. doi: 10.1016/S0031-9422(00)00316-2

Fahey, J. W., Zhang, Y., and Talalay, P. (1997). Broccoli sprouts: An exceptionally rich source of inducers of enzymes that protect against chemical carcinogens. *Proc. Natl. Acad. Sci.* 94, 10367–10372. doi: 10.1073/pnas.94.19.10367

Fao, S. (2017). FAOSTAT database. *Food Agric. Organ. U. N. Rome Italy* 1. doi: 10.17616/R3N614

Finch, S., and Collier, R. H. (2000). Integrated pest management in field vegetable crops in northern Europe - with focus on two key pests. *Crop Prot.* 19, 817–824. doi: 10.1016/S0261-2194(00)00109-5

Giamoustaris, A., and Mithen, R. (1995). The effect of modifying the glucosinolate content of leaves of oilseed rape (Brassica napus ssp. oleifera) on its interaction with specialist and generalist pests. *Ann. Appl. Biol.* 126, 347–363. doi: 10.1111/j.1744-7348.1995.tb05371.x

Glen, D. M., Jones, H., and Fieldsend, J. K. (1990). Damage to oilseed rape seedlings by the field slug Deroceras-reticulatum in relation to glucosinolate concentration. *Ann. Appl. Biol.* 117, 197–207. doi: 10.1111/j.1744-7348.1990.tb04207.x

Grosser, K., and van Dam, N. M. (2017). A straightforward method for glucosinolate extraction and analysis with high-pressure liquid chromatography (HPLC). *J. Vis. Exp.* (121), e55425. doi: 10.3791/55425

Hopkins, R., Griffiths, D., Birch, A., and Mckinlay, R. (1998). Influence of increasing herbivore pressure on modification of glucosinolate content of swedes (Brassica napus spp. rapifera). *J. Chem. Ecol.* 24, 2003–2019. doi: 10.1023/A:1020729524818

Hopkins, R. J., van Dam, N. M., and van Loon, J. J. (2009). Role of glucosinolates in insect-plant relationships and multitrophic interactions. *Annu. Rev. Entomol.* 54, 57–83. doi: 10.1146/annurev.ento.54.110807.090623

Jeschke, V., and Burow, M. (2018). Glucosinolates. In *eLS,* John Wiley & Sons, Ltd (Ed.). 1–8. doi: 10.1002/9780470015902.a0027968

Jørgensen, M. E., Xu, D., Crocoll, C., Ramírez, D., Motawia, M. S., Olsen, C. E., et al. (2017). Origin and evolution of transporter substrate specificity within the NPF family. *Elife* 6, e19466. doi: 10.7554/eLife.19466

Kabouw, P., van Der Putten, W. H., van Dam, N. M., and Biere, A. (2010). Effects of intraspecific variation in white cabbage (Brassica oleracea var. capitata) on soil organisms. *Plant Soil* 336, 509–518. doi: 10.1007/s11104-010-0507-y

Kim, J. H., and Jander, G. (2007). Myzus persicae (green peach aphid) feeding on Arabidopsis induces the formation of a deterrent indole glucosinolate. *Plant J.* 49, 1008–1019. doi: 10.1111/j.1365-313X.2006.03019.x

Li, Q., Eigenbrode, S. D., Stringam, G., and Thiagarajah, M. (2000). Feeding and growth of Plutella xylostella and Spodoptera eridania on Brassica juncea with varying glucosinolate concentrations and myrosinase activities. *J. Chem. Ecol.* 26, 2401–2419. doi: 10.1023/A:1005535129399

Madsen, S. R., Olsen, C. E., Nour-Eldin, H. H., and Halkier, B. A. (2014). Elucidating the role of transport processes in leaf glucosinolate distribution. *Plant Physiol.* 166, 1450–1462. doi: 10.1104/pp.114.246249

Mathur, V., Tytgat, T. O., Hordijk, C. A., Harhangi, H. R., Jansen, J. J., Reddy, A. S., et al. (2013). An ecogenomic analysis of herbivore-induced plant volatiles in B rassica juncea. *Mol. Ecol.* 22, 6179–6196. doi: 10.1111/mec.12555

Mazzucotelli, E., Mastrangelo, A. M., Crosatti, C., Guerra, D., Stanca, A. M., and Cattivelli, L. (2008). Abiotic stress response in plants: when post-transcriptional and post-translational regulations control transcription. *Plant Sci.* 174, 420–431. doi: 10.1016/j.plantsci.2008.02.005

Mcdonald, R., and Sears, M. (1992). Assessment of larval feeding damage of the cabbage maggot (Diptera: Anthomyiidae) in relation to oviposition preference on canola. *J. Econ. Entomol.* 85, 957–962. doi: 10.1093/jee/85.3.957

Nour-Eldin, H. H., and Halkier, B. A. (2009). Piecing together the transport pathway of aliphatic glucosinolates. *Phytochem. Rev.* 8, 53–67. doi: 10.1007/s11101-008-9110-8

Pierre, P. S., Jansen, J. J., Hordijk, C. A., van Dam, N. M., Cortesero, A.-M., and Dugravot, S. (2011). Differences in volatile profiles of turnip plants subjected to single and dual herbivory above-and belowground. *J. Chem. Ecol.* 37, 368. doi: 10.1007/s10886-011-9934-3

Pierre, S., Dugravot, S., Hervé, M., Hasan, H., van Dam, N. M., and Cortesero, A. M. (2013). Belowground induction by Delia radicum or phytohormones affect aboveground herbivore communities on field-grown broccoli. *Front. Plant Sci.* 4, 305. doi: 10.3389/fpls.2013.00305

Poelman, E. H., Galiart, R. J., Raaijmakers, C. E., van Loon, J. J., and van Dam, N. M. (2008). Performance of specialist and generalist herbivores feeding on cabbage cultivars is not explained by glucosinolate profiles. *Entomol. Exp. Appl.* 127, 218–228. doi: 10.1111/j.1570-7458.2008.00700.x

Potter, M. J., Davies, K., and Rathjen, A. J. (1998). Suppressive Impact of Glucosinolates in Brassica Vegetative Tissues on Root Lesion Nematode Pratylenchus neglectus. *J. Chem. Ecol.* 24, 67–80. doi: 10.1023/A:1022336812240

Potter, M. J., Vanstone, V. A., Davies, K. A., Kirkegaard, J. A., and Rathjen, A. J. (1999). Reduced Susceptibility of Brassica napus to Pratylenchus neglectus in Plants with Elevated Root Levels of 2-Phenylethyl Glucosinolate. *J. Nematol.* 31, 291–298.

R Core Team. (2015). *"R: A language and environment for statistical computing [Internet]*. Vienna, Austria: R Foundation for Statistical Computing.

Rasmann, S., Chassin, E., Bilat, J., Glauser, G., and Reymond, P. (2015). Trade-off between constitutive and inducible resistance against herbivores is only partially explained by gene expression and glucosinolate production. *J. Exp. Bot.* 66, 2527–2534. doi: 10.1093/jxb/erv033

Textor, S., and Gershenzon, J. (2009). Herbivore induction of the glucosinolate–myrosinase defense system: major trends, biochemical bases and ecological significance. *Phytochem. Rev.* 8, 149–170. doi: 10.1007/s11101-008-9117-1

Tsunoda, T., Grosser, K., and van Dam, N. M. (2018). Locally and systemically induced glucosinolates follow optimal defence allocation theory upon root herbivory. *Funct. Ecol.* 32, 2127–2137. doi: 10.1111/1365-2435.13147

Untergasser, A., Cutcutache, I., Koressaar, T., Ye, J., Faircloth, B. C., Remm, M., et al. (2012). Primer3—new capabilities and interfaces. *Nucleic Acids Res.* 40, e115–e115. doi: 10.1093/nar/gks596

van Dam, N. M., and Raaijmakers, C. E. (2006). Local and systemic induced responses to cabbage root fly larvae (Delia radicum) in Brassica nigra and B. oleracea. *Chemoecology* 16, 17–24. doi: 10.1007/s00049-005-0323-7

van Geem, M., Harvey, J. A., Cortesero, A. M., Raaijmakers, C. E., and Gols, R. (2015). Interactions between a belowground herbivore and primary and secondary root metabolites in wild cabbage. *J. Chem. Ecol.* 41, 696–707. doi: 10.1007/s10886-015-0605-7

Warwick, S. I. (2011). "Brassicaceae in agriculture," in *Genetics and Genomics of the Brassicaceae* (New York, NY: Springer), 33–65. doi: 10.1007/978-1-4419-7118-0_2

Welte, C. U., De Graaf, R. M., van Den Bosch, T. J. M., Op Den Camp, H. J. M., van Dam, N. M., and Jetten, M. S. M. (2016). Plasmids from the gut microbiome of cabbage root fly larvae encode SaxA that catalyses the conversion of the plant toxin 2-phenylethyl isothiocyanate. *Environ. Microbiol.* 18, 1379–1390. doi: 10.1111/1462-2920.12997

Wittstock, U., and Burow, M. (2010). Glucosinolate breakdown in Arabidopsis: mechanism, regulation and biological significance. *Arabidopsis Book/American Soc. Plant Biologists* 8, e0134. doi: 10.1199/tab.0134

Wurst, S., Langel, R., Rodger, S., and Scheu, S. (2006). Effects of belowground biota on primary and secondary metabolites in Brassica oleracea. *Chemoecology* 16, 69–73. doi: 10.1007/s00049-005-0328-2

Xue, J., Jørgensen, M., Pihlgren, U., and Rask, L. (1995). The myrosinase gene family in Arabidopsis thaliana: gene organization, expression and evolution. *Plant Mol. Biol.* 27, 911–922. doi: 10.1007/BF00037019

Zhang, W., Kwon, S.-T., Chen, F., and Kliebenstein, D. J. (2016). Isolate dependency of Brassica rapa resistance QTLs to Botrytis cinerea. *Front. Plant Sci.* 7, 161. doi: 10.3389/fpls.2016.00161

Conflict of Interest: The authors declare that the research was conducted in the absence of any commercial or financial relationships that could be construed as a potential conflict of interest.

frontiers in Plant Science

ORIGINAL RESEARCH
published: 26 November 2019
doi: 10.3389/fpls.2019.01549

Glucosinolate Content in Dormant and Germinating *Arabidopsis thaliana* Seeds Is Affected by Non-Functional Alleles of Classical Myrosinase and Nitrile-Specifier Protein Genes

*Kathrin Meier, Markus D. Ehbrecht and Ute Wittstock**

Institute of Pharmaceutical Biology, Technische Universität Braunschweig, Braunschweig, Germany

While the defensive function of glucosinolates is well established, their possible role as a nutrient reservoir is poorly understood and glucosinolate turnover pathways have not been elucidated. Previous research showed that glucosinolate content in germinating seeds of *Arabidopsis thaliana* Columbia-0 (Col-0) increases within the first two to four days on culture medium and then decreases below the level at day 0. In this study we used previously characterized T-DNA mutants to investigate if enzymes known to be involved in glucosinolate breakdown upon tissue damage affect the time course of glucosinolate content in germinating seeds. Besides dormant seeds, we analyzed seeds subjected to stratification in water for up to 72 h or germination on plates for up to ten days. Although seeds of *tgg1 tgg2* (deficient in above-ground classical myrosinases) had higher glucosinolate levels than Col-0, the changes during germination were not different to those in seeds of Col-0. This demonstrates that TGG1/TGG2 are not responsible for the decline in glucosinolate content upon germination and suggests the involvement of other enzymes. Expression data extracted from publically available databases show a number of β-glucosidases of the BGLU18–BGLU33 clade to be expressed at specific time points of seed maturation and germination identifying them as good candidates for a role in glucosinolate turnover. Although nitrile-specifier proteins (NSPs) act downstream of myrosinases upon glucosinolate breakdown in tissue homogenates, mutants deficient in either seed-expressed NSP2 or seedling-expressed NSP1 were affected in glucosinolate content in seeds and during stratification or germination when compared to Col-0 indicating a direct role in turnover. The mutant lines *nsp1-1*, *nsp2-1* and *nsp2-2* had significantly higher glucosinolate levels in dry seeds than Col-0. After 24 h of stratification in water, *nsp2-2* seeds contained 2.3 fold higher levels of glucosinolate than Col-0 seeds. This might indicate downregulation of hydrolytic enzymes when nitrile formation following glucosinolate hydrolysis is impaired. The time course of total glucosinolate content during ten days of germination depended on functional *NSP1*. Based on the present data, we propose a number of experiments that might aid in establishing the pathway(s) of glucosinolate turnover in germinating *A. thaliana* seeds.

Keywords: glucosinolates, turnover, germination, seedling, myrosinase, nitrile-specifier protein

OPEN ACCESS

Edited by:
Ralph Kissen, Norwegian University of Science and Technology, Norway

Reviewed by:
Ryohei Thomas Nakano, Max Planck Institute for Plant Breeding Research, Germany
Daniel J. Kliebenstein, University of California, Davis, United States

****Correspondence:***
Ute Wittstock
u.wittstock@tu-bs.de

Specialty section:
This article was submitted to Plant Metabolism and Chemodiversity, a section of the journal Frontiers in Plant Science

Received: *19 July 2019*
Accepted: *06 November 2019*
Published: *26 November 2019*

Citation:
Meier K, Ehbrecht MD and Wittstock U (2019) Glucosinolate Content in Dormant and Germinating Arabidopsis thaliana Seeds Is Affected by Non-Functional Alleles of Classical Myrosinase and Nitrile-Specifier Protein Genes. Front. Plant Sci. 10:1549. doi: 10.3389/fpls.2019.01549

INTRODUCTION

A dual role of specialized metabolites as defenses and nutrient deposits has been discussed for more than 50 years due to the frequent observation that specialized metabolite levels decrease upon germination, maturation or nutrient constraints and more recent reports on growth defects in mutants with reduced levels of specialized metabolites. For example, transgenic cassava lines with RNAi supression of the cyanogenic glycoside biosynthetic pathway did not produce roots *in vitro*, but root growth was restored upon supplementation with nitrogen (Jørgensen et al., 2005). Only in few cases have turnover pathways been elucidated at the molecular level (Rosenthal, 1992; Negi et al., 2014). In addition to serving plant nutrition, turnover of stored specialized metabolites can also contribute to regulation of specialized metabolite levels as in case of flower color changes upon bud opening (Zipor et al., 2015) or diurnal variation of glucosinolate content (Huseby et al., 2013). Thus, "turnover" in the context of specialized metabolism can generally be described as catabolic reactions that yield building blocks (e.g. ammonia, pyruvate, amino acids) for primary metabolism, e.g. under nutrient deficient conditions, or regulate specialized metabolite levels. Although a clear distinction might not always be possible, this differentiates "turnover" from other catabolic reactions, namely "activation" (associated with a gain in biological activity and roles in organismic interactions or signalling) and "detoxification" (conversion to less harmful compounds).

Glucosinolates (**Figure 1**) are characteristic specialized metabolites of the Brassicales with a well-established role in plant defense against both herbivores and pathogens (e.g. Schlaeppi et al., 2008; Bednarek et al., 2009; Clay et al., 2009; Müller et al., 2010; Stotz et al., 2011; Nakazaki et al., 2019). Due to their unusual structure that includes a sulfate group and a thioglucosidic linkage and may comprise an additional sulfur in the variable side chain (**Figure 1**), glucosinolates have long been proposed to serve as sulfur storage compounds in addition to their roles as chemical defenses (reviewed in Falk et al., 2007; Sugiyama and Hirai, 2019). In several different species, glucosinolate content has been reported to rise with sulfur supply and to decrease under sulfur deficiency (reviewed in Hirai et al., 2004; Falk et al., 2007). Moreover, glucosinolate content may decline in certain developmental stages or in response to prolonged darkness and varies diurnally (Brown et al., 2003; Falk et al., 2007; Huseby et al., 2013; Brandt et al., 2018). In support of a role in sulfur supply, seedlings of *Arabidopsis thaliana gtr1 gtr2* are smaller than wildtype seedlings when grown on medium lacking a sulfur source (Nour-Eldin et al., 2012). This mutant is deficient in the glucosinolate transporters which are, among others, responsible for transferring glucosinolates from maternal tissue to the embryo, and the seeds are devoid of glucosinolates, a potential sulfur source (Nour-Eldin et al., 2012).

Glucosinolate turnover during seed germination and seedling development has also been observed under nutrient-sufficient conditions. Inspired by the markedly different glucosinolate

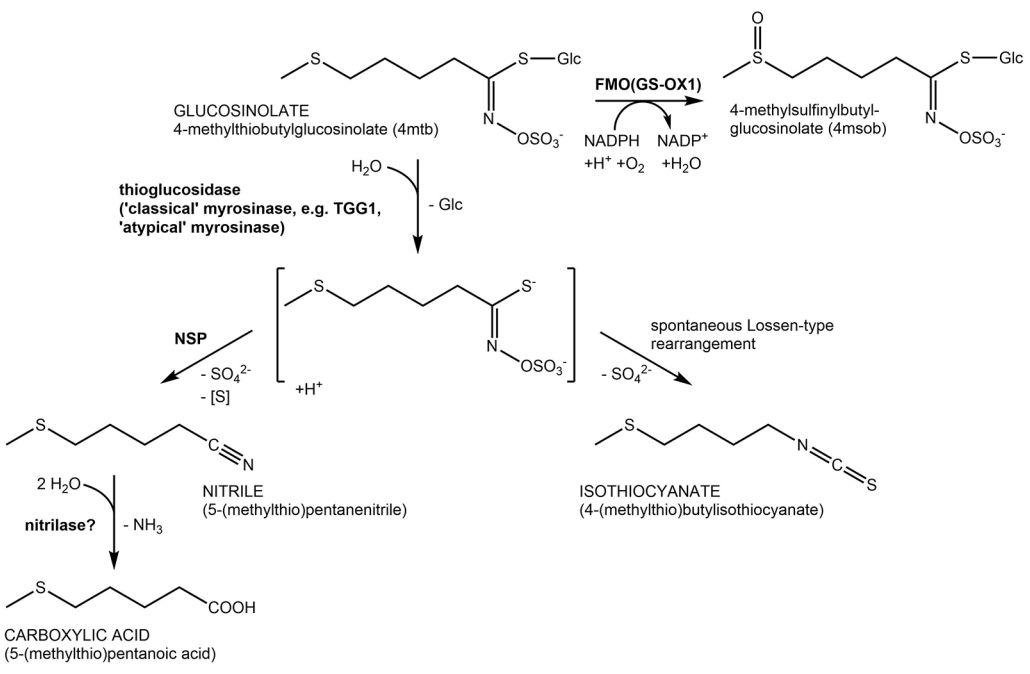

FIGURE 1 | Glucosinolate structures and breakdown pathways. Reactions are shown using the most abundant seed glucosinolate 4-methylthiobutylglucosinolate (4mtb) as an example. Hydrolysis is catalyzed by β-glucosidases with thioglucosidase (myrosinase) activity. In *A. thaliana*, the above ground myrosinases TGG1 and TGG2 are known to hydrolyze glucosinolates upon tissue damage. In the presence of nitrile-specifier proteins (NSPs; left side) the unstable aglucone is converted to a nitrile, a potential substrate of nitrilases. In the absence of specifier proteins (right side), the aglucone rearranges spontaneously yielding an isothiocyanate. Isothiocyanate formation is associated with herbivore and pathogen defense while the NSP-mediated pathway has been proposed as a possible route of safe glucosinolate turnover in intact tissue. Oxidation of 4mtb catalyzed by FMO(GS-OX1) yields 4-methylsulfinylbutylglucosinolate (4msob), the most abundant leaf glucosinolate.

profiles of *A. thaliana* Col-0 seeds and plants in the rosette stage, two studies described changes of glucosinolate content and profile throughout the life cycle of *A. thaliana* Col-0 (Petersen et al., 2002; Brown et al., 2003). This showed that seeds have the highest total glucosinolate concentration among all organs of the plant (Petersen et al., 2002; Brown et al., 2003). Upon seedling development, total glucosinolate concentration decreases dramatically followed by a slight increase upon emergence and growth of the rosette leaves (Petersen et al., 2002; Brown et al., 2003; Barth and Jander, 2006). The initial decline in glucosinolate concentration could be the result of biomass gain ('dilution'), but could also indicate a surplus of glucosinolate turnover relative to biosynthesis. In order to distinguish between these possibilities, Brown et al. (2003) determined glucosinolate content per individual during seed-seedling transition and found a net gain of glucosinolate content per individual in the first two to four days of development followed by a net decrease during the next four days (Brown et al., 2003). Together with the observed changes in glucosinolate profiles, this indicated simultaneous functioning of biosynthesis and turnover reactions with an intial surplus of biosynthesis followed by a period in which turnover outweighs total biosynthesis (Brown et al., 2003).

The defensive role of glucosinolates requires, in most cases, activation through hydrolysis by co-occuring enzymes named myrosinases (**Figure 1**). To prevent premature hydrolysis, enzyme and substrate are usually stored in separate compartments and get mixed to initiate hydrolysis. This happens either upon tissue damage (classical "mustard oil bomb") or in intact tissue by mechanisms that are presently poorly understood (reviewed in Wittstock et al., 2016a). Classical myrosinases can be distinguished from O-glycosidases by the substitution of a catalytic Glu residue in the active site by Gln and are therefore also termed "QE-type" myrosinases (Burmeister et al., 1997). *A. thaliana* possesses six genes (*TGG1-TGG6*) encoding such myrosinases of which two are expressed in the above-ground parts (*TGG1*, *TGG2*) and two in the below-ground parts (*TGG4*, *TGG5*) of the Columbia-0 (Col-0) accession (Wittstock and Burow, 2010). Additionally, the genome of *A. thaliana* harbours a sister clade to *TGG1-TGG6* composed of sixteen genes encoding β-glucosidases (BGLU18-BGLU33), three of which have recently been demonstrated to be functional myrosinases (Bednarek et al., 2009; Clay et al., 2009; Nakano et al., 2017; Nakazaki et al., 2019). These proteins lack the amino acid substitution in the active site and are therefore also refered to as "atypical" or "EE-type" myrosinases (Nakano et al., 2017). Most members of the BGLU18–BGLU33 clade have not been characterized with respect to their activity and specificity with diverse glucosinolates as substrates. In addition, biological roles of BGLU18–BGLU33 that might be associated with activity on glucosinolates are largely unexplored with few exceptions including a role of BGLU18 in herbivore defense and a role of BGLU26 in plant innate immunity (Bednarek et al., 2009; Clay et al., 2009; Nakazaki et al., 2019; Sugiyama and Hirai, 2019).

Pathways of glucosinolate turnover have not been established, and it is unclear how stored glucosinolates would get in contact with breakdown enzymes during turnover in intact tissue. It is generally believed that turnover is initiated by hydrolysis catalyzed by myrosinases/thioglucosidases, but the responsible enzymes have not been identified. Although above-ground parts of the *tgg1 tgg2* mutant had increased concentrations of aliphatic and indolic glucosinolates two weeks after planting, a direct involvement of TGG1 and TGG2 in turnover was considered unlikely (Barth and Jander, 2006). Formation of isothiocyanates upon hydrolysis would potentially be unfavorable for the plant (Urbancsok et al., 2017). A potentially "safe" route of turnover without formation of toxic isothiocyanates would involve nitrile-specifier proteins (NSPs; Burow et al., 2009; Kissen and Bones, 2009) and nitrilases (Janowitz et al., 2009) (**Figure 1**). This would allow complete turnover of glucosinolates to building blocks for primary metabolism (glucose, sulfate, sulfur, ammonia, carboxylic acid; **Figure 1**). *A. thaliana* Col-0 expresses five *NSP* genes in different organs and developmental stages (Kissen and Bones, 2009; Wittstock et al., 2016b). Characterization of T-DNA insertion mutants of each of these genes demonstrated that simple nitrile formation depends entirely on *NSP2* in seed homogenates and mostly on *NSP1* in seedling homogenates (Wittstock et al., 2016b).

In this study, we tested the effects of deficiency in above-ground myrosinases (TGG1 and TGG2) and seed- or seedling-expressed NSPs (NSP1, NSP2) on glucosinolate levels in germinating seeds and developing seedlings in order to evaluate their possible contribution to glucosinolate turnover during seed-seedling transition. We made use of mutant lines that had been characterized previously (Barth and Jander, 2006; Wittstock et al., 2016b) and analyzed their glucosinolate content at different time points during stratification and germination in comparison to Col-0. Following the considerations by Brown et al. (2003), we determined glucosinolate content per individual (as opposed to concentrations relative to dry weight). This enabled us to identify periods in which turnover dominates (relative to *de-novo* biosynthesis) and to rule out reallocation within the plant as a possible cause of changed glucosinolate levels in a particular organ.

MATERIAL AND METHODS

Plant Material

A. thaliana Columbia-0, *nsp1-1* (Burow et al., 2009), *nsp2-1* and *nsp2-2* (Burow et al., 2009; Wittstock et al., 2016b) and *tgg1 tgg2* (Barth and Jander, 2006) were grown in parallel in controlled environment chambers (Percival) at 22°C, 60–70% relative humidity; 300 μmol m^{-2} s^{-1} photosynthetically active radiation (photoperiod 16 h) in several rounds between Spring 2018 and Spring 2019. After harvest, seeds were stored for six to twelve months before analysis. Each mutant-wildtype comparison was done between seed batches harvested and stored in parallel. For glucosinolate analysis, a known number of seeds (100–200) was frozen in liquid nitrogen and freeze-dried. Glucosinolate content was determined and expressed as content [nmol] per individual.

Stratification Time Course

A known number of seeds (100–200) was incubated with 500 μl autoclaved tap water at 4°C in the dark with three replicates (randomly assigned as 1–3) for each time point. After 2, 4, 8, or 24, water was removed, samples were frozen in liquid nitrogen and freeze-dried. Glucosinolate content was determined

and expressed as content (nmol) per individual. To quantify changes of glucosinolate content during imbibition, the ratio of glucosinolate content at two time points of interest was calculated for paired replicates (e.g. 8 h-replicate-1 vs. 2 h-replicate-1).

Germination Time Course

A known number of seeds (100–200) was surface sterilized by incubation with 70% (v/v) ethanol for 2 min and 3% (v/v) sodium hypochlorite for 5 min followed by three washes with sterile water. The duration of this procedure was kept between 45 and 60 min for all samples. Seeds were plated on Murashige & Skoog (MS) medium (Murashige and Skoog, 1962) (0.9% (w/v) agar) and stratified at 4°C in the dark for 48 h. The plates were then kept in a controlled environment chamber (Percival; 22°C, 60–70% relative humidity; 300 µmol m^{-2} s^{-1} photosynthetically active radiation, photoperiod of 16 h). Plant material was harvested 4, 8, or 10 days after plating. In each of three independent experiments, three plates were generated as biological replicates (randomly assigned as 1–3) per genotype and time point. The seedlings of one plate were carefully harvested with tweezers, pooled, frozen in liquid nitrogen, and freeze-dried. Day 0 samples were frozen after sterilization without plating on MS medium. Glucosinolate content was determined and expressed as content [nmol] per individual. To quantify changes of glucosinolate content during germination, the ratio of glucosinolate content at two time points of interest was calculated for paired replicates (e.g. 10 day-replicate-1 vs. 4 day-replicate-1). Dry weight was recorded in two of the three experiments.

Glucosinolate Analysis

Glucosinolates were quantified by HPLC of the corresponding desulfoglucosinolates (Thies, 1979) as described previously (Wittstock et al., 2016b). Desulfoglucosinolates were identified based on comparison of retention times and UV absorption spectra with those of known standards (Reichelt et al., 2002) and quantified based on peak areas at 229 nm relative to the peak area of the internal standard (4-hydroxybenzylglucosinolate; relative response factor 2.0 for aliphatic glucosinolates and 0.5 for indole glucosinolates (Burow et al., 2006; Sarosh et al., 2010). Total glucosinolate content was calculated as the sum of all detected glucosinolates (4-methylthiobutyl-(4mtb), 4-methylsulfinylbutyl-(4msob), 5-methylthiopentyl-(5mtp), 7-methylthioheptyl-(7mth), 7-methylsulfinylheptyl-(7msoh),8-methylthiooctyl-(8mto), 8-methylsulfinyloctyl-(8msoo), 3-hydroxypropyl-(3OHp), 3-benzoyloxypropyl-(3bzo), 4-benzoyloxybutyl-(4bzo), indol-3-ylmethylglucosinolate (i3m), **Table 1**). Two glucosinolates (5mtp, 3OHp) were present in traces and/or inconsistently and were therefore excluded from more detailed analyses of contents of individual glucosinolates and corresponding figures. Plant material did not contain detectable levels of 4-hydroxybutyl glucosinolate.

Statistics

Statistical analyses were done with OriginPro8. Normal distribution was assumed based on Shapiro–Wilk Test. Homogeneity of variance was assessed using ANOVA with Brown–Forsythe Test.

TABLE 1 | Glucosinolates detected in seeds and germinating seedlings of *A. thaliana* and their abbreviations.

Abbreviation	Glucosinolate
4mtb	4-methylthiobutylglucosinolate
4msob	4-methylsulfinylbutylglucosinolate
5mtp	5-methylthiopentylglucosinolate
7mth	7-methylthioheptylglucosinolate
7msoh	7-methylsulfinylheptylglucosinolate
8mto	8-methylthiooctylglucosinolate
8msoo	8-methylsulfinyloctylglucosinolate
3OHp	3-hydroxypropylglucosinolate
3bzop	3-benzoyloxypropylglucosinolate
4bzob	4-benzoyloxybutylglucosinolate
i3m	indol-3-ylmethylglucosinolate

Significant differences in pairwise comparisons between wildtype and each mutant were identified using Two-Sample-t-Test (in case of normal distribution) and Mann–Whitney Test (when normal distribution was not confirmed). Multiple comparisons were done with ANOVA followed by Tukey's test when normal distribution had been confirmed.

RESULTS

To investigate if deficiency in above-ground myrosinases affects glucosinolate content in seeds, we determined glucosinolate levels in *tgg1 tgg2* seeds in comparison to Col-0 wildtype. Although *tgg1 tgg2* seeds had, on average, slightly higher total glucosinolate levels per individual than Col-0 and tended to weight more than Col-0 seeds, these difference were not significant (**Figure 2**, **Figure S1**). With the exception of 4bzo, the four major seed glucosinolates (4mtb, 4bzo, 3bzo, and 8msoo; 75% of the total glucosinolate content) all contributed to the overall increase in glucosinolate content in *tgg1 tgg2* relative to Col-0 (**Figure S2**; compound abbreviations are listed in **Table 1**). Minor glucosinolates (4msob, 7mth, 7msoh, 8mto, i3m) were slightly, but not significantly increased in *tgg1 tgg2* relative to Col-0 (**Figure S2**). As glucosinolates with methylthioalkyl side chain (4mtb, 7mth, 8mto) are biosynthetic precursors of those with methylsulfinylalkyl side chain (4msob, 7msoh, 8msoo) (**Figure 1**), we also considered the total content of each of these pairs and found the level of 4mtb + 4msob to be significantly increased in *tgg1 tgg2* relative to Col-0 (**Figure S2**).

Next we studied the effect of non-functional genes of seed/seedling-expressed NSPs by assessing glucosinolate content in seeds of *nsp1-1* and two independent *nsp2* lines (*nsp2-1*, *nsp2-2*). Seeds of *nsp1-1* and both *nsp2* lines accumulated significantly higher glucosinolate levels per individual than Col-0 seeds (**Figure 2**), but their weight did not differ significantly from that of Col-0 seeds (**Figure S1**). In *nsp1-1* seeds, all glucosinolates except of 4mtb (a major glucosinolate) and 4msob were increased, on average, relative to Col-0 (**Figure S2**). The increase was significant for 7msoh 3bzo, 4bzo, and i3m (**Figure S2**). In case of *nsp2-1*, each of the methylthioalkyl/methylsulfinylalkyl pairs (4mtb + 4msob, 7mth + 7msoh, 8mto + 8msoo) as well as 4bzo, 3bzo, and i3m contributed to the overall increase (**Figure S2**).

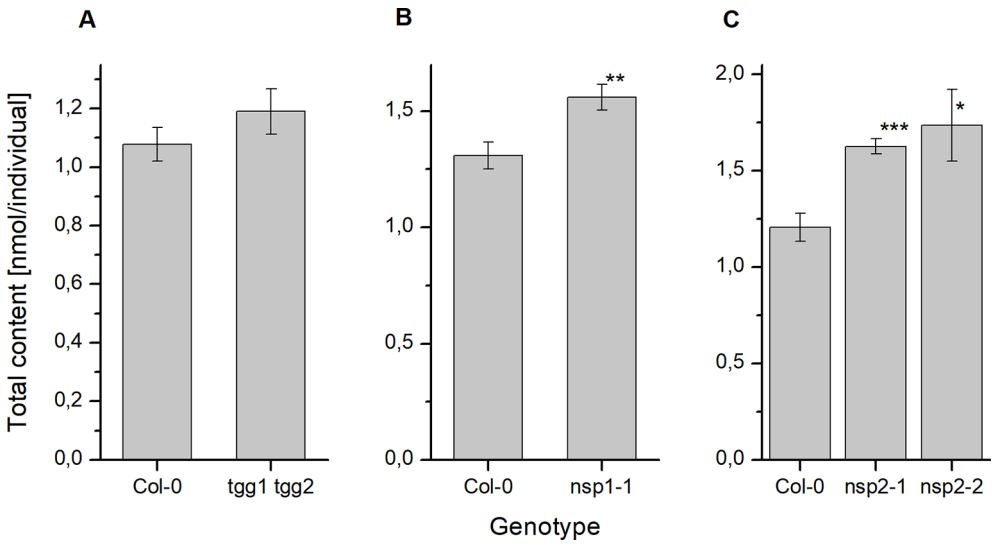

FIGURE 2 | Glucosinolate content in dry seeds of *A. thaliana* Col-0 and breakdown pathway mutants. Total glucosinolate content was determined as nmol per individual in seeds of *tgg1 tgg2* **(A)**, *nsp1-1* **(B)**, as well as *nsp2-1* and *nsp2-2* **(C)** in comparison to seeds of Col-0. Means ± SD of N = 3 biological replicates. Significant differences between mutant and Col-0 are indicated by asterisks (*, $p < 0.05$; **, $p < 0.01$; Two-Sample-t-Test; ***, $p < 0.001$).

However, in case of 7mth + 7msoh and 8mto + 8msoo the increase was entirely due to a higher level of the oxidized form (methylsulfinyl-) relative to Col-0 (**Figure S2**). Seeds of *nsp2-2* showed largely the same trend as *nsp2-1*, with the exception of 8mto + 8msoo which accumulated to a lower mean total level as in Col-0 seeds (**Figure S2**).

To investigate the effect of glucosinolate breakdown pathway genes on glucosinolate levels during germination, we conducted two different treatments. Treatment 1 addressed early timepoints within up to 72 h of stratification and germination. Therefore, the procedure was kept simple. We subjected seeds to imbibition in water at 4°C in the dark and measured glucosinolate content per individual after 2, 6, 8, 12, 24, 48, and (in some experiments) 72 h. We conducted different sets of experiments with either *tgg1 tgg2* and Col-0 or both *nsp2* lines and Col-0. The *nsp2* lines were chosen as *NSP2* is expressed in seeds and during stratification (**Figure 3**), and as simple nitrile formation in seed homogenates depends entirely on *NSP2* (Wittstock et al., 2016b). Treatment 2 considered changes in glucosinolate content during the standard procedure for germination of *A. thaliana* seeds on MS medium under sterile conditions over a total of ten days and included sterilization, plating, stratification for two days and incubation at 22°C and with 16 h photoperiod for another eight days. In these experiments, we analyzed *tgg1 tgg2* and *nsp1-1* in comparison to Col-0. The *nsp1-1* line was chosen as the transfer from stratification to normal growth conditions is associated with a switch from *NSP2* to *NSP1/3/4* expression (**Figure 3**) and *NSP1* is expressed in seedlings (in contrast to *NSP3* and *NSP4*) (Wittstock et al., 2016b).

Based on the overall time course in Treatment 1 (**Figure S3**), we selected three time points (2, 8 and 24 h) for comparison between Col-0 and mutants. To quantify changes, we calculated the ratio (fold change) between the content at a later and an earlier time point (**Figure 4**). Thus, values >1 indicate an increase of glucosinolate content over time, and values <1 a decrease. In *tgg1 tgg2* seeds, glucosinolate content after 8 h was, on average, about 1.2-fold higher than after 2 h of incubation (**Figure 4**), but this difference was not significant ($p > 0.05$, Mann–Whitney Test). Glucosinolate content in seeds of Col-0 and both *nsp2* lines did not change significantly from 2 to 8 h of incubation (**Figure 4**). The 8h/2h ratio did not differ significantly between Col-0 and the mutant lines (**Figure 4**). Between 8 and 24 h of incubation, glucosinolate content of *nsp2-2* seeds increased about 1.2-fold ($p < 0.05$, Two-Sample-t-Test) while the content in seeds of the other tested genotypes decreased on average (**Figure 4**). The 24 h/8 h ratio differed significantly between *nsp2-2* and Col-0 ($p < 0.05$, Two-Sample-t-Test) (**Figure 4**).

As a consequence of these changes, *tgg1 tgg2* seeds contained significantly higher total glucosinolate levels per individual than Col-0 after 24 h of stratification (**Figure 5**). On average, individual glucosinolates were all increased in *tgg1 tgg2* relative to Col-0 with the exception of 4bzo (**Figure 6**), similar to the results with dry seeds (**Figure S2**). Seeds of *nsp2-2* had the highest glucosinolate content among the tested genotypes at this time point and contained, on average, >2.3-fold higher levels per individual than Col-0 seeds after the same treatment (**Figure 6**). All individual glucosinolates were increased, on average, in *nsp2-2* seeds compared to Col-0 (**Figure 6**) with the exception of 7mth which was replaced by 7msoh in *nsp2-2* seeds, i.e. the level of 7msoh in *nsp2-2* was higher than the level of 7mth + 7msoh in Col-0 (**Figure 6B**). The proportion of reduced and oxidized form (7mth/7msoh, 8mto/8msoo) also varied in Col-0 seeds (**Figures 6B, C**). These four glucosinolates were of low abundance. Together with differences between seed batches, this might explain the large variation. Seeds of *nsp2-1* showed the same trend as those of *nsp2-2* with respect to total glucosinolate content (**Figure 5**) and individual glucosinolates (**Figure 6**).

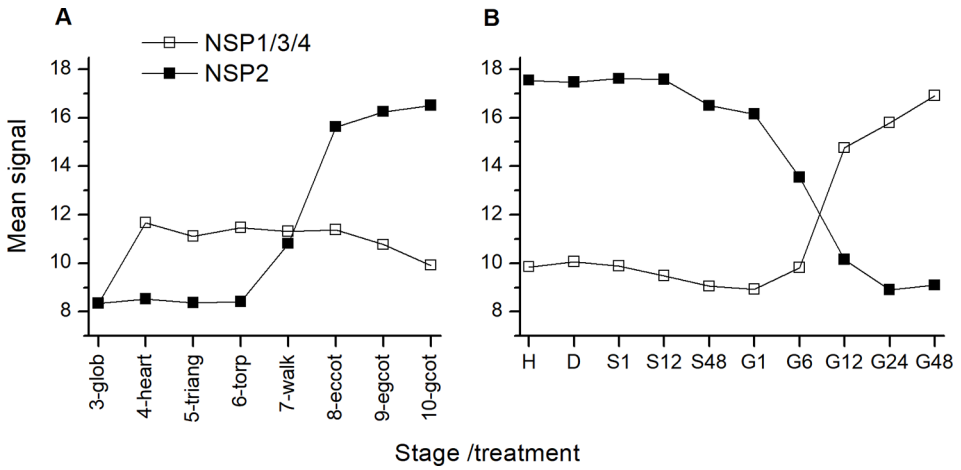

FIGURE 3 | Expression of *NSP* genes during maturation and germination of *A. thaliana* Col-0 seeds. Microarray data (ATH1) from **(A)** (Kleindt et al., 2010) (GEO accession: GSE5634) and **(B)** (Narsai et al., 2011) (GEO accession: GSE30223) for *NSP1/3/4* and *NSP2* were extracted from Genevestigator (Hruz et al., 2008). Each data point represents the mean of three replicates. **(A):** Seed maturation, samples consisted of siliques with seeds (stages 3–5) or seeds (stages 6–10). Stages are defined by embryo development according to (Kleindt et al., 2010): glob, globular to early heart; heart, early to late heart; triang, triangular (late heart to mid torpedo); torp, mid to late torpedo; walk, late torpedo to early walking stick; eccot, walking stick to early curled cotyledons; egcot, curled cotyledons to early green cotyledons; gcot, green cotyledons. **(B):** Germination. Stages/treatments are as follows (with numbers indicating the duration of the treatment in hours): H, freshly harvested; D, dried (15 days in darkness); S, stratification (on MS plates, 4°C in the dark); G, germination (22°C, continuous light). *NSP1*, *NSP3* and *NSP4* are represented by the same probe (259381_s_at).

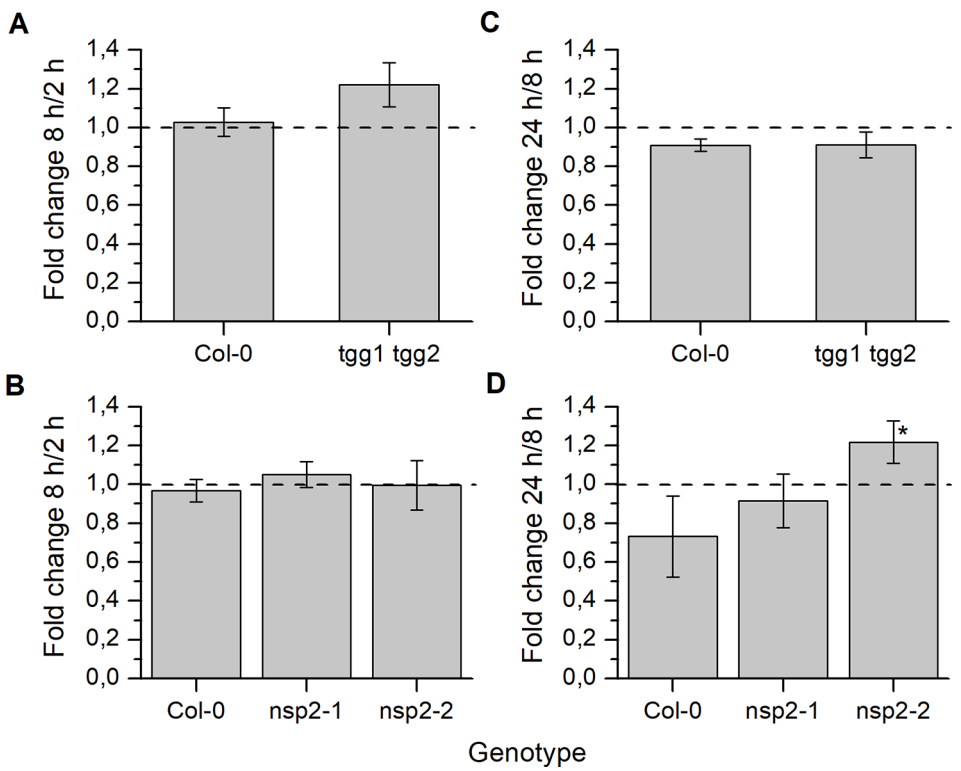

FIGURE 4 | Changes of seed glucosinolate content during stratification. Seeds of Col-0 and *tgg1 tgg2* **(A**, **C)** or Col-0, *nsp2-1*, and *nsp2-2* **(B**, **D)** were incubated in autoclaved tap water at 4°C in the dark for 2, 8, or 24 h. Total glucosinolate content was determined as nmol per individual. Fold change from 2 h to 8 h **(A**, **B)** and from 8 h to 24 h **(C**, **D)** is given. Ratio of 1 (no change) is highlighted by the dashed line. Means ± SD of N = 3 biological replicates. Significant differences between mutant and Col-0 are indicated by asterisks (*, $p < 0.05$, Two-Sample-t-Test).

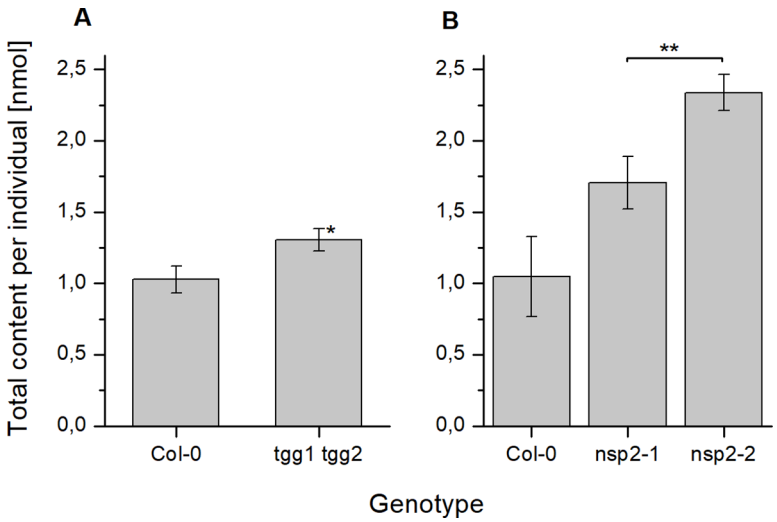

FIGURE 5 | Seed glucosinolate content after 24 h of stratification. Seeds were incubated in autoclaved tap water at 4°C in the dark for 24 h. Total glucosinolate content was determined as nmol per individual in seeds of *tgg1 tgg2* **(A)** and *nsp2-1* and *nsp2-2* **(B)** in comparison to seeds of Col-0. Means ± SD of N = 3 biological replicates. An asterisk next to a bar indicates a significant difference to Col-0. Asterisks at a horizontal bracket denote a significant difference between the bars. *, $p < 0.05$; **, $p < 0.01$ (Two-Sample-t-Test).

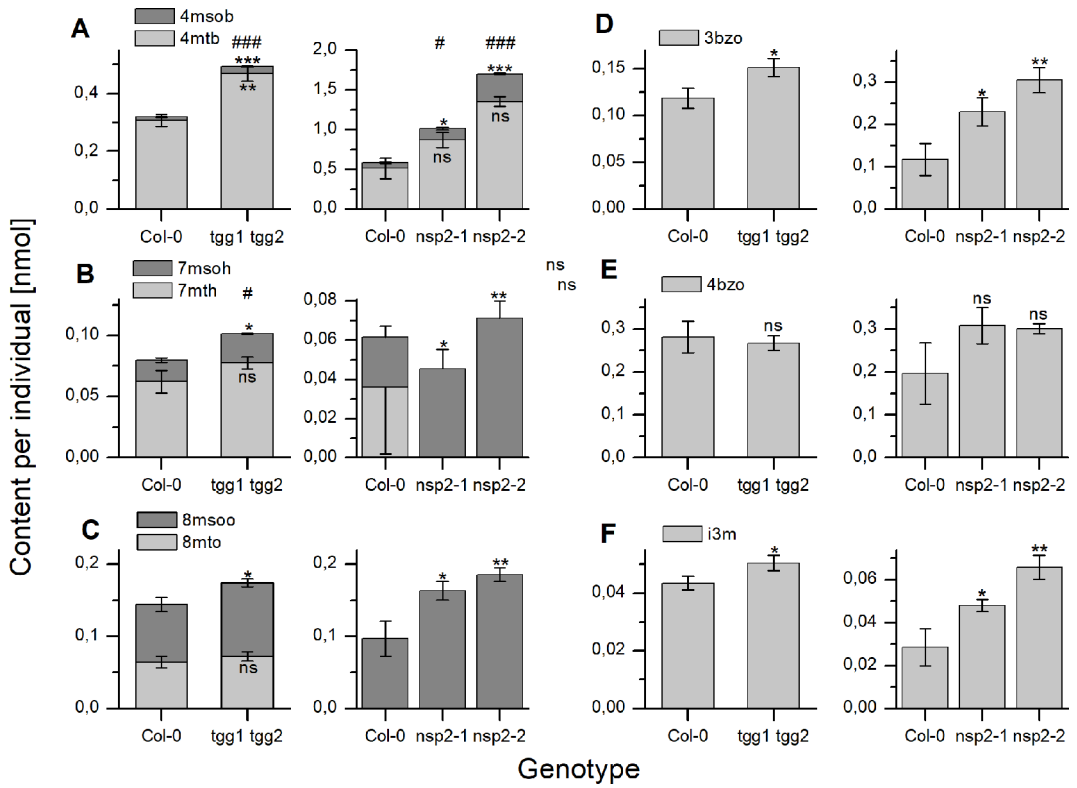

FIGURE 6 | Seed content of individual glucosinolates after 24 h of stratification. Seeds were incubated in autoclaved tap water at 4°C in the dark for 24 h. Glucosinolate content is expressed as nmol per individual. **(A–C)** depict methylthioalkylglucosinolates together with the derived methylsulfinylalkyl derivative. **(D, E)** depict individual benzoylated glucosinolates and **(F)** indol-3-ylmethylglucosinolate. The left graph of each panel shows results of experiments with *tgg1 tgg2* in comparison with Col-0, the right graph in each panel those with two independent *nsp2* lines in comparison with Col-0. Means ± SD from N = 3 biological replicates. Asterisks indicate significant differences for individual glucosinolates relative to Col-0 (*, $p < 0.05$; **, $p < 0.01$; ***, $p < 0.001$) while hashs on top of a bar in **(A–C)** indicate significant differences for the sum of a biosynthetically linked pair relative to wildtype (#, $p < 0.05$; ###, $p < 0.001$). Significant differences were identified by pairwise comparisons using Two-Sample-t-Test with the exception of 4mtb in Col-0 vs. both *nsp2* mutants (A, right graph). In the latter case, Mann–Whitney Test was applied. Levels of 7mth **(B)** and 8mto **(C)** were low, varied strongly and could not be detected in some samples of Col-0 as well as *nsp2-1* and *nsp2-2*. ns, not significant.

Taken together, the differences of total glucosinolate content in seeds between Col-0, *tgg1 tgg2* and both *nsp2* lines determined with dry seeds became more pronounced when seeds were stratified in water at 4°C in the dark for 24 h.

Changes of seed glucosinolate content during germination (Treatment 2) were assessed at four time points after sterilization during up to ten days of growth on MS medium. For Col-0 seeds, we were able to reproduce, in principle, the previously published time course (Brown et al., 2003) with a peak in total glucosinolate content per individual at day 4 and, in our study, no significant difference between total glucosinolate content at days 0 and 10 (**Figure 7A**). The content of most individual glucosinolates or biosynthetically linked pairs (7mth + 7msoh, 8mto + 8msoo, i3m), respectively, showed the same trend (**Figure 8**, top row from left to right), similar to a previous report (Brown et al., 2003). However, the major glucosinolate 3bzo increased steadily over the investigated time period to reach an almost twofold higher level at day 10 when compared with day 0 (**Figure 8D**). The content of the major seed glucosinolate 4mtb and the sum of 4mtb and its derivative 4msob declined below the level at day 0, in our study to about 70% (4mtb) and 80% (4mtb + 4msob) of the content at day 0 indicating turnover (**Figure 8A**). In case of the other two methylthio-/sulfinylalkylglucosinolate pairs, we found increased levels of the methylthioalkyl compounds (7mth, 8mto) at days 8 and 10 relative to day 4, but decreased levels of their oxidized derivatives (7msoh, 8msoo) (**Figures 8B**, **C**). Thus, the oxidized forms might undergo turnover or are converted back to the methylthioalkyl precursors.

The analysis of germinating seeds of *tgg1 tgg2* resulted in a similar time course of glucosinolate content as that obtained for Col-0 seeds (**Figure 7B**). There was no significant difference between *tgg1 tgg2* and Col-0 with respect to the ratio (fold change) between days 0 and 4 as well as between days 4 and 10 ($p > 0.05$, Two-sample-t-Test, **Figure S4**). The time course of each individual glucosinolate (**Figure 8**, middle row from left to right) largely mirrored that found with Col-0 seeds This indicates that TGG1 and TGG2 are not involved in the reactions that determine the time course of glucosinolate content in germinating *A. thaliana* seeds within 10 days of incubation on MS medium.

In contrast to Col-0 and *tgg1 tgg2*, germinating seeds of *nsp1-1* did not contain higher total glucosinolate levels on day 4 relative to days 0 and 10 (**Figure 7C**). Fold change between days 0 and 4 was significantly different from that obtained with Col-0 ($p < 0.05$, Two-sample-t-Test, **Figure S4**). On average, total glucosinolate content of *nsp1-1* seeds decreased slightly and steadily over 10 days of incubation on MS medium, but these changes were not significant ($p > 0.05$, ANOVA; **Figure 7C**). Among individual glucosinolates, time courses of 3bzo and i3m were similar to those found with Col-0 while time courses of all other glucosinolates lacked the peak at day 4 (**Figure 8**, bottom row from left to right). Our results indicate that the time course of glucosinolate content in *A. thaliana* Col-0 seeds upon 10 days of growth on MS medium depends on functional *NSP1*.

To assess if the observed differences between the genotypes can be explained by a developmental defect, we inspected the developing seedlings of Col-0, *tgg1 tgg2*, and *nsp1-1* visually and determined their dry weight over ten days of growth on MS medium (**Figures S5** and **S6**). At day 4, seedlings of all genotypes had emerged with light-green cotyledons and a primary root, and cotyledons had started to open (**Figure S5**). At day 8, seedlings possessed opened, green cotyledons (**Figure S5**). The plumule started to become visible with the naked eye. Cotyledons and

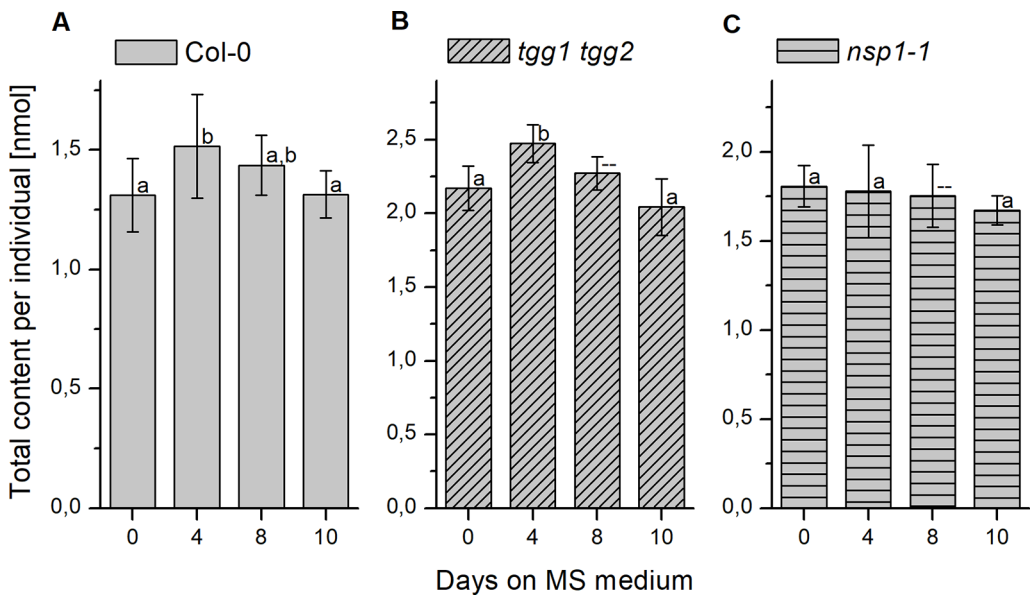

FIGURE 7 | Changes of glucosinolate content in sterilized seeds plated on MS medium. Seeds were sterilized (day 0), plated on MS medium, stratified at 4°C in the dark for two days and then grown at 22°C with 16 h photoperiod. Total glucosinolate content was determined as nmol per individual in seeds of Col-0 **(A)**, *tgg1 tgg2* **(B)**, as well as *nsp1-1* **(C)**. Means ± SD (N = 8 – 9). Different letters above bars indicate a significant difference ($p < 0.05$, ANOVA with Tukey's test; data for day 8 in **(B)** and **(C)** were not included as normal distribution was not confirmed).

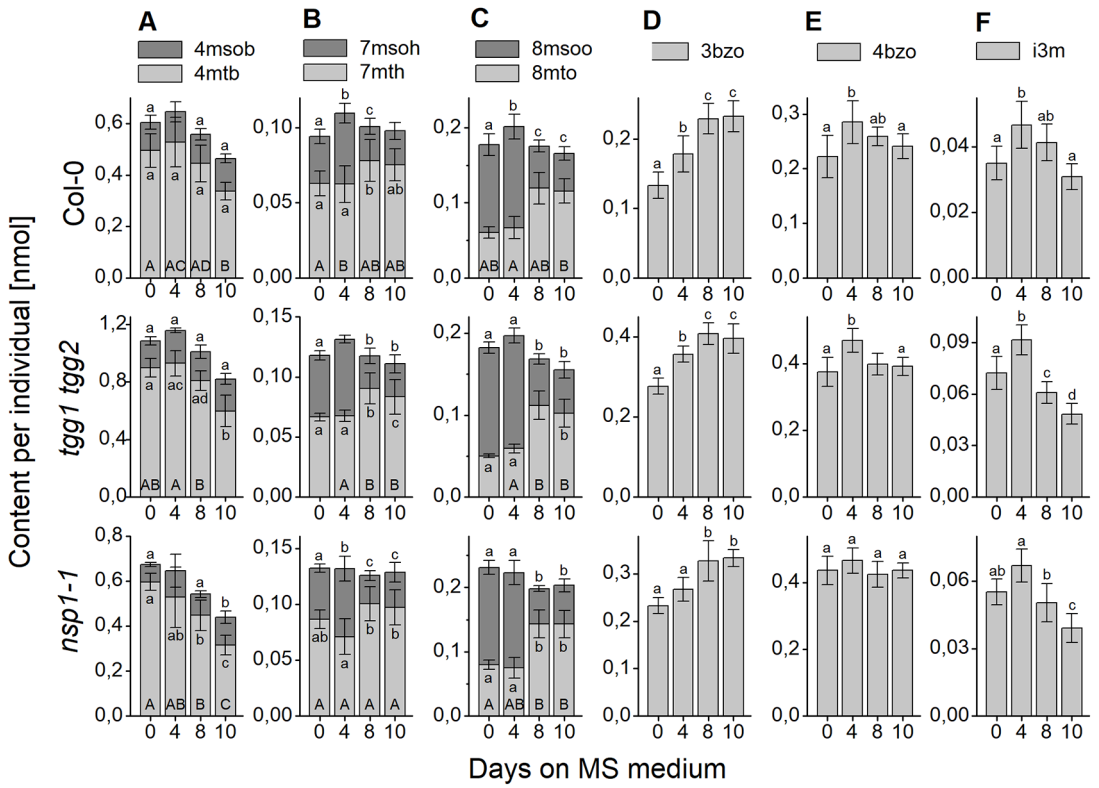

FIGURE 8 | Changes of content of individual glucosinolates in sterilized *A. thaliana* Col-0 seeds plated on MS medium. Seeds were sterilized (day 0), plated on MS medium, stratified at 4°C in the dark for two days and then grown at 22°C with 16 h photoperiod. Glucosinolate content was determined as nmol per individual. **(A–C)** depict methylthioalkylglucosinolates together with the derived methylsulfinylalkyl derivatives. **(D, E)** depict individual benzoylated glucosinolates and **(F)** indol-3-yl-methylglucosinolate. Each panel shows a comparison of Col-0 (top), *tgg1 tgg2* (middle), and *nsp1-1* (bottom). Means ± SD from N = 8–9 biological replicates. Different letters next to error bars indicate a significant difference for individual glucosinolates between time points while those at the base of bars indicate significant differences for the sum of biosynthetically linked pairs ($p < 0.05$, ANOVA with Tukey's test; samples without a label were not included in the analysis as normal distribution could not be assumed).

plumule tended to appear slightly larger in seedlings of *tgg1 tgg2* than in the other genotypes (**Figure S5**). At day 10, *tgg1 tgg2* seedlings were larger than seedlings of the other genotypes and had typically developed the first pair of true leaves while only few seedlings of the other genotypes had reached this stage (**Figure S5**). Thus, *tgg1 tgg2* developed slightly faster than the other genotypes. In agreement with this, *tgg1 tgg2* had, on average, the highest dry weight among the tested genotypes throughout days 4 to 10 (**Figure S6**). Col-0 seedlings had the lowest dry weight and *nsp1-1* seedlings reached intermediate levels (**Figure S6**) with the exception of day 8 where dry weight of *nsp1-1* was the same as that of *tgg1 tgg2*. Taken together, we found *tgg1 tgg2* to gain weight and develop slightly faster than Col-0 and *nsp1-1*, but we did not find developmental differences among the genotypes that could explain the changed time course of glucosinolate content in *nsp1-1* relative to Col-0 and *tgg1 tgg2*.

DISCUSSION

While turnover of seed glucosinolates during germination and seedling development of *A. thaliana* has been described previously based on different experimental approaches (Petersen et al., 2002; Brown et al., 2003; Barth and Jander, 2006) and was confirmed here (**Figure 7**), pathways of glucosinolate turnover have remained unresolved. The present study was set up to evaluate the time course of glucosinolate content during stratification and germination in dependency of enzymes known to be involved in glucosinolate breakdown upon tissue damage, namely TGG1, TGG2, NSP1 and NSP2, using previously characterized T-DNA mutants. The *tgg1 tgg2* mutant lacked myrosinase activity in the above-ground parts of plants in the vegetative as well as generative stages when myrosinase activity of plant extracts was determined with allylglucosinolate as substrate but had residual myrosinase activity on indolic glucosinolates (Barth and Jander, 2006). TGG1 seems to be the major myrosinase of the above-ground organs because the single mutant *tgg1* gave similar results as the double mutant while results for *tgg2* were similar to wildtype (Barth and Jander, 2006). *NSP2* is expressed only in seeds and solely responsible for simple nitrile formation in Col-0 seed homogenates without contributions from other *NSPs* (Wittstock et al., 2016b). Under laboratory conditions, the switch from *NSP2* to *NSP1* expression coincides with the transfer from stratification to germination (**Figure 3**).

However, *NSP2* expression seems to be confined to late stages of seed maturation and to the mature seed until the onset of germination (**Figure 3**). Among non-functional alleles of *NSP1–NSP5*, only the *nsp1-1* allele caused a significant decrease of absolute and relative levels of the simple nitrile and a significant increase of the corresponding isothiocyanate derived from 4mtb (the most abundant aliphatic glucosinolate) in seedling homogenates, but did not result in a complete lack of simple nitrile formation (Wittstock et al., 2016b). Hence, other NSPs are likely to contribute, albeit to a low extent. It would, therefore, be interesting to include mutants with multiple non-functional *NSP* alleles in future studies on glucosinolate turnover. As *NSP1*, *NSP3*, and *NSP4* are tandem genes, a triple mutant cannot be obtained by crossing of the existing genotypes but has to be generated by alternative methods, e.g. gene editing. In *nsp5-1*, *NSP5* expression was downregulated, but not lacking (Wittstock et al., 2016b). Once a real knockout has been obtained, it should also be studied in a background with other non-functional *NSPs*.

We did not find differences between *tgg1 tgg2* and Col-0 with respect to the time course of total glucosinolate content over 10 days of incubation on MS medium (**Figure 7**, **Figure S4**). Thus, TGG1/TGG2 are not responsible for the decline of glucosinolate content between days 4 and 10 of the germination time course in agreement with the conclusions drawn by Barth and Jander (2006). However, glucosinolate content in dry seeds of *tgg1 tgg2* was, on average, higher than that of Col-0, and after 24 h of stratification this difference was larger and significant (**Figures 2A** and **5A**). As a possible explanation, TGG1/TGG2 could be involved in breakdown of glucosinolates in developing siliques/seeds, for example for the release of volatile breakdown products. In fact, *TGG1/TGG2* are expressed in early stages of silique development (stages 3–6, Kleindt et al., 2010) according to microarray data (GEO: GSE5634; *TGG1* and *TGG2* are represented by the same probe). Lacking *TGG1/TGG2* expression could also have an effect on glucosinolate import into the developing seed or biosynthesis. Even though we did not observe higher herbivore or pathogen infestation rates of *tgg1 tgg2* plants as compared to simultaneously grown Col-0 plants, defense pathways could have been induced in the mutant relative to Col-0 leading to enhanced glucosinolate biosynthesis in the parent plants of the analyzed *tgg1 tgg2* seeds. Upon stratification in water, we observed a steep increase of glucosinolate content in *tgg1 tgg2* between 6 and 10 h of incubation, and the resulting difference in content relative to Col-0 remained largely unchanged for the following 40 h (**Figure S3**). This might indicate that glucosinolate breakdown by TGG1/TGG2 happens only within a small time window during stratification (maybe due to reorganization of tissues upon onset of imbibition), but is normally compensated by biosynthesis. Further experiments will need to be performed to investigate this possibility in more detail. Seedlings of *tgg1 tgg2* grew faster than Col-0 seedlings. It is tempting to speculate that this could be due to the benefit provided by increased levels of glucosinolates as substrates fed into TGG1/TGG2-independent turnover pathways for nutrient release. As an alternative explanation, lack of expression of TGG1, a highly abundant protein in wildtype plants, might safe considerable resources which *tgg1 tgg2* plants can invest in growth.

If TGG1/TGG2 are not responsible for the observed decline in glucosinolate content between days 4 and 10 of the germination time course, as our data suggest, other enzymes must initiate glucosinolate turnover. To test if any of the genes of the *BGLU18-BGLU33* cluster are expressed in germinating seeds, we analyzed microarray data using Genevestigator (Hruz et al., 2008) (**Figures 9C**, **D**). This identified *BGLU21/BGLU22*, *BGLU23*, *BGLU26*, and *BGLU28* to be induced upon transfer to light. All of these genes except for *BGLU28* reached the highest expression level at 24–48 h of incubation in light, i.e. days 3 to 4 of incubation on medium, and are therefore candidates for future studies on glucosinolate turnover in germinating seeds of *A. thaliana*. Based on the present knowledge, BGLU23 and BGLU26 are active on indolic glucosinolates, and BGLU23 is unable to hydrolyze allylglucosinolate (Bednarek et al., 2009; Clay et al., 2009; Ahn et al., 2010; Nakano et al., 2017). However, a broad spectrum of structurally diverse glucosinolates needs to be tested to evaluate possible roles of these and other atypical myrosinases in processes such as glucosinolate turnover during seedling development.

As NSPs act downstream of glucosinolate hydrolysis (**Figure 1**; (Eisenschmidt-Bönn et al., 2019), we did not expect large effects of mutations in *NSP* genes on glucosinolate content and its time course during germination. Surprisingly, we found non-functional alleles of *NSP1* and *NSP2* to have significant effects on glucosinolate content in dry seeds, seeds stratified in water and germinating seeds, respectively. Mutant lines deficient in *NSP1* or *NSP2* had significantly higher glucosinolate contents in seeds than Col-0 (**Figures 2B**, **C**), but did not differ from Col-0 seeds in weight (**Figure S1**). As the two NSPs are expressed at different time points during seed development (**Figure 3**), we assume that the high glucosinolate content is due to effects exerted at different stages of seed development including effects on the mother plant. For example, NSP1 could be involved in turnover reactions that take place during early silique development, while NSP2 would act at later time points of seed maturation. If these NSPs are involved in turnover pathways by converting the glucosinolate aglucone to a nitrile (**Figure 1**), our results could indicate downregulation of glucosinolate hydrolysis in response to accumulation of undesirable breakdown products, e.g. isothiocyanates. Besides *TGG1/TGG2*, several *BGLUs* of the BGLU18–BGLU33 clade are expressed in early stages of silique development (*BGLU18*, *BGLU26*, *BGLU28*, *BGLU29*, *BGLU30*, *BGLU33*; **Figure 9**) and could be affected by *NSP1* deficiency. At the later stages of seed maturation, when *NSP2* is expressed, *BGLU19* and *BGLU30* are induced in Col-0 (**Figure 9**). Future experiments will have to show if these genes are downregulated in developing seeds of the *nsp2* mutant lines. There is presently no experimental support for a regulatory role of NSP1 and NSP2 that is independent of their enzymatic activity, but we cannot rule out alternative mechanisms of action based on current knowledge.

In our stratification time course experiments with *nsp2* mutants, we found elevated glucosinolate levels in both *nsp2* lines relative to Col-0 at 24 h of incubation in water at 4°C in the dark (**Figure 5**). This was, on one hand, a consequence of the increased content in the seeds. On the other hand, we found glucosinolates to increase in *nsp2-2* especially between 8 and 24 h of incubation while glucosinolate content decreased in Col-0. Although only

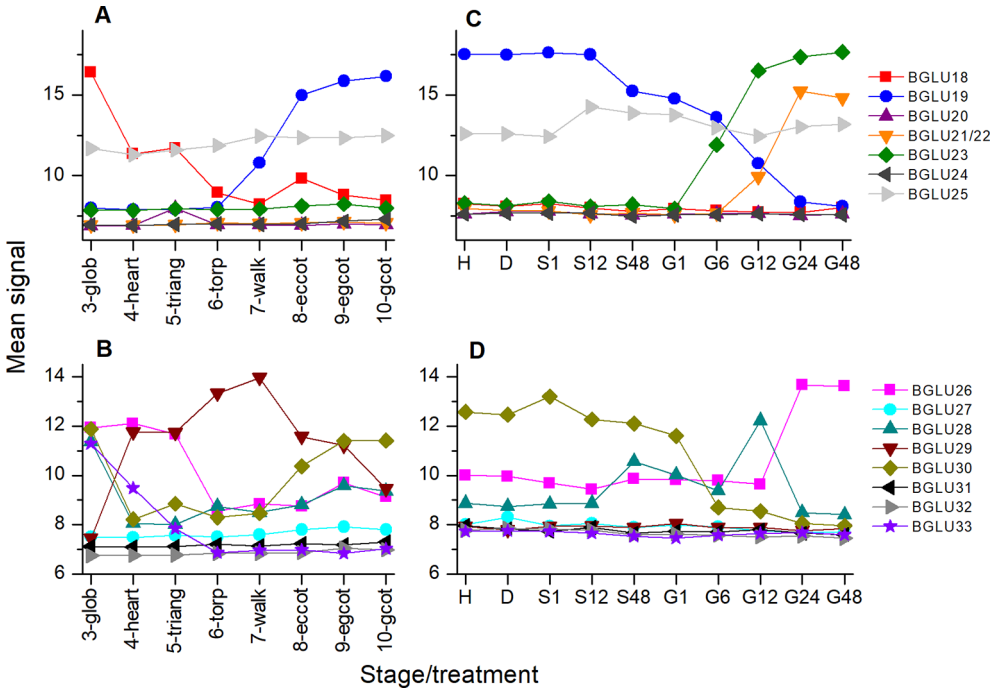

FIGURE 9 | Expression of *BGLU* genes during maturation and germination of *A. thaliana* Col-0 seeds. Microarray data (ATH1) from (Kleindt et al., 2010) (GEO accession: GSE5634) **(A**, **B)** and (Narsai et al., 2011) (GEO accession: GSE30223) **(C**, **D)** for *BGLU18-25* **(A**, **C)** and *BGLU26-BGLU33* **(B**, **D)** were extracted from Genevestigator (Hruz et al., 2008). Each data point represents the mean of three replicates. **(A**, **B)** Seed maturation, samples consisted of siliques with seeds (stages 3–5) or seeds (stages 6–10). Stages are defined by embryo development according to (Kleindt et al., 2010): glob, globular to early heart; heart, early to late heart; triang, triangular (late heart to mid torpedo); torp, mid to late torpedo; walk, late torpedo to early walking stick; eccot, walking stick to early curled cotyledons; egcot, curled cotyledons to early green cotyledons; gcot, green cotyledons. **(C**, **D)** Germination. Stages/treatments are as follows (with numbers indicating the duration of the treatment in hours): H, freshly harvested; D, dried (15 days in darkness); S, stratification (on MS plates, 4°C in the dark); G, germination (22°C, continuous light). *BGLU21* and *BGLU22* are represented by the same probe (260130_s_at).

one of the *nsp2* lines showed this increase, this result might again indicate that a non-functional pathway of nitrile formation may result in downregulation of hydrolysis. At 24 h of stratification, *TGG1/TGG2* as well as *BGLU19*, *BGLU28* and *BGLU30* could be involved (**Figure 9**).

The germination time course experiments with *nsp1-1* showed that *NSP1* deficiency affects the time course significantly (**Figure 7**, **Figure S4**). While total glucosinolate content increased in Col-0 seeds between days 0 and 4 of germination on MS medium and then decreased, the content in *nsp1-1* seeds did not increase or decrease over the entire observation period (**Figure 7**). If *NSP1* is involved in turnover during germination, its lacking expression appears to have a different effect at this stage when compared to seeds or lacking *NSP2* expression during stratification. But as indicated above and illustrated in **Figure 9**, other BGLUs might be involved in glucosinolate turnover during germination than during seed maturation and stratification, and maybe they react differently to the inability to form nitriles. Additionally, genes/enzymes involved in biosynthesis could be affected as well, and biosynthesis could be downregulated as a consequence of *NSP1* deficiency. Of note, accumulation of isothiocyanates (instead of nitriles) would likely reduce the amount of glutathione available for glucosinolate biosynthesis as isothiocyanates readily react with glutathione, either spontaneously or enzymatically catalyzed (Czerniawski and Bednarek, 2018; Urbancsok et al., 2018).

In addition to the evaluation of total glucosinolate contents, we have also recorded the levels of the most abundant individual glucosinolates and compared them between different time points and the different genotypes analyzed. Although we found individual glucosinolates or biosynthetically linked pairs of glucosinolates to largely mirror the trends found for total glucosinolate content in mutants vs. Col-0, we noticed some interesting exceptions. For example, *tgg1 tgg2* had increased total glucosinolate contents in dry seeds and after 24 h of stratification in water compared to Col-0, but the level of 4bzo did not differ between the two genotypes (**Figure S2**, **Figure 6**). In case of *nsp1-1*, 4mtb+4msob did not contribute to the increased glucosinolate content in dry seeds relative to Col-0, but 3bzo and 4bzo were increased overproportionally in *nsp1-1* relative to Col-0 (**Figure S2**). During germination, the levels of 3bzo and i3m in *nsp1-1* underwent a time course similar to Col-0 while all other glucosinolates and the total glucosinolate content did not change in *nsp1-1* (**Figure 8**). At present, we can only speculate that these observations might be explained by different substrate specificities of the hydrolytic enzymes involved in turnover pathways or by specific localization of certain glucosinolates in some stages of development.

Although our data confirm glucosinolate turnover during seed-seedling transition and provide some indication for involvement of NSPs, more experiments are required to establish a direct participation of NSPs in turnover pathways. For example,

experiments should be directed at capturing metabolites formed specifically in developing and germinating seeds of mutants impaired in nitrile formation, but not or to lesser extent in Col-0. Furthermore, the effects of non-functional *NSP* alleles on expression of other genes involved in glucosinolate breakdown and glucosinolate biosynthesis should be studied in detail in these stages. In order to establish pathways of glucosinolate turnover, it would also be essential to biochemically characterize more BGLUs of the BGLU18–BGLU33 cluster to find out if they accept glucosinolates as substrates. It has to be clarified how substrate and enzyme(s) come together in intact tissue to allow hydrolysis of glucosinolates to occur with a high level of spacial and temporal control. Although the analysis of whole individuals allowed us to rule out reallocation between organs as a possible course of changed glucosinolate content, we might have missed tissue-specific effects (e.g. a surplus of turnover in one tissue balanced out by a surplus of biosynthesis in another tissue) in this setup. The design of experiments directed at tissue specific variation will be facilitated by a better knowledge of genes and enzymes involved in turnover pathways. Last but not least, the physiological roles of glucosinolate turnover in germinating seeds deserves more attention. Apart from a role in nutrient supply [which has been discussed controversially (Aghajanzadeh et al., 2014)], turnover could represent a mechanism of regulating glucosinolate levels or it could generate signals upon which biosynthesis rates are adjusted. Interestingly, glucosinolate concentrations per unit dry weight differed significantly between Col-0, *tgg1 tgg2* and *nsp1-1* at day 0 of the germination time course, but were equal at day 10 (**Figure S7**). This would be in agreement with mechanisms that allow the plant to sense glucosinolate concentration and to maintain it at a fixed level as suggested previously (Brown et al., 2003).

The presence and abundance of different glucosinolate types and the structural outcome of glucosinolate hydrolysis in tissue homogenates are subject to an enormous natural variation (Lambrix et al., 2001; Witzel et al., 2015; Wentzell and Kliebenstein, 2008). It would, therefore, be worthwhile to extend investigations on glucosinolate turnover during seed-seedling transition to other accessions of *A. thaliana* and to other species of the Brassicaceae as well as other families of the Brassicales. To our knowledge, natural variation of the *NSP* genes in *A. thaliana* or other Brassicaceae has not been assessed systematically yet. In case of the epithiospecifier protein (ESP), a large proportion of the *A. thaliana* accessions analyzed so far (including Col-0) does not possess a functional allele at the *ESP* locus. The presence of a functional allele seems to correlate with the presence of alkenyl glucosinolates (Lambrix et al., 2001) which give rise to formation of epithionitriles upon hydrolysis in the presence of ESP. It remains to be tested if both NSPs and ESP affect glucosinolate turnover in *A. thaliana* accessions with alkenyl glucosinolates as predominant glucosinolates. Interestingly, there is presently no indication for the presence of functional specifier proteins in other families than the Brassicaceae (Kuchernig et al., 2012). This raises the question if turnover of seed glucosinolates during germination is a general phenomenon of glucosinolate-producing plants and if so, if the mechanisms are evolutionarily conserved. In the absence of specifier proteins, isothiocyanates are likely to be formed as initial hydrolysis products upon turnover. The ability to generate nitriles instead and to recycle them into primary metabolism could potentially represent an innovation that contributed to the evolutionary success of the Brassicaceae.

In conclusion, our study demonstrates that the decline of glucosinolate content in *A. thaliana* Col-0 seeds during germination (days 4 to 10) does not depend on functional TGG1 and TGG2. This indicates involvement of other enzymes, e.g. members of the BGLU18–BGLU33 clade of β-glucosidases, in glucosinolate turnover at this stage of development. Furthermore, the observed time course with highest glucosinolate content at day 4 of germination requires functional *NSP1*. Increased glucosinolate levels in dormant and stratified seeds deficient in TGG1/TGG2, NSP1 or NSP2 suggest turnover to take place during seed maturation and stratification and to depend on these enzymes. However, more research is required to provide evidence for a direct participation of TGG1/TGG2, NSP1 and NSP2 in corresponding turnover pathways. Based on our study, we hypothesize that different enzymes are involved in such pathways at different stages of seed maturation and germination.

DATA AVAILABILITY STATEMENT

All datasets generated for this study are included in the article/ **Supplementary Material**.

AUTHOR CONTRIBUTIONS

UW conceived the study. KM and ME designed and conducted experiments. KM, ME, and UW analyzed data. UW and ME performed statistical analysis. UW analyzed gene expression data. UW wrote the manuscript. All authors contributed to manuscript revision, read and approved the submitted version.

FUNDING

This research was funded by Technische Universität Braunschweig. We acknowledge support by the German Research Foundation and the Open Access Publication Funds of the Technische Universität Braunschweig.

ACKNOWLEDGMENTS

The authors wish to thank Dr. Georg Jander (Boyce Thompson Institute, Ithaka) for providing seeds of the *tgg1 tgg2* mutant. We also acknowledge the contributions of our undergraduate students Paula García Gamarro, Jesús Felipe Mozo Casado, Tom Eisenack and Lee Roy Oldfield to some pilot experiments that paved the way for the present study.

SUPPLEMENTARY MATERIAL

The Supplementary Material for this article can be found online at: https://www.frontiersin.org/articles/10.3389/fpls.2019.01549/full#supplementary-material

REFERENCES

Aghajanzadeh, T., Hawkesford, M. J., and De Kok, L. J. (2014). The significance of glucosinolates for sulfur storage in Brassicaceae seedlings. *Front. In Plant Sci.* 5 (704), 1–10. doi: 10.3389/fpls.2014.00704

Ahn, Y. O., Shimizu, B. I., Sakata, K., Gantulga, D., Zhou, Z., Bevan, D. R., et al. (2010). Scopolin-hydrolyzing β-glucosidases in roots of Arabidopsis. *Plant Cell Physiol.* 51 (1), 132–143. doi: 10.1093/pcp/pcp174

Barth, C., and Jander, G. (2006). Arabidopsis myrosinases TGG1 and TGG2 have redundant function in glucosinolate breakdown and insect defense. *Plant J.* 46 (4), 549–562. doi: 10.1111/j.1365-313X.2006.02716.x

Bednarek, P., Piślewska-Bednarek, M., Svatoš, A., Schneider, B., Doubsky, J., Mansurova, M., et al. (2009). A glucosinolate metabolism pathway in living plant cells mediates broad-spectrum antifungal defense. *Science* 323 (5910), 101–106. doi: 10.1126/science.1163732

Brandt, S., Fachinger, S., Tohge, T., Fernie, A. R., Braun, H. P., and Hildebrandt, T. M. (2018). Extended darkness induces internal turnover of glucosinolates in Arabidopsis thaliana leaves. *PloS One* 13 (8), 1–15. doi: 10.1371/journal.pone.0202153

Brown, P. D., Tokuhisa, J. G., Reichelt, M., and Gershenzon, J. (2003). Variation of glucosinolate accumulation among different organs and developmental stages of Arabidopsis thaliana. *Phytochemistry* 62 (3), 471–481. doi: 10.1016/S0031-9422(02)00549-6

Burmeister, W. P., Cottaz, S., Driguez, H., Iori, R., Palmieri, S., and Henrissat, B. (1997). The crystal structures of Sinapis alba myrosinase and a covalent glycosyl-enzyme intermediate provide insights into the substrate recognition and active-site machinery of an S-glycosidase. *Structure* 5 (5), 663–675. doi: 10.1016/S0969-2126(97)00221-9

Burow, M., Müller, R., Gershenzon, J., and Wittstock, U. (2006). Altered glucosinolate hydrolysis in genetically engineered Arabidopsis thaliana and its influence on the larval development of Spodoptera littoralis. *J. Chem. Ecol.* 32 (11), 2333–2349. doi: 10.1007/s10886-006-9149-1

Burow, M., Losansky, A., Mueller, R., Plock, A., Kliebenstein, D. J., and Wittstock, U. (2009). The genetic basis of constitutive and herbivore-induced ESP-independent nitrile formation in Arabidopsis. *Plant Physiol.* 149 (1), 561–574. doi: 10.1104/pp.108.130732

Clay, N. K., Adio, A. M., Denoux, C., Jander, G., and Ausubel, F. M. (2009). Glucosinolate metabolites required for an Arabidopsis innate immune response. *Science* 323 (5910), 95–101. doi: 10.1126/science.1164627

Czerniawski, P., and Bednarek, P. (2018). Glutathione S-transferases in the biosynthesis of sulfur-containing secondary metabolites in brassicaceae plants. *Front. In Plant Sci.* 9 (1639), 1–8. doi: 10.3389/fpls.2018.01639

Eisenschmidt-Bönn, D., Schneegans, N., Backenköhler, A., Wittstock, U., and Brandt, W. (2019). Structural diversification during glucosinolate breakdown: mechanisms of thiocyanate, epithionitrile and simple nitrile formation. *Plant J.* 99 (2), 329–343. doi: 10.1111/tpj.14327

Falk, K. L., Tokuhisa, J. G., and Gershenzon, J. (2007). The effect of sulfur nutrition on plant glucosinolate content: physiology and molecular mechanisms. *Plant Biol.* 9 (5), 573–581. doi: 10.1055/s-2007-965431

Hirai, M. Y., Yano, M., Goodenowe, D. B., Kanaya, S., Kimura, T., Awazuhara, M., et al. (2004). Integration of transcriptomics and metabolomics for understanding of global responses to nutritional stresses in Arabidopsis thaliana. *Proc. Natl. Acad. Sci. U. States America* 101 (27), 10205–10210. doi: 10.1073/pnas.0403218101

Hruz, T., Laule, O., Szabo, G., Wessendorp, F., Bleuler, S., Oertle, L., et al. (2008). Genevestigator V3: a reference expression database for the meta-analysis of transcriptomes. *Adv. In Bioinf.* 2008 (420747), 1–5. doi: 10.1155/2008/420747

Huseby, S., Koprivova, A., Lee, B. R., Saha, S., Mithen, R., Wold, A. B., et al. (2013). Diurnal and light regulation of sulphur assimilation and glucosinolate biosynthesis in Arabidopsis. *J. Exp. Bot.* 64 (4), 1039–1048. doi: 10.1093/jxb/ers378

Jørgensen, K., Bak, S., Busk, P. K., Sørensen, C., Olsen, C. E., Puonti-Kaerlas, J., et al. (2005). Cassava plants with a depleted cyanogenic glucoside content in leaves and tubers. Distribution of cyanogenic glucosides, their site of synthesis and transport, and blockage of the biosynthesis by RNA interference technology. *Plant Physiol.* 139 (1), 363–374. doi: 10.1104/pp.105.065904

Janowitz, T., Trompetter, I., and Piotrowski, M. (2009). Evolution of nitrilases in glucosinolate-containing plants. *Phytochemistry* 70 (15-16), 1680–1686. doi: 10.1016/j.phytochem.2009.07.028

Kissen, R., and Bones, A. M. (2009). Nitrile-specifier proteins involved in glucosinolate hydrolysis in Arabidopsis thaliana. *J. Biol. Chem.* 284 (18), 12057–12070. doi: 10.1074/jbc.M807500200

Kleindt, C. K., Stracke, R., Mehrtens, F., and Weisshaar, B. (2010). Expression analysis of flavonoid biosynthesis genes during Arabidopsis thaliana silique and seed development with a primary focus on the proanthocyanidin biosynthetic pathway. *BMC Res. Notes* 3 (255), 1–12. doi: 10.1186/1756-0500-3-255

Kuchernig, J. C., Burow, M., and Wittstock, U. (2012). Evolution of specifier proteins in glucosinolate-containing plants. *BMC Evol. Biol.* 12, 127. doi: 10.1186/1471-2148-12-127

Lambrix, V., Reichelt, M., Mitchell-Olds, T., Kliebenstein, D. J., and Gershenzon, J. (2001). The Arabidopsis epithiospecifier protein promotes the hydrolysis of glucosinolates to nitriles and influences Trichoplusia ni herbivory. *Plant Cell* 13, 2793–2807. doi: 10.1105/tpc.010261

Müller, R., de Vos, M., Sun, J. Y., Sønderby, I. E., Halkier, B. A., Wittstock, U., et al. (2010). Differential effects of indole and aliphatic glucosinolates on lepidopteran herbivores. *J. Chem. Ecol.* 36 (8), 905–913. doi: 10.1007/s10886-010-9825-z

Murashige, T., and Skoog, F. (1962). A revised medium for rapid growth and bio assays with tobacco tissue cultures. *Physiol. Plantarum* 15 (3), 473–497. doi: 10.1111/j.1399-3054.1962.tb08052.x

Nakano, R. T., Piślewska-Bednarek, M., Yamada, K., Edger, P. P., Miyahara, M., Kondo, M., et al. (2017). PYK10 myrosinase reveals a functional coordination between endoplasmic reticulum bodies and glucosinolates in Arabidopsis thaliana. *Plant J.* 89 (2), 204–220. doi: 10.1111/tpj.13377

Nakazaki, A., Yamada, K., Kunieda, T., Sugiyama, R., Hirai, M. Y., Tamura, K., et al. (2019). Leaf endoplasmic reticulum bodies identified in Arabidopsis rosette leaves are involved in defense against herbivory. *Plant Physiol.* 179 (4), 1515–1524. doi: doi.org/10.1104/pp.18.00984

Narsai, R., Law, S. R., Carrie, C., and Xu, L. (2011). In-depth temporal transcriptome profiling reveals a crucial developmental switch with roles for RNA processing and organelle metabolism that are essential for germination in Arabidopsis. *Plant Physiol.* 157 (3), 1342–1362. doi: 10.1104/pp.111.183129

Negi, V. S., Bingham, J. P., Li, Q. X., and Borthakur, D. (2014). A carbon-nitrogen lyase from Leucaena leucocephala catalyzes the first step of mimosine degradation. *Plant Physiol.* 164 (2), 922–934. doi: 10.1104/pp.113.230870

Nour-Eldin, H. H., Andersen, T. G., Burow, M., Madsen, S. R., Jørgensen, M. E., Olsen, C. E., et al. (2012). NRT/PTR transporters are essential for translocation of glucosinolate defence compounds to seeds. *Nature* 488 (7412), 531–534. doi: 10.1038/nature11285

Petersen, B. L., Chen, S. X., Hansen, C. H., Olsen, C. E., and Halkier, B. A. (2002). Composition and content of glucosinolates in developing Arabidopsis thaliana. *Planta* 214 (4), 562–571. doi: 10.1007/s004250100659

Reichelt, M., Brown, P. D., Schneider, B., Oldham, N. J., Stauber, E., Tokuhisa, J., et al. (2002). Benzoic acid glucosinolate esters and other glucosinolates from Arabidopsis thaliana. *Phytochemistry* 59 (6), 663–671. doi: 10.1016/S0031-9422(02)00014-6

Rosenthal, G. A. (1992). Purification and characterization of the higher plant enzyme L-canaline reductase. *Proc. Natl. Acad. Sci. U. States America* 89 (5), 1780–1784. doi: 10.1073/pnas.89.5.1780

Sarosh, B. R., Wittstock, U., Halkier, B. A., and Ekbom, B. (2010). The influence of metabolically engineered glucosinolates profiles in Arabidopsis thaliana on Plutella xylostella preference and performance. *Chemoecology* 20 (1), 1–9. doi: 10.1007/s00049-009-0028-4

Schlaeppi, K., Bodenhausen, N., Buchala, A., Mauch, F., and Reymond, P. (2008). The glutathione-deficient mutant pad2-1 accumulates lower amounts of glucosinolates and is more susceptible to the insect herbivore Spodoptera littoralis. *Plant J.* 55 (5), 774–786. doi: 10.1111/j.1365-313X.2008.03545.x

Stotz, H. U., Sawada, Y., Shimada, Y., Hirai, M. Y., Sasaki, E., Krischke, M., et al. (2011). Role of camalexin, indole glucosinolates, and side chain modification of glucosinolate-derived isothiocyanates in defense of Arabidopsis against Sclerotinia sclerotiorum. *Plant J.* 67, 81–93. doi: 10.1111/j.1365-313X.2011.04578.x

Sugiyama, R., and Hirai, M. Y. (2019). Atypical myrosinase as a mediator of glucosinolate functions in plants. *Front. In Plant Sci.* 10 (1008), 1–14. doi: 10.3389/fpls.2019.01008

Thies, W. (1979). Detection and utilization of a glucosinolate sulfohydrolase in the edible snail, Helix pomatia. *Naturwissenschaften* 66, 364–365. doi: 10.1007/BF00368477

Urbancsok, J., Bones, A. M., and Kissen, R. (2017). Glucosinolate-derived isothiocyanates inhibit Arabidopsis growth and the potency depends on their side chain structure. *Int. J. Mol. Sci.* 18 (11), 1–18. doi: 10.3390/ijms18112372

Urbancsok, J., Bones, A. M., and Kissen, R. (2018). Arabidopsis mutants impaired in glutathione biosynthesis exhibit higher sensitivity towards the glucosinolate hydrolysis product allyl-isothiocyanate. *Sci. Rep.* 8 (1), 1–13. doi: 10.1038/s41598-018-28099-1

Wentzell, A. M., and Kliebenstein, D. J. (2008). Genotype, age, tissue, and environment regulate the structural outcome of glucosinolate activation. *Plant Physiol.* 147, 415–428. doi: 10.1104/pp.107.115279

Wittstock, U., and Burow, M. (2010). "Glucosinolate breakdown in Arabidopsis - mechanism, regulation and biological significance," in *The Arabidopsis Book* (http://www.aspb.org/publications/arabidopsis/). Eds. R. Last, C. Chang, G. Jander, D. Kliebenstein, R. McClung, H. Millar, K. Torii, and D. Wagner (The American Society of Plant Biologists, Rockville, USA). doi: 10.1199/tab.0134

Wittstock, U., Kurzbach, E., Herfurth, A.-M., and Stauber, E. J. (2016a). "Glucosinolate breakdown," in *Advances in Botanical Research*. Ed. S. Kopriva (London: Academic Press), 125–169. doi: 10.1016/bs.abr.2016.06.006

Wittstock, U., Meier, K., Dörr, F., and Ravindran, B. M. (2016b). NSP-dependent simple nitrile formation dominates upon breakdown of major aliphatic glucosinolates in roots, seeds, and seedlings of Arabidopsis thaliana Columbia-0. *Front. In Plant Sci.* 7, 1821. doi: 10.3389/fpls.2016.01821

Witzel, K., Hanschen, F. S., Klopsch, R., Ruppel, S., Schreiner, M., and Grosch, R. (2015). Verticillium longisporum infection induces organ-specific glucosinolate degradation in arabidopsis thaliana. *Front. In Plant Sci.* 6, 508. doi: 10.3389/fpls.2015.00508

Zipor, G., Duarte, P., Carqueijeiro, I., Shahar, L., Ovadia, R., Teper-Bamnolker, P., et al. (2015). In planta anthocyanin degradation by a vacuolar class III peroxidase in Brunfelsia calycina flowers. *New Phytol.* 205 (2), 653–665. doi: 10.1111/nph.13038

Conflict of Interest: The authors declare that the research was conducted in the absence of any commercial or financial relationships that could be construed as a potential conflict of interest.

frontiers in Plant Science

ORIGINAL RESEARCH
published: 06 December 2019
doi: 10.3389/fpls.2019.01560

Coordination of Glucosinolate Biosynthesis and Turnover Under Different Nutrient Conditions

*Verena Jeschke, Konrad Weber, Selina Sterup Moore and Meike Burow**

DynaMo Center, Department of Plant and Environmental Sciences, University of Copenhagen, Frederiksberg, Denmark

Dynamically changing environmental conditions promote a complex regulation of plant metabolism and balanced resource investments to development and defense. Plants of the Brassicales order constitutively allocate carbon, nitrogen, and sulfur to synthesize glucosinolates as their primary defense metabolites. Previous findings support a model in which steady-state levels of glucosinolates in intact tissues are determined by biosynthesis and turnover through a yet uncharacterized turnover pathway. To investigate glucosinolate turnover in the absence of tissue damage, we quantified exogenously applied allyl glucosinolate and endogenous glucosinolates under different nutrient conditions. Our data shows that, in seedlings of *Arabidopsis thaliana* accession Columbia-0, glucosinolate biosynthesis and turnover are coordinated according to nutrient availability. Whereas exogenous carbon sources had general quantitative effects on glucosinolate accumulation, sulfur or nitrogen limitation resulted in distinct changes in glucosinolate profiles, indicating that these macronutrients provide different regulatory inputs. Raphanusamic acid, a breakdown product that can potentially be formed from all glucosinolate structures appears not to reflect *in planta* turnover rates, but instead correlates with increased accumulation of endogenous glucosinolates. Thus, raphanusamic acid could represent a metabolic checkpoint that allows glucosinolate-producing plants to measure the flux through the biosynthetic and/or turnover pathways and thereby to dynamically adjust glucosinolate accumulation in response to internal and external signals.

Keywords: glucosinolate metabolism, nutrient conditions, seedling development, nitrogen limitation, sulfur limitation, metabolic regulation

OPEN ACCESS

Edited by:
Tamara Gigolashvili, University of Cologne, Germany

Reviewed by:
Kei Hiruma, Nara Institute of Science and Technology (NAIST), Japan
Paweł Bednarek, Institute of Bioorganic Chemistry (PAS), Poland
Ute Wittstock, Technische Universitat Braunschweig, Germany

****Correspondence:***
Meike Burow
mbu@plen.ku.dk

Specialty section:
This article was submitted to Plant Metabolism and Chemodiversity, a section of the journal Frontiers in Plant Science

Received: *29 July 2019*
Accepted: *07 November 2019*
Published: *06 December 2019*

Citation:
Jeschke V, Weber K, Moore SS and Burow M (2019) Coordination of Glucosinolate Biosynthesis and Turnover Under Different Nutrient Conditions. Front. Plant Sci. 10:1560. doi: 10.3389/fpls.2019.01560

INTRODUCTION

Plants rely on a multitude of constitutive and inducible specialized metabolites that mediate interactions with the environment. These range from deterring pathogen and herbivores, over attracting beneficial organisms and enemies, to providing protection from, for example, UV radiation or drought. The chemodiversity of specialized metabolites and their regulation in terms of quantity and composition across tissues and developmental stages is beyond comparison (Moore et al., 2014). *Arabidopsis thaliana*, a small herbaceous plant of the Brassicaceae family, is a widely used and well-studied model organism for plant specialized metabolism, particularly the metabolism of glucosinolates (D'Auria and Gershenzon, 2005; Jensen et al., 2014; Burow and Halkier, 2017). Glucosinolates are chemically diverse amino acid-derived, sulfur- and nitrogen-containing thioglucosides almost solely found in plants of the order Brassicales with more than 130

identified structures to date (Blažević et al., 2019). The activation of glucosinolates has been intensively studied, both for their defensive roles against pathogens and herbivores and for their health beneficial roles for humans (Burow et al., 2010; Pastorczyk and Bednarek, 2016; Traka, 2016; Wittstock et al., 2016a). In recent years, more and more studies uncovering additional roles of glucosinolates and glucosinolate-derived metabolites in feedback regulation of plant metabolism, growth and defense emerged (Zhao et al., 2008; Kerwin et al., 2011; Burow et al., 2015; Jensen et al., 2015; Katz et al., 2015; Francisco et al., 2016a; Malinovsky et al., 2017; Urbancsok et al., 2017; Urbancsok et al., 2018). These studies have connected primary and specialized metabolism *via* glucosinolate-mediated signaling networks, and provided first insights into the regulatory interplay between glucosinolate metabolism and plant development.

As precursors of defensive metabolites, glucosinolates are constitutively biosynthesized in almost all tissues of *A. thaliana* throughout all developmental stages of the plant. Sufficient amounts of glucosinolates must be present in a given tissue for the glucosinolate-myrosinase system to function as defense. In the flower stalk, S-cells store glucosinolates accounting for 40% of the total sulfur in that tissue and these have also been identified in petioles (Koroleva et al., 2000; Koroleva et al., 2010). A considerable proportion of glucosinolates thus seems to be stored in these idioblasts. Nevertheless, glucosinolate quantity and composition vary dynamically depending on the age of the plant, the tissue studied and the environmental conditions (Petersen et al., 2002; Brown et al., 2003; Kliebenstein et al., 2005; Mewis et al., 2005; Gigolashvili et al., 2009; Textor and Gershenzon, 2009; Mewis et al., 2012; Züst et al., 2012; Huseby et al., 2013; Augustine and Bisht, 2016; Burow, 2016). Furthermore, a growing number of studies have identified additional functions of glucosinolates; often of distinct of glucosinolate structures, that are not directly linked to plant defense, but instead to hormone signaling, stomatal aperture, the circadian clock, root growth, biomass, and the onset of flowering (Zhao et al., 2008; Kerwin et al., 2011; Burow et al., 2015; Jensen et al., 2015; Katz et al., 2015; Francisco et al., 2016a; Francisco et al., 2016b; Malinovsky et al., 2017; Urbancsok et al., 2017; Urbancsok et al., 2018). These observations illustrate how intricately glucosinolate metabolism connects to a multitude of metabolic and developmental processes; and they may explain the dynamic nature of glucosinolate profiles, also in the absence of a biotic attacker.

Glucosinolate content reaches levels of up to 3% of the dry weight (Brown et al., 2003; Falk et al., 2007) making it a potentially costly investment for the plant (Bekaert et al., 2012; Züst and Agrawal, 2017). Because glucosinolates contain sulfur and nitrogen, their metabolism is tightly linked with sulfur and nitrogen assimilation and metabolism (Kopriva and Gigolashvili, 2016; Marino et al., 2016). Changes in abundance and composition depending on sulfur and nitrogen availability has been intensely studied in *A. thaliana* and glucosinolate-producing vegetables. Generally, sulfur availability and assimilation is positively correlated with aliphatic glucosinolate levels, while nitrogen availability is positively correlated with indolic glucosinolate levels [for example: (Booth et al., 1991; Withers and O'Donnell, 1994; Koprivova et al., 2000; Krumbein et al., 2001; Kopsell et al., 2007; Omirou et al., 2009; Frerigmann and Gigolashvili, 2014)]. However, increasing nitrogen concentrations have also been shown to have negative effects on total and aliphatic glucosinolate levels depending on the proportion of other macronutrients present such as sulfur, potassium and phosphorous (Li et al., 2007; Schonhof et al., 2007; Chun et al., 2017). Further, the type of nitrogen source (nitrate versus ammonium) can affect glucosinolate levels (Marino et al., 2016). Besides aforementioned inorganic macronutrients, different sugars have been shown to have a positive effect on glucosinolate levels in broccoli sprouts (Guo et al., 2011). Up to 30% of the total sulfur pool are bound in glucosinolates, which were therefore discussed as potential sulfur storage that can be remobilized under conditions of sulfur deficiency or starvation (Falk et al., 2007). The general ability of *A. thaliana* to metabolize glucosinolates has been directly demonstrated. When *p*-hydroxybenzyl glucosinolate (sinalbin) was provided as the only sulfur source, seedlings accumulated higher levels of sulfur-containing metabolites, including glucosinolates, than seedlings on glucosinolate-free, sulfur-deficient medium (Zhang et al., 2011). However, endogenous glucosinolates were shown not to be a sulfur source in Brassica seedlings when other sources of organic sulfur were present (Aghajanzadeh et al., 2014). This suggests that seedlings are capable of utilizing glucosinolates as a nutrient under conditions of deficiency, but glucosinolates are not a preferred source for sulfur remobilization. Unlike cyanogenic glycosides (Pičmanová et al., 2015), glucosinolates have not been investigated for a potential function as storage form of nitrogen.

Studies on glucosinolate breakdown have traditionally focused on the enzymatic activation of glucosinolates to bioactive compounds initiated by myrosinases upon tissue damage, i.e. caused by feeding insects (Matile, 1980; Kissen et al., 2009; Wittstock and Burow, 2010). Turnover in intact tissue (i.e. their *in planta* metabolization in absence of tissue-damage induced breakdown) is less well understood and the pathways and their regulation are yet to be uncovered (**Figure 1**). Earlier studies that investigated the dynamics of glucosinolates in *A. thaliana* during plant development or in adult rosettes at different times of day suggested turnover processes in concurrence with *de novo* biosynthesis (Petersen et al., 2002; Brown et al., 2003; Huseby et al., 2013). For example, relative and absolute amounts of glucosinolates change considerably during the transitions from seeds to seedlings and from seedlings to adult rosette (Brown et al., 2003). Furthermore, in *A. thaliana* Col-0, some methionine-derived glucosinolates (embryo-synthesized glucosinolates, **Supplementary Figure 1**) are only present in seeds and seedlings but not in vegetative rosette tissue of young plants indicative of *in planta* turnover of glucosinolates in seedlings (Petersen et al., 2002; Brown et al., 2003). Indeed, labeled [^{14}C] *p*-hydroxybenzyl glucosinolate fed to rosette leaves of flowering plants accumulated in the seeds and subsequently showed a decline to 70% within the first weeks of plant development in the next generation (Petersen et al., 2002).

It is currently unknown which enzymes and pathways are involved in *in planta* turnover of glucosinolates. Hydrolysis of the thioglucosidic bond by a β-glucosidase has been proposed as the first step (**Figure 1**). Experimental evidence suggests that the classical myrosinases TGG1 and TGG2 are not involved in

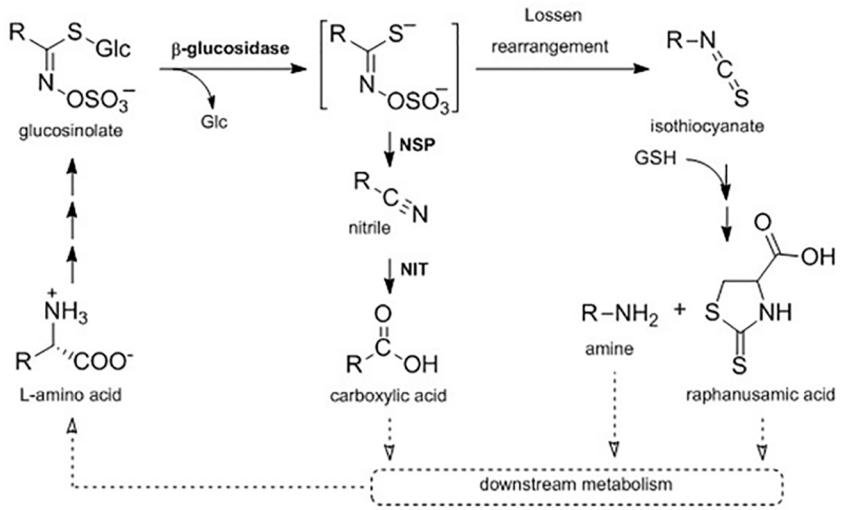

FIGURE 1 | A proposed metabolic pathway connecting primary and specialized metabolism in intact *A. thaliana* Col-0 seedlings. *In planta* turnover of glucosinolates may proceed *via* hydrolytic cleavage of the glucose (Glc) moiety by a ß-glucosidase to form an aglucone, which is either metabolized to the corresponding nitrile in dependency of nitrile-specifier proteins (NSPs) or rearranged to the isothiocyanate. Nitriles can be further metabolized by nitrilases (NIT) to carboxylic acids, while isothiocyanates can be conjugated to glutathione (GSH) and metabolized to the corresponding amine and raphanusamic acid. Further downstream metabolization of those metabolites is not yet elucidated (dotted arrows).

glucosinolate turnover in the absence of tissue damage (Barth and Jander, 2006), but in total, 40 family 1 β-glucosidases are encoded in the *A. thaliana* Col-0 genome (Xu et al., 2004). For three of these enzymes besides classical myrosinases, it has been shown that they can hydrolyze glucosinolates under certain conditions and in certain tissues (Bednarek et al., 2009; Nakano et al., 2017; Nakazaki et al., 2019). In *A. thaliana* Col-0, damage-induced glucosinolate activation by myrosinases results in the formation of aglucones that can either arrange to isothiocyanates or be converted into simple nitriles (**Figure 1**) (Wittstock and Burow, 2007; Wittstock and Burow, 2010; Wittstock et al., 2016a). Nitrile-formation is dependent on action of nitrile-specifier proteins (NSPs), which are expressed in seeds, seedlings, leaves, and roots with an organ-specific regulation in *A. thaliana* Col-0 (Burow et al., 2009; Wittstock et al., 2016b). Glucosinolate-derived nitriles were suggested to be further converted to the corresponding carboxylic acids by nitrilases (NITs), yet these conversions were not considered to contribute to growth regulation *via* auxin signaling (Piotrowski, 2008; Janowitz et al., 2009). More recently, *in silico* modelling did, however, not hint to a major impact of nitrilase activity on auxin signaling (Vik et al., 2018). Spontaneous rearrangement of the aglucones yields isothiocyanates, which are highly reactive electrophiles (Brown and Hampton, 2011). Upon activation of 4-methoxyindol-3-ylmethyl glucosinolate (4MOI3M) by the atypical myrosinase PEN2, the resulting isothiocyanate is conjugated with glutathione and undergoes further metabolization to the corresponding amine bearing the indolic side-chain, a reaction that also yields the sulfur-containing raphanusamic acid (**Figure 1**) (Bednarek et al., 2009; Piślewska-Bednarek et al., 2018). Raphanusamic acid has been reported to have inhibitory properties on plant growth (Inamori et al., 1992) and to be involved in plant immunity (Bednarek, 2012), but the *in planta* mode of action remained elusive.

Here, to investigate the dynamics of glucosinolate biosynthesis and turnover in seedlings of *A. thaliana* Col-0 in the absence of tissue damage, we quantitatively analyzed the profiles of endogenous glucosinolates and the dynamics of the exogenous allyl glucosinolate under different nutrient conditions, specifically sulfur and nitrogen limitation as well as availability of exogenous sugars. Our data shows that glucosinolate biosynthesis and its downstream *in planta* turnover are coordinated according to nutrient availability. Under our experimental conditions, raphanusamic acid accumulation correlated with glucosinolate accumulation, suggesting that this turnover pathway intermediate can provide the plant with information on total glucosinolate levels.

MATERIALS AND METHODS

Plant Treatments

A. thaliana seedling Col-0 (NASC, N1093) were sterilized with chlorine gas (generated by mixing 100 ml 14% sodium hypochlorite and 3 ml 37% HCL) for 3h. Growth medium was prepared as described in a published protocol (dx.doi.org/10.17504/protocols.io.5q6g5ze). Total nitrogen concentrations were 3 mM (+N) and 0.3 mM (−N) and total sulfur concentrations 1.68 mM (+S) and 0.015 mM (−S). ½ MS medium (**Figure 3B**) was purchased from Duchefa Biochemie (product no. M0222) and had a total sulfur concentration of 0.82 mM and total nitrogen concentration of 30 mM. Sugars were added to the growth medium solution prior to autoclaving. The concentrations of sugars used correspond to 1% (w/v, 29.2 mM) and 2% (w/v, 58.4 mM) for the monosaccharides glucose and fructose and the sugar alcohols mannitol and sorbitol, and 1.9% (w/v, 29.2 mM) and 3.8% (w/v, 58.4 mM) for the disaccharide sucrose. To study allyl glucosinolate accumulation and turnover,

100 mM allyl glucosinolate (Sinigrin, Sigma-Aldrich, No. S1647) stock solution in water was added to 50 ml of the autoclaved hand warm medium to the final concentrations indicated in the figures and carefully mixed by inversion. For all media treatments, 50 ml medium was poured into a square plate (120 ×120 × 16 mm, Frisenette, Denmark) and the medium was allowed to cool. After plating of the seeds, plates were placed for four days in the dark at 4°C for stratification and subsequently moved to a growth chamber (16 h light/8 h dark, 22/21°C, average light intensity 160 µE), in a vertical orientation. Germination was scored daily as the emergence of the radicle. Only seedlings that germinated one day after stratification were considered for further analysis. To investigate turnover of glucosinolates under different nutrient conditions, seedlings were carefully transferred after phase 1 (accumulation of exogenously applied allyl glucosinolate) using soft forceps onto plates containing different media compositions but no allyl glucosinolate (phase 2) (**Supplementary Figure 3**). Seedling weight was recorded for a single seedling using a fine-balance prior to metabolite sampling if indicated.

Metabolite Analyses

For glucosinolate and raphanusamic acid analysis, seedlings were harvested into 300 µl 85% (v/v) methanol (HPLC grade) containing 10 µM *p*-hydroxybenzyl glucosinolate (pOHb; PhytoLab, cat. No. 89793) as internal standard and subsequently homogenized in a bead mill (3 mm bearing balls, 2 × 30 s at 30 Hz). After centrifugation (5 min, 4,700×*g*, 4°C), 20 µl of the supernatant was diluted with 180 µL MilliQ-grade water (1:10) and filtered (Durapore® 0.22 µm PVDF filters, Merck Millipore, Tullagreen, Ireland) for the analysis of raphanusamic acid. For glucosinolate analysis, samples were prepared as desulfo-glucosinolates as previously described (alternate protocol 2, Crocoll et al., 2016) and analysed with LC-MS/MS. LC-MS/MS analysis was carried out on an Advance UHPLC system (Bruker, Bremen, Germany) equipped with a Kinetex® XB-C18 column (100 × 2.1 mm, 1.7 µm, 100 Å, Phenomenex, USA) coupled to an EVOQ Elite TripleQuad mass spectrometer (Bruker, Bremen, Germany) equipped with an electrospray ionization source (ESI). The injection volume was 1 µL. Separation was achieved with a gradient of water/0.05% (v/v) formic acid (solvent A)–acetonitrile (solvent B) at a flow rate of 0.4 ml/min at 40°C (formic acid, Sigma-Aldrich, cat. no. F0507, reagent grade; acetonitrile, HPLC grade). The elution profile was: 0–0.5 min 2% B; 0.5–1.2 min 2-30% B; 1.2–2.0 min 30–100% B; 2.0–2.5 min 100% B; 2.5–2.6 min 100–2% B; 2.6–4.0 min 2% B. For raphanusamic acid the instrument parameters were optimized by infusion with the pure standard (Sigma-Aldrich, No. 273449). The mass spectrometer parameters were as follows: ionspray voltage was maintained at 3,500 V, cone temperature was set to 300°C and heated probe temperature to 400°C, cone gas flow was set to 20 psi, probe gas flow to 40 psi, nebulizer gas 60 psi, and collision gas to 1.5 mTorr. Nitrogen was used as cone and nebulizer gas, and argon as collision gas. Multiple reaction monitoring (MRM) was used to monitor analyte parent ion > product ion transitions [collision energy]: (pos) 164 > 118 [15 V] (quantifier) and 164 > 59 [15 V] (qualifier). Both Q1 and Q3 quadrupoles were maintained at unit resolution. Glucosinolates were quantified relative pOHb using experimentally determined response factors with commercially available standards in a representative plant matrix. Raphanusamic acid was quantified based on external calibration using a dilution series of an authentic standard.

Statistical Analysis

Statistical analyses (parametric and non-parametric standard tests) were performed using the software R (version 3.3.2, R Core Team, 2017) after checking the suitability of the model for scedasticity and distribution of the data. Models used for analysis are indicated in the figure and supplementary table legends. Figures were generated using the package "ggplot2." MFA (multiple factor analysis) was performed and visualized using the packages "FactoMineR" and "factoextra."

RESULTS

Exogenous Carbon Sources Affect Total Amounts of Glucosinolates During Seedling Development

Glucosinolate profiles differ markedly between seeds and seedlings of A. thaliana (Haughn et al., 1991; Brown et al., 2003). In the accession Col-0, glucosinolates with hydroxyalkyl and benzoyloxyalkyl side chains are synthesized in the developing seeds and still present in seedlings but not at later developmental stages (**Supplementary Figure 2**) (Kliebenstein et al., 2001; Brown et al., 2003; Kliebenstein et al., 2007). We refer here to these structures as embryo-synthesized glucosinolates. During the transition from seed to seedling, the total glucosinolate content transiently increases, but then drops again to seed level within two to six days after planting. Interestingly, the content of embryo-synthesized glucosinolates is stable during germination (Brown et al., 2003), suggesting that they are not yet catabolized at this early stage of seed-to-seedling transition. To study glucosinolate turnover kinetics, we therefore focused on seedling development after germination.

We analyzed glucosinolates in individual seedlings, starting three days after germination. Overall glucosinolate content continuously increased by 4-fold within six days ($P < 0.001$, **Figure 2A**) and more than 30-fold within 20 days after germination ($P < 0.001$, **Figure 3A**). This increase affects all three main glucosinolate classes of short- and long-chain aliphatic and indolic glucosinolates but is initially mainly driven by indolic glucosinolates (most dominantly NMOI3M; **Supplementary Tables 1** and **2**) and then later also by long-chain aliphatic glucosinolates (**Supplementary Table 3**). The group of embryo-synthesized glucosinolates (**Supplementary Figure 1**), herein 3bzo and 4bzo glucosinolates, slightly decrease with seedling development ($P = 0.062$) until they are not detected at nine days after germination (**Figure 2B**). Interestingly, we detected relatively high levels of embryo-synthesized glucosinolates decreasing at later developmental stages in a different developmental setup (see below).

Noticeable increases of glucosinolate content between five and seven days after germination correlated with the development of

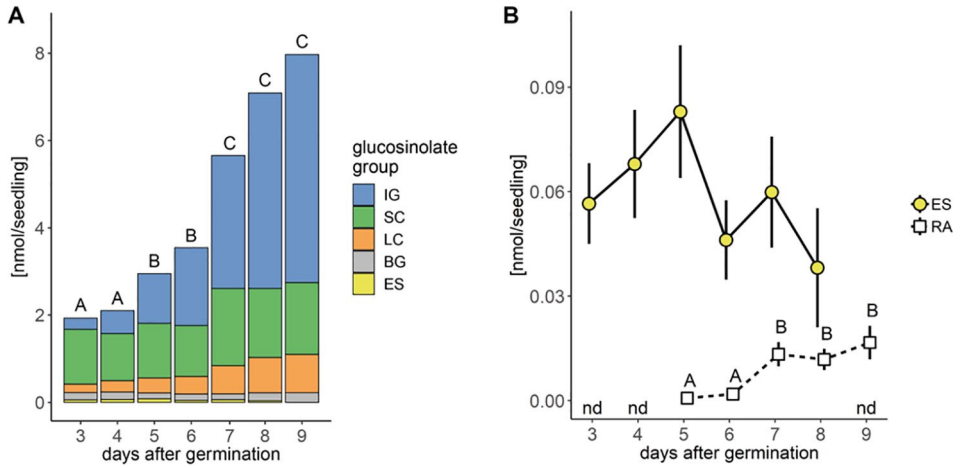

FIGURE 2 | Glucosinolate accumulation during *A. thaliana* Col-0 seedling development. **(A)** Plotted are means (N = 6–18, one experimental round) of glucosinolate classes: IG, indolic glucosinolates; SC, short-chain aliphatic glucosinolates; LC, long-chain aliphatic glucosinolates; BG, benzenic glucosinolates; ES, embryo-synthesized glucosinolates. Letters denote significant differences at the level on total glucosinolate levels ($P < 0.05$). **(B)** Levels of embryo-synthesized glucosinolates (ES; $P = 0.62$) and raphanusamic acid (RA; $P < 0.001$). Embryo-synthesized glucosinolates were not detected (nd) in nine-day-old seedlings and raphanusamic acid was not detected in three- and four-day-old seedlings. Depicted are means ± SE, N = 6–18. Statistical testing was performed with Kruskal–Wallis rank sum test followed by pairwise comparisons using Wilcoxon rank sum test (P-value adjustment method: Benjamini & Hochberg). Details on the statistical analysis including means and standard deviations are provided in **Supplementary Table 1** for glucosinolate groups and **Supplementary Table 2** for individual glucosinolates.

the first lateral roots and the expansion of the first true leaves, respectively. Concurrent with these physiological changes in seedling development and the pattern of glucosinolate accumulation, levels of raphanusamic acid show increases at five and seven days after germination ($P < 0.001$, **Figure 2B**).

The addition of exogenous carbon sources to the growth medium, as frequently done in studies on *A. thaliana* seedlings, had several effects on the dynamics of glucosinolate accumulation (**Figure 3**) and seedling development (**Supplementary Figure 4**). Exogenously supplied sucrose affected the rate and timing of the accumulation of all individual glucosinolates in whole seedlings (**Figures 3A**, **B**, top panel, **Supplementary Table 3**). Most dominantly affected by 29.2 mM sucrose treatment were the dynamics of long-chain aliphatic and indolic glucosinolate accumulation while the changes in short-chain aliphatic glucosinolates over time seemed unaffected (**Supplementary Table 3**). Compared to sucrose treatment, the effects of glucose treatment on glucosinolate levels was similar, while that of fructose was weaker (**Figure 3B**). Twelve-day-old seedlings showed a clear distribution of short-chain aliphatic glucosinolates predominantly in shoots and long-chain aliphatic glucosinolates mostly in roots. This tissue-specific distribution remained unaffected by all sugar treatments, albeit the absolute levels and ratios between all glucosinolate groups changed depending on the sugar applied (**Figure 3B** and **Supplementary Table 5**). The tested sugars additionally had considerable growth and developmental effects (**Supplementary Figure 4**). While seedlings grown in the presence of sucrose or glucose show an increase in lateral root formation and shoot size, fructose and mannitol caused an overall stunted growth phenotype. This suggests that the increase in glucosinolates in sucrose and glucose treated seedlings relates to the increased seedling size, while fructose treated seedlings accumulate considerably lower glucosinolate contents, possibly due to their smaller size (**Figure 3B** and **Supplementary Figure 4**).

Sulfur and Nitrogen Limitation Differentially Affects Total and Relative Glucosinolate Levels

Next, we tested the effect of sulfur and nitrogen limitation, alone and in combination, on glucosinolate accumulation and growth of *A. thaliana* Col-0 seedlings for several days. Before the seedlings were exposed to different nutrient regimes, seeds were germinated and grown for six days on control medium containing sufficient amounts of sulfur and nitrogen. Seedlings were then transferred to different media limited in sulfur and/or nitrogen (**Supplementary Figure 3**) and their development and glucosinolate profile was followed for several days. Nitrogen limitation led to reduced seedling weight (**Supplementary Figure 5**) and significantly affected accumulation of all *de novo* synthesized glucosinolate classes (indolic, short- and long-chain aliphatic glucosinolates) within ten to 13 days after transfer (16 to 19 day-old seedlings) and caused stagnation in glucosinolate accumulation (**Figure 4A** and **Supplementary Table 7**). After 13 days, nitrogen limitation alone (+S/−N medium) reduces short-chain aliphatic glucosinolate levels to 8%, long-chain aliphatic glucosinolate levels to 20% and indolic glucosinolate levels to 15% compared to the nutrient-sufficient control group (+S/+N medium). Within the long-chain aliphatic glucosinolates, this reduction was more pronounced for methylthioalkyl glucosinolates (7MTH, 8MTO) than for methylsulfinylalkyl glucosinolates (7MSH, 8MSO) (**Supplementary Table 7**).

Sulfur limitation resulted in an overall reduced accumulation of glucosinolates, but when looking at the three main classes, only the reduced levels of aliphatic glucosinolates were statistically

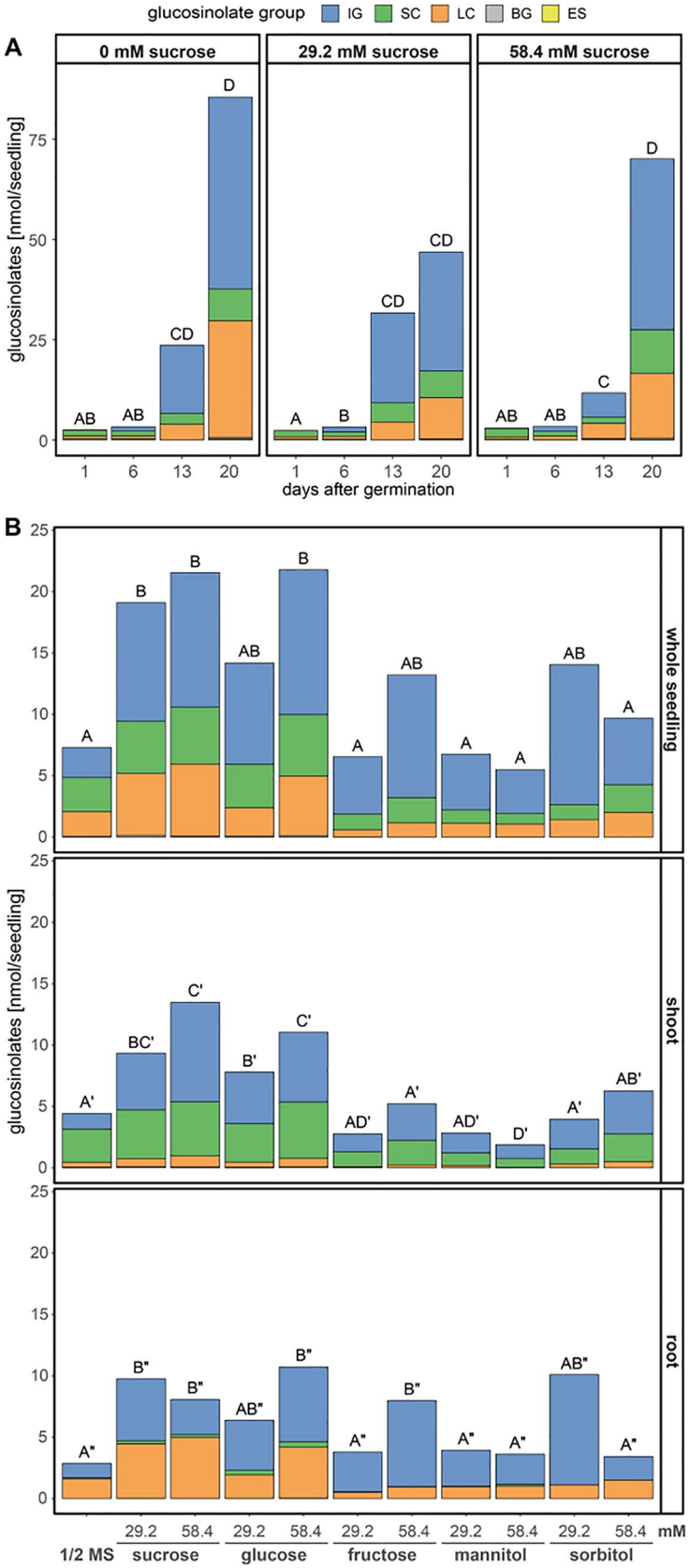

FIGURE 3 | Continued

FIGURE 3 | Glucosinolate accumulation in *A. thaliana* Col-0 seedlings depending on the presence and concentration of different sugars in the growth media. Plotted are the means of glucosinolate classes: IG, indolic glucosinolates; SC, short-chain aliphatic glucosinolates; LC, long-chain aliphatic glucosinolates; BG, benzenic glucosinolates; ES, embryo-synthesized glucosinolates. Letters denote significant differences at the 0.05 level on total glucosinolate levels. **(A)** Seedlings were grown on medium (1.68 mM S, 3 mM N) with three different sucrose concentrations and harvested 1–20 days after germination, (N = 6–8, one experimental round). Different letters indicate statistical differences across all treatments and days. Statistical details including means and standard deviations are in **Supplementary Table 3** for glucosinolate groups and **Supplementary Table 4** for individual glucosinolates. **(B)** Seedlings grew for twelve days after germination on ½ MS medium (0.82 mM S, 30 mM N) supplemented with different sugars, before shoot and root tissue were separately harvested per individual seedling. Letters denote significant differences of total glucosinolates levels within a tissue determined by pairwise comparison using Wilcoxon rank sum test (P-value adjustment method: Benjamini & Hochberg) (N = 12, one experimental round). Details on the statistical analysis including means and standard deviations are provided in **Supplementary Table 5** for glucosinolate groups and **Supplementary Table 6** for individual glucosinolates. Growth phenotypes are depicted in **Supplementary Figure 4**. ½ MS, half strength Murashige & Skoog medium.

significant. Long-chain aliphatic glucosinolate levels were reduced to 14% and short-chain aliphatic glucosinolate levels to 40% of the nutrient-sufficient control group with similar effects on the individual structures within these classes. Although the levels of total indolic glucosinolates and the levels of NMOI3M were not affected by sulfur limitation, the levels of I3M and 4MOI3M were significantly reduced (**Supplementary Tables 7** and **8**). Almost exclusively for long-chain aliphatic glucosinolates, we observed synergistic effects of sulfur and nitrogen limitation (**Supplementary Table 8**).

Levels of embryo-synthesized glucosinolates decreased over time after transfer, but their turnover rate was not affected by nitrogen or sulfur limitation or the combination thereof (**Figure 4B** and **Supplementary Table 7**). Accumulation of the general turnover metabolite raphanusamic acid was highest under nitrogen sufficient conditions and thus did not follow the turnover of embryo-synthesized glucosinolates (**Figure 4B**). Instead, we found the levels of raphanusamic acid to be positively correlated with total glucosinolate accumulation (**Figure 4C** and **Supplementary Figure 5**). Availability of nitrogen and sulfur significantly affected seedling growth (**Supplementary Figure 6**). Nitrogen limitation showed the strongest negative effect on seedling growth ($P < 0.001$), resulting in stagnation of growth after eight days. The seedling weight was reduced to 13% compared to the nutrient-sufficient group after 13 days under limiting conditions irrespective of the availability of sulfur, which had a smaller negative effect on seedling weight ($P = 0.047$; **Supplementary Table 9**). Thus, total endogenous glucosinolate accumulation followed the pattern of seedling growth under nutrient limiting conditions.

Allyl Glucosinolate Accumulation Is Time- and Dose-Dependent and Promotes the Accumulation of Raphanusamic Acid

A. thaliana Col-0 does not biosynthesize allyl glucosinolate at any developmental stage (Kliebenstein et al., 2001; Li and Quiros, 2003; Wentzell et al., 2007; Burow et al., 2015). Accordingly, we did not detect allyl glucosinolate in this study unless it had been applied exogenously. Feeding this glucosinolate to Col-0 seedlings therefore makes it possible to experimentally uncouple biosynthesis and turnover (Francisco et al., 2016a). Seedlings grown on medium containing 50 μM allyl glucosinolate steadily accumulated increasing amounts of allyl glucosinolate (**Figure 5A**) and reached levels corresponding to approx. 5% of the total endogenous glucosinolates (**Figure 5B** and **Supplementary Tables 10** and **11**). Notably, raphanusamic acid levels were considerably higher in allyl glucosinolate-treated seedlings. Nine days after germination, seedlings that had grown on allyl glucosinolate-containing medium accumulated 1.3 nmol raphanusamic acid, whereas the control seedlings only accumulated less than 0.02 nmol (**Figures 2B** and **5C**). Feeding of allyl glucosinolate moreover coincided with accumulation of 0.56 nmol allyl glucosinolate per seedling and increased levels of total endogenous glucosinolates (11 nmol/seedling compared to 8 nmol/seedling grown on control medium) nine days after germination, indicating that the turnover of endogenous glucosinolates might contribute to the accumulation of raphanusamic acid at this developmental stage.

Furthermore, allyl glucosinolate accumulated to higher levels with increasing concentrations of allyl glucosinolate in sucrose-free growth medium (**Figure 6**). The presence of 29.2 mM sucrose in the growth medium decreased the accumulation in seedlings grown on high relative to low allyl glucosinolate concentrations six days after germination (white diamonds, **Figure 6**) and allyl glucosinolate accumulation remained sucrose-dependent over time (**Supplementary Figure 7** and **Supplementary Table 12**). To investigate the turnover of allyl glucosinolate, allyl glucosinolate-containing seedlings were transferred to glucosinolate-free medium with the same sucrose concentration and grown for another seven days (**Figure 6**). Allyl glucosinolate levels were reduced by 54%, 58% and 72% for seedlings treated with 10 μM, 50 μM and 200 μM allyl glucosinolate, respectively, after growing on 0 mM sucrose compared to the levels on the day of transfer (black diamonds, **Figure 6**). In comparison, allyl glucosinolate levels were reduced only by up to 20% for seedlings grown on 29.2 mM sucrose (**Figure 6**) suggesting a reduced rate of allyl glucosinolate turnover. We further investigated the effect of nitrogen and sulfur limitation on allyl glucosinolate turnover, which had only a minor effect within our time frame of investigation depending on the initial allyl glucosinolate concentration applied in the medium (**Supplementary Figure 8** and **Supplementary Table 12**). Seedling weight, however, was significantly affected by both, the concentration of allyl glucosinolate supplied in the accumulation phase (Phase 1, $P < 0.001$) and nitrogen limitation in the turnover phase (Phase 2, $P < 0.001$) for 0 mM sucrose treatment (**Supplementary Figure 9** and **Supplementary Table 13**).

The accumulation of raphanusamic acid was positively correlated with increased allyl glucosinolate accumulation

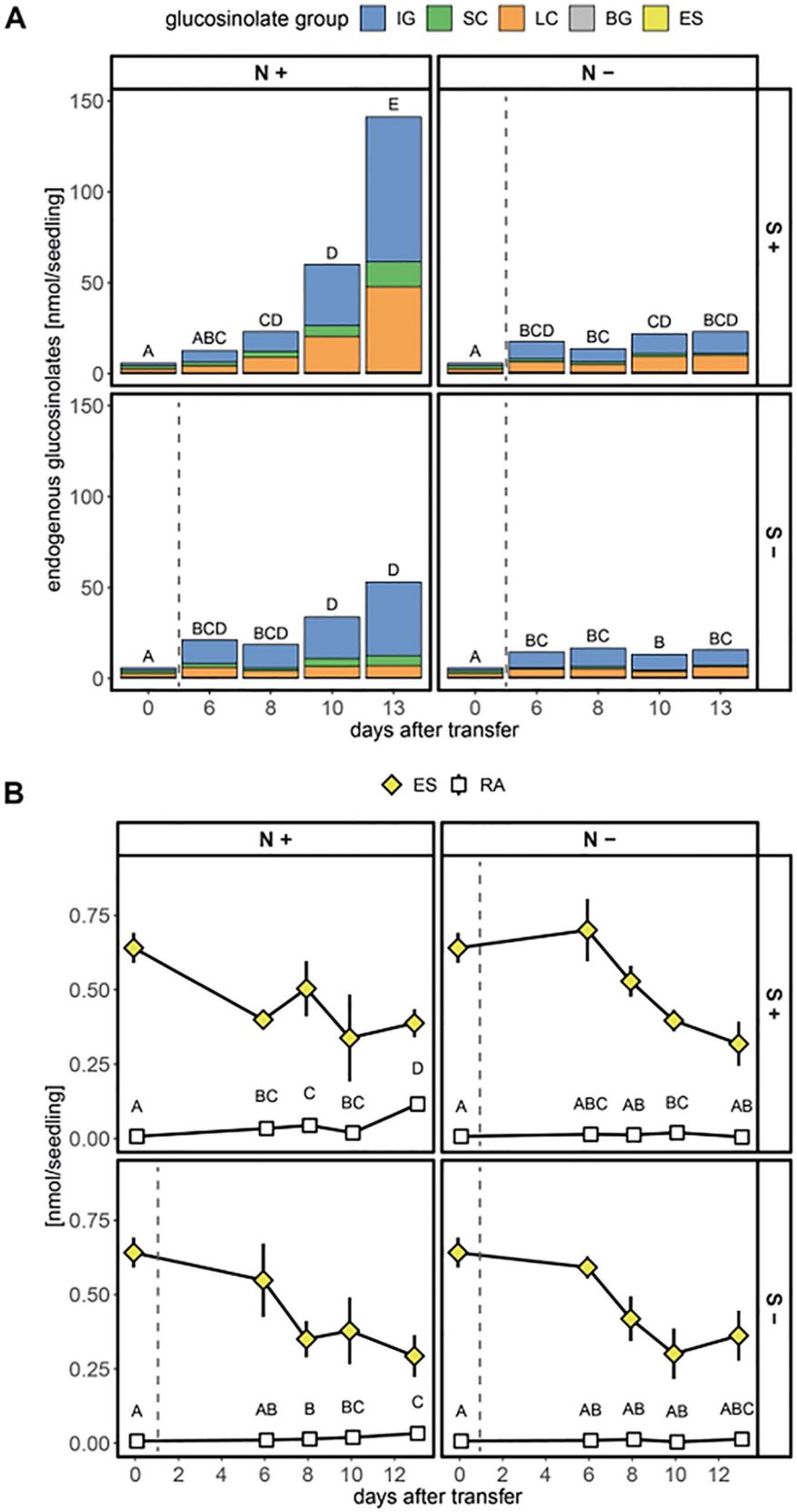

FIGURE 4 | Continued

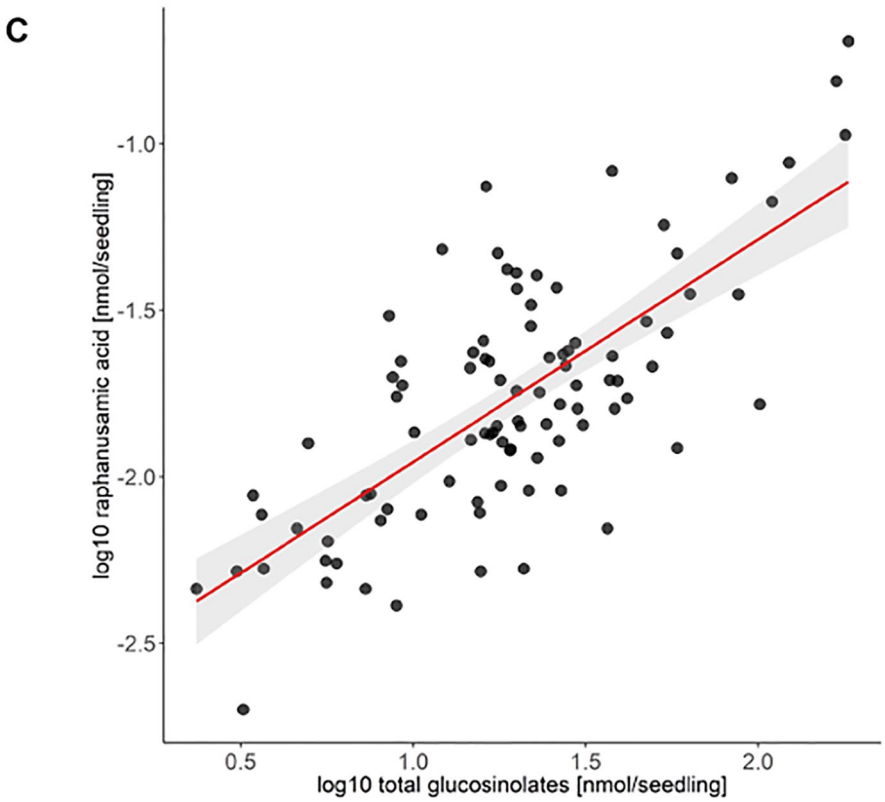

FIGURE 4 | Accumulation of glucosinolates and raphanusamic acid in *A. thaliana* Col-0 seedlings under different sulfur (S) and nitrogen (N) regimes. Seeds were germinated on control medium containing sufficient amounts of sulfur (+S) and nitrogen (+N) and seedlings were grown for six days (phase 1) before they were transferred to media with varying sulfur and nitrogen nutrition (phase 2, **Supplementary Figure 3**). Day 0 describes the day of transfer and reflects the metabolite levels of six-day-old seedlings grown on +S/+N medium. The dashed grey line indicates that seedlings had a change to a limiting medium condition. **(A)** Total glucosinolate levels and **(B)** levels of embryo-synthesized glucosinolates (ES) and accumulation of raphanusamic acid (RA) under sufficient and limiting sulfur and nitrogen nutrition. Plotted are **(A)** means of the glucosinolate classes: IG, indolic glucosinolates; SC, short-chain aliphatic glucosinolates; LC, long-chain aliphatic glucosinolates; BG, benzenic glucosinolates; ES, embryo-synthesized glucosinolates, and **(B)** means ± SE (N = 5–16, two independent experiments pooled). Letters denote significant difference at the 0.05 level determined by pairwise comparison using Wilcoxon rank sum test (P-value adjustment method: Benjamini & Hochberg). Details on the statistical analysis including means and standard deviations are provided in **Supplementary Table 7** for glucosinolate groups and **Supplementary Table 8** for individual glucosinolates. Seedling fresh weight in nitrogen and/or sulfur sufficient and limiting conditions is plotted in **Supplementary Figure 5**. **(C)** Correlation between total levels of glucosinolates and raphanusamic acid for seedlings grown on sulfur and nitrogen sufficient medium harvested daily three to nine days after germination. Slope = 0.667 ± 0.066, $P < 0.001$ (F = 103.30), adj. R2 = 0.521 of the linear model lm(logRA~logGLS). Correlations of raphanusamic acid to levels of indolic, short-chain aliphatic and long-chain aliphatic glucosinolates for seedlings grown on glucosinolate-free medium are depicted in **Supplementary Figures 5A–C**, correlations of raphanusamic acid to total glucosinolate levels and accumulated allyl glucosinolate for seedlings grown on medium supplemented with 50 μM allyl glucosinolate are depicted in **Supplementary Figures 5D–E**.

(P(concentration) < 0.001) and nitrogen availability (P(N) < 0.001; **Figure 7**). This effect was stronger for seedlings that had initially grown on high allyl glucosinolate concentrations (P(N * concentration) < 0.001). Although allyl glucosinolate levels were similar across all four media seven days after transfer depending on the initial allyl glucosinolate concentration in Phase 1 (**Supplementary Figure 8**), raphanusamic acid levels varied among media (**Figure 7**). Raphanusamic acid accumulated to amounts expected based on turnover of allyl glucosinolate under nitrogen limiting conditions (–N) if 1 nmol allyl glucosinolate is detected as 1 nmol raphanusamic acid. For nitrogen sufficient conditions (+N), appr. 2-fold higher amounts were detected as could be expected from allyl glucosinolate turnover alone (comparing the difference of days 0 and 7, **Figure 6**, to the levels in **Figure 7**), suggesting that raphanusamic acid also stems from turnover of endogenous glucosinolates in intact plant tissue.

Allyl Glucosinolate Treatment Alters the Turnover of Embryo-Synthesized Glucosinolates

In seedlings grown on 50 μM allyl glucosinolate-containing medium, short-chain aliphatic glucosinolates showed the same pronounced increase seven days after germination (**Figures 2A** and **8**), but accumulated to higher levels compared to those in seedlings grown on allyl glucosinolate-free medium (P = 0.024, **Supplementary Table 10**). This was driven by a 30% higher accumulation of 4mtb glucosinolate compared to the control group (**Supplementary Table 15**). Indolic glucosinolates, showing

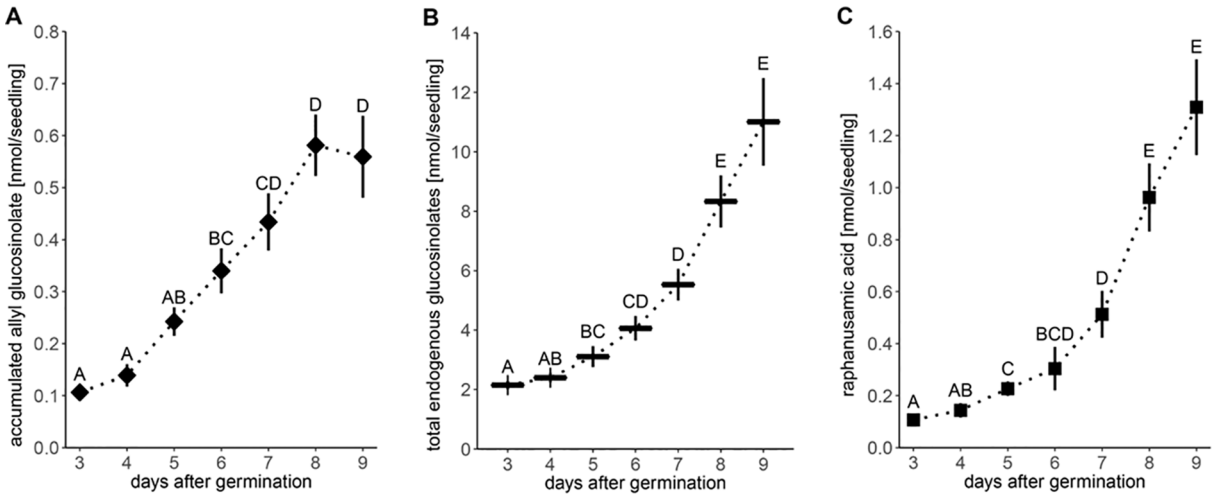

FIGURE 5 | Accumulation of allyl glucosinolate **(A)**, total endogenous glucosinolates **(B)** and raphanusamic acid, **(C)** in *A. thaliana* Col-0 seedlings grown continuously on media containing 50 µM allyl glucosinolate. Depicted are means ± SE (N = 17–19, one experimental round) and letters denote significant difference at the 0.05 level. Details on the statistical analysis including means and standard deviation are provided in **Supplementary Table 10** for allyl glucosinolate, glucosinolate groups and raphanusamic acid.

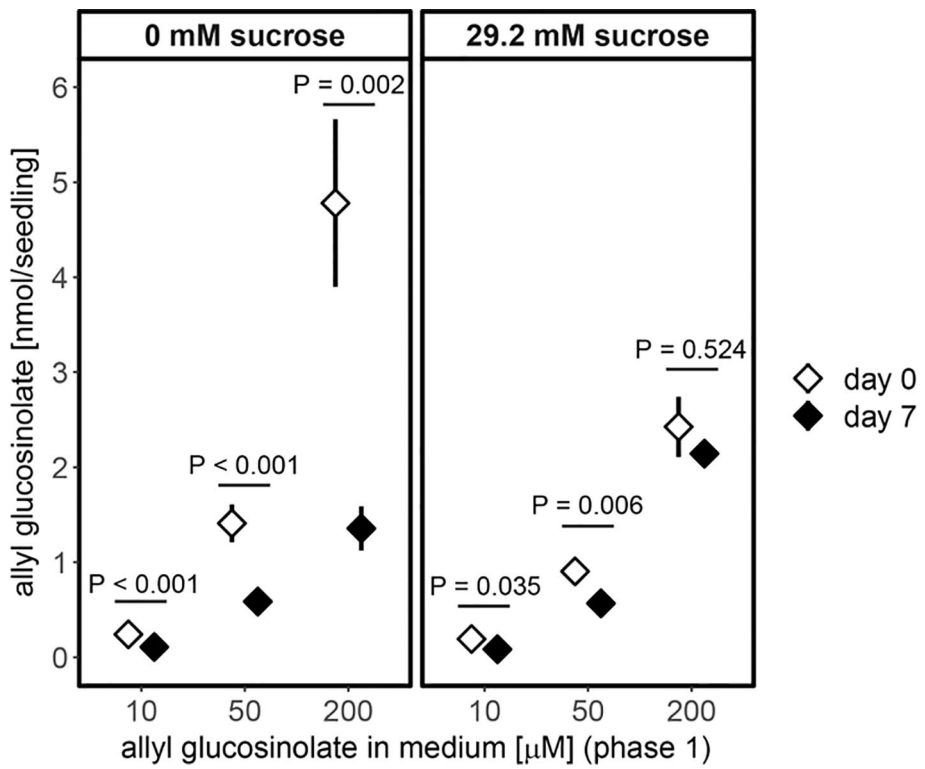

FIGURE 6 | Accumulation of allyl glucosinolates in six-day-old seedlings (white diamond, transfer day) and its turnover after seven days on allyl glucosinolate-free medium (black diamond, end of phase 2) is dependent on the concentration of allyl glucosinolate present in the growth medium (phase 1) and the absence (left panel) and presence of 29.2 mM sucrose (right panel). Depicted are means ± SE, N = 15–18 for 0 mM sucrose (data pooled from two independent experiments) and N = 5–8 for 29.2 mM sucrose treatment (one experiment). Pairwise comparison of day 0 to day 7 within an allyl glucosinolate and sucrose treatment group was performed using Wilcoxon rank sum test (P-value adjustment method: Benjamini & Hochberg). Details on the statistical analysis are provide in **Supplementary Table 11**. For details on the experimental set-up refer to **Supplementary Figure 3**. For the effect of varying nitrogen and sulfur content on the growth medium on allyl glucosinolate turnover refer to **Supplementary Figure 8**. Fresh weight of seedlings grown on nitrogen and/or sulfur sufficient and limiting conditions (phase 2) depending on the allyl glucosinolate concentration in phase 1 on sucrose-free medium is plotted in **Supplementary Figure 9**.

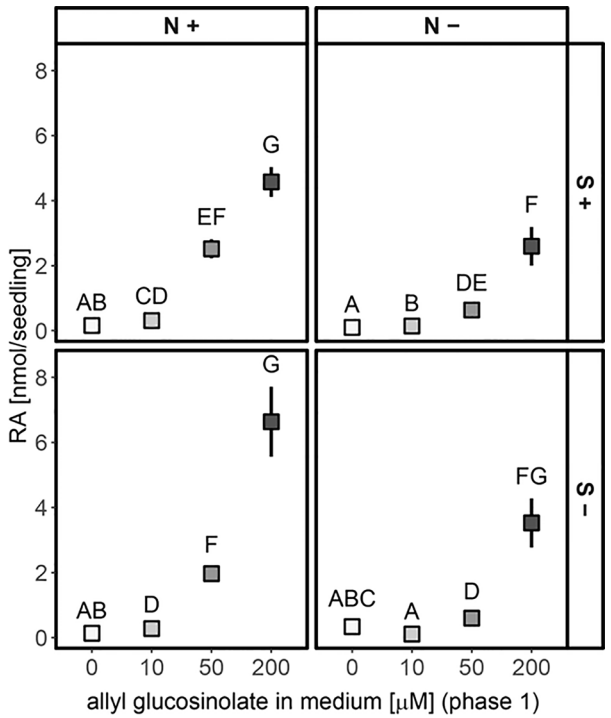

FIGURE 7 | Accumulation of raphanusamic acid in 13-day-old seedlings dependent on the concentration of allyl glucosinolate supplied in the growth medium in the first six days of seedling development (phase 1, grey scale) and the sulfur (S) and nitrogen (N) availability for additional seven days (phase 2) on 0 mM sucrose medium. Depicted are means ± SE, N = 15–18, data pooled from two independent experiments. Letters denote significant differences at the 0.05 level with pairwise comparison using Wilcoxon rank sum test (P-value adjustment method: Benjamini & Hochberg). Details on the statistical analysis are provided in **Supplementary Table 14**. For details on the experimental set-up refer to **Supplementary Figure 3**.

the strongest increase rate at this developmental stage, increased continuously over time and reached 43% higher levels in allyl glucosinolate-treated seedlings than in control seedlings nine days after germination. In contrast, neither total long-chain aliphatic glucosinolates nor any individual glucosinolate in the group was affected by allyl glucosinolate feeding **Figures 2A**, **8**, and **Supplementary Table 15**). Until eight days after germination, allyl glucosinolate-treated seedlings also maintained significantly higher levels of embryo-synthesized glucosinolates compared to the control group (P = 0.008) (**Figure 8**). In this experimental setup, the levels of embryo-synthesized glucosinolates decreased over time until they were not detectable nine days after germination irrespective of the presence of allyl glucosinolate in the medium.

Nine days after germination, seedlings grown on 50 μM allyl glucosinolate-containing medium had accumulated >35% higher total levels of glucosinolates than seedlings grown on control medium (**Figures 2A** and **8**). To compare the effects of allyl glucosinolate feeding to those of nitrogen and sulfur availability, and sucrose on endogenous glucosinolate profiles, we performed a multiple factor analysis (MFA) on a principle component analysis (PCA) on the entirety of the individual glucosinolates detected with our method (for all values and treatment combinations, **Supplementary Table 17**). The analysis was performed on single seedlings that were first grown on various concentrations of allyl glucosinolate with or without the addition of 29.2 mM sucrose (phase 1). Six days after germination, the seedlings were grown for another seven days (in sum, 13-day-old seedlings) on glucosinolate-free media that were sufficient or limiting in nitrogen and/or sulfur and either contained 29.2mM sucrose, or not (phase 2, **Supplementary Figure 3**). These four variations in medium composition (allyl glucosinolate concentration in Phase 1; nitrogen content, sulfur content and sucrose content in Phase 2) were considered as categorical variables in the principal component analysis, and the individual glucosinolates were further divided into groups (as in **Supplementary Table 17**) as continuous variables for the MFA-PCA analysis. Of the treatments, the absence or presence of sucrose (**Figure 9**, bottom right panel) is the dominant factor describing the separation of the data in the first dimension.

Overall, the presence of sucrose in the growth medium correlates with lowered total glucosinolate levels (**Supplementary Tables 16** and **17**) independent of other variable factors in this experiment. The glucosinolates most strongly contributing to this dimension (thus correlating with the effect of sucrose treatment) are 2PE and NMOI3M, followed by C8 aliphatic glucosinolates, embryo-synthesized glucosinolates and short-chain aliphatic glucosinolate to a lesser extent (**Supplementary Figure 10**, bottom left panel). Dimension 2 best describes the effect of nitrogen variation, followed by allyl glucosinolate feeding (**Figure 9**, top panels; **Supplementary Figure 10**, top right panel). In the 0 mM sucrose treatment group, we find that total glucosinolate levels are negatively correlated with allyl glucosinolate concentration affecting aliphatic and indolic glucosinolates (**Supplementary Table 16**). Nitrogen limitation negatively impacts short-chain aliphatic glucosinolate levels dependent on the allyl glucosinolate concentration fed, particularly negatively affecting 4mtb levels (but not raising 4msb levels) (**Supplementary Figure 10**, bottom right panel; **Supplementary Table 17**). Variation in sulfur availability has a negligible effect on the overall changes in in glucosinolate profiles, and this effect could not be resolved in any other dimension described in this model (dimensions 3 and upwards not shown).

DISCUSSION

Glucosinolate Biosynthesis and Turnover Are Coordinated According to Nutrient Availability

Steady-state levels of metabolites are determined by the rates of biosynthesis and turnover. Whereas the regulation of the biosynthetic pathways and their regulators has been intensely studied, especially at the transcriptional level, glucosinolate turnover pathways remained largely elusive and their impact on steady-state levels of glucosinolates awaits to be determined. To this end, we investigated the nutrient-driven dynamics of glucosinolate levels during seedling development in *A. thaliana*, i.e. at a developmental stage at which biosynthesis and turnover of glucosinolates coincide. Between three and nine days after germination, the average rate of total glucosinolate accumulation

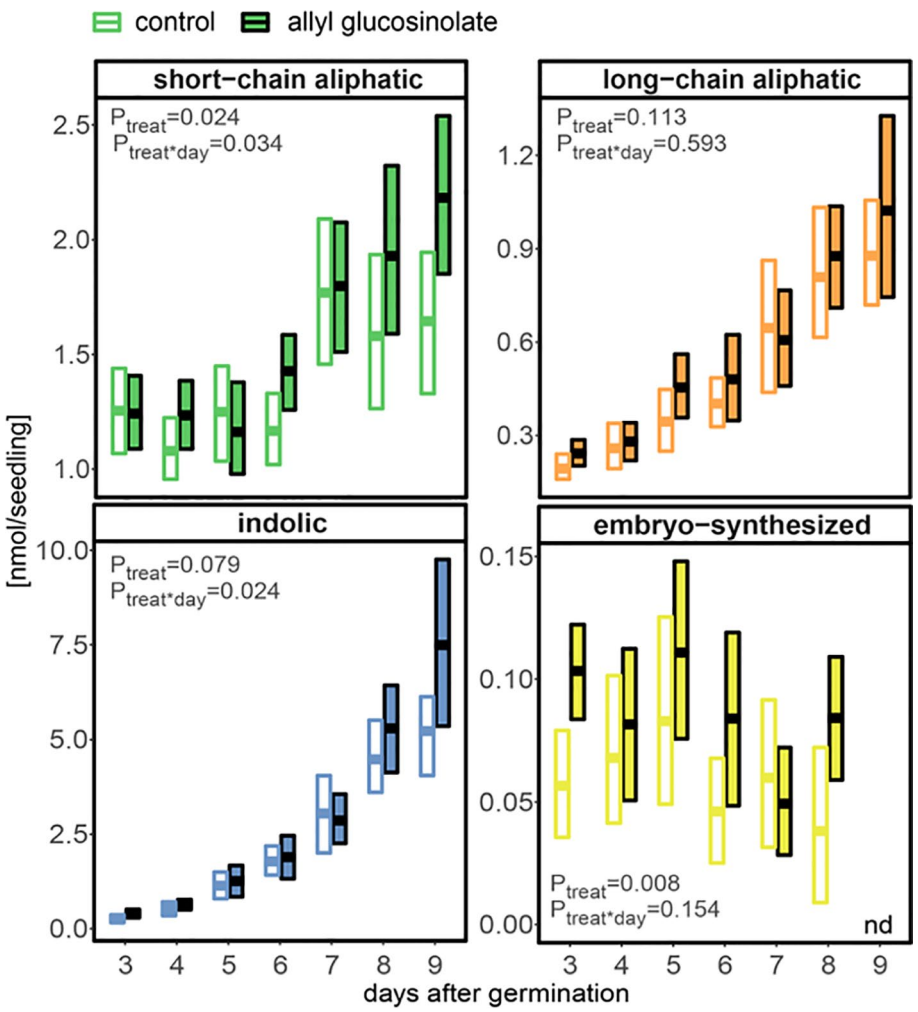

FIGURE 8 | The influence of exogenously applied allyl glucosinolate on endogenous glucosinolate profiles in *A. thaliana* Col-0 seedlings. Seedlings were grown on control (glucosinolate-free) medium (white fill) and medium containing 50 µM allyl glucosinolate (colored fill) for nine days after germination. Plotted are means (bold bar) and 95% confidence interval (box), N = 6–19 (one experimental round). Embryo-synthesized glucosinolates were not detected (nd) in nine-day-old seedlings. Statistical comparison of the control and allyl glucosinolate treatment was performed with a linear model of the following function: aov(analyte ~ treat*day), with treat = treatment. Details on the statistical analysis including means, standard error and post-hoc tests are in **Supplementary Table 1** for the control treatment and **Supplementary Table 15** for allyl glucosinolate treatment.

was ca. 1 nmol/day (**Figure 2A**), indicating that the rate of biosynthesis exceeds the rate of turnover at this stage. Embryo-synthesized glucosinolates were detectable at least nine days after germination under our experimental conditions (**Figure 2B**) and generally found to decrease during seedling development (**Figures 2B**, **4B**, and **Supplementary Table 7**) demonstrating turnover of these compounds. Similarly, the levels of allyl glucosinolate exogenously applied during the first days of seedling development decreased after the seedlings had been moved to allyl glucosinolate-free medium (**Figure 6**). Although, we cannot determine the relative impact of biosynthesis and turnover on those glucosinolate structures that are *de novo* synthesized in the seedlings, our data confirm previous findings (Petersen et al., 2002; Brown et al., 2003) that seedlings possess the enzymatic machinery to metabolize glucosinolates.

Metabolic processes, growth and development in *A. thaliana* seedlings are regulated by nutrient availability, for example a balanced carbon to nitrogen ratio (Martin et al., 2002). The addition of 29.2 mM (1 %) sucrose to the growth medium with sufficient concentrations of sulfur and nitrogen alters glucosinolate profiles (**Figure 3**) (Gigolashvili et al., 2007; Francisco et al., 2016a). Under our experimental conditions, external sucrose had a stronger effect on the dynamics of long-chain aliphatic and indolic glucosinolate accumulation than on short-chain aliphatic glucosinolates, without changes in glucosinolate composition within these three groups (**Figure 3A** and **Supplementary Table 3**). In twelve-day-old seedlings, sucrose and glucose led to higher glucosinolate accumulation in roots and shoots, whereas fructose treatment did not result in significant changes in glucosinolate content (**Figure 3B**).

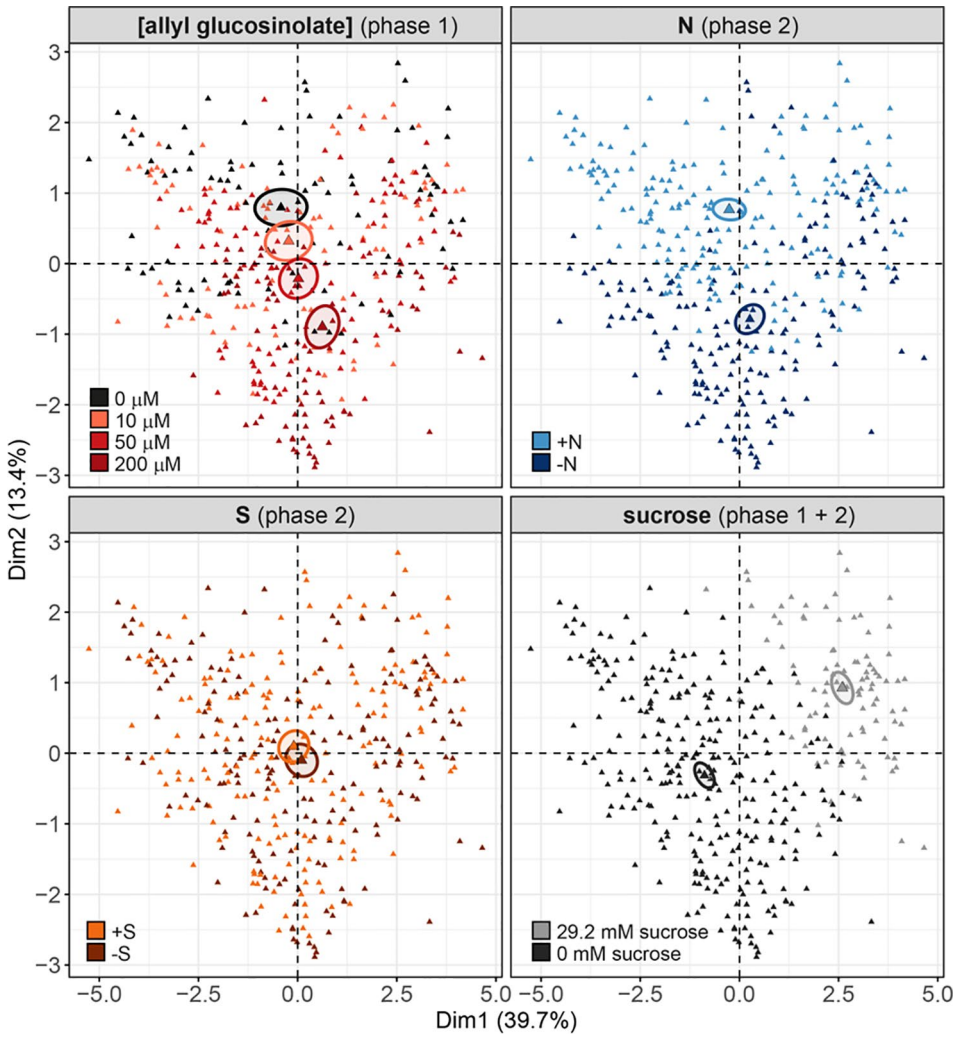

FIGURE 9 | Multiple factor analysis (MFA) of the effects of exogenously feeding allyl glucosinolate (in 0, 10, 50 and 200 µM), varying nitrogen in the growth medium (0.3 mM (–N) and 3 mM (+N)), varying sulfur in the growth medium (0.015 mM (–S) and 1.68 mM (+S) and the effects of the presence (29.2 mM) and absence and sucrose on endogenous glucosinolate levels. Seedlings were grown on medium containing different concentrations of allyl glucosinolate for six days (phase 1) and transferred to glucosinolate-free medium varying in their nitrogen and sulfur content for seven days (phase 2, for details on the experimental set-up refer to **Supplementary Figure 3**). Sucrose treatment was constant over phase 1 and phase 2. Each triangle represents the sum of all individual glucosinolate concentrations of one single seedling, data pooled from two independent experiments. For a list of the glucosinolate concentrations and the statistical analysis by treatment group refer to **Supplementary Tables 16** and **17**. For a list of the contribution of the treatment and glucosinolate classes, and of the contributions of the individual glucosinolates to the separation of dimensions 1 and 2, refer to **Supplementary Figure 10**.

Although the expression of *MYB28*, a positive regulator of aliphatic glucosinolate biosynthesis, is short-term inducible by glucose (Gigolashvili et al., 2007), long term exposure to external carbon sources appears to affect overall glucosinolate content by regulating seedling growth (**Supplementary Figure 4**) without fine-tuning glucosinolate composition.

Sucrose treatment further affected accumulation of the exogenous allyl glucosinolate, which could reflect a negative effect of sucrose on allyl glucosinolate uptake or a positive effect on turnover (**Figure 6**). When we subsequently followed the turnover of allyl glucosinolate after transfer of the seedlings from plates containing 200 µM allyl glucosinolate to allyl glucosinolate-free media, lower amounts were metabolized in seedlings kept on sucrose-containing plates. This observation suggests a lower turnover rate of allyl glucosinolate in the presence of sucrose and shows that sucrose treatment regulates not only glucosinolate biosynthesis but also turnover.

Also sulfur and nitrogen limitation negatively affected the accumulation of all *de novo* synthesized glucosinolate classes (indolic, short- and long-chain aliphatic glucosinolates). Under nitrogen limiting conditions, the strongest fold-reduction was detected for short-chain aliphatic glucosinolates, which are, however, less abundant than indolic and long-chain aliphatic glucosinolates at this developmental stage (**Figure 4A**). In contrast, sulfur limitation had the strongest negative impact on long-chain aliphatic glucosinolates. Although nitrogen has the more pronounced quantitative effect on

glucosinolate levels, both nitrogen and sulfur negatively affected *de novo* synthesis of all three groups under conditions of long-term nutrient limitation. In addition to the overall reduction in glucosinolates, sulfur or nitrogen limitation resulted in distinct changes in the levels of individual glucosinolates (**Supplementary Table 7**), indicating that these macronutrients provide a regulatory input different from sucrose.

Because glucosinolates can represent up to 30 % of the total sulfur in a given tissue, they have been discussed as potential source for sulfur under sulfur limiting conditions (Falk et al., 2007). However, in seedlings of *Brassica juncea* and *B. napus* challenged by sulfate deprivation, sulfur is not mobilized from glucosinolates (Aghajanzadeh et al., 2014). Similarly, neither sulfur nor nitrogen limitation had a significant effect on the turnover of embryo-synthesized glucosinolates under our experimental conditions (**Figure 4**) or on the turnover of exogenously fed allyl glucosinolate (**Supplementary Figure 8**). Although sulfur and nitrogen availability do not seem to change glucosinolate turnover rates in Brassicaceae seedlings, this may nevertheless happen at later developmental stages.

Exogenously Applied Allyl Glucosinolate Is Metabolized and Fine-Tunes Glucosinolate Biosynthesis and Turnover

When grown on medium containing allyl glucosinolate, *A. thaliana* seedlings gradually accumulated allyl glucosinolate until eight days after germination in a dose-dependent manner (**Figures 5A** and **6**). Although exogenously applied glucosinolates have previously been shown to be transported between root and shoot in the same way as endogenous glucosinolates and to undergo further side chain modification by the glucosinolate biosynthetic machinery (Li and Quiros, 2003; Andersen et al., 2013; Burow et al., 2015; Francisco et al., 2016a; Malinovsky et al., 2017), it cannot be ruled out that an unknown proportion of allyl glucosinolate provided in the medium will encounter myrosinase-catalyzed breakdown. Nevertheless, the addition of sucrose to the growth medium quantitatively affects allyl glucosinolate accumulation depending on seedling development (**Figure 6** and **Supplementary Figure 7**) (Francisco et al., 2016a). Exogenously applied allyl glucosinolate further affects the endogenous glucosinolate profile (**Figures 5** and **8**) (Francisco et al., 2016a). Short -chain aliphatic and indolic glucosinolates accumulated to higher levels in seedlings grown on allyl glucosinolate compared to seedlings grown on allyl glucosinolate-free medium, although this trend was not significant for long-chain aliphatic glucosinolates (**Figure 8**). This further supports the positive regulatory effect of allyl glucosinolate on the biosynthesis of glucosinolates from methionine and tryptophan (Francisco et al., 2016a).

The presence of sucrose resulted in decreased accumulation of allyl glucosinolate depending on the initial allyl glucosinolate concentration in the growth medium (**Figure 6**), which is likely due to a lower uptake rate of allyl glucosinolate as discussed above. In the absence of external sucrose, seedlings grown on allyl glucosinolate-containing medium maintained higher levels of the embryo-synthesized glucosinolates (**Figure 8**). Likewise, allyl glucosinolate feeding did not lead to altered levels of the short-chain aliphatic 4-methylsulfinylbutyl glucosinolate predominantly present in adult plants, but resulted in altered levels of 4mtb glucosinolate depending on seedling age, illustrating the fine-tuning effect of allyl glucosinolate on the glucosinolate profile in seedlings. Because a substantial proportion of 4mtb but not 4msb glucosinolate in seedlings is derived from the seed, we cannot conclude whether allyl glucosinolate affects biosynthesis and/or turnover at this developmental stage.

Structure-specific effects on growth and development have also been shown for the structurally unrelated 3ohp glucosinolate, which belongs to the embryo-synthesized glucosinolates in *A. thaliana* Col-0. 3ohp glucosinolate was recently shown to inhibit seedling root growth due to its signaling function *via* genes in the sugar sensing Target Of Rapamycin (TOR) pathway (Malinovsky et al., 2017). Dose-dependent effects on root growth have further been shown for the glucosinolate breakdown products indole-3-carbinol and allyl isothiocyanate, although at much higher concentrations and in case of indole-3-carbinol through auxin signaling (Katz et al., 2015; Urbancsok et al., 2017). Based on these observations, we propose a model in which the glucosinolate composition and the metabolic status coordinately feedback regulate glucosinolate profiles and seedling development.

Raphanusamic Acid Levels Reflect the Levels of Endogenous Glucosinolates

Turnover of glucosinolates *via* the formation of isothiocyanates and their conjugation with glutathione yields raphanusamic acid (Bednarek et al., 2009; Piślewska-Bednarek et al., 2018). Although glucosinolates are predominantly metabolized to simple nitriles in homogenates of *A. thaliana* seedlings (Wittstock et al., 2016b), we monitored the levels of raphanusamic acid as potential indicator of glucosinolate turnover during seedling development and indeed detected increasing amounts from five days after germination (**Figure 2B**). Over time, the kinetics of raphanusamic acid accumulation did, however, not follow the turnover of the embryo-synthesized glucosinolates (**Figures 2** and **4B**). Raphanusamic acid levels were instead correlated with the accumulation of total glucosinolate levels (**Figure 4C**). Considering that one week after germination, the indolic glucosinolate NMOI3M constitutes >40% of total glucosinolates and accumulates at high rate (**Supplementary Table 1**), raphanusamic acid may at least partially reflect the biosynthetic rate of indolic or possibly of total glucosinolates.

In support of this hypothesis, higher levels of raphanusamic acid repeatedly coincided with high flux through the glucosinolate biosynthetic pathways. The levels of raphanusamic acid and glucosinolates were reduced under nitrogen and sulfur limiting conditions (**Figure 4**). Further, the accumulation of allyl glucosinolate over time positively correlated with raphanusamic acid, an effect that persisted seven days after the seedlings had been transferred to allyl glucosinolate-free media (**Figure 7**). These increased levels of raphanusamic acid upon and after allyl glucosinolate feeding may stem from allyl glucosinolate itself but may also reflect an allyl glucosinolate-mediated increased biosynthetic rate. Because raphanusamic acid can possibly be formed form all glucosinolates irrespective of their side chain chemistry, it cannot carry glucosinolate structure-specific

regulatory information. Nevertheless, this intermediate of glucosinolate metabolism could serve as checkpoint allowing the plant to measure the flux through the glucosinolate biosynthetic and turnover pathways and thereby to dynamically adjust glucosinolate levels to internal and external signals.

DATA AVAILABILITY STATEMENT

All datasets generated for this study are included in the article/ **Supplementary Material**.

AUTHOR CONTRIBUTIONS

VJ and MB design the experiments. KW and SM conducted the sugar dependency experiments. VJ carried out all other experimental work, the statistical analyses and made the figures. VJ and MB wrote the manuscript.

FUNDING

This work was supported by The Danish National Research Foundation, DNRF grant 99 (VJ, KW, MB) and Villumfonden, project no. 13169 (VJ, MB).

ACKNOWLEDGMENTS

We would like to thank Christoph Crocoll and the DynaMo Metabolomics Facility for help with Data Acquisition.

SUPPLEMENTARY MATERIAL

The Supplementary Material for this article can be found online at: https://www.frontiersin.org/articles/10.3389/fpls.2019.01560/full#supplementary-material

REFERENCES

Aghajanzadeh, T., Hawkesford, M. J., and De Kok, L. J. (2014). The significance of glucosinolates for sulfur storage in Brassicaceae seedlings. *Front. Plant Sci.* 5, 704. doi: 10.3389/fpls.2014.00704

Andersen, T. G., Nour-Eldin, H. H., Fuller, V. L., Olsen, C. E., Burow, M., and Halkier, B. A. (2013). Integration of biosynthesis and long-distance transport establish organ-specific glucosinolate profiles in vegetative Arabidopsis. *Plant Cell* 25, 3133–3145. doi: 10.1105/tpc.113.110890

Augustine, R., and Bisht, N. C. (2016). "*Glucosinolates*," in *Regulation of Glucosinolate Metabolism: From Model Plant Arabidopsis thaliana to Brassica Crops*. Eds. J.-M. Mérillon, and K. G. Ramawat (Cham: Springer International Publishing), 1–37. doi: 10.1007/978-3-319-26479-0_3-1

Barth, C., and Jander, G. (2006). Arabidopsis myrosinases TGG1 and TGG2 have redundant function in glucosinolate breakdown and insect defense. *Plant J.* 46, 549–562. doi: 10.1111/j.1365-313X.2006.02716.x

Bednarek, P., Pislewska-Bednarek, M., Svatos, A., Schneider, B., Doubsky, J., Mansurova, M., et al. (2009). A glucosinolate metabolism pathway in living plant cells mediates broad-spectrum antifungal defense. *Science* 323, 101–106. doi: 10.1126/science.1163732

Bednarek, P. (2012). Sulfur-containing secondary metabolites from Arabidopsis thaliana and other Brassicaceae with function in plant immunity. *Chembiochem* 13, 1846–1859. doi: 10.1002/cbic.201200086

Bekaert, M., Edger, P. P., Hudson, C. M., Pires, J. C., and Conant, G. C. (2012). Metabolic and evolutionary costs of herbivory defense: systems biology of glucosinolate synthesis. *New Phytol.* 196, 596–605. doi: 10.1111/j.1469-8137.2012.04302.x

Blažević, I., Montaut, S., Burcul, F., Olsen, C. E., Burow, M., Rollin, P., et al. (2019). Glucosinolate structural diversity, identification, chemical synthesis and metabolism in plants. *Phytochemistry*. doi: 10.1016/j.phytochem.2019.112100

Booth, E. J., Walker, K. C., and Griffiths, D. W. (1991). A time-course study of the effect of sulphur on glucosinolates in oilseed rape (Brassica napus) from the vegetative stage to maturity. *J. Sci. Food Agric.* 56, 479–493. doi: 10.1002/jsfa.2740560408

Brown, K. K., and Hampton, M. B. (2011). Biological targets of isothiocyanates. *Biochim. Biophys. Acta* 1810, 888–894. doi: 10.1016/j.bbagen.2011.06.004

Brown, P. D., Tokuhisa, J. G., Reichelt, M., and Gershenzon, J. (2003). Variation of glucosinolate accumulation among different organs and developmental stages of *Arabidopsis thaliana*. *Phytochemistry* 62, 471–481. doi: 10.1016/S0031-9422(02)00549-6

Burow, M., and Halkier, B. A. (2017). How does a plant orchestrate defense in time and space? Using glucosinolates in *Arabidopsis* as case study. *Curr. Opin. Plant Biol.* 38, 142–147. doi: 10.1016/j.pbi.2017.04.009

Burow, M., Losansky, A., Müller, R., Plock, A., Kliebenstein, D. J., and Wittstock, U. (2009). The genetic basis of constitutive and herbivore-induced ESP-independent nitrile formation in *Arabidopsis*. *Plant Physiol.* 149, 561–574. doi: 10.1104/pp.108.130732

Burow, M., Halkier, B. A., and Kliebenstein, D. J. (2010). Regulatory networks of glucosinolates shape *Arabidopsis thaliana* fitness. *Curr. Opin. Plant Biol.* 13, 348–353. doi: 10.1016/j.pbi.2010.02.002

Burow, M., Atwell, S., Francisco, M., Kerwin, R. E., Halkier, B. A., and Kliebenstein, D. J. (2015). The glucosinolate biosynthetic gene aop2 mediates feed-back regulation of jasmonic acid signaling in *Arabidopsis*. *Mol. Plant* 8, 1201–1212. doi: 10.1016/j.molp.2015.03.001

Burow, M. (2016). "*Gucosinolates* Advances in Botanical Research," in *Complex Environments Interact With Plant Development to Shape Glucosinolate Profiles*. Ed. S. Kopriva (Elsevier Ltd.), 15–30. doi: 10.1016/bs.abr.2016.06.001

Chun, J.-H., Kim, S., Arasu, M. V., Al-Dhabi, N. A., Chung, D. Y., and Kim, S.-J. (2017). Combined effect of Nitrogen, Phosphorus and Potassium fertilizers on the contents of glucosinolates in rocket salad (Eruca sativa Mill.). *Saudi J. Biol. Sci.* 24, 436–443. doi: 10.1016/j.sjbs.2015.08.012

Crocoll, C., Halkier, B. A., and Burow, M. (2016). Analysis and quantification of glucosinolates. *Curr. Protoc. Plant Biol.* 1 (2), 385–409. doi: 10.1002/cppb.20027

D'Auria, J. C., and Gershenzon, J. (2005). The secondary metabolism of *Arabidopsis thaliana*: growing like a weed. *Curr. Opin. Plant Biol.* 8, 308–316. doi: 10.1016/j.pbi.2005.03.012

Falk, K. L., Tokuhisa, J. G., and Gershenzon, J. (2007). The effect of sulfur nutrition on plant glucosinolate content: physiology and molecular mechanisms. *Plant Biol. (Stuttg.)* 9, 573–581. doi: 10.1055/s-2007-965431

Francisco, M., Joseph, B., Caligagan, H., Li, B., Corwin, J. A., Lin, C., et al. (2016a). The defense metabolite, allyl glucosinolate, modulates *Arabidopsis thaliana* biomass dependent upon the endogenous glucosinolate pathway. *Front. Plant Sci.* 7, 774. doi: 10.3389/fpls.2016.00774

Francisco, M., Joseph, B., Caligagan, H., Li, B., Corwin, J. A., Lin, C., et al. (2016b). Genome wide association mapping in *Arabidopsis thaliana* identifies novel genes involved in linking allyl glucosinolate to altered biomass and defense. *Front. Plant Sci.* 7, 1010. doi: 10.3389/fpls.2016.01010

Frerigmann, H., and Gigolashvili, T. (2014). Update on the role of R2R3-MYBs in the regulation of glucosinolates upon sulfur deficiency. *Front. Plant Sci.* 5, 626. doi: 10.3389/fpls.2014.00626

Gigolashvili, T., Yatusevich, R., Berger, B., Müller, C., and Flügge, U.-I. (2007). The R2R3-MYB transcription factor HAG1/MYB28 is a regulator of methionine-derived glucosinolate biosynthesis in *Arabidopsis thaliana*. *Plant J.* 51, 247–261. doi: 10.1111/j.1365-313X.2007.03133.x

Gigolashvili, T., Berger, B., and Flügge, U.-I. (2009). Specific and coordinated control of indolic and aliphatic glucosinolate biosynthesis by R2R3-MYB transcription factors in *Arabidopsis thaliana*. *Phytochem. Rev.* 8, 3–13. doi: 10.1007/s11101-008-9112-6

Guo, R., Yuan, G., and Wang, Q. (2011). Sucrose enhances the accumulation of anthocyanins and glucosinolates in broccoli sprouts. *Food Chem.* 129, 1080–1087. doi: 10.1016/j.foodchem.2011.05.078

Haughn, G. W., Davin, L., Giblin, M., and Underhill, E. W. (1991). Biochemical genetics of plant secondary metabolites in *Arabidopsis thaliana*: the glucosinolates. *Plant Physiol.* 97, 217–226. doi: 10.1104/pp.97.1.217

Huseby, S., Koprivova, A., Lee, B.-R., Saha, S., Mithen, R., Wold, A.-B., et al. (2013). Diurnal and light regulation of sulphur assimilation and glucosinolate biosynthesis in *Arabidopsis*. *J. Exp. Bot.* 64, 1039–1048. doi: 10.1093/jxb/ers378

Inamori, Y., Muro, C., Tanaka, R., Adachi, A., Miyamoto, K., and Tsujibo, H. (1992). Phytogrowth-inhibitory activity of sulphur-containing compounds. I. Inhibitory activities of thiazolidine derivatives on plant growth. *Chem. Pharm. Bull.* 40, 2854–2856. doi: 10.1248/cpb.40.2854

Janowitz, T., Trompetter, I., and Piotrowski, M. (2009). Evolution of nitrilases in glucosinolate-containing plants. *Phytochemistry* 70, 1680–1686. doi: 10.1016/j.phytochem.2009.07.028

Jensen, L. M., Halkier, B. A., and Burow, M. (2014). How to discover a metabolic pathway? An update on gene identification in aliphatic glucosinolate biosynthesis, regulation and transport. *Biol. Chem.* 395, 529–543. doi: 10.1515/hsz-2013-0286

Jensen, L. M., Jepsen, H. S. K., Halkier, B. A., Kliebenstein, D. J., and Burow, M. (2015). Natural variation in cross-talk between glucosinolates and onset of flowering in *Arabidopsis*. *Front. Plant Sci.* 6, 697. doi: 10.3389/fpls.2015.00697

Katz, E., Nisani, S., Yadav, B. S., Woldemariam, M. G., Shai, B., Obolski, U., et al. (2015). The glucosinolate breakdown product indole-3-carbinol acts as an auxin antagonist in roots of *Arabidopsis thaliana*. *Plant J.* 82, 547–555. doi: 10.1111/tpj.12824

Kerwin, R. E., Jimenez-Gomez, J. M., Fulop, D., Harmer, S. L., Maloof, J. N., and Kliebenstein, D. J. (2011). Network quantitative trait loci mapping of circadian clock outputs identifies metabolic pathway-to-clock linkages in *Arabidopsis*. *Plant Cell* 23, 471–485. doi: 10.1105/tpc.110.082065

Kissen, R., Rossiter, J. T., and Bones, A. M. (2009). The "mustard oil bomb": not so easy to assemble?! Localization, expression and distribution of the components of the myrosinase enzyme system. *Phytochem. Rev.* 8, 69–86. doi: 10.1007/s11101-008-9109-1

Kliebenstein, D. J., Lambrix, V. M., Reichelt, M., Gershenzon, J., and Mitchell-Olds, T. (2001). Gene duplication in the diversification of secondary metabolism: tandem 2-oxoglutarate-dependent dioxygenases control glucosinolate biosynthesis in *Arabidopsis*. *Plant Cell* 13, 681–693. doi: 10.1105/tpc.13.3.681

Kliebenstein, D. J., Rowe, H. C., and Denby, K. J. (2005). Secondary metabolites influence *Arabidopsis*/Botrytis interactions: variation in host production and pathogen sensitivity. *Plant J.* 44, 25–36. doi: 10.1111/j.1365-313X.2005.02508.x

Kliebenstein, D. J., D'Auria, J. C., Behere, A. S., Kim, J. H., Gunderson, K. L., Breen, J. N., et al. (2007). Characterization of seed-specific benzoyloxyglucosinolate mutations in *Arabidopsis thaliana*. *Plant J.* 51, 1062–1076. doi: 10.1111/j.1365-313X.2007.03205.x

Kopriva, S., and Gigolashvili, T. (2016). Chapter five - glucosinolate synthesis in the context of plant metabolism. *Adv. In Botanical Res.* 80, 99–124. doi: 10.1016/bs.abr.2016.07.002

Koprivova, A., Suter, M., den Camp, R. O., Brunold, C., and Kopriva, S. (2000). Regulation of sulfate assimilation by nitrogen in *Arabidopsis*. *Plant Physiol.* 122, 737–746. doi: 10.1104/pp.122.3.737

Kopsell, D. A., Barickman, T. C., Sams, C. E., and McElroy, J. S. (2007). Influence of nitrogen and sulfur on biomass production and carotenoid and glucosinolate concentrations in watercress (Nasturtium officinale R. Br.). *J. Agric. Food Chem.* 55, 10628–10634. doi: 10.1021/jf072793f

Koroleva, O. A., Davies, A., Deeken, R., Thorpe, M. R., Tomos, A. D., and Hedrich, R. (2000). Identification of a new glucosinolate-rich cell type in *Arabidopsis* flower stalk. *Plant Physiol.* 124, 599–608. doi: 10.1104/pp.124.2.599

Koroleva, O. A., Gibson, T. M., Cramer, R., and Stain, C. (2010). Glucosinolate-accumulating S-cells in *Arabidopsis* leaves and flower stalks undergo programmed cell death at early stages of differentiation. *Plant J.* 64, 456–469. doi: 10.1111/j.1365-313X.2010.04339.x

Krumbein, A., Schonhof, I., Rühlmann, J., and Widell, S. (2001). "Influence of sulphur and nitrogen supply on flavour and health-affecting compounds in Brassicaceae," in *Plant Nutrition*. Eds. W. J. Horst, M. K. Schenk, A. Bürkert, N. Claassen, H. Flessa, W. B. Frommer, H. Goldbach, H. W. Olfs, V. Römheld, and B. Sattelmacher (Dordrecht: Springer Netherlands), 294–295. doi: 10.1007/0-306-47624-X_141

Li, G., and Quiros, C. F. (2003). In planta side-chain glucosinolate modification in Arabidopsis by introduction of dioxygenase Brassica homolog BoGSL-ALK. *Theor. Appl. Genet.* 106, 1116–1121. doi: 10.1007/s00122-002-1161-4

Li, S., Schonhof, I., Krumbein, A., Li, L., Stützel, H., and Schreiner, M. (2007). Glucosinolate concentration in turnip (Brassica rapa ssp. rapifera L.) roots as affected by nitrogen and sulfur supply. *J. Agric. Food Chem.* 55, 8452–8457. doi: 10.1021/jf070816k

Malinovsky, F. G., Thomsen, M. F., Nintemann, S. J., Jagd, L. M., Bourgine, B., Burow, M., et al. (2017). An evolutionarily young defense metabolite influences the root growth of plants *via the* ancient TOR signaling pathway. *Elife* 6. doi: 10.7554/eLife.29353

Marino, D., Ariz, I., Lasa, B., Santamaría, E., Fernández-Irigoyen, J., González-Murua, C., et al. (2016). Quantitative proteomics reveals the importance of nitrogen source to control glucosinolate metabolism in *Arabidopsis thaliana* and *Brassica oleracea*. *J. Exp. Bot.* 67, 3313–3323. doi: 10.1093/jxb/erw147

Martin, T., Oswald, O., and Graham, I. A. (2002). *Arabidopsis* seedling growth, storage lipid mobilization, and photosynthetic gene expression are regulated by carbon:nitrogen availability. *Plant Physiol.* 128, 472–481. doi: 10.1104/pp.010475

Matile, P. H. (1980). The mustard oil bomb-compartmentation of the myrosinase system. *Biochemie und Physiol. der. Pflanzen*. 175 (8–9), 722–731. doi: 10.1016/S0015-3796(80)80059-X

Mewis, I., Appel, H. M., Hom, A., Raina, R., and Schultz, J. C. (2005). Major signaling pathways modulate *Arabidopsis* glucosinolate accumulation and response to both phloem-feeding and chewing insects. *Plant Physiol.* 138, 1149–1162. doi: 10.1104/pp.104.053389

Mewis, I., Khan, M. A. M., Glawischnig, E., Schreiner, M., and Ulrichs, C. (2012). Water stress and aphid feeding differentially influence metabolite composition in *Arabidopsis thaliana* (L.). *PloS One* 7, e48661. doi: 10.1371/journal.pone.0048661

Moore, B. D., Andrew, R. L., Külheim, C., and Foley, W. J. (2014). Explaining intraspecific diversity in plant secondary metabolites in an ecological context. *New Phytol.* 201, 733–750. doi: 10.1111/nph.12526

Nakano, R. T., Piślewska-Bednarek, M., Yamada, K., Edger, P. P., Miyahara, M., Kondo, M., et al. (2017). PYK10 myrosinase reveals a functional coordination between endoplasmic reticulum bodies and glucosinolates in *Arabidopsis thaliana*. *Plant J.* 89, 204–220. doi: 10.1111/tpj.13377

Nakazaki, A., Yamada, K., Kunieda, T., Sugiyama, R., Hirai, M. Y., Tamura, K., et al. (2019). Leaf endoplasmic reticulum bodies identified in *Arabidopsis* rosette leaves are involved in defense against herbivory. *Plant Physiol.* 179, 1515–1524. doi: 10.1104/pp.18.00984

Omirou, M. D., Papadopoulou, K. K., Papastylianou, I., Constantinou, M., Karpouzas, D. G., Asimakopoulos, I., et al. (2009). Impact of nitrogen and sulfur fertilization on the composition of glucosinolates in relation to sulfur assimilation in different plant organs of broccoli. *J. Agric. Food Chem.* 57, 9408–9417. doi: 10.1021/jf901440n

Pastorczyk, M., and Bednarek, P. (2016). Chapter seven - the function of glucosinolates and related metabolites in plant innate immunity. *Adv. In Botanical Res.* 80, 171–198. doi: 10.1016/bs.abr.2016.06.007

Petersen, B. L., Chen, S., Hansen, C. H., Olsen, C. E., and Halkier, B. A. (2002). Composition and content of glucosinolates in developing *Arabidopsis thaliana*. *Planta* 214, 562–571. doi: 10.1007/s004250100659

Pičmanová, M., Neilson, E. H., Motawia, M. S., Olsen, C. E., Agerbirk, N., Gray, C. J., et al. (2015). A recycling pathway for cyanogenic glycosides evidenced by the comparative metabolic profiling in three cyanogenic plant species. *Biochem. J.* 469, 375–389. doi: 10.1042/BJ20150390

Piślewska-Bednarek, M., Nakano, R. T., Hiruma, K., Pastorczyk, M., Sanchez-Vallet, A., Singkaravanit-Ogawa, S., et al. (2018). Glutathione transferase U13 functions in pathogen-triggered glucosinolate metabolism. *Plant Physiol.* 176, 538–551. doi: 10.1104/pp.17.01455

Piotrowski, M. (2008). Primary or secondary? Versatile nitrilases in plant metabolism. *Phytochemistry* 69, 2655–2667. doi: 10.1016/j.phytochem.2008.08.020

R Core Team (2017). R: A language and environment for statistical computing. R Foundation for Statistical Computing, Vienna, Austria. https://www.R-project.org/

Schonhof, I., Blankenburg, D., Müller, S., and Krumbein, A. (2007). Sulfur and nitrogen supply influence growth, product appearance, and glucosinolate

concentration of broccoli. *Z. Pflanzenernähr. Bodenk.* 170, 65–72. doi: 10.1002/jpln.200620639

Textor, S., and Gershenzon, J. (2009). Herbivore induction of the glucosinolate–myrosinase defense system: major trends, biochemical bases and ecological significance. *Phytochem. Rev.* 8, 149–170. doi: 10.1007/s11101-008-9117-1

Traka, M. H. (2016). Chapter Nine - Health Benefits of Glucosinolates. *Adv. In Botanical Res.* 80, 247–279. doi: 10.1016/bs.abr.2016.06.004

Urbancsok, J., Bones, A. M., and Kissen, R. (2017). Glucosinolate-derived isothiocyanates inhibit *Arabidopsis* growth and the potency depends on their side chain structure. *Int. J. Mol. Sci.* 18 (11), 2372. doi: 10.3390/ijms18112372

Urbancsok, J., Bones, A. M., and Kissen, R. (2018). Benzyl Cyanide Leads to auxin-like effects through the action of nitrilases in *Arabidopsis thaliana*. *Front. Plant Sci.* 9, 1240. doi: 10.3389/fpls.2018.01240

Vik, D., Mitarai, N., Wulff, N., Halkier, B. A., and Burow, M. (2018). Dynamic modeling of indole glucosinolate hydrolysis and its impact on auxin signaling. *Front. Plant Sci.* 9, 550. doi: 10.3389/fpls.2018.00550

Wentzell, A. M., Rowe, H. C., Hansen, B. G., Ticconi, C., Halkier, B. A., and Kliebenstein, D. J. (2007). Linking metabolic QTLs with network and cis-eQTLs controlling biosynthetic pathways. *PLoS Genet.* 3, 1687–1701. doi: 10.1371/journal.pgen.0030162

Withers, P. J. A., and O'Donnell, F. M. (1994). The response of double-low winter oilseed rape to fertiliser sulphur. *J. Sci. Food Agric.* 66, 93–101. doi: 10.1002/jsfa.2740660114

Wittstock, U., and Burow, M. (2007). Tipping the scales–specifier proteins in glucosinolate hydrolysis. *IUBMB Life* 59, 744–751. doi: 10.1080/15216540701736277

Wittstock, U., and Burow, M. (2010). Glucosinolate breakdown in *Arabidopsis*: mechanism, regulation and biological significance. *Arabidopsis Book* 8, e0134. doi: 10.1199/tab.0134

Wittstock, U., Kurzbach, E., Herfurth, A. M., and Stauber, E. J. (2016a). Chapter six - glucosinolate breakdown. *Adv. In Botanical Res.* 80, 125–169. doi: 10.1016/bs.abr.2016.06.006

Wittstock, U., Meier, K., Dörr, F., and Ravindran, B. M. (2016b). NSP-dependent simple nitrile formation dominates upon breakdown of major aliphatic glucosinolates in roots, seeds, and seedlings of *Arabidopsis thaliana* Columbia-0. *Front. Plant Sci.* 7, 1821. doi: 10.3389/fpls.2016.01821

Xu, Z., Escamilla-Treviño, L., Zeng, L., Lalgondar, M., Bevan, D., Winkel, B., et al. (2004). Functional genomic analysis of *Arabidopsis thaliana* glycoside hydrolase family 1. *Plant Mol. Biol.* 55, 343–367. doi: 10.1007/s11103-004-0790-1

Züst, T., and Agrawal, A. A. (2017). Trade-offs between plant growth and defense against insect herbivory: an emerging mechanistic synthesis. *Annu. Rev. Plant Biol.* 68, 513–534. doi: 10.1146/annurev-arplant-042916-040856

Züst, T., Heichinger, C., Grossniklaus, U., Harrington, R., Kliebenstein, D. J., and Turnbull, L. A. (2012). Natural enemies drive geographic variation in plant defenses. *Science* 338, 116–119. doi: 10.1126/science.1226397

Zhang, J., Sun, X., Zhang, Z., Ni, Y., Zhang, Q., Liang, X., et al. (2011). Metabolite profiling of *Arabidopsis* seedlings in response to exogenous sinalbin and sulfur deficiency. *Phytochemistry* 72, 1767–1778. doi: 10.1016/j.phytochem.2011.06.002

Zhao, Z., Zhang, W., Stanley, B. A., and Assmann, S. M. (2008). Functional proteomics of *Arabidopsis thaliana* guard cells uncovers new stomatal signaling pathways. *Plant Cell* 20, 3210–3226. doi: 10.1105/tpc.108.063263

Conflict of Interest: The authors declare that the research was conducted in the absence of any commercial or financial relationships that could be construed as a potential conflict of interest.

frontiers in Plant Science

ORIGINAL RESEARCH
published: 19 December 2019
doi: 10.3389/fpls.2019.01552

Identification and Characterization of Three Epithiospecifier Protein Isoforms in *Brassica oleracea*

Katja Witzel[1], *Marua Abu Risha*[1], *Philip Albers*[1], *Frederik Börnke*[1,2] *and Franziska S. Hanschen*[1]*

[1] *Leibniz Institute of Vegetable and Ornamental Crops, Großbeeren, Germany,* [2] *Institute of Biochemistry and Biology, University of Potsdam, Potsdam, Germany*

Glucosinolates present in *Brassicaceae* play a major role in herbivory defense. Upon tissue disruption, glucosinolates come into contact with myrosinase, which initiates their breakdown to biologically active compounds. Among these, the formation of epithionitriles is triggered by the presence of epithiospecifier protein (ESP) and a terminal double bond in the glucosinolate side chain. One *ESP* gene is characterized in the model plant *Arabidopsis thaliana* (AtESP; At1g54040.2). However, *Brassica* species underwent genome triplication since their divergence from the *Arabidopsis* lineage. This indicates the presence of multiple ESP isoforms in *Brassica* crops that are currently poorly characterized. We identified three *B. oleracea* ESPs, specifically *BoESP1* (LOC106296341), *BoESP2* (LOC106306810), and *BoESP3* (LOC106325105) based on *in silico* genome analysis. Transcript and protein abundance were assessed in shoots and roots of four *B. oleracea* vegetables, namely broccoli, kohlrabi, white, and red cabbage, because these genotypes showed a differential pattern for the formation of glucosinolate hydrolysis products as well for their ESP activity. BoESP1 and BoESP2 were expressed mainly in shoots, while BoESP3 was abundant in roots. Biochemical characterization of heterologous expressed BoESP isoforms revealed different substrate specificities towards seven glucosinolates: all isoforms showed epithiospecifier activity on alkenyl glucosinolates, but not on non-alkenyl glucosinolates. The pH-value differently affected BoESP activity: while BoESP1 and BoESP2 activities were optimal at pH 6-7, BoESP3 activity remained relatively stable from pH 4 to 7. In order test their potential for the *in vivo* modification of glucosinolate breakdown, the three isoforms were expressed in *A. thaliana* Hi-0, which lacks AtESP expression, and analyzed for the effect on their respective hydrolysis products. The BoESPs altered the hydrolysis of allyl glucosinolate in the *A. thaliana* transformants to release 1-cyano-2,3-epithiopropane and reduced formation of the corresponding 3-butenenitrile and allyl isothiocyanate. Plants expressing BoESP2 showed the highest percentage of released epithionitriles. Given these results, we propose a model for isoform-specific roles of *B. oleracea* ESPs in glucosinolate breakdown.

Keywords: epithionitrile, expression profile, functional complementation, glucosinolate hydrolysis, nitrile, specifier proteins, tissue specificity

OPEN ACCESS

Edited by:
Ralph Kissen, Norwegian University of Science and Technology, Norway

Reviewed by:
Rehna Augustine, National Institute of Plant Genome Research (NIPGR), India
Luke Bell, University of Reading, United Kingdom

***Correspondence:**
Franziska S. Hanschen
hanschen@igzev.de

Specialty section:
This article was submitted to Plant Metabolism and Chemodiversity, a section of the journal Frontiers in Plant Science

Received: *11 September 2019*
Accepted: *06 November 2019*
Published: *19 December 2019*

Citation:
Witzel K, Abu Risha M, Albers P, Börnke F and Hanschen FS (2019) Identification and Characterization of Three Epithiospecifier Protein Isoforms in Brassica oleracea. Front. Plant Sci. 10:1552. doi: 10.3389/fpls.2019.01552

INTRODUCTION

In the order Brassicales, glucosinolate (GLS) hydrolysis products play a vital role in plant defense, but are also well recognized for their health beneficial effects exerted by the consumption of *Brassicaceae* vegetables. The enzyme myrosinase initiates the breakdown of the sulfur-containing compounds when cells are disrupted and compartmentation is destroyed, for example by herbivore feeding (Wittstock and Burow, 2010; Hanschen et al., 2014). While releasing glucose, a thiohydroximate-*O*-sulfate is formed, which can spontaneously degrade by a Lossen-like rearrangement to an isothiocyanate (ITC) or a nitrile (Rossiter et al., 2007). ITCs are the pungent principle found in mustard, wasabi, and radish (Terada et al., 2015), among others. Moreover, ITCs have antimicrobial, anti-inflammatory, and most frequently investigated, anticarcinogenic properties (Traka and Mithen, 2009; Veeranki et al., 2015). Several *Brassica* vegetables mainly release nitriles and epithionitriles (ETNs) upon GLS hydrolysis (Matusheski et al., 2006; Hanschen and Schreiner, 2017; Klopsch et al., 2017). This is due to the presence of specifier proteins that interact during the degradation of the GLS aglucon (Wittstock and Burow, 2010; Backenköhler et al., 2018). Nitrile specifier proteins (NSPs) were previously identified in *Arabidopsis thaliana* as the evolutionary oldest specifier proteins. Their presence leads to an increased formation of nitriles (Kissen and Bones, 2009; Kuchernig et al., 2012). Occurrence and activity of the epithiospecifier protein (ESP) leads to the generation of ETNs from alkenyl-GLS aglucons as well as nitriles from non-alkenyl-GLS-aglucons (Burow et al., 2006; Matusheski et al., 2006). Many *Brassica* species release nitriles and ETNs upon GLS hydrolysis, among them *B. oleracea* and also *B. campestris, B. carinata,* and *B. rapa* (Macleod and Rossiter, 1985; Matusheski et al., 2004; Hanschen and Schreiner, 2017; Klopsch et al., 2017; Klopsch et al., 2018; Hanschen et al., 2019). So far, ESPs were characterized in *A. thaliana* (Lambrix et al., 2001; De Torres Zabala et al., 2005; Hanschen et al., 2018b) and in *Brassica* species, such as broccoli (*B. oleracea* var. *italica*) (Matusheski et al., 2006) and *B. napus* (Bernardi et al., 2000; Foo et al., 2000). The thiocyanate forming protein (TFP) has evolved from ESP and was reported in *Lepidium sativum*, *Thlaspi arvense,* and *Alliaria petiolate*, where it catalyzes the formation of thiocyanates and ETNs from selected GLS, and nitriles from other GLS (Kuchernig et al., 2011; Kuchernig et al., 2012). A recent study shows that the enlargement in the 3L2 loop of TaTFP is associated with a higher flexibility compared to ESP which enables an alternative loop conformation (alternative to the loop conformation leading to ETN formation due to C-S lyase activity) being the prerequisite for an additional activity as C-C-lyase leading to thiocyanate formation (Eisenschmidt-Bönn et al., 2019).

Tookey was the first to isolate an ESP-rich fraction in 1973 from *Crambe abyssinica* and to show that ESP activity depends on the availability of Fe^{2+} (Tookey, 1973). Fe^{2+} most likely is bound to ESP by the amino acids E260, D264, and H268 (Brandt et al., 2014; Backenköhler et al., 2018). Concerning ESP-catalyzed ETN formation, it is known that the sulfur from its thiirane ring originates from the thioglucosidic sulfur of the GLS (Brocker and Benn, 1983). Thus, Fe^{2+} most likely enables the intramolecular transfer and insertion of the sulfur into the terminal double bond to form the thiirane ring (Brocker and Benn, 1983; Foo et al., 2000; Backenköhler et al., 2018).

Vegetables belonging to *B. oleracea* species (such as broccoli, kohlrabi, Brussels sprouts, white, red, or savoy cabbages) are of high importance with regard to human consumption (FAOSTAT, 2018). As ESP activity reduces formation of health-promoting ITCs (Matusheski and Jeffery, 2001; Matusheski et al., 2006), knowledge on function of specifier proteins in vegetables is essential. Until now, one *ESP* was cloned form *B. oleracea*, expressed in *Escherichia coli* and the recombinant protein was characterized for its role in sulforaphane [4-(methylsulfinyl)butyl isothiocyanate] and sulforaphane nitrile [5-(methylsulfinyl) pentanenitrile] formation (Matusheski et al., 2006). However, it can be assumed that genome triplication of *B. oleracea* ($n = 9$) (Cheng et al., 2014; Liu et al., 2014) resulted in the presence and activity of multiple ESP isoforms with distinct expression patterns as shown for aquaporins (Diehn et al., 2015) and flavonoid biosynthesis genes (Qu et al., 2016).

Here we report the identification of three ESPs from *B. oleracea*. The transcript and protein abundance was investigated in shoots and roots of four *B. oleracea* genotypes, namely broccoli, kohlrabi, white, and red cabbage. Further, heterologous expressed BoESPs were characterized for their substrate specificity towards specific GLS. Finally, their potential for the *in vivo* modification of GLS hydrolysis was tested and the three isoforms were expressed in *A. thaliana* Hi-0, which has very low intrinsic ESP activity.

MATERIALS AND METHODS

Chemicals

Benzonitrile (≥99.9%), 3-butenenitrile (Allyl-CN, ≥98%), 3-(methylsulfanyl)propyl ITC (3MTP-ITC; ≥98%), D/L-dithiothreitol, $FeSO_4(H_2O)_7$ (≥ 99%), myrosinase (thioglucosidase from *Sinapis alba* seeds; ≥100 units/g), $CH_3COONa(H_2O)_3$ (≥ 99%), allyl ITC (Allyl-ITC, ≥99%), Coomassie Brilliant Blue R staining solution, Gamborg's vitamin solution, isopropyl-β-D-thiogalactopyranoside (IPTG), kanamycin sulfate, Murashige and Skoog medium, 4-pentenenitrile (3But-CN, ≥97%), 3-phenylpropanenitrile (2PE-CN) ≥99%), and 2-phenylethyl isothiocyanate (2PE-ITC, ≥99%) were purchased from Sigma-Aldrich Chemie GmbH (Steinheim, Germany). 3-Indoleacetonitrile (IAN) (≥98%) was acquired from Acros Organics (Fischer Scientific GmbH, Schwerte, Germany). 3-Butenyl ITC (3But-ITC, ≥95%) was obtained from TCI Deutschland GmbH (Eschborn, Germany). 3-(Methylsulfinyl) propyl ITC (3MSOP-ITC) and 4-(methylsulfanyl)butyl ITC (4MTB-ITC, ≥98%) were purchased from Santa Cruz Biotechnology (Heidelberg, Germany). 4-(Methylsulfinyl) butyl ITC (4MSOB-ITC) was bought from Enzo Life Sciences GmbH (Lörrach, Germany). (*R*)-5-Vinyloxazolidine-2-thione (*R*-OZT) was purchased from Biosynth AG (Staad, Switzerland). Acetic acid (≥99.5%), 4-hydroxybenzyl GLS (≥99%), methylene chloride (GC Ultra grade), allyl GLS · H_2O (ROTICHROM® CHR, and vitamin C [L-(+)-ascorbic acid, ≥99%] were obtained

from Carl Roth GmbH (Karlsruhe, Germany). 1-Cyano-2,3-epithiopropane [CETP, ≥97.6% (by GC-MS)] was purchased from Taros Chemicals GmbH Co. KG (Dortmund, Germany). 1-Cyano-3,4-epithiobutane (CETB, ≥99%) was purchased from ASCA GmbH Angewandte Synthesechemie Adlershof (Berlin, Germany). Methanol (≥99.95%), acetonitrile (LC-MS grade), and arylsulfatase were purchased from Th. Geyer GmbH & Co. KG (Renningen, Germany). $NaSO_4$ (≥99%) was purchased from VWR International GmbH (Darmstadt, Germany). 3-Butenyl (3But), (*R*)-2-hydroxy-3-butenyl- (2OH3But), 4-(methylsulfanyl)butyl- (4MTB), 3-(methylsulfinyl)propyl- (3MSOP), 4-(methylsulfinyl) butyl- (4MSOB), and 2-phenylethyl-GLS (2PE) were purchased from Phytolab GmbH & Co. KG (Vestenbergsgreuth, Germany).

All solvents were of LC-MS or GC-MS grade, ultrapure water was used for all experiments.

Plant Material

Seeds of white cabbage *B. oleracea* var. *capitata* f. *alba* cv. Jetma (Rijk Zwaan Welver GmbH, Welver, Germany), kohlrabi *B. oleracea* var. *gongylodes* cv. Kolibri, and red cabbage *B. oleracea* var. *capitata* f. *rubra* cv. Integro (both Volmary GmbH, Münster, Germany), and broccoli *B. oleracea* var. *italica* cv. Ironman (Seminis Vegetable Seeds Deutschland GmbH, Neustadt am Rübenberge, Germany) all being F1 hybrids, were germinated on perlite. Sprouts were grown for 8 days in a climate chamber at controlled light (15 h photoperiod, 500 $\mu mol \cdot m^{-2} \cdot s^{-1}$) and temperature regime (day 22°C/night 18°C) as well as 70% humidity. Water was given as needed.

At harvest, sprouts were separated into root and shoot (tissue in between was discarded). Aliquots for RNA (100 mg) and for protein extraction (500 mg) were frozen in liquid nitrogen and stored at -80°C until further sample preparation. For analysis of GLS, an aliquot was weighed and frozen immediately in liquid nitrogen and lyophilized subsequently. Determination of GLS hydrolysis products was performed on 250 mg of fresh plant material, mixed with 250 mg of water and homogenized using a mixer mill at 30 Hz as described earlier (Hanschen and Schreiner, 2017). For determination of ESP activity of *B. oleracea* tissues, 250 mg of tissue was mixed 1:1 with water and ESP-rich plant extracts were prepared as described previously (Hanschen et al., 2018a). Samples from three (protein profiling, GLS, GLS hydrolysis products, ESP activity) or four (transcript profiling) independent experiments were analyzed.

A. thaliana seeds of T2 transgenic lines were surface sterilized and germinated on half-strength Murashige Skoog medium (pH 5.8), supplemented with 1.5% sucrose and 50 µg/ml kanamycin, the latter except for Hi-0 wildtype plants. Two weeks after germination, plants were transferred to pots filled with sand and watered with nutrient solution (Gibeaut et al., 1997). Plants were grown for 5 weeks under short-day conditions (8 h light/16 h dark, 22°C, 40–60% humidity). At harvest, roots were carefully removed from pots, blotted dry and samples of rosette leaves and roots were taken and analyzed for GLS breakdown products: 5–55 mg of root and 60–250 mg of shoot tissue were exactly weighed, mixed with water 1: 1, homogenized as described above and analyzed. Three independent experiments were performed to test BoESP activity in Hi-0, with 3–4 replicates consisting of 1–2 plants.

Analysis of Glucosinolates

To determine the profiles and concentrations of GLS in root and shoot tissue of *B. oleracea*, lyophilized powder was extracted and GLS were analyzed in their desulfo-form (Hanschen and Schreiner, 2017).

Determination of Glucosinolate Hydrolysis Products in Roots and Shoots

The extraction and quantification of the enzymatically formed GLS hydrolysis products in homogenized plant material or the BoESP activity assay *via* GC-MS was performed as described earlier (Hanschen and Schreiner, 2017) with small modifications: The transfer line was set to 270°C and He flow was 1 ml min^{-1} in the ESP-assay experiments and GLS hydrolysis profile screenings of *B. oleracea*. He flow was 1.8 ml min^{-1} for analyzing GLS hydrolysis products in *A. thaliana*.

Database Search and Gene Sequence Analyses

The *A. thaliana* ESP nucleotide sequence (At1g54040.2) was used as query to search the *B. oleracea* genome data set at NCBI using BLASTn (https://blast.ncbi.nlm.nih.gov/Blast.cgi). Primers were designed using NCBI Primer-BLAST tool (https://www.ncbi.nlm.nih.gov/tools/primer-blast/). Multiple sequence alignments and assessment of sequence identities were done with MegAlign (DNASTAR, United States) and T-Coffee program (Di Tommaso et al., 2011).

cDNA Synthesis and qPCR Analysis

RNA was isolated from 100 mg root or shoot material using RNeasy Plant Mini Kit (QIAGEN, Hilden, Germany), according to the manufacturer's specifications, including DNase treatment. Briefly, cDNA was synthesized from 2 µg total RNA with iScript™ cDNA Synthesis Kit (Bio-Rad Laboratories GmbH, Munich, Germany), according to the manufacturer's protocol. Transcript abundance of *BoESP*s was estimated by qPCR based on primer pairs detailed in **Table S1**. Two primer pairs were selected for *B. oleracea* reference genes based on geNORM (Vandesompele et al., 2002) analysis of expression stability and previous evaluation (Brulle et al., 2014). The two reference genes chosen were *BoSAND1* (GenBank accession no. KF218596) and *BoTUB6* (GenBank accession no. KF218597). The PCR program comprised an initial denaturation (95°C/3 min) followed by 40 cycles of 95°C/10 s, 54°C/30 s. A melting curve was generated by denaturing (95°C/10 s), then holding the reaction for 5 s at a temperature between 65°C and 95°C in 0.5°C increments. The template cDNA was diluted 10-fold in sterile water to an approximate concentration of 50 ng/µl. qPCRs were set up, measured and analyzed as described earlier (Witzel et al., 2018). Statistical analysis of transcript abundance data was assessed using Student's t-test implemented in SigmaPlot 12.3 (Systat Software GmbH, Germany).

Protein Extraction and Label Free Protein Quantification

Proteins in shoots and roots of the four *B. oleracea* genotypes were extracted using phenol extraction method (Faurobert et al., 2007). Resulting protein pellets were solubilized in 30 mM Tris, 7 M urea, 2 M thiourea, 4% CHAPS (pH 8.5), and concentration was measured using Bradford Red reagent (Expedeon, United Kingdom) and bovine serum albumin as standard. For tryptic digest of proteins, the filter aided sample preparation (FASP) protocol was applied as outlined in detail (Jozefowicz et al., 2018), using a Microcon-10 kDa Centrifugal Filter Unit (Merck Millipore, United States). After completion of digest, peptides were eluted from the filter and the eluate was dried. Desalting of peptides was done using Peptide Desalting Spin Columns (Pierce, Thermo Scientific, United States) following the manufacturer's instructions. Eluted and desalted peptides were re-suspended in 2% acetonitrile/0.1% trifluoroacetic acid to a concentration of 100 ng μl^{-1}.

Five µl of protein digest were separated by nanoflow liquid chromatography on a Dionex UltiMate 3000 system (Thermo Scientific) coupled to a Q Exactive Plus mass spectrometer (Thermo Scientific). Peptides were loaded onto a C18 trap-column (0.3 × 5 mM, PepMap100 C18, 5 µm, Thermo Scientific) and then eluted onto an Acclaim PepMap 100 C18 column (0.075 x 150 mM, 3 µm, Thermo Scientific) at a flow rate of 300 nl min^{-1}. The mobile phases consisted of 0.1% formic acid (solvent A) and 0.1% formic acid in 80% ACN (solvent B). Peptides were separated chromatographically by a 70 min gradient from 2% to 44% solvent B, with the column temperature set at 40°C. For electrospray ionization of peptides, a Nanospray Flex ion source was used, with spray voltage set at 1.80 kV, capillary temperature at 275°C, and S-lens RF level at 60. Mass spectra were acquired in positive ion and data-dependent mode. Full-scan spectra (375 to 1,500 m/z) were acquired at 140,000 resolution and MS/MS scans (200 to 2,000 m/z) were conducted at 17,500 resolution. Maximum ion injection time was 50 ms for both scan types. The 20 most intense MS ions were selected for collision-induced dissociation fragmentation. Singly charged ions and unassigned charge states were rejected; dynamic exclusion duration was set to 45 s.

The raw files were processed using Proteome Discoverer v2.3.0.523 (Thermo Scientific) and Mascot search engine v2.5.1.1 (Matrix Science Inc, United States), searching the *B. oleracea* protein database (release 42, http://plants.ensembl.org/Brassica_oleracea/Info/Index). The false discovery rate was set to 0.01 for proteins and peptides. Further parameters for database search were: peptide tolerance, 10 ppm; fragment ion tolerance, 0.02 Da; tryptic cleavage with max. 2 missed cleavages; carbamidomethylation of cysteine as fixed modification and oxidation of methionine as variable modification. The result lists were filtered for high confident peptides and their signals were mapped across all LC-MS experiments (four *B. oleracea* genotypes x two analyzed organs x three independent experiments x three replicate measurements = 72 LC-MS experiments) and normalized to the total peptide amount per same LC-MS experiment. Only unique peptides were selected for quantification and abundances of all peptides allocated to a specific protein were summed and compared. Statistical analysis of protein abundance data was assessed using Student's t-test implemented in SigmaPlot 13.0 (Systat Software GmbH, Germany).

Plasmid Construction

Due to the high sequence similarity of *BoESP* isoforms, cloning of specific full-length cDNA fragments from *B. oleracea* was not successful. Therefore, cDNAs were commercially synthesized (Eurofins Genomics Germany GmbH, Germany) and subsequently PCR amplified using the primers listed in **Table S2**. The resulting fragments were inserted into the pENTR-D/TOPO vector according to the manufacturer's instructions (Thermo Fisher Scientific, Germany) and verified by sequencing. Subsequently, the individual ESP coding regions were recombined into the technique-specific destination vector, using L/R-Clonase (Thermo Fisher Scientific). To generate constructs for *A. thaliana* transformation, the destination vector pRB-35S-3xmyc (Bartetzko et al., 2009) was used while *E. coli* expression constructs were based on a Gateway®-compatible version of pMal-C2 (New England Biolabs GmbH, Germany).

Protein Expression and Purification

For *in vitro* ESP assays, MBP-BoESP1, MBP-BoESP2, and MBP-BoESP3 were individually expressed in *E. coli* BL21 cells at 37°C for 3 h after induction with 0.5 mM IPTG. Bacteria were harvested, lysed by sonication and after centrifugation, the recombinant proteins were purified using amylose resin (New England Biolabs GmbH, Germany) according to the manufacturer's instructions. The purity of the proteins was approximately 90% as analyzed by SDS-PAGE and Coomassie Blue staining.

Generation of Stable *Arabidopsis thaliana* Transformants Expressing BoESP1-3

A. thaliana ecotype Hi-0 was transformed using the floral dip method (Clough and Bent, 1998). For the selection of transgenic plants, seeds of T0 plants were sterilized and sown onto Murashige and Skoog medium supplemented with Gamborg's vitamin solution (1:1,000) and 50 µg ml^{-1} kanamycin. Primary transformants were allowed to self-fertilize and then propagated into the T2 generation.

Western Blotting

Immunoblotting analysis and membrane staining was performed as described previously (Witzel et al., 2017). Ten µg of protein were separated on SDS gels (SERVAGel™ TG PRiME™ 8–16%, Serva, Germany). The blots were probed with the anti-c-myc-peroxidase conjugate antibody (Roche, Mannheim, Germany) in a dilution of 1:1,000. Immunodetection was carried out using Pierce ECL Western Blotting Substrate (Thermo Fisher Scientific, USA) and Octoplus QPLEX Fluorescence Imager (NH DyeAGNOSTICS, Germany). After image capture, total protein load was assessed by staining the blots using amido black 10B staining method (Witzel et al., 2017).

Determination of ESP Activity

BoESP Activity With Pure GLS Standards

To compare the substrate specificities of the three recombinant BoESPs, the protocol of (Matusheski et al., 2004) was modified and adapted. In order to maximize GLS hydrolysis, vitamin C was added and Fe^{2+} concentration in the assay was reduced to 0.2 mM to optimize ITC formation while maintaining ETN formation from alkenyl GLS in the assay: Briefly, 50 µl of purified ESP (containing in total 6.5 µg ESP as determined by Bradford assay (Bradford, 1976), 350 µl of a 50 mM sodium acetate buffer (pH 5.5) containing 1 mM dithiothreitol and 0.2 mM of $FeSO_4$, 10 µl of a 25.5 mM vitamin C solution, 50 µl of 0.5 U ml^{-1} myrosinase and 50 µl of a 10 mM solution of the GLS to be tested were mixed in an extraction tube and incubated for 1 h at room temperature. Then, hydrolysis products of the respective GLS were extracted and quantified according to the protocol described above. Water controls (without ESP) were analyzed as well for each GLS.

ESP activity was expressed as the % of ETN [or nitrile (CN) formation for nonalkenyl GLS]: % ETN = [ETN]/([ETN]+[ITC]+[CN])*100%; % CN = [CN]/([CN] + [ITC]) *100%. Each analysis consisted of three independent experiments (freshly purified ESP extract) that consisted of 2–3 technical replicates.

ESP Activity in *B. oleracea* Tissues

In order to analyze the ESP activity of *B. oleracea* root and shoot samples, ESP-rich plant extracts, prepared as described previously (Hanschen et al., 2018a) were used for the assays. The protocol described above was used in a slightly modified way: 50 µL of ESP-rich plant extract were mixed with 350 µl of the sodium acetate buffer containing dithiothreitol and $FeSO_4$, 10 µl of the vitamin C solution, 50 µl of myrosinase solution and finally 50 µl of 5 mg ml^{-1} solution of allyl GLS were added and samples were incubated and analyzed as described above. As some of the ESP-extracts already could contain CETP, water controls were analyzed as well, by adding water instead of allyl GLS. These values were used to correct the sample values. The % of CEPT on all allyl GLS hydrolysis products was calculated (% CETP = [CEPT]/([CEPT]+[Allyl-ITC]+[Allyl-CN])*100%).

Influence of pH on ESP Activity

In order to investigate the influence of pH value on allyl GLS hydrolysis by the three ESPs, the ESP assay described above was performed, except that the pH value of the sodium acetate buffer was set to pH 4, pH 5, pH 6, and pH 7. Three technical replicates were analyzed.

Statistical Analysis

To investigate statistical significant differences, one-way analysis of variance (ANOVA) was performed. For the comparison of means, Tukeys HSD test was applied using the STATISTICA version 13 software (StatSoft, Hamburg, Germany) (data in **Figures 1**, **2** and **7**, **Figure S2**) or the SigmaPlot version 13.0 (Systat Software GmbH, Germany) (data in **Figures 4**, **5** and **6**).

RESULTS

Glucosinolate and Glucosinolate Hydrolysis Pattern in *B. oleracea* Genotypes

Previously, we have shown that *Brassica* vegetables exhibit a huge variation in the pattern of intact and hydrolyzed GLS (Hanschen and Schreiner, 2017; Klopsch et al., 2018). In order to characterize the plant material with regard to those specific plant secondary compounds, seedlings of four *B. oleracea* varieties, namely broccoli, kohlrabi, white cabbage, and red cabbage were investigated for their GLS profile and GLS hydrolysis product formation in roots and shoots. Both, broccoli and kohlrabi where rich in methylsulfanyl- and methylsulfinylalkyl GLS, but

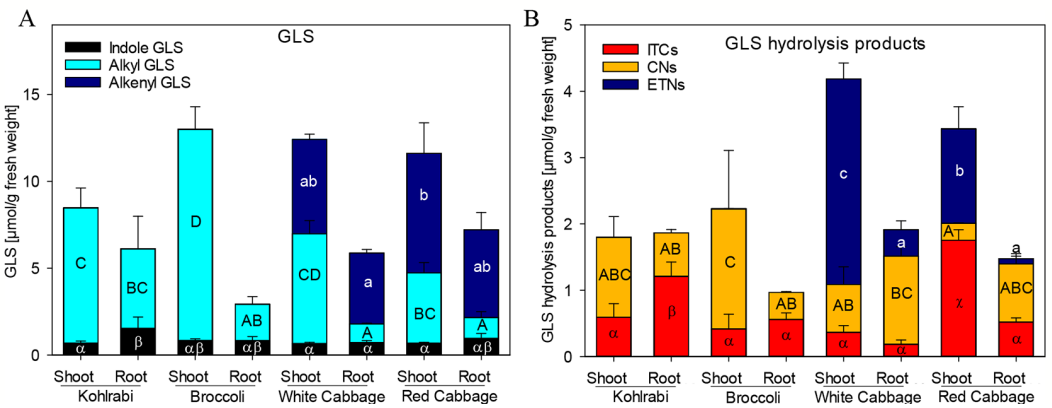

FIGURE 1 | Glucosinolate (GLS) accumulation **(A)** and formation of hydrolysis products **(B)** in shoots and roots of four *B. oleracea* genotypes. ITCs, isothiocyanates; CNs, nitriles; ETNs, epithionitriles. Values represent mean ± standard deviation (SD) of three independent experiments (n = 3). Significant differences in means between the formation of), alkenyl GLS (small letters), alkyl GLS (capital letters), and indole GLS (Greek letters) in **(A)** or ETNs (small letters), CNs (capital letters), or ITC (Greek letters) in **(B)** as tested by ANOVA and Tukey HSD test at the $p \leq 0.05$ level.

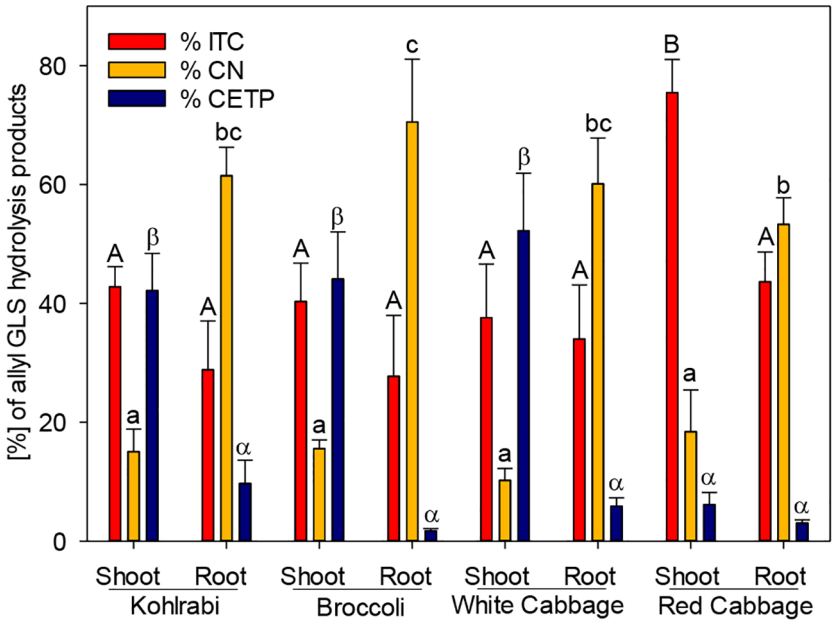

FIGURE 2 | The effect of epithiospecifier protein activity of shoots and roots of four *B. oleracea* genotypes on the proportion of 1-cyano-2,3-epithiopropane (CEPT), the corresponding isothiocyanate (ITC) and nitrile (CN) produced from allyl glucosinolate (GLS). Values represent mean ± standard deviation of three independent experiments (n = 3). Significant differences in means between the formation of ITC (capital letters) or CN (small letters) or CETP (Greek letters) as tested by ANOVA and Tukey HSD test at the $p \leq 0.05$ level.

contained no alkenyl GLS (**Figure 1A**, **Table S3**). While shoot tissue was rich in the methylsulfinylalkyl GLS, 3MSOP, and 4MSOB, roots contained mainly the less oxidized 3MTP and 4MTB as well as 1-methoxyindol-3-ylmethyl GLS (**Table S3**). Shoots and roots of white and red cabbage accumulated alkenyl GLS (**Figure 1A**): allyl GLS in white cabbage and 2OH3But in red cabbage. Further, methylsulfanylalkyl GLS were present and shoots were rich in methylsulfinylalkyl GLS. Here, white cabbage contained mainly 3MSOP, whereas red cabbage was rich in 4MSOB. Additionally, white cabbage shoots contained 2PE (**Table S3**).

To screen for GLS hydrolysis products, the GLS in these plant genotypes and tissues were degraded upon endogenous enzymatic hydrolysis and corresponding nitriles, ITCs and ETNs (from alkenyl GLS) were produced (**Figure 1B**, **Table S4**). Nitriles were formed mainly in shoots of kohlrabi and broccoli, while roots released mainly ITCs; however, no ETNs was found in kohlrabi and only very low levels of ETNs (below 0.3%) were detected in broccoli (**Table S4**). Most abundant in white cabbage shoots were ETNs with 74% of degradation products, while roots formed mainly nitriles (70%) and less ETNs (20%). Shoots of red cabbage released mainly ITCs (51%), followed by ETNs (41%) and root tissue released mainly nitriles (59%) and low amounts of ETNs (5%). Of note is that, compared to total GLS contents, the overall recovery of GLS hydrolysis products was relatively low with 18–46%. The recovery of products from allyl GLS ranged from 39–63%, while that of the products of sulfinylalkyl GLS, 3MSOP and 4MSOB, was low with only 13%.

ESP Activity in *B. oleracea* Is Genotype- and Organ-Specific

While ESP activity *via* plant tissue autolysis assay was detected only in white and red cabbage, an additional assay was performed to analyze plant tissue ESP activity on allyl GLS. The potential of the tested genotypes to form ETN as an indicator of ESP activity was assessed by studying the hydrolysis of allyl GLS to the corresponding ETN (1-cyano-2,3-epithiopropane, CETP) in presence of myrosinase. ESP activity of shoots was high in kohlrabi, broccoli, and white cabbage (42%, 44%, and 52%, respectively), while it was lower in shoots of red cabbage (**Figure 2**). ESP activity was in general inversely correlated to CN formation in this assay. Roots possessed a lower ESP activity as compared to shoots, but root tissue of kohlrabi had by tendency higher ESP activity than shoot tissue of red cabbage (9.7% vs. 6.1%). Shoot tissue of red cabbage significantly released more ITC than the other tissues in this assay (**Figure 2**). These results indicate that all *B. oleracea* genotypes and tissues exhibit ESP activity, including kohlrabi and broccoli.

Identification of Genes in *B. oleracea* With Sequence Similarity to AtESP

Based on our observation of differential ETN formation in the tested genotypes and plant organs, we hypothesized the presence of multiple ESP isoforms in *B. oleracea*. Sequence similarity search using *AtESP* nucleotide sequence (At1g54040.2) against the whole genome of *B. oleracea* revealed six predicted ESP-like sequences (**Table 1**). Amino acid sequence alignment

TABLE 1 | Predicted and characterized ESP-like genes present in *Brassica oleracea*.

Protein isoform	NCBI gene ID	NCBI protein ID	Ensembl Plants ID	Phytozome ID	ORF (aa)
BoESP1	LOC106296341	XP_013587912.1	Bo6g032960.1	Bol039072	343
BoESP2	LOC106306810	XP_013599019.1	Bo7g067530	Bol006380	343
BoESP3	LOC106325105	XP_013618586.1	Bo2g124420.1	Bol024137	343
–	LOC106297542	XP_013589216.1	Bo6g050860	Bol013374	158
–	LOC106306884X1, LOC106306884X2	XP_013599116.1, XP_013599117.1	Bo7g067500	Bol006378	343

The AtESP nucleotide sequence (At1g54040.2) was used to Blast B. oleracea *entries of the NCBI database (https://www.ncbi.nlm.nih.gov),* B. oleracea *entries of the Ensembl Plants v43 database (https://plants.ensembl.org/index.html) and* B. oleracea *var.* capitata *v1.0 entries of the Phytozome v12.1 database (https://phytozome.jgi.doe.gov/pz/portal.html#).*

showed that three of the predicted genes were almost identical: LOC106306810 (designated *BoESP2*), LOC106306884X1, and LOC106306884X2 (**Table 2**). Hence, these three predicted genes were considered as one isoform. The amino acid sequence of LOC106297542 was considerably shorter as compared to the remaining ESPs and shared only N-terminal sequence similarity to AtESP. Since the protein contained only two Kelch domains, this gene was omitted from further analysis. In order to test if the predicted genes are actively transcribed in shoots of the four *B. oleracea* genotypes, the open reading frames of the putative sequences were aligned and primers were designed to bind to their isoform-specific regions (**Table S1**, **Figure S1**). The specificity of amplification was verified by sequencing of PCR products. PCR products were obtained for LOC106296341 (designated *BoESP1*), LOC106306810 (designated *BoESP2*), and LOC106325105 (designated *BoESP3*) and, therefore, those three ESP isoforms were investigated further. Sequence comparison with *AtESP* showed that *BoESP1-3* had a sequence similarity between 79 and 81% at nucleotide level (**Figure S1**), and 77% on amino acid level (**Figure 3**).

Transcript and Protein Expression Pattern of BoESP1-3

In order to analyze transcript abundance levels in shoot and roots of sprouts, quantitative real-time PCR was performed. The analysis revealed a higher expression level of *BoESP1* in shoots as compared to roots (**Figures 4A**, **B**). *BoESP2* was higher abundant in shoots of broccoli, white cabbage, and red cabbage as compared to the respective root samples, although this pattern was reversed in kohlrabi. *BoESP3* expression was barely detected in shoots, while a transcript accumulation was detected in roots of kohlrabi and white cabbage.

We further extended the expression analysis to profile protein abundance pattern based on label-free LC-MS analysis. A total of 20,896 peptide groups were identified by this approach in shoots and roots of the four genotypes, leading to the identification of 6,986 proteins, which were grouped into 3,996 protein groups based on sequence similarity. Then, the data was inspected for BoESP1-3 presence and abundance. Protein coverage was higher for BoESP1 (69%) and BoESP2 (75%) as compared to BoESP3 (42%). Nevertheless, a sufficient amount of isoform-specific peptides was detected allowing the quantification of isoforms based on peptides that were unique to the respective isoform. Nine unique peptides were found for BoESP1, 16 unique peptides were detected for BoESP2, and eight unique peptides were specific for BoESP3. Overall, the protein abundance pattern (**Figures 4C**, **D**) was in agreement with the transcript abundance. However, while transcript levels were threefold higher in shoots as compared to roots, the level of accumulation of the respective gene products was similar between both plant organs.

Substrate Specificity of BoESP Isoforms

Since the three BoESP isoforms exhibited a differential expression pattern, their substrate specificity was tested next, using recombinant BoESP1-3 proteins. Open reading frames of BoESP1-3 were cloned, expressed in *E.coli* and proteins purified using the maltose-binding protein tag. The effect of the substrate structure on the activity of the three BoESPs was investigated using three alkenyl GLS, three alkyl GLS and one aromatic GLS. With all three alkenyl GLS investigated, namely allyl GLS (releasing CETP), 3But (releasing CETB) and 2OH3But (forming CHETB), BoESP3 showed the highest ESP activity, and BoESP2 (by tendency for allyl GLS hydrolysis) the lowest ESP activity (**Figure 5**). BoESPs did not increase nitrile release from the

TABLE 2 | Amino acid sequence similarity of identified ESP-like genes found in *B. oleracea*, given as per cent identity.

LOC 106325105 (BoESP3)	LOC 106296341 (BoESP1)	LOC 106297542	LOC 106306810 (BoESP2)	LOC 106306884X1	LOC 106306884X2	
	86.0	79.1	86.3	86.6	86.6	**LOC106325105**
		73.2	84.5	84.8	84.8	**LOC106296341**
			77.1	77.8	77.8	**LOC106297542**
				99.7	99.7	**LOC106306810**
					100.0	**LOC106306884X1**
						LOC106306884X2

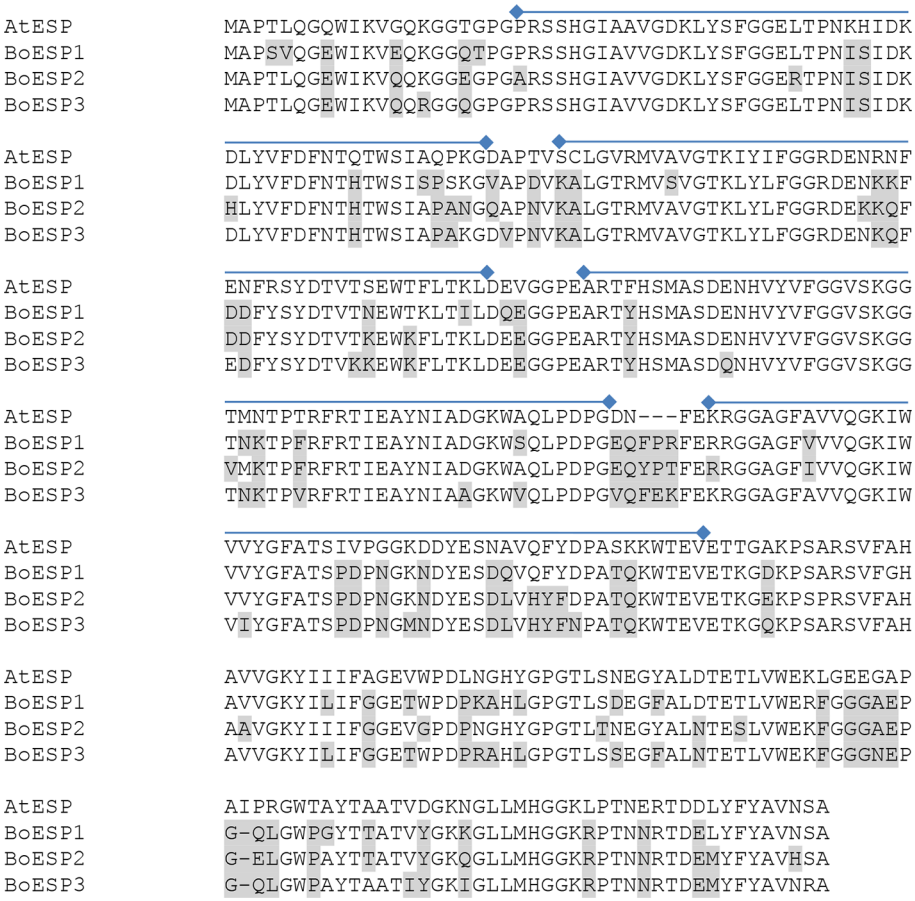

FIGURE 3 | Alignment of the amino acid sequences of AtESP (At1g54040.2) and *Brassica oleracea* ESPs BoESP1 (LOC106296341), BoESP2 (LOC106306810), and BoESP3 (LOC106325105) using T-Coffee program (Tommaso et al., 2011). Residues variant from AtESP are shaded in grey. Kelch domains (PF01344, Kelch_1) of AtESP are indicated by lines above the alignment and were derived from pfam (http://pfam.xfam.org).

alkenyl GLS (**Table S5**). Moreover, there was no effect of the three BoESPs on the hydrolysis of nonalkenyl GLS [4MTB releasing 5-(methylsulfanyl)pentanenitrile (4MTB-CN), 3MSOP releasing 4-(methylsulfinyl)butanenitrile (3MSOP-CN), and 4MSOB releasing 5-(methylsulfinyl)pentanenitrile (4MSOB-CN)] (**Figure S2**).

The pH Affects BoESP Activity Differently

The pH-optimum can be used as a measure to assess protein adaptation to cellular and subcellular pH as well as to get insight into protein-protein interactions that take place in the same microenvironment (Talley and Alexov, 2010). The optimal pH value for *B. napus* (Bernardi et al., 2000) and *Crambe abyssinica* (Tookey, 1973) ESPs was reported to be pH 6, but so far the pH optimum for BoESP was not published. Therefore, the effect of pH values on the activity of the three BoESP was investigated in a pH range of pH 4 to pH 7 (**Figure 6**). While BoESP3 activity was high at all pH values, both BoESP1 and BoESP2 were affected. Being at optimal pH from 6–7, their activity decreased with decreasing pH value. This effect was stronger for BoESP2 compared to BoESP1, especially at pH 4.

Expression of BoESP1-3 in *A. thaliana* Hi-0

In order to test whether BoESP1-3 isoforms are able to perform ESP activity *in planta*, the three isoforms were expressed in *A. thaliana* Hi-0, an ecotype with a GLS pattern that is characterized by high allyl GLS content and barely detectable own ESP activity (Hanschen et al., 2018b). Two independent lines expressing cDNAs of BoESP1 and three independent lines expressing BoESP2 and BoESP3, respectively, were characterized in comparison to the Hi-0 wildtype. Western blot analyses using an antibody directed against the C-terminal myc-tag confirmed BoESP protein in all transgenic lines (**Figure S3**). Analysis of transgenic *A. thaliana* plants revealed a modified hydrolysis pattern of allyl GLS (**Figure 7**). Levels of released GLS hydrolysis products are given in the **Table S6**. Whereas Hi-0 wildtype plants released mainly Allyl-CN [1.09 ± 0.17µmol/g fresh weight (FW)], Allyl-ITC (0.56 ± 0.09 µmol/g FW), and very low CETP (0.006 ± 0.002 µmol/g FW) from allyl GLS in shoots and roots, BoESP1-3 transformants released mainly CETP from these tissues. Shoots of *A. thaliana* BoESP2 constructs showed a slightly higher percentage of CETP-formation compared to BoESP3 constructs. The shift

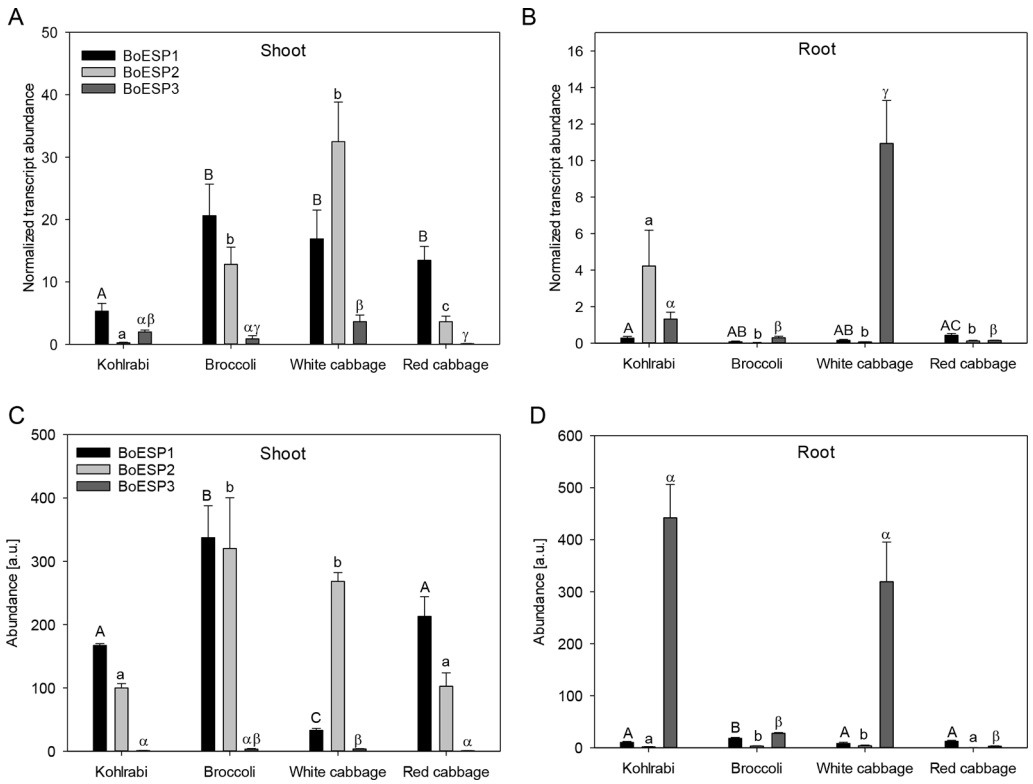

FIGURE 4 | Expression profiles of BoESP1-3 transcripts **(A**, **B)** and proteins **(C**, **D)** in shoots and roots of four *B. oleracea* genotypes. Values represent mean ± standard error of measurements based on three technical replicates from four independent biological experiments for transcript abundance, and based on three technical replicate runs from three independent biological experiments for protein abundance. Letters denote statistical significant differences ($p \leq 0.05$) of BoESP1 (capital letters), BoESP2 (small letters), or BoESP3 (Greek letters) between the genotypes within a given plant organ.

in allyl GLS hydrolysis in shoot tissue was accompanied with reduced formation of both Allyl-ITC and Allyl-CN in the transgenic lines. Since the overall amount of allyl GLS in roots is 10-times lower as compared to shoots (Witzel et al., 2013), the detection of respective breakdown products in wildtype and transgenic lines was near the method detection limit, resulting in substantial standard deviations. Nonetheless, ESP activity was increased in BoESP1-3 transformants, as compared to the wildtype. The hydrolysis of the alkyl GLS 8-(methylsulfanyl) octyl (8MTO) in *A. thaliana* was not affected by the BoESPs (**Figure S4**).

DISCUSSION

GLS hydrolysis in *Brassica* vegetables often results in the release of nitriles and ETN instead of ITCs, and presence of ESP is made responsible (Petroski and Tookey, 1982; Matusheski et al., 2006; Hanschen and Schreiner, 2017; Klopsch et al., 2018). Here, we report the identification and characterization of three BoESP isoforms in *B. oleracea* varieties, namely kohlrabi, broccoli, white cabbage, and red cabbage and their functional characterization in *A. thaliana*.

GLS hydrolysis in root and shoot tissue of four *B. oleracea* genotypes was investigated and was correlated with ESP activity in order to characterize the role of ESP in the GLS hydrolysis. The genotypes that contained no alkenyl GLS (kohlrabi, broccoli) were producers of nitriles, while the genotypes containing alkenyl GLS (white cabbage, red cabbage) formed ETN in high amounts, which is in line with previous reports (Matusheski et al., 2006; Hanschen and Schreiner, 2017; Hanschen et al., 2018a). In contrast to this, the ESP activity assay revealed that all genotypes and tissues possess ESP activity. This is mirrored by the high ETN release in alkenyl rich genotypes (white cabbage, red cabbage) or high nitrile release in shoot tissue of alkyl GLS rich genotypes and points to the dual role of ESPs in generating nitriles as well as ETNs (Lambrix et al., 2001), depending on the GLS substrate.

Our analysis identified six genes in the *B. oleracea* genome with sequence homology to *AtESP*. Screening the transcript abundance of these genes revealed that three of them were expressed in shoots of seedlings. It remains open whether those genes, where no expression was detected, are transcribed at older developmental stages, in other tissues or genotypes as investigated, have lost their function or are induced under specific environmental conditions. One of the expressed genes, *BoESP1*, was identical to a previously characterized ESP from *B. oleracea* (Matusheski et al., 2006). Expression of *BoESP*s was regulated differentially with respect to the analyzed tissue and the investigated genotypes. *BoESP1* and *BoESP2* were detected mainly in shoots, while *BoESP3* was

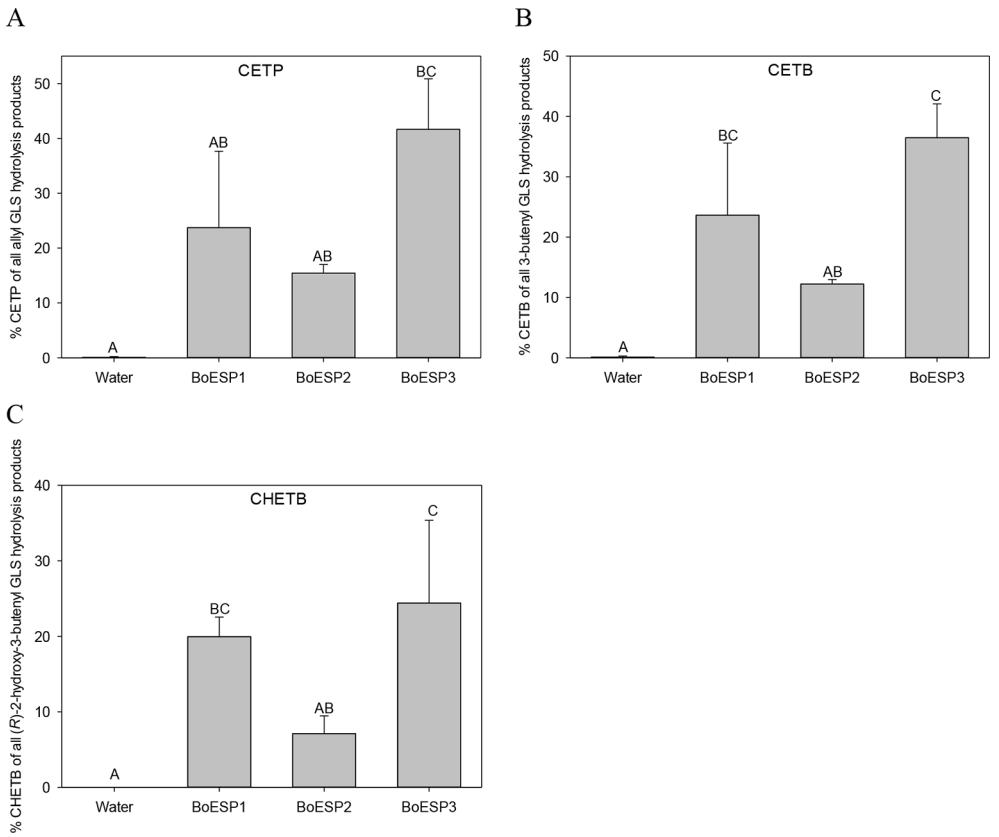

FIGURE 5 | Glucosinolate (GLS) substrate-specific epithiospecifier protein (ESP) activity of recombinant BoESP1-3 as assessed by the formation of epithionitriles from the three GLS **(A)** allyl GLS, **(B)** 3-butenyl GLS and **(C)** (R)-2-hydroxy-3-butenyl GLS. CETP, 1-cyano-2,3-epithiopropane; CETB, 1-cyano-3,4-epithiobutane; CHETB, 1-cyano-2-hydroxy-3,4-epithiobutane. Values represent mean ± standard deviation of three independent experiments, comprising of 2–3 technical replicates each. Different capital letters indicate significant differences in means between the formation of the epithionitrile from one GLS by the different BoESP and a water control as tested by ANOVA and Tukey test at the $p \leq 0.05$ level.

found in shoots but accumulated more in roots, confirming previous data from RNAseq experiments (Wang et al., 2017). The presence of *BoESP3* in roots distinguishes it from *AtESP*, for which only low transcript levels and no protein abundance were detected in this plant organ (Burow et al., 2007; Kissen et al., 2012). In general, pattern of transcripts were reflected by those of protein abundances. However, the overlap between protein expression pattern (**Figure 4**) and GLS hydrolysis generation (**Figures 1** and **2**) was limited to the shoot. In roots, although BoESP3 expression was high in kohlrabi and white cabbage, white cabbage produced nitriles and ETNs from endogenous GLS, while kohlrabi produced only small amounts of nitriles (**Figure 1**). In addition, the hydrolysis pattern of allyl GLS was almost identical between genotypes with high BoESP3 expression in roots (kohlrabi and white cabbage) and those with barely detected BoESP3 abundance (broccoli and red cabbage) (**Figure 2**). These observations could indicate the presence and functionality of other specifier proteins that are not elucidated yet. This research question is particularly interesting since roots were mainly excluded from past investigations on GLS degradation, although GLS and GLS degradation products were detected in root exudates and might play a role in below ground chemical communication between plants and rhizosphere biota (Schreiner et al., 2011; Auger et al., 2012; Xu et al., 2017). Moreover, future research should be directed to enlighten the cellular and subcellular localization of BoESP1 and BoESP2, which would explain their biological role in more detail. RNAseq data from *B. oleracea* indicate that BoESP2 is highly expressed in leaves, while BoESP1 expression peaks in stems, flowers, and siliques (Wang et al., 2017).

The recombinant BoESPs differed in their activity towards alkenyl GLS, with BoESP3 being most active and BoESP2 being least active under the assay conditions. In contrast, *A. thaliana* lines expressing BoESP2 showed the highest percentage of ETN release during GLS hydrolysis. The activity of ESPs is strongly dependent on Fe^{2+} (Backenköhler et al., 2018) and probably differs in their requirement of Fe^{2+} as previous reports suggest (Williams et al., 2010). Therefore, it is likely that BoESPs activities will vary according to hydrolysis conditions present.

The recombinant BoESPs showed no activity in terms of the hydrolysis of the tested non-alkenyl GLS, implying that these proteins do not possess NSP activity (**Figure S2**) as this would have been linked with the increased formation of simple nitriles (Wittstock

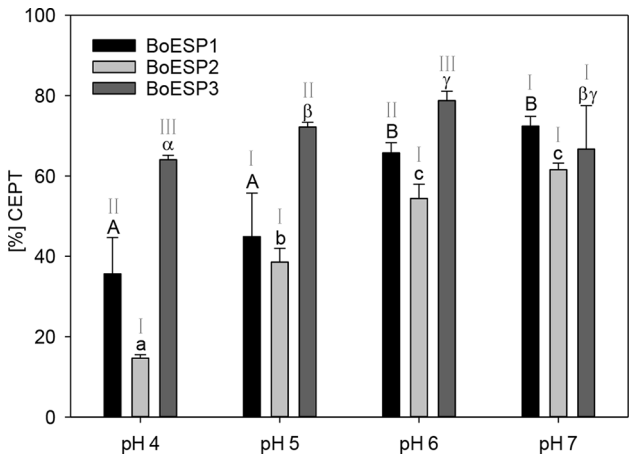

FIGURE 6 | Influence of the pH value on the epithiospecifier protein (ESP) activity of BoESP1-3 assessed by the formation of 1-cyano-2,3-epithiopropane (CETP) from allyl glucosinolate (GLS). Values represent mean ± standard deviation of three replicate measurements. Different letters indicate significant differences in means for the influence of pH on CETP-formation by BoESP1 (capital letters), BoESP2 (small letters), or BoESP3 (Greek letters) as tested by ANOVA and Tukey test at the $p \leq 0.05$ level or, in case of BoESP3, by pairwise comparison using t-test. Roman letters indicate significant differences in means between the formation of CETP by the different BoESP at a given pH value as tested by ANOVA and Tukey test at the $p \leq 0.05$ level.

et al., 2016). This corresponds to the hydrolysis pattern of alkyl GLS 8MTO, observed in the *A. thaliana* transgenic lines (**Figure S4**). An absent NSP activity of recombinant AtESP on 4MSOB GLS substrate was reported earlier (De Torres Zabala et al., 2005). However, NSP activities of ESPs on alkyl GLS have been observed by other groups (Burow et al., 2006; Matusheski et al., 2006) and the tested non-alkenyl GLS are hydrolyzed to nitriles *in vivo* in the tested genotypes (**Table S2**). Hence, our results could indicate the presence of NSPs in *B. oleracea* that have not been characterized yet. The gene expression of two NSP in the related *B. rapa* species was already reported (Wang et al., 2017). Interestingly, the *Pieris rapae* NSP activity was differently affected by Fe^{2+} concentrations. More 4MTB-CN was released in presence of ESP from 4MTB (13-fold of ESP free control) when Fe^{2+} was absent as compared to 0.01 mM Fe^{2+}, while more 4MSOB-CN was formed at the 0.01mM Fe^{2+} level as compared to no added Fe^{2+} (Burow et al., 2006).

Moreover, as tested here, the BoESPs differed in their susceptibility towards a shifting pH. BoESP1 and BoESP2 activity decreased with a lower pH, whereas the activity of BoESP3 was stable in a pH range of pH 4 to pH 7. This stability of BoESP3 could point to a different subcellular localization as compared to BoESP1 and BoESP2. Cellular compartmentation is crucial to control the complex system of GLS hydrolysis. GLS accumulate in vacuoles of sulfur-rich S-cells that are found in close proximity of myrosin cells and guard cells, which both store myrosinases in their vacuoles (Shirakawa and Hara-Nishimura, 2018). In contrast to this, AtESP is localized in the cytosol (Burow et al., 2007; Chhajed et al., 2019). Measurements of the *in vivo* organelle pH revealed an acidification gradient from the cytosol and endoplasmatic reticulum, with pH around pH 7, to lytic vacuoles ranging from pH 5–6 (Martinière et al., 2013; Shen et al., 2013). The pH of the leaf apoplast is even more acidic and was determined to range from 4.5–5 (Geilfus and Muehling, 2011). Hence, one possible explanation for the pH stability of BoESP3 could be the additional localization to the root apoplast. So far, apoplast proteome studies demonstrated the presence of myrosinase and myrosinase-associated proteins in *B. juncea* (Sehrawat and Deswal, 2014) and *A. thaliana* (Trentin et al., 2015) leaves, but not for ESPs. Since BoESP3 is expressed mainly in roots, future experiments should concentrate on the subcellular localization of this isoform to further study its possible involvement in root exudation of GLS hydrolysis products.

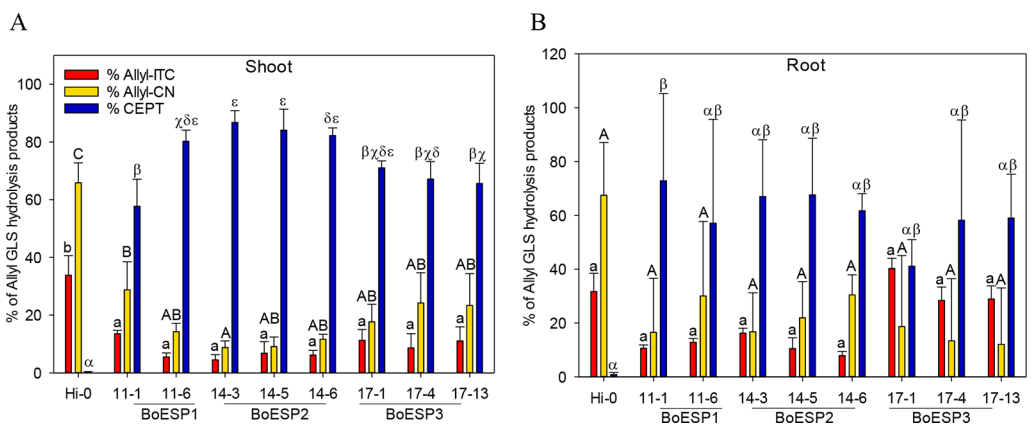

FIGURE 7 | Formation of allyl GSL hydrolysis products allyl isothiocyanate (Allyl-ITC), 3-butenenitrile (Allyl-CN) and 1-cyano-2,3-epithiopropane (CETP) in % relative to all allyl GLS hydrolysis products in *Arabidopsis thaliana* Hi-0 control and BoESP1-3 transgenic lines in shoots **(A)** and roots **(B)**. Values represent mean ± standard deviation of three independent experiments. Significant differences in means between the formation of Allyl-CN (small letters), Allyl-ITC (capital letters) or CETP (Greek letters) as tested by ANOVA and Tukey HSD test at the $p \leq 0.05$ level.

The general role of specifier proteins *in planta* is still part of scientific debate. In *Arabidopsis*, the NSP-catalyzed release of simple nitriles often increases due to herbivory (Lambrix et al., 2001; Burow et al., 2009). Moreover, ESP/NSP-expressing nitrile-producing plants are more susceptible to herbivore feeding (Lambrix et al., 2001; Burow et al., 2009; Jeschke et al., 2016). However, increased nitrile formation can reduce attractiveness for ovipositing herbivorous specialist insects and attracts natural enemies of the larvae (Mumm et al., 2008; Jeschke et al., 2016). So far, the specific role of ESP-catalyzed ETN formation and, hence, their specific role in biotic interactions is still unclear (Jeschke et al., 2016). With regard to human consumption, the aroma and taste of fresh Brassicaceae vegetables likely is influenced by the ESP activity (Zhang et al., 2018). While ITC contribute to the characteristic flavor and pungency of these vegetables (Bell et al., 2018), ETNs have a lower aroma impact. Using GC-olfactometry, the overall odor impression of the ETN CETP was described as weak and onion-like, pungent, spicy, fatty, but also garlic-like and fecal notes were attributed to this compound (Kroener and Buettner, 2017). Therefore, a higher ESP activity might reduce the taste and flavor of fresh *Brassica* vegetables. Further, vegetables rich in ESP-activity might have lower health beneficial properties, as protective effects are mainly attributed to ITCs (Zhang et al., 2018). Thus, it is crucial to unravel the role of ESP *in planta* and to identify strategies for ESP activity reduction in these vegetables.

DATA AVAILABILITY STATEMENT

All datasets generated for this study are included in the article/**Supplementary Material**.

AUTHOR CONTRIBUTIONS

FH and KW designed the study. FH, KW, MA, and PA performed the experiments. FH, MA, FB, and KW analyzed the data. FH and KW wrote the manuscript, with contributions from all authors.

FUNDING

FH is funded by the German Leibniz Association (Leibniz-Junior Research Group OPTIGLUP; J16/2017).

ACKNOWLEDGMENTS

The technical assistance of Sabine Breitkopf, Jessica Eichhorn, Mandy Heinze, Susanne Jeserigk, Vanda Púčiková, and Maria Skoruppa is gratefully acknowledged.

SUPPLEMENTARY MATERIAL

The Supplementary Material for this article can be found online at: https://www.frontiersin.org/articles/10.3389/fpls.2019.01552/full#supplementary-material

REFERENCES

Auger, B., Pouvreau, J.-B., Pouponneau, K., Yoneyama, K., Montiel, G., Le Bizec, B., et al. (2012). Germination stimulants of *Phelipanche ramosa* in the rhizosphere of *Brassica napus* are derived from the glucosinolate pathway. *Mol. Plant-Microbe Interact.* 25, 993–1004. doi: 10.1094/MPMI-01-12-0006-R

Backenköhler, A., Eisenschmidt, D., Schneegans, N., Strieker, M., Brandt, W., and Wittstock, U. (2018). Iron is a centrally bound cofactor of specifier proteins involved in glucosinolate breakdown. *PloS One* 13, e0205755. doi: 10.1371/journal.pone.0205755

Bartetzko, V., Sonnewald, S., Vogel, F., Hartner, K., Stadler, R., Hammes, U. Z., et al. (2009). The *Xanthomonas campestris* pv. *vesicatoria* type III effector protein XopJ inhibits protein secretion: evidence for interference with cell wall-associated defense responses. *Mol. Plant-Microbe Interact.* 22, 655–664. doi: 10.1094/MPMI-22-6-0655

Bell, L., Oloyede, O. O., Lignou, S., Wagstaff, C., and Methven, L. (2018). Taste and flavor perceptions of glucosinolates, isothiocyanates, and related compounds. *Mol. Nutr. Food Res.* 62, 1700990. doi: 10.1002/mnfr.201700990

Bernardi, R., Negri, A., Ronchi, S., and Palmieri, S. (2000). Isolation of the epithiospecifier protein from oil-rape (*Brassica napus ssp. oleifera*) seed and it's characterization. *FEBS Lett.* 467, 296–298. doi: 10.1016/S0014-5793(00)01179-0

Bradford, M. M. (1976). A rapid and sensitive method for the quantitation of microgram quantities of protein utilizing the principle of protein-dye binding. *Anal. Biochem.* 72, 248–254. doi: 10.1016/0003-2697(76)90527-3

Brandt, W., Backenköhler, A., Schulze, E., Plock, A., Herberg, T., Roese, E., et al. (2014). Molecular models and mutational analyses of plant specifier proteins suggest active site residues and reaction mechanism. *Plant Mol. Biol.* 84, 173–188. doi: 10.1007/s11103-013-0126-0

Brocker, E. R., and Benn, M. H. (1983). The intramolecular formation of epithioalkanenitriles from alkenylglucosinolates by *Crambe abyssinica* seed flour. *Phytochemistry* 22, 770–772. doi: 10.1016/S0031-9422(00)86982-4

Brulle, F., Bernard, F., Vandenbulcke, F., Cuny, D., and Dumez, S. (2014). Identification of suitable qPCR reference genes in leaves of *Brassica oleracea* under abiotic stresses. *Ecotoxicol.* 23, 459–471. doi: 10.1007/s10646-014-1209-7

Burow, M., Markert, J., Gershenzon, J., and Wittstock, U. (2006). Comparative biochemical characterization of nitrile-forming proteins from plants and insects that alter myrosinase-catalysed hydrolysis of glucosinolates. *FEBS J.* 273, 2432–2446. doi: 10.1111/j.1742-4658.2006.05252.x

Burow, M., Rice, M., Hause, B., Gershenzon, J., and Wittstock, U. (2007). Cell- and tissue-specific localization and regulation of the epithiospecifier protein in *Arabidopsis thaliana*. *Plant Mol. Biol.* 64, 173–185. doi: 10.1007/s11103-007-9143-1

Burow, M., Losansky, A., Müller, R., Plock, A., Kliebenstein, D. J., and Wittstock, U. (2009). The genetic basis of constitutive and herbivore-induced ESP-independent nitrile formation in *Arabidopsis*. *Plant Physiol.* 149, 561–574. doi: 10.1104/pp.108.130732

Cheng, F., Wu, J., and Wang, X. (2014). Genome triplication drove the diversification of *Brassica* plants. *Hortic. Res.* 1, 14024–14024. doi: 10.1038/hortres.2014.24

Chhajed, S., Misra, B. B., Tello, N., and Chen, S. (2019). Chemodiversity of the glucosinolate-myrosinase system at the single cell type resolution. *Front. Plant Sci.* 10: 618 doi: 10.3389/fpls.2019.00618

Clough, S. J., and Bent, A. F. (1998). Floral dip: a simplified method for Agrobacterium -mediated transformation of *Arabidopsis thaliana*. *Plant J.* 16, 735–743. doi: 10.1046/j.1365-313x.1998.00343.x

De Torres Zabala, M., Grant, M., Bones, A. M., Bennett, R., Lim, Y. S., Kissen, R., et al. (2005). Characterisation of recombinant epithiospecifier protein and its over-expression in *Arabidopsis thaliana*. *Phytochemistry* 66, 859–867. doi: 10.1016/j.phytochem.2005.02.026

Di Tommaso, P., Moretti, S., Xenarios, I., Orobitg, M., Montanyola, A., Chang, J.-M., et al. (2011). T-Coffee: a web server for the multiple sequence alignment of protein and RNA sequences using structural information and homology extension. *Nucleic Acids Res.* 39, W13–W17. doi: 10.1093/nar/gkr245

Diehn, T. A., Pommerrenig, B., Bernhardt, N., Hartmann, A., and Bienert, G. P. (2015). Genome-wide identification of aquaporin encoding genes in *Brassica oleracea* and their phylogenetic sequence comparison to Brassica crops and Arabidopsis. *Front. Plant Sci.* 6, 166. doi: 10.3389/fpls.2015.00166

Eisenschmidt-Bönn, D., Schneegans, N., Backenköhler, A., Wittstock, U., and Brandt, W. (2019). Structural diversification during glucosinolate breakdown: mechanisms of thiocyanate, epithionitrile and simple nitrile formation. *Plant J.* 99, 329–343. doi: 10.1111/tpj.14327

Faostat (2018). Food and Agriculture Organization of the United Nations).

Faurobert, M., Pelpoir, E., and Chaïb, J. (2007). "Phenol extraction of proteins for proteomic studies of recalcitrant plant tissues," in *Plant Proteomics: Methods and Protocols*. Eds. H. Thiellement, M. Zivy, and V. Méchin. (Totowa, NJ: Humana Press), 9–14. doi: 10.1385/1-59745-227-0:9

Foo, H. L., Grønning, L. M., Goodenough, L., Bones, A. M., Danielsen, B.-E., Whiting, D. A., et al. (2000). Purification and characterisation of epithiospecifier protein from *Brassica napus*: enzymic intramolecular sulphur addition within alkenyl thiohydroximates derived from alkenyl glucosinolate hydrolysis. *FEBS Lett.* 468, 243–246. doi: 10.1016/S0014-5793(00)01176-5

Geilfus, C.-M., and Muehling, K. (2011). Real-time imaging of leaf apoplastic pH dynamics in response to NaCl stress. *Front. Plant Sci.* 2, 13 doi: 10.3389/fpls.2011.00013

Gibeaut, D. M., Hulett, J., Cramer, G. R., and Seemann, J. R. (1997). Maximal biomass of *Arabidopsis thaliana* using a simple, low-maintenance hydroponic method and favorable environmental conditions. *Plant Physiol.* 115, 317–319. doi: 10.1104/pp.115.2.317

Hanschen, F. S., and Schreiner, M. (2017). Isothiocyanates, nitriles, and epithionitriles from glucosinolates are affected by genotype and developmental stage in *Brassica oleracea* varieties. *Front. Plant Sci.* 8, 1095. doi: 10.3389/fpls.2017.01095

Hanschen, F. S., Lamy, E., Schreiner, M., and Rohn, S. (2014). Reactivity and stability of glucosinolates and their breakdown products in foods. *Angew. Chem. Int. Ed.* 53, 11430–11450. doi: 10.1002/anie.201402639

Hanschen, F. S., Kühn, C., Nickel, M., Rohn, S., and Dekker, M. (2018a). Leaching and degradation kinetics of glucosinolates during boiling of *Brassica oleracea* vegetables and the formation of their breakdown products. *Food Chem.* 263, 240–250. doi: 10.1016/j.foodchem.2018.04.069

Hanschen, F. S., Pfitzmann, M., Witzel, K., Stützel, H., Schreiner, M., and Zrenner, R. (2018b). Differences in the enzymatic hydrolysis of glucosinolates increase the defense metabolite diversity in 19 *Arabidopsis thaliana* accessions. *Plant Physiol. Biochem.* 124, 126–135. doi: 10.1016/j.plaphy.2018.01.009

Hanschen, F. S., Baldermann, S., Brobrowski, A., Maikath, A., Wiesner-Reinhold, M., Rohn, S., et al. (2019). Identification of *N*-acetyl-*S*-(3-cyano-2-(methylsulfanyl)propyl-cysteine as a major human urine metabolite from the epithionitrile 1-cyano-2,3-epithiopropane, the main glucosinolate hydrolysis product from cabbage. *Nutrients* 11, 908. doi: 10.3390/nu11040908

Jeschke, V., Gershenzon, J., and Vassão, D. G. (2016). "Chapter Eight - insect detoxification of glucosinolates and their hydrolysis products," in *Advances in Botanical Research*. Ed. K. Stanislav (Massachusetts, USA: Cambridge), 199–245. doi: 10.1016/bs.abr.2016.06.003

Jozefowicz, A. M., Matros, A., Witzel, K., and Mock, H.-P. (2018). "Mini-scale isolation and preparation of plasma membrane proteins from potato roots for LC/MS analysis," in *Plant Membrane Proteomics: Methods and Protocols*. Eds. H.-P. Mock, A. Matros, and K. Witzel (New York, NY: Springer New York), 195–204. doi: 10.1007/978-1-4939-7411-5_13

Kissen, R., and Bones, A. M. (2009). Nitrile-specifier proteins involved in glucosinolate hydrolysis in *Arabidopsis thaliana*. *J. Biol. Chem.* 284, 12057–12070. doi: 10.1074/jbc.M807500200

Kissen, R., Hyldbakk, E., Wang, C. W. V., Sørmo, C. G., Rossiter, J. T., and Bones, A. M. (2012). Ecotype dependent expression and alternative splicing of epithiospecifier protein (ESP) in *Arabidopsis thaliana*. *Plant Mol. Biol.* 78, 361–375. doi: 10.1007/s11103-011-9869-7

Klopsch, R., Witzel, K., Börner, A., Schreiner, M., and Hanschen, F. S. (2017). Metabolic profiling of glucosinolates and their hydrolysis products in a germplasm collection of *Brassica rapa* turnips. *Food Res. Int.* 100, 392–403. doi: 10.1016/j.foodres.2017.04.016

Klopsch, R., Witzel, K., Artemyeva, A., Ruppel, S., and Hanschen, F. S. (2018). Genotypic variation of glucosinolates and their breakdown products in leaves of *Brassica rapa*. *J. Agric. Food Chem.* 66, 5481–5490. doi: 10.1021/acs.jafc.8b01038

Kroener, E.-M., and Buettner, A. (2017). Unravelling important odorants in horseradish (*Armoracia rusticana*). *Food Chem.* 232, 455–465. doi: 10.1016/j.foodchem.2017.04.042

Kuchernig, J.-C., Backenköhler, A., Lübbecke, M., Burow, M., and Wittstock, U. (2011). A thiocyanate-forming protein generates multiple products upon allylglucosinolate breakdown in *Thlaspi arvense*. *Phytochemistry* 72, 1699–1709. doi: 10.1016/j.phytochem.2011.06.013

Kuchernig, J. C., Burow, M., and Wittstock, U. (2012). Evolution of specifier proteins in glucosinolate-containing plants. *BMC Evol. Biol.* 12, 127. doi: 10.1186/1471-2148-12-127

Lambrix, V., Reichelt, M., Mitchell-Olds, T., Kliebenstein, D. J., and Gershenzon, J. (2001). The *Arabidopsis* epithiospecifier protein promotes the hydrolysis of glucosinolates to nitriles and influences *Trichoplusia ni* herbivory. *Plant Cell* 13, 2793–2807. doi: 10.1105/tpc.010261

Liu, S., Liu, Y., Yang, X., Tong, C., Edwards, D., Zhao, M., et al. (2014). The *Brassica oleracea* genome reveals the asymmetrical evolution of polyploid genomes. *Nat. Commun.* 5, 3930. doi: 10.1038/ncomms4930

Macleod, A. J., and Rossiter, J. T. (1985). The occurrence and activity of epithiospecifier protein in some cruciferae seeds. *Phytochemistry* 24, 1895–1898. doi: 10.1016/S0031-9422(00)83087-3

Martinière, A., Bassil, E., Jublanc, E., Alcon, C., Reguera, M., Sentenac, H., et al. (2013). *In vivo* intracellular pH measurements in tobacco and *Arabidopsis* reveal an unexpected pH gradient in the endomembrane system. *Plant Cell* 25, 4028–4043. doi: 10.1105/tpc.113.116897

Matusheski, N. V., and Jeffery, E. H. (2001). Comparison of the bioactivity of two glucoraphanin hydrolysis products found in broccoli, sulforaphane and sulforaphane nitrile. *J. Agric. Food Chem.* 49, 5743–5749. doi: 10.1021/jf010809a

Matusheski, N. V., Juvik, J. A., and Jeffery, E. H. (2004). Heating decreases epithiospecifier protein activity and increases sulforaphane formation in broccoli. *Phytochemistry* 65, 1273–1281. doi: 10.1016/j.phytochem.2004.04.013

Matusheski, N. V., Swarup, R., Juvik, J. A., Mithen, R., Bennett, M., and Jeffery, E. H. (2006). Epithiospecifier protein from broccoli (*Brassica oleracea* L. ssp. *italica*) inhibits formation of the anticancer agent sulforaphane. *J. Agric. Food Chem.* 54, 2069–2076. doi: 10.1021/jf0525277

Mumm, R., Burow, M., Bukovinszkine'kiss, G., Kazantzidou, E., Wittstock, U., Dicke, M., et al. (2008). Formation of simple nitriles upon glucosinolate hydrolysis affects direct and indirect defense against the specialist herbivore, *Pieris rapae*. *J. Chem. Ecol.* 34, 1311–1321. doi: 10.1007/s10886-008-9534-z

Petroski, R. J., and Tookey, H. L. (1982). Interactions of thioglucoside glucohydrolase and epithiospecifier protein of cruciferous plants to form 1-cyanoepithioalkanes. *Phytochemistry* 21, 1903–1905. doi: 10.1016/0031-9422(82)83011-2

Qu, C., Zhao, H., Fu, F., Wang, Z., Zhang, K., Zhou, Y., et al. (2016). Genome-wide survey of flavonoid biosynthesis genes and gene expression analysis between black- and yellow-seeded *Brassica napus*. *Front. Plant Sci.* 7, 1755. doi: 10.3389/fpls.2016.01755

Rossiter, J. T., Pickett, J. A., Bennett, M. H., Bones, A. M., Powell, G., and Cobb, J. (2007). The synthesis and enzymic hydrolysis of (*E*)-2-[2,3-$^2H_2$]propenyl glucosinolate: Confirmation of the rearrangement of the thiohydroximate moiety. *Phytochemistry* 68, 1384–1390. doi: 10.1016/j.phytochem.2007.02.030

Schreiner, M., Krumbein, A., Knorr, D., and Smetanska, I. (2011). Enhanced glucosinolates in root exudates of *Brassica rapa* ssp. *rapa* mediated by salicylic acid and methyl jasmonate. *J. Agric. Food Chem.* 59, 1400–1405. doi: 10.1021/jf103585s

Sehrawat, A., and Deswal, R. (2014). S-Nitrosylation analysis in *Brassica juncea* apoplast highlights the importance of nitric oxide in cold-stress signaling. *J. Proteome Res.* 13, 2599–2619. doi: 10.1021/pr500082u

Shen, J., Zeng, Y., Zhuang, X., Sun, L., Yao, X., Pimpl, P., et al. (2013). Organelle pH in the *Arabidopsis* endomembrane system. *Mol. Plant* 6, 1419–1437. doi: 10.1093/mp/sst079

Shirakawa, M., and Hara-Nishimura, I. (2018). Specialized vacuoles of myrosin cells: Chemical defense strategy in Brassicales plants. *Plant Cell Physiol.* 59, 1309–1316. doi: 10.1093/pcp/pcy082

Talley, K., and Alexov, E. (2010). On the pH-optimum of activity and stability of proteins. *Proteins: Struct. Funct. Bioinf.* 78, 2699–2706. doi: 10.1002/prot.22786

Terada, Y., Masuda, H., and Watanabe, T. (2015). Structure-activity relationship study on isothiocyanates: comparison of TRPA1-activating ability between allyl isothiocyanate and specific flavor components of wasabi, horseradish, and white mustard. *J. Natural Prod.* 78, 1937–1941. doi: 10.1021/acs.jnatprod.5b00272

Tommaso, P., Moretti, S., Xenarios, I., Orobitg, M., Montanyola, A., Chang, J. M., et al. (2011). T-Coffee: a web server for the multiple sequence alignment of protein and RNA sequences using structural information and homology extension. *Nucleic Acids Res.* 39, W13–W17. doi: 10.1093/nar/gkr245

Tookey, H. L. (1973). Crambe thioglucoside glucohydrolase (EC 3.2.3.1): separation of a protein required for epithiobutane formation. *Can. J. Biochem.* 51, 1654–1660. doi: 10.1139/o73-222

Traka, M., and Mithen, R. (2009). Glucosinolates, isothiocyanates and human health. *Phytochem. Rev.* 8, 269–282. doi: 10.1007/s11101-008-9103-7

Trentin, A. R., Pivato, M., Mehdi, S. M. M., Barnabas, L. E., Giaretta, S., Fabrega-Prats, M., et al. (2015). Proteome readjustments in the apoplastic space of *Arabidopsis thaliana* ggt1 mutant leaves exposed to UV-B radiation. *Front. Plant Sci.* 6: 128. doi: 10.3389/fpls.2015.00128

Vandesompele, J., De Preter, K., Pattyn, F., Poppe, B., Van Roy, N., De Paepe, A., et al. (2002). Accurate normalization of real-time quantitative RT-PCR data by geometric averaging of multiple internal control genes. *Genome Biol.* 3. research0034.1. doi: 10.1186/gb-2002-3-7-research0034

Veeranki, O., Bhattacharya, A., Tang, L., Marshall, J., and Zhang, Y. (2015). Cruciferous vegetables, isothiocyanates, and prevention of bladder cancer. *Curr. Pharmacol. Rep.* 1, 272–282. doi: 10.1007/s40495-015-0024-z

Wang, J., Qiu, Y., Wang, X., Yue, Z., Yang, X., Chen, X., et al. (2017). Insights into the species-specific metabolic engineering of glucosinolates in radish (*Raphanus sativus* L.) based on comparative genomic analysis. *Sci. Rep.* 7, 16040–16040. doi: 10.1038/s41598-017-16306-4

Williams, D. J., Critchley, C., Pun, S., Chaliha, M., and O'hare, T. J. (2010). Key role of Fe^{2+} in epithiospecifier protein activity. *J. Agric. Food Chem.* 58, 8512–8521. doi: 10.1021/jf904532n

Wittstock, U., and Burow, M. (2010). Glucosinolate breakdown in Arabidopsis: Mechanism, regulation and biological significance. *Arabidopsis Book*, 8, e0134. doi: 10.1199/tab.0134

Wittstock, U., Meier, K., Dörr, F., and Ravindran, B. M. (2016). NSP-Dependent simple nitrile formation dominates upon breakdown of major aliphatic glucosinolates in roots, seeds, and seedlings of *Arabidopsis thaliana* Columbia-0. *Front. Plant Sci.* 7, 1821. doi: 10.3389/fpls.2016.01821

Witzel, K., Hanschen, F. S., Schreiner, M., Krumbein, A., Ruppel, S., and Grosch, R. (2013). Verticillium suppression is associated with the glucosinolate composition of *Arabidopsis thaliana* leaves. *PloS One* 8, e71877. doi: 10.1371/journal.pone.0071877

Witzel, K., Buhtz, A., and Grosch, R. (2017). Temporal impact of the vascular wilt pathogen *Verticillium dahliae* on tomato root proteome. *J. Proteomics* 169, 215–224. doi: 10.1016/j.jprot.2017.04.008

Witzel, K., Matros, A., Møller, A. L. B., Ramireddy, E., Finnie, C., Peukert, M., et al. (2018). Plasma membrane proteome analysis identifies a role of barley membrane steroid binding protein in root architecture response to salinity. *Plant Cell Environ.* 41, 1311–1330. doi: 10.1111/pce.13154

Xu, D., Hanschen, F. S., Witzel, K., Nintemann, S. J., Nour-Eldin, H. H., Schreiner, M., et al. (2017). Rhizosecretion of stele-synthesized glucosinolates and their catabolites requires GTR-mediated import in Arabidopsis. *J. Exp. Bot.* 68, 3205–3214. doi: 10.1093/jxb/erw355

Zhang, Z., Bergan, R., Shannon, J., Slatore, C. G., Bobe, G., and Takata, Y. (2018). The role of cruciferous vegetables and isothiocyanates for lung cancer prevention: current status, challenges, and future research directions. *Mol. Nutr. Food Res.* 62, 1700936. doi: 10.1002/mnfr.201700936

Conflict of Interest: The authors declare that the research was conducted in the absence of any commercial or financial relationships that could be construed as a potential conflict of interest.

frontiers in Plant Science

CORRECTION
published: 28 April 2020
doi: 10.3389/fpls.2020.00523

Corrigendum: Identification and Characterization of Three Epithiospecifier Protein Isoforms in *Brassica oleracea*

Katja Witzel[1], *Marua Abu Risha*[1], *Philip Albers*[1], *Frederik Börnke*[1,2] *and Franziska S. Hanschen*[1]*

[1] Leibniz Institute of Vegetable and Ornamental Crops, Großbeeren, Germany, [2] Institute of Biochemistry and Biology, University of Potsdam, Potsdam, Germany

OPEN ACCESS

Approved by:
Frontiers Editorial Office, Frontiers Media SA, Switzerland

***Correspondence:**
Franziska S. Hanschen
hanschen@igzev.de

Specialty section:
This article was submitted to Plant Metabolism and Chemodiversity, a section of the journal Frontiers in Plant Science

Received: *03 April 2020*
Accepted: *06 April 2020*
Published: *28 April 2020*

Citation:
Witzel K, Abu Risha M, Albers P, Börnke F and Hanschen FS (2020) Corrigendum: Identification and Characterization of Three Epithiospecifier Protein Isoforms in Brassica oleracea. Front. Plant Sci. 11:523. doi: 10.3389/fpls.2020.00523

Keywords: epithionitrile, expression profile, functional complementation, glucosinolate hydrolysis, nitrile, specifier proteins, tissue specificity

A Corrigendum on

Identification and Characterization of Three Epithiospecifier Protein Isoforms in *Brassica oleracea*

by Witzel, K., Abu Risha, M., Albers, P., Börnke, F., and Hanschen, F. S. (2019). Front. Plant Sci. 10:1552. doi: 10.3389/fpls.2019.01552

In the original article, there was a mistake in Figure 1 as published. In Figure 1A as well as in Figure 1B the colors in the bar of the "Red Cabbage Root" were not shown correctly: In Figure 1A the "Indole GLS" in the bar of "Red Cabbage Root" were turquois instead of black. In Figure 1B in the bar of "Red Cabbage Root" the ITCs were orange instead of red and the CNs were dark blue instead of orange (and therefore could be mistaken for ETNs). The corrected **Figure 1** appears below.

The authors apologize for this error and state that this does not change the scientific conclusions of the article in any way. The original article has been updated.

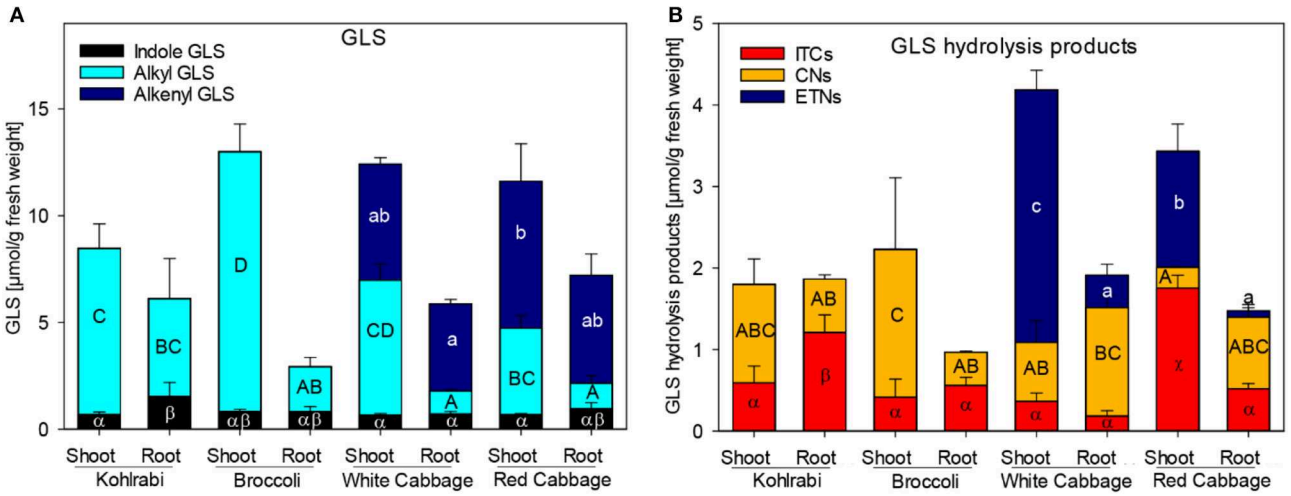

FIGURE 1 | Glucosinolate (GLS) accumulation **(A)** and formation of hydrolysis products **(B)** in shoots and roots of four *B. oleracea* genotypes. ITCs, isothiocyanates; CNs, nitriles; ETNs, epithionitriles. Values represent mean ± standard deviation (SD) of three independent experiments (n = 3). Significant differences in means between the formation of), alkenyl GLS (small letters), alkyl GLS (capital letters), and indole GLS (Greek letters) in **(A)** or ETNs (small letters), CNs (capital letters), or ITC (Greek letters) in **(B)** as tested by ANOVA and Tukey HSD test at the $p \leq 0.05$ level.

frontiers in Plant Science

ORIGINAL RESEARCH
published: 10 January 2020
doi: 10.3389/fpls.2019.01653

Both Biosynthesis and Transport Are Involved in Glucosinolate Accumulation During Root-Herbivory in *Brassica rapa*

Axel J. Touw[1,2]*, *Arletys Verdecia Mogena*[3], *Anne Maedicke*[1,2], *Rebekka Sontowski*[1,2], *Nicole M. van Dam*[1,2] *and Tomonori Tsunoda*[4]

[1] Molecular Interaction Ecology, German Center for Integrative Biodiversity Research (iDiv) Halle-Jena-Leipzig, Leipzig, Germany, [2] Institute of Biodiversity, Friedrich Schiller University Jena, Jena, Germany, [3] Research and Development Department, Center for Genetic Engineering and Biotechnology, Camagüey, Cuba, [4] Faculty of Agriculture and Life Science, Shinshu University, Kamiina-County, Japan

OPEN ACCESS

Edited by:
Ralph Kissen,
Norwegian University of Science and Technology, Norway

Reviewed by:
Jim Tokuhisa,
Virginia Tech, United States
Richard James Hopkins,
Natural Resources Institute, United Kingdom

***Correspondence:**
Axel J. Touw
axel.touw@idiv.de

Specialty section:
This article was submitted to Plant Metabolism and Chemodiversity, a section of the journal Frontiers in Plant Science

Received: 05 July 2019
Accepted: 22 November 2019
Published: 10 January 2020

Citation:
Touw AJ, Verdecia Mogena A, Maedicke A, Sontowski R, van Dam NM and Tsunoda T (2020) Both Biosynthesis and Transport Are Involved in Glucosinolate Accumulation During Root-Herbivory in Brassica rapa. Front. Plant Sci. 10:1653. doi: 10.3389/fpls.2019.01653

The optimal defense theory predicts that plants invest most energy in those tissues that have the highest value, but are most vulnerable to attacks. In *Brassica* species, root-herbivory leads to the accumulation of glucosinolates (GSLs) in the taproot, the most valuable belowground plant organ. Accumulation of GSLs can result from local biosynthesis in response to herbivory. In addition, transport from distal tissues by specialized GSL transporter proteins can play a role as well. GSL biosynthesis and transport are both inducible, but the role these processes play in GSL accumulation during root-herbivory is not yet clear. To address this issue, we performed two time-series experiments to study the dynamics of transport and biosynthesis in local and distal tissues of *Brassica rapa*. We exposed roots of *B. rapa* to herbivory by the specialist root herbivore *Delia radicum* for 7 days. During this period, we sampled above- and belowground plant organs 12 h, 24 h, 3 days and 7 days after the start of herbivory. Next, we measured the quantity and composition of GSL profiles together with the expression of genes involved in GSL biosynthesis and transport. We found that both benzyl and indole GSLs accumulate in the taproot during root-herbivory, whereas we did not observe any changes in aliphatic GSL levels. The rise in indole GSL levels coincided with increased local expression of biosynthesis and transporter genes, which suggest that both biosynthesis and GSL transport play a role in the accumulation of GSLs during root herbivory. However, we did not observe a decrease in GSL levels in distal tissues. We therefore hypothesize that GSL transporters help to retain GSLs in the taproot during root-herbivory.

Keywords: cabbage root fly, plant–insect interactions, above–belowground interactions, induced plant responses, optimal defense theory

INTRODUCTION

In their role as primary producers plants form the basis of most natural communities. Consequently, plants are involved in interactions with many different organisms, including aboveground and belowground herbivores. To limit the negative effects of herbivory, plants have evolved an elaborate defense system, including structural traits such as thorns and trichomes,

antidigestive proteins, and an extensive arsenal of defense-related metabolites (Schoonhoven et al., 2005). The classes of these metabolites vary by taxon and are often characteristic for distinct plant families (reviewed in Piasecka et al., 2015).

Glucosinolates (GSLs) are a class of well-studied defense metabolites that are characteristic for brassicaceous plants. They are derived from amino acids, and are broadly divided into three groups based on their amino acid precursor (reviewed in Sønderby et al., 2010). Indole GSLs have a side chain derived from tryptophan, aliphatic GSLs from methionine and benzyl GSLs from phenylalanine or tyrosine. GSLs are stored in the vacuoles of specific cells (Kissen et al., 2009). Upon herbivore damage, GSLs mix with the enzyme myrosinase, which is stored in separate cells. This leads to the formation of breakdown products, the structure and biological activity of which strongly depend on the structure of the GSL. In general, the hydrolysis of indole GSLs leads to the formation of instable isothiocyanates (ITCs) and nitriles, whereas aliphatic and benzyl GSLs mostly produce noxious ITCs (Wittstock and Burow, 2010). Due to this difference in breakdown products, structurally different GSL groups cause resistance against distinct groups of attackers. In general, indole GSLs act against phloem feeders and pathogens (Kim et al., 2008; Bednarek et al., 2009), whereas aliphatic, indole and benzyl GSLs can affect the performance of chewing insects (Beekwilder et al., 2008; Schlaeppi et al., 2008; Bejai et al., 2012).

GSLs are constitutively present in all tissues of brassicaceous plants (Wittstock and Gershenzon, 2002), but quantitative and qualitative differences in GSL composition occur between different plant parts. Constitutive GSL concentrations are generally higher in roots compared to shoots (reviewed in van Dam et al., 2009). Moreover, GSLs are differentially distributed over different organs. Recent studies showed that the distribution of GSLs over different parts follows optimal defense theory (ODT) (Tsunoda et al., 2018). The ODT predicts that plants allocate defenses preferentially to the plant parts that are highly attractive to potential attackers and are most valuable to the plant at the same time (McKey, 1974; Meldau et al., 2012). This implies that in aboveground tissues young leaves and reproductive organs, such as flowers and seeds, contain the highest GSL concentrations. In belowground tissues, constitutive GSLs accumulate mainly in the tap- and lateral roots, whereas GSL levels are lower in fine roots (Tsunoda et al., 2017). In addition, GSLs accumulate in damaged tissue in response to insect herbivory (van Dam and Raaijmakers, 2006). The strength of this induced response and the composition of the resulting GSL profile depends in large on the feeding guild of the attacker. Feeding by chewing herbivores such as beetles, caterpillars and fly larvae generally leads to strong increases in total GSL levels (reviewed in Textor and Gershenzon, 2009). In contrast, sucking insects such as aphids do not induce GSL accumulation, or in some cases even inhibit production of certain GSL classes (Kim and Jander, 2007). Similar to the allocation of constitutive defenses, induced plant responses to herbivory follow ODT predictions (reviewed in Meldau et al., 2012). In shoot tissues of *Nicotiana sylvestris*, accumulation of nicotine is more inducible in younger leaves (Ohnmeiss and Baldwin, 2000). In belowground tissues of *Brassica*, the taproot responds more strongly to root-herbivory compared to lateral and fine roots, leading to accumulation of high GSL levels in the taproot (Tsunoda et al., 2018). In line with the ODT, herbivore damage on the taproot had a larger impact on plant biomass than herbivore feeding on fine roots (Tsunoda et al., 2018).

The distribution of GSLs over the plant is the combined result of several, tightly coordinated processes. Increased local biosynthesis plays an important part in GSL accumulation upon induction (Tytgat et al., 2013), whereas transport of GSLs from other parts towards the feeding site may play a role as well (Johnson et al., 2016). In undamaged plants, long-distance transport of GSLs to designated plant parts is regulated through the activity of GSL transporter proteins (GTRs) (Nour-Eldin et al., 2012; Andersen et al., 2013; Madsen et al., 2014). The role of GTRs is twofold: they either play a role in selective loading of GSLs into the phloem for transport to other plant compartments, or by retaining GSLs in certain parts by preventing transport *via* the xylem (Madsen et al., 2014; Jørgensen et al., 2017). Because of their partial substrate specificity, GTRs can fine-tune the distribution of GSLs belonging to different classes and of GSLs of different chain lengths (Andersen et al., 2013).

Since the production of GTRs is inducible, biotic and abiotic factors can affect the allocation of GSLs over specific plant parts (Nour-Eldin et al., 2012). However, how transport and biosynthesis act in concert to change GSL accumulation patterns in plant–herbivore interactions has not been studied so far (Jørgensen et al., 2015; Burow and Halkier, 2017). The aim of this study was to explore the temporal and spatial dynamics of GSL accumulation and the underlying molecular mechanisms during root herbivory in line with ODT. We expected that the accumulation of GSLs in response to root herbivory would not only be the result of local biosynthesis, but also of active transport from distal tissues. We tested this hypothesis in two time course experiments using wild mustard plants (*Brassica rapa*) and the cabbage root-fly (*Delia radicum*), a specialist root-herbivore on brassicaceous plants. Adult females typically oviposit on the lower part of the stem. After hatching, the larvae mine into the taproot, where they cause extensive damage. Because of this feeding behavior, GSL induction is mainly seen in the taproot (Tsunoda et al., 2018). This makes *D. radicum* an attractive organism to study local and systemic defense induction in belowground tissues. In the first experiment, we investigated the effects of root-herbivory on the accumulation of GSLs in both above- and belowground organs after 3 and 7 days, when GSL accumulation is known to occur (Tsunoda et al., 2018). In the second experiment, we focused on the dynamics of the molecular mechanisms underlying this accumulation at earlier time points after the onset of herbivory, and therefore sampled at 12 and 24 h after infestation. Specifically, we tested the following hypotheses: (i) there is a negative correlation between allocation of GSL to local- and distal tissues (ii) transporter genes are expressed earlier than biosynthesis genes and (iii) transporter genes are expressed earlier in distal root tissues than in damaged root tissues.

MATERIALS AND METHODS

Plants and Insects

Brassica rapa seeds used during the first experiment were bought from a commercial supplier (Horti Tops, the Netherlands), whereas the seeds used during the second experiment were collected in 2009 from a wild population in Maarsen (the Netherlands) (Danner et al., 2015). Both *B. rapa* varieties are fast-cycling, which flower without vernalization. The seeds were germinated on fine-grained vermiculite in plastic containers. The containers were kept in a climate chamber (E-36L Reach in Plant Growth Chamber, CLF Plant Climatics GmbH, Wertingen, Germany) at 20°C (16:8 h day:night) and 60% relative humidity for one week. After germination, the seedlings were transplanted to 2.5 L pots filled with river sand and placed in a greenhouse chamber belonging to the botanical gardens of Leipzig University (Leipzig, Germany) at 27°C (day, 16 h) and 21°C (night, 8 h) at 50% relative humidity. Two batches of sand that were used during transplanting were weighed, dried for 24 h at 50°C and weighed again to determine initial water content. After transplanting, the seedlings were supplied with 2P Hoagland solution (double KH_2PO_4 compared to regular Hoagland solution) (Van Dam et al., 2004) so that the total water content of the sand amounted to 14% w/w of the dry mass. Every 2–3 days, five randomly chosen pots were weighed to determine the volume of water needed to keep the water content of the sand at 14%. Once a week, plants were watered with 2P Hoagland solution instead of water. Plants were placed in a full-factorial block design with time point of harvest as the blocking factor. Within each block, control plants were paired with treatment plants of similar size and habit.

Delia radicum L. (Diptera: Anthomyiidae) larvae used during the experiments originated from our rearing, which was established 4 years ago. The rearing was started from a culture kindly provided by Dr. Anne-Marie Cortesero (University of Rennes, France). The colony has been maintained since in a climate chamber at 20°C (16:8 h day:night) on cabbage turnip (*Brassica oleracea*). Second instar larvae were used during the experiments.

Experimental Design

We tested the defense response of *B. rapa* to herbivory by *D. radicum* in two experiments. The experimental setup of both experiments was based on a paired block design with six biological replicates per treatment group. The two factors were root herbivory and duration of root herbivory. The root herbivory treatment had two levels: control (no larvae) or infestation by three second-instar *D. radicum* larvae. The duration of root herbivory had two levels in the first experiment (3 and 7 days) and four levels in the second experiment (12 h, 24 h, 3 days and 7 days).

Infestation with *D. radicum* took place after around 40 days after transplanting the seedlings to the pots. This coincided with the moment when plants had developed three leaf pairs (BBCH code 13, according to Feller et al., 1995). Separate sets of plants were destructively harvested 3 and 7 days after the start of herbivory in the first experiment, and after 0.5, 1, 3, and 7 days in the second. During harvest, plants were first split in above- and belowground parts by cutting the stem immediately above the taproot using garden scissors. After flushing the sand out with cold water, the root systems were split into two organs: fine roots and taproots. Fine roots were collected from the lower half of the root system to clearly separate them from lateral or taproots. The shoots were split into two organs: leaf lamina and stem or hypocotyl. We divided leaves into three groups: young leaves (two most recently developed leaves), mature leaves (two leaves directly below the young leaves) and old leaves (two leaves directly below the mature leaves). In the first experiment, one leaf of each group were pooled together for later analysis. After harvest, the separate plant organs were wrapped in aluminum foil, flash-frozen in liquid nitrogen and stored at -80°C. Afterwards, we finely ground each sample in liquid nitrogen using a mortar and pestle. For the first experiment two of the six plants belonging to the same treatment were pooled, resulting in three biological replicates per treatment (n = 3). For the second experiment all six biological replicates were analyzed individually (n = 6).

Gene Expression Analysis

Total RNA was extracted from ±100 mg ground plant tissue following a protocol adapted from Oñate-Sánchez and Vicente-Carbajosa (2008). The extracted RNA was subsequently treated with DNAse I (Thermo Scientific, Waltham, MA, USA) following the manufacturer's instructions. The quality of RNA was checked visually by gel-electrophoresis and by measuring 260/230 and 260/280 absorbance ratios using a NanoPhotometer® P330 (Implen, Munich, Germany). Next, first-strand cDNA was synthesized from 1 µg purified total RNA using Revert Aid H minus reverse transcriptase (Thermo Scientific, Waltham, MA, USA) following the manufacturer's instructions. The samples were incubated at 42°C for 60 min, 50° C for 15 min, and finally 70°C for 15 min in a thermal cycler (Techne, Stone, UK). Real-time quantitative PCR (RT-qPCR) procedures were performed on a CFX384 Real-time system (BioRad, Munich, Germany) using the gene-specific primers as described in **Table S1**. The qPCR conditions were: 2 min at 50°C, 5 min at 95°C, and 40 cycles of 30 s at 95°C, 30 s at 58°C, 45 s at 72°C. Three technical replicates were analyzed per gene for each of the three biological replicates in experiment 1 and of the six biological replicates in experiment 2. Relative expression of target genes was calculated using the comparative $2^{-\Delta\Delta CT}$ method as described in Livak and Schmittgen (2001). The data was normalized to expression of the housekeeping gene *GAPDH* in the first experiment and *ACTIN 7* in the second experiment. Expression levels were then normalized to those in the control plants. The genes selected for this study play a role in either GSL biosynthesis or transport. *CYP83A1* (CYTOCHROME P450, FAMILY 83, SUBFAMILY A, POLYPEPTIDE 1) is involved in the biosynthesis of aliphatic GSLs. *CYP79B2* (CYTOCHROME P450, FAMILY 79, SUBFAMILY B, POLYPEPTIDE 2) is involved in the biosynthesis of indole GSLs. *GTR1A2* and *GTR2A2* (GLUCOSINOLATE TRANSPORTER 1&2) regulate transport of aliphatic and indole GSLs, whereas *GTR3A1* exclusively regulates transport of indole GSLs (Jørgensen et al.,

2017). Primer sequences used in this experiment are shown in **Table S1**.

Glucosinolate Analysis

GSL extraction was performed following the method as described in Grosser and van Dam (2017). In brief, freshly ground plant tissue was freeze-dried, after which ±100 mg of material was used for extraction from three biological replicates in experiment 1 and from six biological replicates in experiment 2. GSLs were extracted in 70% methanol at 90°C, after which the supernatant was transferred to an ion-exchange column with Sephadex G-25 (Merck, Darmstadt, Germany) as column material. After washing the extracts with 70% methanol and adding a NaOAc buffer to the column, sulfatase (from Helix pomatia type H-1, Merck, Darmstadt, Germany) was pipetted onto the extracts to remove the sulfate group from the GSLs. The desulfo-GSLs that were released from the ion-exchange column as a result of sulfatase activity were eluted in ultrapure water and collected. Next, the samples were freeze-dried and re-dissolved in 1 ml of ultrapure water. The GSLs in the samples were separated using a reversed phase high-pressure liquid chromatography (HPLC) set-up equipped with a photodiode array detector (PDA; Thermo Scientific Ultimate 3000 series) at wavelengths of 229 nm and 272 nm. A reversed-phase Acclaim™ 300 C18 column (4.6 × 150 mm, 3 µm, 300 Å, Acclaim 300, Thermo Fisher Scientific) was used for separation with 100% H_2O (solvent A) and 99% acetonitrile in water (solvent B) as solvents. The separation conditions were as follows: equilibration took place at a gradient profile of 98% of solvent A for 4.3 min, followed by a gradient to 35% solvent B within 24.3 min, and a hold until 29° min at 35% solvent B. Next, the gradient went back to the initial 98% of solvent A within 1 min and held at initial conditions for 10 min at a flow of 0.6 ml/min. Desulfo-GSLs were identified based on retention time and UV spectra compared to commercially available reference standards (Phytoplan, Heidelberg, Germany). We used sinigrin as an external standard for GSL quantification. The resulting data were processed using Chromeleon 7.2 SR5 MUa (9624; Thermo Fisher Scientific, Waltham, MA, USA). Response factors and approximate retention times of each GSL are shown in **Table S2**. Detailed results of individual GSL accumulation are shown in **Table S3** for the first experiment and **Table S4** for the second experiment.

Statistical Analysis

All statistical analyses were performed with version 3.4.3 of R (RStudio Team, 2018). Normality of the data and homogeneity of variance were inspected visually using QQ- and residual plots. When the assumptions were not met, the respective data were log-transformed. Within each plant organ, concentrations of total GSLs and of each GSL class individually, and of transcript accumulation of each gene were analyzed by two-way ANOVA with treatment and time as fixed factors. When either factor had a significant effect, student's t-tests where used to test for significant differences between treatments at individual time points. Samples that could not be analyzed due to technical problems during sample processing were treated as missing values.

RESULTS

Experiment 1: Late Time-Points

Indole GSLs Accumulate in the Taproot During Root Herbivory

In the first experiment, we studied the accumulation of GSLs in the taproot, fine roots, stem and leaf lamina after 3 and 7 days of herbivory. We did not observe any changes in the total amount of GSLs in the taproot during root-herbivory by *D. radicum*. Indole GSL levels were significantly elevated both after 3 and 7 days (**Figure 1**, $P < 0.001$, $F = 26.10$, two-way ANOVA, **Table 1**), whereas aliphatic and benzyl GSLs in the taproot were not affected by root herbivory. We did not observe any changes in total GSL levels or in the accumulation of individual GSL classes in the fine roots. Moreover, we did not detect benzyl GSLs in the fine roots, neither in control plants nor after root herbivory (**Figure 1**). In the stem, benzyl GSL levels decreased after 3 days of herbivory (**Figure S1**, $P < 0.01$, $F = 17.45$, **Table S5**) but returned to control levels after 7 days. We did not observe any changes in GSL levels in the leaf lamina (**Figure S1**).

Root Herbivory Affects Expression of Biosynthesis and Transporter Genes in the Taproot

The observed increase in indole GSLs in the taproot coincided with an increased expression of the indole GSL biosynthesis gene *CYP79B2* (**Figure 2**, $P < 0.001$, $F = 37.48$, two-way ANOVA, **Table 2**) and downregulation of *CYP83A1* (**Figure 2**, $P < 0.01$, $F = 16.624$), which is involved in aliphatic GSL biosynthesis. In addition, we observed an increased expression of *GTR1* in the taproot after 7 days (**Figure 3**, $P < 0.01$, $F = 11.535$). No changes in the expression of biosynthesis (**Figure S2**) or transporter genes (**Figure S3**) were found in distal tissues, although a trend towards decreased expression of *GTR1* was observed in the stem after 3 days of herbivory (**Figure S3**, $P = 0.08$, $F = 3.848$, **Table S7**).

Experiment 2: Early Time-Points

The results of the first experiment showed that biosynthesis and transporter genes were already significantly upregulated in the taproot by 3 days of herbivory. We therefore performed a second experiment, in which we focused on the accumulation of GSLs in the early stages of herbivory. We focused only on the taproot and fine roots since we observed hardly any changes in biosynthesis or transport dynamics in aboveground tissues.

Root Herbivory Affects Glucosinolates Accumulation in Local But Not in Distal Tissues

Root herbivory by *D. radicum* leads to an increased total GSL accumulation in the taproot after 3 days (**Figure 4**, $P < 0.05$, $F = 5.80$, two-way ANOVA, **Table 3**). The levels of indole GSLs (**Figure 4**, $P < 0.0001$, $F = 30.59$) and benzyl GSLs increased after 24 h and 3 days (**Figure 4**, $P < 0.0001$, $F = 19.70$), whereas

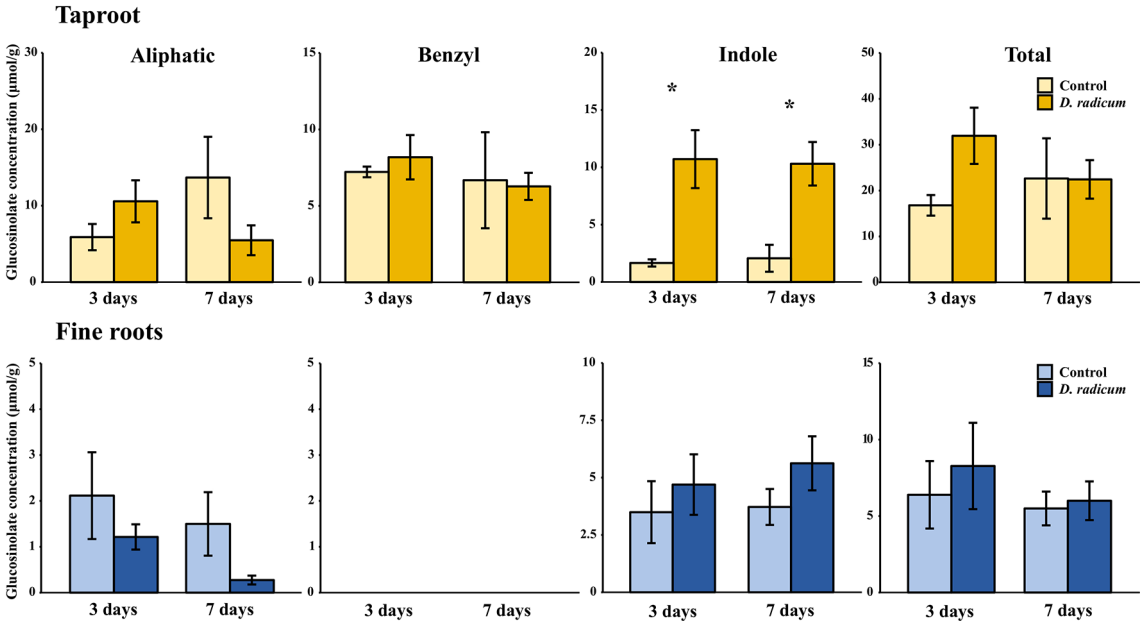

FIGURE 1 | Concentration (µmol/g dry mass) of aliphatic, benzyl, indole and total GSLs in the tap root and fine roots of *B. rapa* plants after 3 and 7 days of root-herbivory by *D. radicum* (mean (SE), *n* = 3). At each time-point, the asterisk indicates significant differences according to student's t-tests (P < 0.05, **Table S6**). *, P < 0.05.

TABLE 1 | Statistical comparison of aliphatic, benzyl, indole and total GSL concentrations [(µmol/g) in the taproot and fine roots of *B. rapa* plants after 3 and 7 days of root-herbivory by *D. radicum* (two-way ANOVA, *n* = 3)]. Bold indicates significant difference P-values (P < 0.05).

GSL	Factors	Taproot					Fine roots				
		Df	Sum Sq	Mean Sq	F	P value	Df	Sum Sq	Mean Sq	F	P value
Aliphatic	Treatment	1	9.32	9.32	0.29	0.60	1	3.39	3.39	3.09	0.12
	Timepoint	1	5.45	5.45	0.17	0.69	1	1.82	1.82	1.66	0.23
	Treatment * Timepoint	1	124.66	124.66	3.90	0.08	1	0.08	0.08	0.07	0.80
	Residuals	8	256.04	32.01			8	8.75	1.09		
Benzyl	Treatment	1	0.24	0.24	0.02	0.88	–	–	–	–	–
	Timepoint	1	4.51	4.51	0.47	0.51	–	–	–	–	–
	Treatment * Timepoint	1	1.40	1.40	0.15	0.71	–	–	–	–	–
	Residuals	8	77.26	9.66			–	–	–	–	–
Indole	Treatment	1	224.40	224.40	26.10	**9.20E-04**	1	7.24	7.24	1.73	0.22
	Timepoint	1	0.00	0.00	0.00	1.00	1	1.00	1.00	0.24	0.64
	Treatment * Timepoint	1	0.50	0.50	0.06	0.82	1	0.37	0.37	0.09	0.77
	Residuals	8	68.79	8.60			8	33.39	4.17		
Total	Treatment	1	151.50	151.51	1.41	0.27	1	1.61	1.61	0.36	0.57
	Timepoint	1	5.30	5.32	0.05	0.83	1	20.97	20.97	4.65	0.06
	Treatment * Timepoint	1	199.00	198.96	1.85	0.21	1	0.16	0.16	0.04	0.86
	Residuals	8	862.00	107.75			8	36.06	4.51		

aliphatic GSL levels were not affected. We did not observe any changes in GSL levels in the fine roots.

Root Herbivory Only Elicits Local Transcript Accumulation

We observed a strongly increased expression of *CYP79B2* in the taproot over the entire period of herbivory (**Figure 5**, P < 0.0001, F = 61.96, two-way ANOVA, **Table 4**). In contrast, *CYP83A1* was upregulated only at 12 h after the start of root herbivory (**Figure 5**, P < 0.01, F = 12.18) and returned to control levels after 24 h. For genes involved in GSL transport, *GTR1A2* expression increased after 12 h (**Figure 6**, P < 0.001, F = 16.68) and stayed elevated until 24 h and 3 days after herbivory. The expression levels of *GTR2A2* were increased over the entire period of herbivory (**Figure 6**, P < 0.0001, F = 21.43), whereas we did not observe any changes in expression of *GTR3A1*. We did not observe any changes in expression of the biosynthesis genes *CYP83A* (**Figure 5**) or *CYP79B2* in the fine roots. The expression of the transporter *GTR1A2* increased after 24 h (**Figure 6**, P < 0.01, F = 7.68) and returned to control levels after 3 days. Root herbivory did not affect the expression of *GTR2A2* or *GTR3A1* in the fine roots (**Figure 6**).

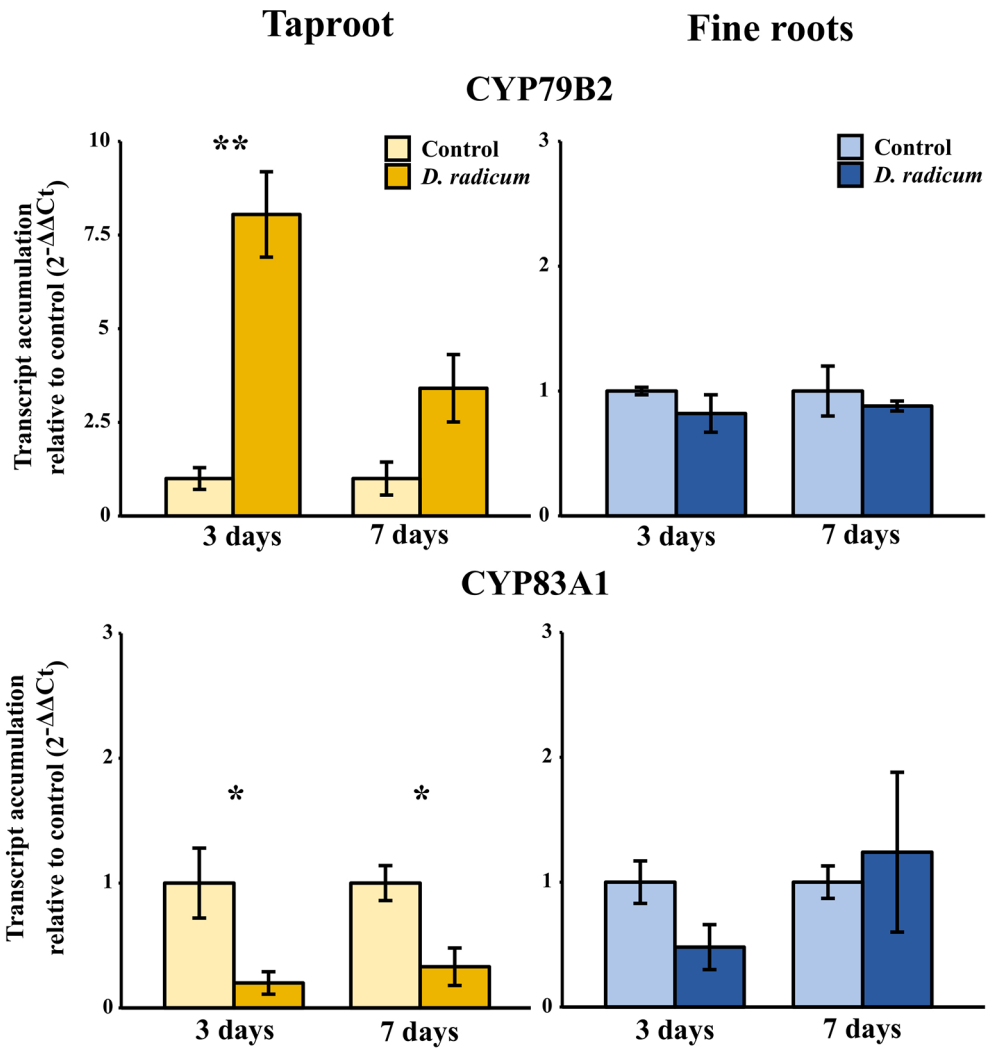

FIGURE 2 | Transcript accumulation ($2^{-\Delta\Delta CT}$) of GSL biosynthesis genes *CYP79B2* and *CYP83A1* in the tap root and fine roots of *B. rapa* plants after 3 and 7 days of root-herbivory by *D. radicum* normalized to the housekeeping gene *GAPDH* (mean (SE), $n = 3$). At each time-point, the asterisk indicates significant differences according to student's t-tests ($P < 0.05$, **Table S8**). *, $P < 0.05$; **, $P < 0.01$.

DISCUSSION

Our study revealed that local accumulation of total GSLs in response to *D. radicum* root feeding coincided with an increased local expression of both GSL biosynthesis and transporter genes in *B. rapa*. We observed similar patterns in both experiments, demonstrating the reproducibility of our results. We hypothesized that activation of GSL transport genes to transport GSLs from distal tissues would precede local *de novo* biosynthesis gene activity. However, we did not observe such temporal dynamics in our experiments. Similarly, we did not find that systemic GSL levels or transporter gene expression are suppressed in favor of locally increasing taproot levels. As predicted by the ODT, we found that GSL levels increased in the taproot in response to local root herbivory. For benzyl and indole GSL, this increase occurred one day after the start of herbivory, and lasted for the complete 7-day period of herbivory. Contrary to our hypothesis, we did not observe a decline in GSL levels in distal tissues during this period. This makes it unlikely that rapid re-allocation of distal GSLs from the shoots contributed to the increase of GSLs in the taproot.

Over the two experiments, the increase of total GSL levels in the taproot was mainly driven by elevated indole GSL levels, whereas aliphatic GSL concentrations did not increase upon root herbivory in either experiment. The increase in indole GSL levels in response to feeding by the specialist *D. radicum* as observed in this study is comparable to that of *B. rapa* to herbivory by the generalist *Anomala cuprea* (Tsunoda et al., 2018). This suggests that chewing root-herbivores with different degrees of host-plant specialization induce similar GSL profiles in *B. rapa*. In addition to indole GSL accumulation, the levels of the benzyl GSL gluconasturtiin (2-phenylethylglucosinolate) also increased in response to root-herbivory. Gluconasturtiin is a dominant GSL present in roots of *Brassica* species (van Dam et al., 2009). Its

TABLE 2 | Statistical comparison of transcript accumulation of GSL transporters 1, 2,and 3 and biosynthesis genes *CYP79B2* and *CYP83A1* in the taproot and fine roots of *B. rapa* plants after 3 and 7 days of root-herbivory by *D. radicum* (two-way ANOVA, $n = 3$). Bold indicates significant difference P-values ($P < 0.05$).

Gene	Factor	Tap root					Fine roots				
		Df	Sum Sq	Mean Sq	F	P value	Df	Sum Sq	Mean Sq	F	P value
GTR1A2	Treatment	1	26.74	26.74	11.535	**0.009**	1	0.145	0.145	0.485	0.506
	Timepoint	1	1.583	1.583	0.683	0.433	1	0.125	0.125	0.418	0.536
	Treatment * Timepoint	1	1.583	1.583	0.683	0.433	1	0.125	0.125	0.418	0.536
	Residuals	8	18.545	2.318			8	2.382	0.298		
GTR2A2	Treatment	1	0.832	0.832	2.397	0.160	1	0.307	0.307	4.089	0.078
	Timepoint	1	0.055	0.055	0.158	0.701	1	0.000	0.000	0.002	0.970
	Treatment * Timepoint	1	0.055	0.055	0.158	0.701	1	0.000	0.000	0.002	0.970
	Residuals	8	2.778	0.347			8	0.601	0.075		
GTR3A1	Treatment	1	0.495	0.495	0.766	0.407	1	0.629	0.629	3.793	0.087
	Timepoint	1	0.298	0.298	0.462	0.516	1	0.179	0.179	1.08	0.329
	Treatment * Timepoint	1	0.298	0.298	0.462	0.516	1	0.179	0.179	1.08	0.329
	Residuals	8	5.165	0.646			8	1.327	0.166		
CYP79B2	Treatment	1	67.150	67.150	37.48	**2.83E-04**	1	0.070	0.070	1.472	0.260
	Timepoint	1	16.130	16.130	9	**0.017**	1	0.003	0.003	0.056	0.820
	Treatment * Timepoint	1	16.130	16.130	9	**0.017**	1	0.003	0.003	0.056	0.820
	Residuals	8	14.330	1.790			8	0.379	0.047		
CYP83A1	Treatment	1	1.621	1.621	16.624	**0.004**	1	0.058	0.058	0.161	0.699
	Timepoint	1	0.013	0.013	0.134	0.724	1	0.437	0.437	1.211	0.303
	Treatment * Timepoint	1	0.013	0.013	0.134	0.724	1	0.437	0.437	1.211	0.303
	Residuals	8	0.780	0.098			8	2.885	0.361		

breakdown product 2-phenylethyl ITC, which is formed upon root fly feeding (Crespo et al., 2012), has chemical traits that are advantageous in soil conditions, such as low volatility and hydrophobicity (Sarwar et al., 1998; Laegdsmand et al., 2007). In addition, gluconasturtiin can have a negative effect on belowground herbivore performance, as was shown for *D. radicum* larvae feeding on *Barberea vulgaris* plants with differential GSL profiles (Van Leur et al., 2008). Pupae of *D. radicum* larvae feeding on *B. vulgaris* roots with gluconasturtiin as the dominant GSL where underdeveloped compared to those feeding from plants that mainly produced glucobarbarin (2(S)-OH-2-phenylethylglucosinolate). Although aliphatic GSLs have shown to play an important role in immunity against several chewing insect species in shoot tissues (Beekwilder et al., 2008; Müller et al., 2010; Jeschke et al., 2017), we did not find an induction of aliphatic GSL accumulation in response to the root-herbivore *D. radicum*. These observations are in accordance with the theory that shoot and root tissues rely on distinct GSL profiles as chemical defenses against a different community of chewing insect herbivores (Tsunoda and van Dam, 2017).

The accumulation patterns that we observed during root-herbivory can be largely explained by local expression levels of biosynthesis genes. The accumulation of indole GSLs in the taproot was preceded by an increased local expression of the biosynthesis gene CYP79B2, which lasted for the entire three-day period of herbivory. Interestingly, we also observed an initial increase in CYP83A1 expression after 12 h, suggesting that root-herbivory also would increase biosynthesis of aliphatic GSLs. However, CYP83A1 transcript levels dropped back to control conditions one day after the start of herbivory. This decrease in CYP83A1 expression coincided with a rise in CYP79B2 expression, suggesting that crosstalk occurred between the indole- and aliphatic GSL biosynthesis pathways. Such crosstalk between GSL biosynthetic pathways in favor of indole GSL synthesis was also observed in interactions between *A. thaliana* and the oomycete pathogen *Phytophthora brassicae* (Schlaeppi et al., 2010). Because specialist herbivores, such as *D. radicum*, may be able to detoxify GSL-based defenses, crosstalk might serve to switch from production of aliphatic GSLs which are ineffective against specialist herbivores, towards to the production of antimicrobial indole GSLs. Because of this antimicrobial effect of indole GSLs (Bednarek et al., 2009; Schlaeppi et al., 2010), we hypothesize that the observed accumulation of indole GSLs in the taproot may serve to prevent secondary infection by soil-borne pathogens. Root-herbivores generally cause damage to plant tissue over an extended period (Johnson et al., 2016), which increases secondary infections by microbial invaders. This may be particularly so for roots, as soils may contain up to 1 billion microbial cells per 10 grams of soil (Prosser, 2015). In *Arabidopsis thaliana*, indole GSLs work in concert with the structurally related phytoalexin camalexin to battle pathogen infection (Schlaeppi et al., 2010). In this case, indole GSLs slow down the infection cycle of pathogens by limiting penetration of the epidermal cell layer, after which camalexin serves as a late-acting antimicrobial defense-barrier. Although camalexin is not present in *B. rapa*, there are other phytoalexins that the species produces in response to biotic stressors. A prominent phytoalexin in several *Brassica* species is brassinin (Klein and Sattely, 2017), which is synthesized from the unstable ITCs that are formed during hydrolysis of glucobrassicin (indol-3-ylmethylglucosinolate) (Pedras et al., 2009; Bednarek, 2012). Glucobrassicin is one of the indole GSL that was induced by *D. radicum* feeding in this study. In addition, the biosynthesis of

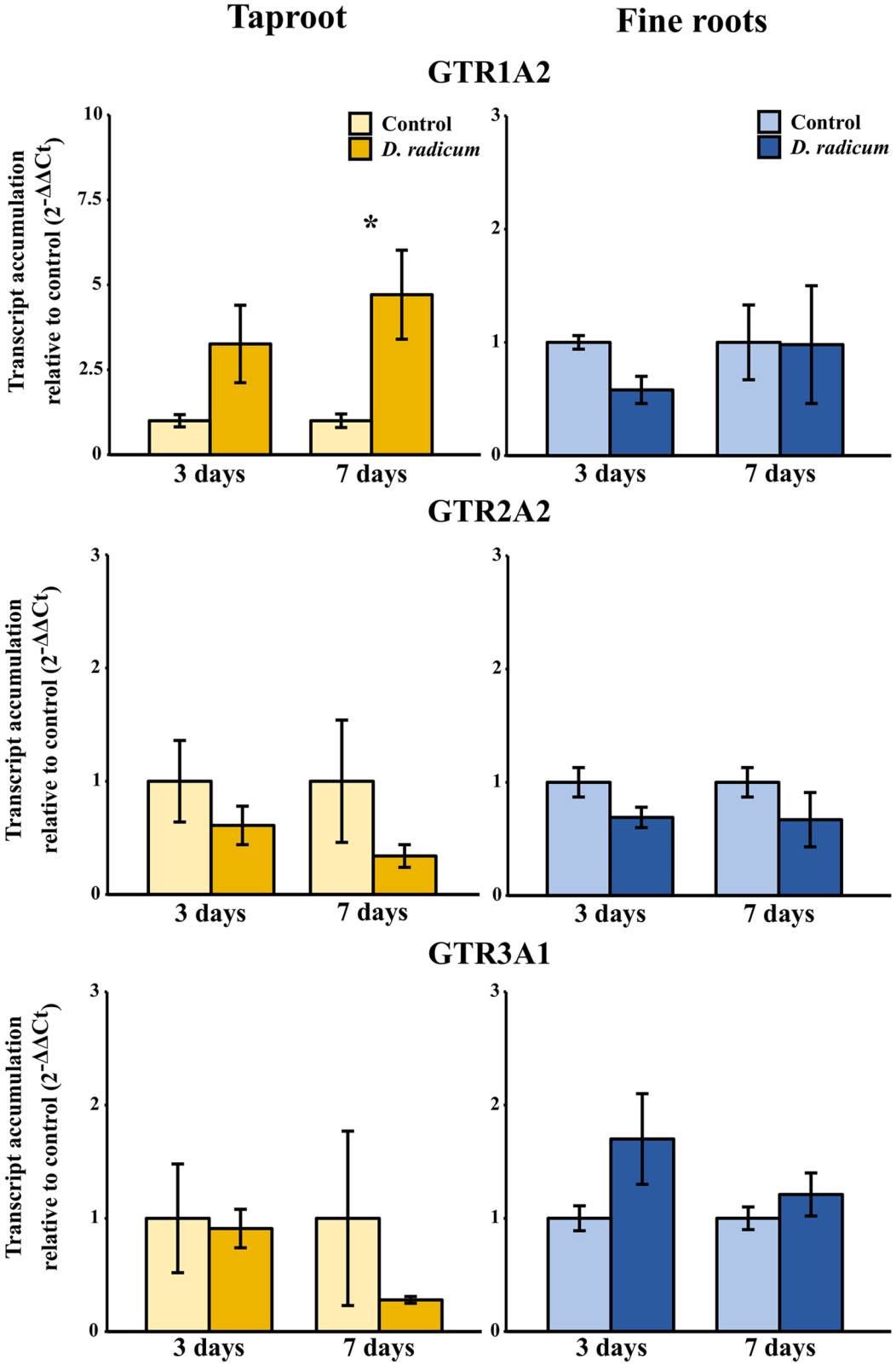

FIGURE 3 | Transcript accumulation ($2^{-\Delta\Delta CT}$) of GSL transporters GTR 1, 2 and 3 in the tap root and fine roots of *B. rapa* plants after 3 and 7 days of root-herbivory by *D. radicum* normalized to the housekeeping gene *GAPDH* (mean (SE), $n = 3$). At each time-point, the asterisk indicates significant differences according to student's t-tests ($P < 0.05$, **Table S8**). *, $P < 0.05$; **, $P < 0.01$, ***, $P < 0.001$.

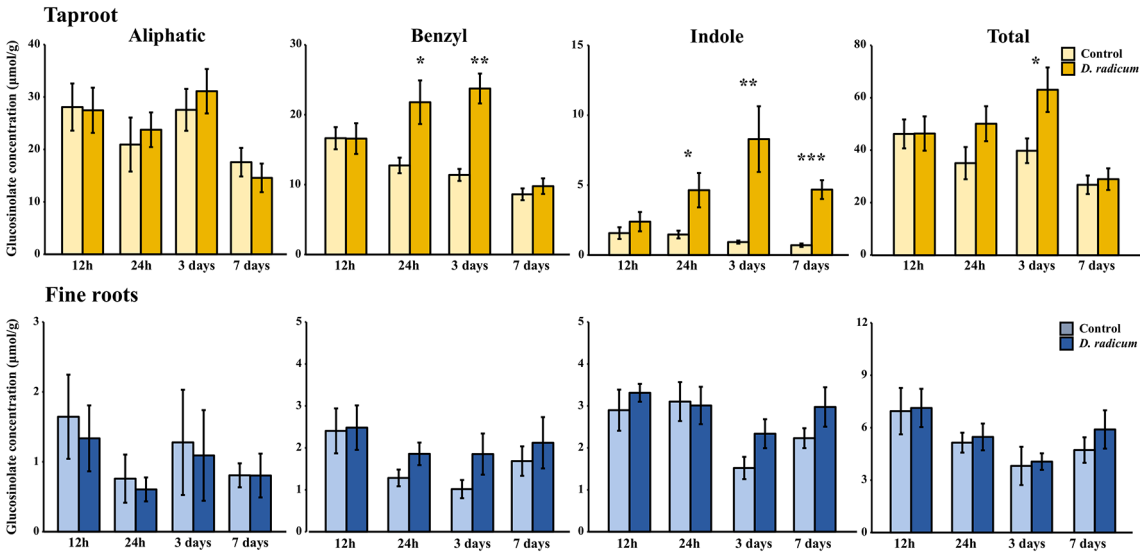

FIGURE 4 | Concentration (µmol/g dry mass) of aliphatic, benzyl, indole and total GSLs in the tap root and fine roots of *B. rapa* plants after 12 h, 24 h, 3 days and 7 days of root-herbivory by *D. radicum* (mean (SE), $n = 6$). At each time-point, the asterisk indicates significant differences according to student's t-tests ($P < 0.05$, **Table S9**). *, $P < 0.05$; **, $P < 0.01$, ***, $P < 0.001$.

TABLE 3 | Statistical comparison of aliphatic, benzyl, indole and total GSL concentrations [(µmol/g) in the taproot and fine roots of *B. rapa* plants after 12 h, 24 h, 3 and 7 days of root-herbivory by *D. radicum* (two-way ANOVA, $n = 6$)]. Bold indicates significant difference P-values ($P < 0.05$).

GSL	Factors	Taproot					Fine roots				
		Df	Sum Sq	Mean Sq	F	P value	Df	Sum Sq	Mean Sq	F	P value
Aliphatic	Treatment	1	4.00	3.70	0.04	0.84	1	0.31	0.31	0.23	0.63
	Timepoint	3	1415.00	471.50	5.04	**4.50E-03**	3	4.97	1.66	1.24	0.31
	Treatment * Timepoint	3	91.00	30.20	0.32	0.81	3	0.16	0.05	0.04	0.99
	Residuals	42	3929.00	93.50			42	56.20	1.34		
Benzyl	Treatment	1	371.10	371.10	19.70	**6.44E-05**	1	2.87	2.87	2.57	0.12
	Timepoint	3	643.00	214.30	11.38	**1.36E-05**	3	7.29	2.43	2.18	0.11
	Treatment * Timepoint	3	337.40	112.50	5.97	**1.74E-03**	3	0.89	0.30	0.27	0.85
	Residuals	42	791.00	18.80			42	46.95	1.12		
Indole	Treatment	1	184.17	184.17	30.59	**1.87E-06**	1	2.88	2.89	3.31	0.08
	Timepoint	3	44.79	14.93	2.48	0.07	3	10.73	3.58	4.10	**0.01**
	Treatment * Timepoint	3	66.04	22.01	3.66	**0.02**	3	1.58	0.53	0.61	0.62
	Residuals	42	252.86	6.02			42	36.63	0.87		
Total	Treatment	1	1207.00	1207.40	5.80	**2.05E-02**	1	8.10	8.10	1.29	0.26
	Timepoint	3	4068.00	1355.90	6.51	**1.02E-03**	3	40.24	13.41	2.13	0.11
	Treatment * Timepoint	3	1111.00	370.40	1.78	0.17	3	3.65	1.22	0.19	0.90
	Residuals	42	8743.00	208.20			42	264.72	6.30		

indole GSLs is closely linked to that of indole-3-acetic acid (IAA) (Malka and Cheng, 2017), the most commonly occurring plant hormone belonging to the auxin class (reviewed in Zhao, 2010). Next to its role in growth and development, IAA is a regulator of callus formation in response to wounding. By forming a physical barrier, callus can reduce infection by closing the wounds, thereby reducing infection by pathogens (Ikeuchi et al., 2013). Last but not least, the root flies themselves bring along microbial communities in their guts, which may help them to overcome their host plant's chemical defenses (Welte et al., 2016). Some of these gut microbes, for example *Pectobacterium* spp, are also root pathogens in *Brassica* crops (van den Bosch et al., 2018). Taken together, it is very likely that the responses triggered by root herbivory are partly triggered by and targeted to microbial pathogens (Sellam et al., 2007). Brassinin and IAA are therefore interesting targets for future studies on interactions with root-herbivores and related microbial infections in *Brassica*.

Next to the induction of biosynthesis, herbivory induced the local expression of transporters GTR1 and GTR2, whereas expression of GTR3 was not affected. Since the induction of GTRs preceded the rise in indole GSL concentration, this suggests that active transport from distal tissues potentially plays a role in local accumulation of indole GSLs. However, contrary to our hypotheses, we did not observe any changes in

TABLE 4 | Statistical comparison of transcript accumulation of GSL transporters 1, 2, and 3 and biosynthesis genes *CYP79B2* and *CYP83A1* in the taproot and fine roots of *B. rapa* plants after 12 h, 24 h, 3 and 7 days of root-herbivory by *D. radicum* (two-way ANOVA $n = 6$). Bold indicates significant difference P-values ($P < 0.05$).

Gene	Factors	Taproot					Fine roots				
		Df	Sum Sq	Mean Sq	F	P value	Df	Sum Sq	Mean Sq	F	P value
GTR1A2	Treatment	1	4171.00	4171.00	16.68	**3.03E-04**	1	4.27	4.27	7.68	**0.01**
	Timepoint	2	509.00	254.00	1.02	0.37	2	3.31	1.65	2.97	0.07
	Treatment * Timepoint	2	509.00	254.00	1.02	0.37	2	3.75	1.87	3.37	**0.05**
	Residuals	30	7502.00	250.00			29	16.12	0.56		
GTR2A2	Treatment	1	40.27	40.27	21.43	**6.62E-05**	1	1.09	1.09	2.54	0.12
	Timepoint	2	7.61	3.81	2.03	0.15	2	1.87	0.93	2.17	0.13
	Treatment * Timepoint	2	7.61	3.81	2.03	0.15	2	1.97	0.99	2.29	0.12
	Residuals	30	56.37	1.88			29	12.47	0.43		
GTR3A1	Treatment	1	0.00	0.00	0.04	0.84	1	0.48	0.48	1.66	0.21
	Timepoint	2	0.08	0.04	0.39	0.68	2	0.30	0.15	0.51	0.61
	Treatment * Timepoint	2	0.08	0.04	0.39	0.68	2	0.30	0.15	0.51	0.61
	Residuals	30	2.92	0.10			28	8.11	0.29		
CYP79B2	Treatment	1	5866.00	5866.00	61.96	**8.75E-09**	1	1.94	1.94	1.22	0.28
	Timepoint	2	415.00	208.00	2.19	0.13	2	1.32	0.66	0.41	0.67
	Treatment * Timepoint	2	415.00	208.00	2.19	0.13	2	1.46	0.73	0.46	0.64
	Residuals	30	2840.00	95.00			29	46.12	1.59		
CYP83A1	Treatment	1	6.10	6.10	12.18	**1.52E-03**	1	0.49	0.49	0.96	0.34
	Timepoint	2	1.91	0.96	1.91	0.17	2	0.25	0.13	0.24	0.79
	Treatment * Timepoint	2	1.91	0.96	1.91	0.17	2	0.25	0.13	0.25	0.78
	Residuals	30	15.03	0.50			29	14.96	0.52		

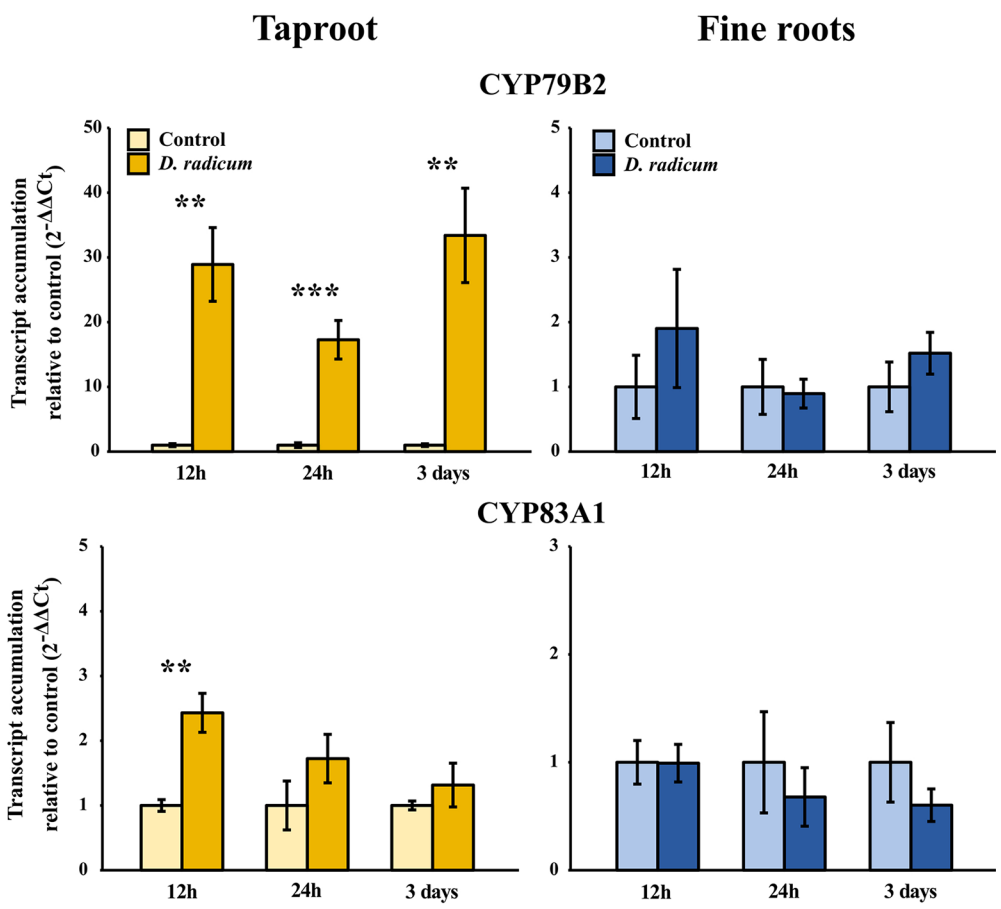

FIGURE 5 | Transcript accumulation ($2^{-\Delta\Delta CT}$) of GSL biosynthesis genes *CYP79B2* and *CYP83A1* in the tap root and fine roots of *B. rapa* plants after 12 h, 24 h and 3 days of root-herbivory by *D. radicum* normalized to the housekeeping gene *ACTIN 7* (mean (SE), $n = 6$). At each time-point, the asterisk indicates significant differences according to student's t-tests ($P < 0.05$, **Table S10**). **, $P < 0.01$, ***, $P < 0.001$.

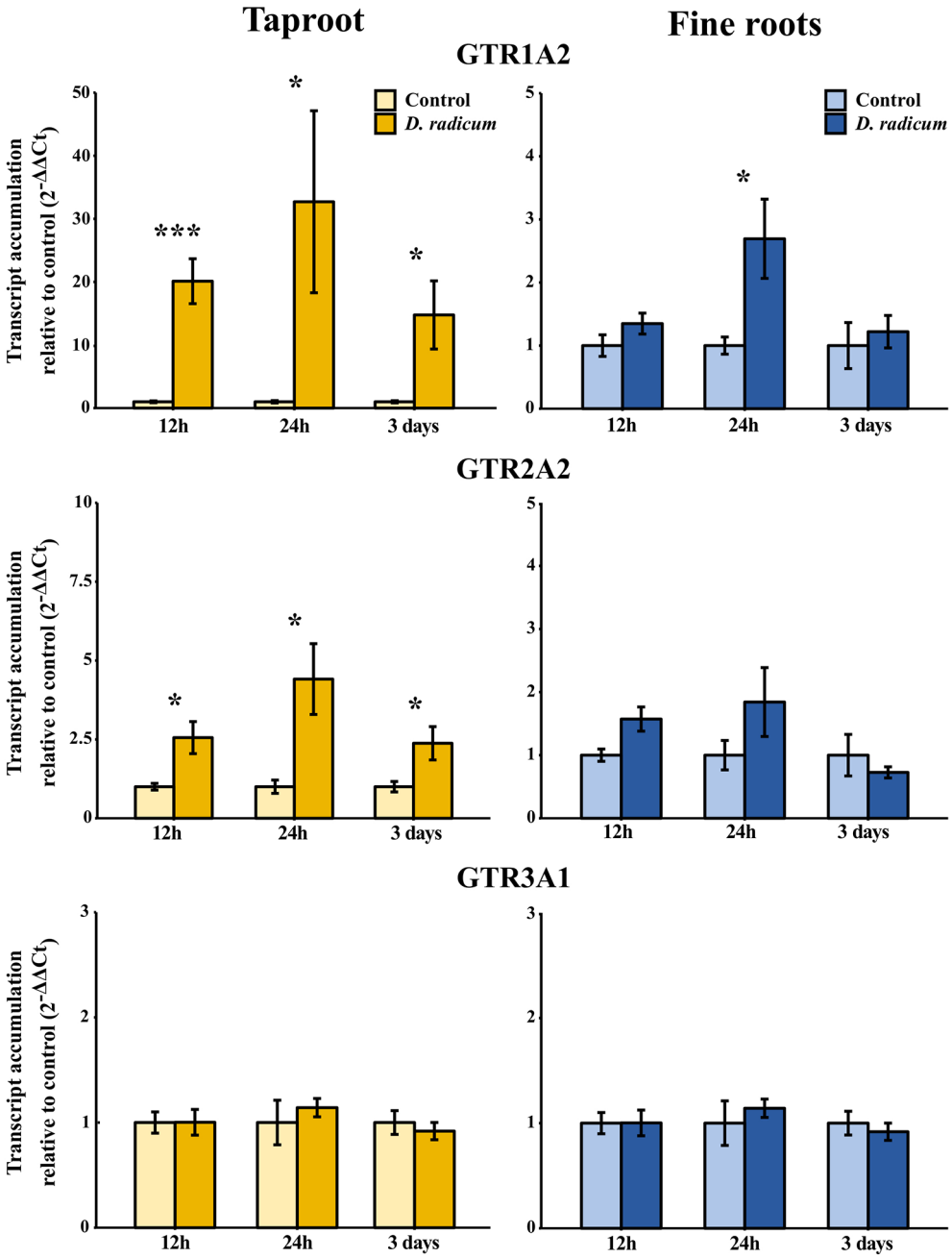

FIGURE 6 | Transcript accumulation ($2^{-\Delta\Delta CT}$) of GSL transporters GTR 1, 2 and 3 in the tap root and fine roots of *B. rapa* plants after 12h, 24 h and 3 days of root-herbivory by *D. radicum* normalized to the housekeeping gene *ACTIN 7* (mean (SE), $n = 6$). At each time-point, the asterisk indicates significant differences according to student's t-tests ($P < 0.05$, **Table S10**). *, $P < 0.05$; ***, $P < 0.001$.

GSL concentrations or expression of GTRs in distal tissues. This implies that local biosynthesis, and not transport from distal tissues, drives the accumulation of indole GSLs in response to root-herbivory. To confirm this hypothesis, the origin of GSLs that accumulated in the taproot should be studied by excluding the effects of transport from distal organs. This could be achieved by introducing isotope labelled GSLs or precursors into organs distal from the taproot, after which their distribution upon root herbivory can be studied. Next to transporting GSLs towards distal plant parts, GTRs also play a role in the retention of GSLs in designated plant parts (Jørgensen et al., 2017). An alternative hypothesis is that the increased expression of GTRs we observed in the taproot serves to prevent allocation of indole GSLs to plant parts that are not under imminent threat. By using specific GTR-knockout mutants, the role of transporter proteins in the retention of GSLs in the taproot can be studied. In conclusion,

our study suggests that both biosynthesis and transport processes play a role in the accumulation of GSLs in the taproot during root-herbivory. However, the exact function and relative importance of transporters upon belowground plant–herbivore interactions needs to be confirmed in future studies.

DATA AVAILABILITY STATEMENT

All datasets generated for this study are included in the article/ **Supplementary Material**.

AUTHOR CONTRIBUTIONS

TT, ND, and AT designed the experiments. TT performed the first experiment. AT and TT performed molecular analysis of the first experiment. AT and AVM carried out chemical analysis of the first experiment. AT and AVM performed the second experiment as well as molecular and chemical analyses. AT performed data analysis, supervised by TT and ND. AT, ND, and TT interpreted the results. AT wrote the manuscript under supervision of ND and TT. AM and RS assisted in molecular and chemical analyses and together with AVM provided helpful feedback on the manuscript.

FUNDING

The authors acknowledge support from the Open Access Fund of the ThULB (Thüringer Universitäts-und Landesbibliothek Jena) and the iDiv Open Science Publication Fund for their contribution to the publication fee.

ACKNOWLEDGMENTS

We are grateful to Dr. Andreas Schedl and Christian Ristok (Molecular Interaction Ecology, iDiv) for their help with chemical and statistical analyses, and to Harry Brown (Cardiff University) for his help during the experiments. AJT, AM and NMvD. gratefully acknowledge the support of the German Centre for Integrative Biodiversity Research (iDiv) Halle-Jena-Leipzig, which is funded by the German Research Foundation (FZT 118). RS is funded within the framework of the Collaborative Research Centre ChemBioSys (CRC1127) of the German Research Foundation (DFG). TT acknowledges the financial support of the Japan Society for the Promotion of Science Grant-in-Aid for Scientific Research (19K16227). AVM acknowledges the support of the German Academic Exchange Service (Short-Term Research Grant, 57381332). We thank the editor and our two reviewers for providing helpful comments on earlier drafts of the manuscript.

SUPPLEMENTARY MATERIAL

The Supplementary Material for this article can be found online at: https://www.frontiersin.org/articles/10.3389/fpls.2019.01653/full#supplementary-material

REFERENCES

Andersen, T. G., Nour-Eldin, H. H., Fuller, V. L., Olsen, C. E., Burow, M., and Halkier, B. A. (2013). Integration of biosynthesis and long-distance transport establish organ-specific glucosinolate profiles in vegetative *Arabidopsis*. *Plant Cell* 25, 3133–3145. doi: 10.1105/tpc.113.110890

Bednarek, P., Piślewska-Bednarek, M., Svatoš, A., Schneider, B., Doubský, J., Mansurova, M., et al. (2009). A glucosinolate metabolism pathway in living plant cells mediates broad-spectrum antifungal defense. *Science (80-.)* 323, 101 LP–106. doi: 10.1126/science.1163732

Bednarek, P. (2012). Sulfur-containing secondary metabolites from *Arabidopsis thaliana* and other Brassicaceae with function in plant immunity. *ChemBioChem* 13, 1846–1859. doi: 10.1002/cbic.201200086

Beekwilder, J., van Leeuwen, W., van Dam, N. M., Bertossi, M., Grandi, V., Mizzi, L., et al. (2008). The impact of the absence of aliphatic glucosinolates on insect herbivory in *Arabidopsis*. *PloS One* 3, e2068. doi: 10.1371/journal.pone.0002068

Bejai, S., Fridborg, I., and Ekbom, B. (2012). Varied response of *Spodoptera littoralis* against *Arabidopsis thaliana* with metabolically engineered glucosinolate profiles. *Plant Physiol. Biochem.* 50, 72–78. doi: 10.1016/j.plaphy.2011.07.014

Burow, M., and Halkier, B. A. (2017). How does a plant orchestrate defense in time and space? Using glucosinolates in *Arabidopsis* as case study. *Curr. Opin. Plant Biol.* 38, 142–147. doi: 10.1016/j.pbi.2017.04.009

Crespo, E., Hordijk, C. A., de Graaf, R. M., Samudrala, D., Cristescu, S. M., Harren, F. J. M., et al. (2012). On-line detection of root-induced volatiles in *Brassica nigra* plants infested with *Delia radicum L.* root fly larvae. *Phytochemistry* 84, 68–77. doi: 10.1016/j.phytochem.2012.08.013

Danner, H., Brown, P., Cator, E. A., Harren, F. J. M., van Dam, N. M., and Cristescu, S. M. (2015). Aboveground and belowground herbivores synergistically induce volatile organic sulfur compound emissions from shoots but not from roots. *J. Chem. Ecol.* 41, 631–640. doi: 10.1007/s10886-015-0601-y

Feller, C., Bleiholder, H., Buhr, L., Hack, H., Hess, M., Klose, R., et al. (1995). Phänologische Entwicklungsstadien von Gemüsepflanzen II. Fruchtgemüse und Hülsenfrüchte Codierung und Beschreibung nach der erweiterten BBCH-Skala - mit Abbildungen.

Grosser, K., and van Dam, N. M. (2017). A straightforward method for glucosinolate extraction and analysis with high-pressure liquid chromatography (HPLC). *J. Vis. Exp.*, (121) e55425. doi: 10.3791/55425

Ikeuchi, M., Sugimoto, K., and Iwase, A. (2013). Plant callus: mechanisms of induction and repression. *Plant Cell* 25, 3159–3173. doi: 10.1105/tpc.113.116053

Jørgensen, M. E., Nour-Eldin, H. H., and Halkier, B. A. (2015). Transport of defense compounds from source to sink: lessons learned from glucosinolates. *Trends Plant Sci.* 20, 508–514. doi: 10.1016/j.tplants.2015.04.006

Jørgensen, M. E., Xu, D., Crocoll, C., Ramírez, D., Motawia, M. S., Olsen, C. E., et al. (2017). Origin and evolution of transporter substrate specificity within the NPF family. *Elife* 6, e19466. doi: 10.7554/eLife.19466

Jeschke, V., Kearney, E. E., Schramm, K., Kunert, G., Shekhov, A., Gershenzon, J., et al. (2017). How glucosinolates affect generalist lepidopteran larvae: growth, development and glucosinolate metabolism. *Front. Plant Sci.* 8, 1995. doi: 10.3389/fpls.2017.01995

Johnson, S. N., Erb, M., and Hartley, S. E. (2016). Roots under attack: contrasting plant responses to below- and aboveground insect herbivory. *New Phytol.* 210, 413–418. doi: 10.1111/nph.13807

Kim, J. H., and Jander, G. (2007). *Myzus persicae* (green peach aphid) feeding on *Arabidopsis* induces the formation of a deterrent indole glucosinolate. *Plant J.* 49, 1008–1019. doi: 10.1111/j.1365-313X.2006.03019.x

Kim, J. H., Lee, B. W., Schroeder, F. C., and Jander, G. (2008). Identification of indole glucosinolate breakdown products with antifeedant effects on *Myzus*

persicae (green peach aphid). *Plant J.* 54, 1015–1026. doi: 10.1111/j.1365-313X.2008.03476.x

Kissen, R., Rossiter, J. T., and Bones, A. M. (2009). The `mustard oil bomb': not so easy to assemble?! Localization, expression and distribution of the components of the myrosinase enzyme system. *Phytochem. Rev.* 8, 69–86. doi: 10.1007/s11101-008-9109-1

Klein, A. P., and Sattely, E. S. (2017). Biosynthesis of cabbage phytoalexins from indole glucosinolate. *Proc. Natl. Acad. Sci. U. S. A.* 114, 1910–1915. doi: 10.1073/pnas.1615625114

Laegdsmand, M., Gimsing, A. L., Strobel, B. W., Sørensen, J. C., Jacobsen, O. H., and Hansen, H. C. B. (2007). Leaching of isothiocyanates through intact soil following simulated biofumigation. *Plant Soil* 291, 81–92. doi: 10.1007/s11104-006-9176-2

Livak, K. J., and Schmittgen, T. D. (2001). Analysis of relative gene expression data using real-time quantitative PCR and the 2–ΔΔCT method. *Methods* 25, 402–408. doi: 10.1006/meth.20011262

Madsen, S. R., Olsen, C. E., Nour-Eldin, H. H., and Halkier, B. A. (2014). Elucidating the role of transport processes in leaf glucosinolate distribution. *Plant Physiol.* 166, 1450–1462. doi: 10.1104/pp.114.246249

Malka, S. K., and Cheng, Y. (2017). Possible interactions between the biosynthetic pathways of indole glucosinolate and auxin. *Front. Plant Sci.* 8, 2131. doi: 10.3389/fpls.2017.02131

McKey, D. (1974). Adaptive patterns in alkaloid physiology. *Am. Nat.* 108, 305–320. doi: 10.1086/282909

Meldau, S., Erb, M., and Baldwin, I. T. (2012). Defence on demand: mechanisms behind optimal defence patterns. *Ann. Bot.* 110, 1503–1514. doi: 10.1093/aob/mcs212

Müller, R., de Vos, M., and Sun, J. Y. (2010). Differential effects of indole and aliphatic glucosinolates on lepidopteran herbivores. *J. Chem. Ecol.* 36, 905–913. doi: 10.1007/s10886-010-9825-z

Nour-Eldin, H. H., Andersen, T. G., Burow, M., Madsen, S. R., Jorgensen, M. E., Olsen, C. E., et al. (2012). NRT/PTR transporters are essential for translocation of glucosinolate defence compounds to seeds. *Nature* 488, 531–534. doi: 10.1038/nature11285

Oñate-Sánchez, L., and Vicente-Carbajosa, J. (2008). DNA-free RNA isolation protocols for *Arabidopsis thaliana*, including seeds and siliques. *BMC Res. Notes* 1, 93. doi: 10.1186/1756-0500-1-93

Ohnmeiss, T. E., and Baldwin, I. T. (2000). Optimal defense theory predicts the ontogeny of an induced nicotine defense. *Ecology* 81, 1765–1783. doi: 10.1890/0012-9658(2000)081[1765:ODTPTO]2.0.CO;2

Pedras, M. S. C., Okinyo-Owiti, D. P., Thoms, K., and Adio, A. M. (2009). The biosynthetic pathway of crucifer phytoalexins and phytoanticipins: de novo incorporation of deuterated tryptophans and quasi-natural compounds. *Phytochemistry* 70, 1129–1138. doi: 10.1016/j.phytochem.2009.05.015

Piasecka, A., Jedrzejczak-Rey, N., and Bednarek, P. (2015). Secondary metabolites in plant innate immunity: conserved function of divergent chemicals. *New Phytol.* 206, 948–964. doi: 10.1111/nph.13325

Prosser, J. I. (2015). Dispersing misconceptions and identifying opportunities for the use of *omics* in soil microbial ecology. *Nat. Rev. Microbiol.* 13, 439. doi: 10.1038/nrmicro3468

RStudio Team. (2018). RStudio: Integrated Development for R. (Boston, MA: RStudio, Inc.). Available at: http://www.rstudio.com/.

Sønderby, I. E., Geu-Flores, F., and Halkier, B. A. (2010). Biosynthesis of glucosinolates - gene discovery and beyond. *Trends Plant Sci.* 15, 283–290. doi: 10.1016/j.tplants.2010.02.005

Sarwar, M., Kirkegaard, J. A., Wong, P. T. W., and Desmarchelier, J. M. (1998). Biofumigation potential of brassicas. *Plant Soil* 201, 103–112. doi: 10.1023/A:1004381129991

Schlaeppi, K., Bodenhausen, N., Buchala, A., Mauch, F., and Reymond, P. (2008). The glutathione-deficient mutant pad2-1 accumulates lower amounts of glucosinolates and is more susceptible to the insect herbivore *Spodoptera littoralis*. *Plant J.* 55, 774–786. doi: 10.1111/j.1365-313X.2008.03545.x

Schlaeppi, K., Abou-Mansour, E., Buchala, A., and Mauch, F. (2010). Disease resistance of *Arabidopsis* to *Phytophthora brassicae* is established by the sequential action of indole glucosinolates and camalexin. *Plant J.* 62, 840–851. doi: 10.1111/j.1365-313X.2010.04197.x

Schoonhoven, L. M., van Loon, J. A., and Dicke, M. (2005). *Insect-Plant Biology* (Oxford, UK: Oxford University Press).

Sellam, A., Iacomi-Vasilescu, B., Hudhomme, P., and Simoneau, P. (2007). In vitro antifungal activity of brassinin, camalexin and two isothiocyanates against the crucifer pathogens *Alternaria brassicicola* and *Alternaria brassicae*. *Plant Pathol.* 56, 296–301. doi: 10.1111/j.1365-3059.2006.01497.x

Textor, S., and Gershenzon, J. (2009). Herbivore induction of the glucosinolate–myrosinase defense system: major trends, biochemical bases and ecological significance. *Phytochem. Rev.* 8, 149–170. doi: 10.1007/s11101-008-9117-1

Tsunoda, T., and van Dam, N. M. (2017). Root chemical traits and their roles in belowground biotic interactions. *Pedobiologia* 65, 58–67. doi: 10.1016/j.pedobi.2017.05.007

Tsunoda, T., Krosse, S., and van Dam, N. M. (2017). Root and shoot glucosinolate allocation patterns follow optimal defence allocation theory. *J. Ecol.* 105, 1256–1266. doi: 10.1111/1365-2745.12793

Tsunoda, T., Grosser, K., and van Dam, N. M. (2018). Locally and systemically induced glucosinolates follow optimal defence allocation theory upon root herbivory. *Funct. Ecol.* 32, 2127–2137. doi: 10.1111/1365-2435.13147

Tytgat, T. O. G., Verhoeven, K. J. F., Jansen, J. J., Raaijmakers, C. E., Bakx-Schotman, T., McIntyre, L. M., et al. (2013). Plants know where it hurts: root and shoot jasmonic acid induction elicit differential responses in *Brassica oleracea*. *PloS One* 8, e65502–e65502. doi: 10.1371/journal.pone.0065502

van Dam, N. M., and Raaijmakers, C. E. (2006). Local and systemic induced responses to cabbage root fly larvae (*Delia radicum*) in *Brassica nigra* and *B. oleracea*. *Chemoecology* 16, 17–24. doi: 10.1007/s00049-005-0323-7

Van Dam, N. M., Witjes, L., and Svatoš, A. (2004). Interactions between aboveground and belowground induction of glucosinolates in two wild *Brassica* species. *New Phytol.* 161, 801–810. doi: 10.1111/j.1469-8137.2004.00984.x

van Dam, N. M., Tytgat, T. O. G., and Kirkegaard, J. A. (2009). Root and shoot glucosinolates: a comparison of their diversity, function and interactions in natural and managed ecosystems. *Phytochem. Rev.* 8, 171–186. doi: 10.1007/s11101-008-9101-9

van den Bosch, T. J. M., Tan, K., Joachimiak, A., and Welte, C. U. (2018). Functional profiling and crystal structures of isothiocyanate hydrolases found in gut-associated and plant-pathogenic bacteria. *Appl. Environ. Microbiol.* 84, e00478–e00418. doi: 10.1128/AEM.00478-18

Van Leur, H., Raaijmakers, C. E., and Van Dam, N. M. (2008). Reciprocal interactions between the cabbage root fly (*Delia radicum*) and two glucosinolate phenotypes of *Barbarea vulgaris*. *Entomol. Exp. Appl.* 128, 312–322. doi: 10.1111/j.1570-7458.2008.00722.x

Welte, C. U., de Graaf, R. M., van den Bosch, T. J. M., den Camp, H. J. M., van Dam, N. M., and Jetten, M. S. M. (2016). Plasmids from the gut microbiome of cabbage root fly larvae encode SaxA that catalyses the conversion of the plant toxin 2-phenylethyl isothiocyanate. *Environ. Microbiol.* 18, 1379–1390. doi: 10.1111/1462-2920.12997

Wittstock, U., and Burow, M. (2010). Glucosinolate breakdown in *Arabidopsis*: mechanism, regulation and biological significance. *Arab. B.* 8, e0134–e0134. doi: 10.1199/tab0134

Wittstock, U., and Gershenzon, J. (2002). Constitutive plant toxins and their role in defense against herbivores and pathogens. *Curr. Opin. Plant Biol.* 5, 300–307. doi: 10.1016/S1369-5266(02)00264-9

Zhao, Y. (2010). Auxin biosynthesis and its role in plant development. *Annu. Rev. Plant Biol.* 61, 49–64. doi: 10.1146/annurev-arplant-042809-112308

Conflict of Interest: The authors declare that the research was conducted in the absence of any commercial or financial relationships that could be construed as a potential conflict of interest.

frontiers in Plant Science

ORIGINAL RESEARCH
published: 10 March 2020
doi: 10.3389/fpls.2020.00257

The Role of a Glucosinolate-Derived Nitrile in Plant Immune Responses

Hieng-Ming Ting[1], Boon Huat Cheah[2], Yu-Cheng Chen[1], Pei-Min Yeh[1], Chiu-Ping Cheng[1], Freddy Kuok San Yeo[3], Ane Kjersti Vie[4], Jens Rohloff[4], Per Winge[4], Atle M. Bones[4] and Ralph Kissen[4]**

[1] Institute of Plant Biology and Department of Life Science, National Taiwan University, Taipei, Taiwan, [2] Department of Agronomy, National Taiwan University, Taipei, Taiwan, [3] Faculty of Resource Science and Technology, Universiti Malaysia Sarawak, Kota Samarahan, Malaysia, [4] Cell, Molecular Biology and Genomics Group, Department of Biology, Norwegian University of Science and Technology, Trondheim, Norway

Glucosinolates are defense-related secondary metabolites found in Brassicaceae. When Brassicaceae come under attack, glucosinolates are hydrolyzed into different forms of glucosinolate hydrolysis products (GHPs). Among the GHPs, isothiocyanates are the most comprehensively characterized defensive compounds, whereas the functional study of nitriles, another group of GHP, is still limited. Therefore, this study investigates whether 3-butenenitrile (3BN), a nitrile, can trigger the signaling pathways involved in the regulation of defense responses in *Arabidopsis thaliana* against biotic stresses. Briefly, the methodology is divided into three stages, (i) evaluate the physiological and biochemical effects of exogenous 3BN treatment on Arabidopsis, (ii) determine the metabolites involved in 3BN-mediated defense responses in Arabidopsis, and (iii) assess whether a 3BN treatment can enhance the disease tolerance of Arabidopsis against necrotrophic pathogens. As a result, a 2.5 mM 3BN treatment caused lesion formation in Arabidopsis Columbia (Col-0) plants, a process found to be modulated by nitric oxide (NO). Metabolite profiling revealed an increased production of soluble sugars, Krebs cycle associated carboxylic acids and amino acids in Arabidopsis upon a 2.5 mM 3BN treatment, presumably via NO action. Primary metabolites such as sugars and amino acids are known to be crucial components in modulating plant defense responses. Furthermore, exposure to 2.0 mM 3BN treatment began to increase the production of salicylic acid (SA) and jasmonic acid (JA) phytohormones in Arabidopsis Col-0 plants in the absence of lesion formation. The production of SA and JA in nitrate reductase loss-of function mutant (*nia1nia2*) plants was also induced by the 3BN treatments, with a greater induction for JA. The SA concentration in *nia1nia2* plants was lower than in Col-0 plants, confirming the previously reported role of NO in controlling SA production in Arabidopsis. A 2.0 mM 3BN treatment prior to pathogen assays effectively alleviated the leaf lesion symptom of Arabidopsis Col-0 plants caused by *Pectobacterium carotovorum* ssp. *carotovorum* and *Botrytis cinerea* and reduced the pathogen growth on leaves. The findings of this study demonstrate that 3BN can elicit defense response pathways in Arabidopsis, which potentially involves a coordinated crosstalk between NO and phytohormone signaling.

Keywords: secondary metabolites, glucosinolates, nitriles, metabolomics, transcriptomics, plant innate immunity

OPEN ACCESS

Edited by:
Aleš Svatoš, Max Planck Institute for Chemical Ecology, Germany

Reviewed by:
Irene García, Institute of Plant Biochemistry and Photosynthesis (IBVF), Spain
Thomas Leustek, Rutgers, The State University of New Jersey, United States

****Correspondence:***
Hieng-Ming Ting
jimmytinghm@ntu.edu.tw
Ralph Kissen
ralph.kissen@ntnu.no

Specialty section:
This article was submitted to Plant Metabolism and Chemodiversity, a section of the journal Frontiers in Plant Science

Received: *31 October 2019*
Accepted: *19 February 2020*
Published: *10 March 2020*

Citation:
Ting H-M, Cheah BH, Chen Y-C, Yeh P-M, Cheng C-P, Yeo FKS, Vie AK, Rohloff J, Winge P, Bones AM and Kissen R (2020) The Role of a Glucosinolate-Derived Nitrile in Plant Immune Responses. Front. Plant Sci. 11:257. doi: 10.3389/fpls.2020.00257

INTRODUCTION

Plants are sessile organisms constantly exposed to a wide range of natural enemies, ranging from microbes, small insect herbivores to large herbivores. Once their physical defenses are breached, plants initiate a two-layered innate immune system that allow them to recognize, relay warning signals and mount defense against the invaders (Chisholm et al., 2006; Jones and Dangl, 2006).

The first layer of the innate immune system is primarily regulated by the membrane-bound pattern recognition receptors (PRRs), which enable plants to perceive the pathogen-/microbe-associated molecular patterns (PAMPs/MAMPs) and damage-associated molecular patterns (DAMPs) during a pathogen attack. DAMPs are self-elicitors as they are signal molecules released from damaged or dying plant cells (Roh and Sohn, 2018). The molecular pattern-bound PRRs trigger an innate immune response [PAMP-triggered immunity, (PTI); MAMP-triggered immunity, (MTI); DAMP-triggered immunity; (DTI)] to stop the invasion of pathogens (Heil and Land, 2014; Zipfel, 2014). The pathogens can overcome PTI/MTI/DTI (generally referred as PTI here onward) by deploying specific effector proteins, but may trigger the second layer of the innate immune system.

In the second layer of the innate immune system, plants can recognize the pathogen effector proteins through resistance proteins to activate effector-triggered immunity (ETI) (Rajamuthiah and Mylonakis, 2014). The ETI response is quicker and more intense than PTI. Both PTI and ETI initiate a battery of defense maneuvers, including increase of intracellular calcium and oxidative burst, activation of mitogen-activated protein kinase (MAPK) cascades, activation of transcription factors (such as WRKY family) and defense-related genes regulation (Couto and Zipfel, 2016; Kushalappa et al., 2016). Moreover, ETI response also triggers a hypersensitive response cell death to prevent the spread of pathogens (Vlot et al., 2017). Subsequently, hypersensitive response triggers the synthesis of secondary signal molecules, such as salicylic acid (SA), jasmonic acid (JA), nitric oxide (NO), reactive oxygen species (ROS), and lipid-derived molecules, to induce systemic acquired resistance (Fu and Dong, 2013; Gao et al., 2015).

Phytohormones are small endogenous, low-molecular-weight organic compounds that regulate a plethora of developmental and physiological processes (Bedini et al., 2018). Apart from developmental regulation, the phytohormone signaling cascades of SA, JA, and ethylene have also been associated with the aforementioned two layers of plant immunity, PTI and ETI (Mine et al., 2018). Each of the phytohormones has specific roles yet they can interact/crosstalk with one another either synergistically or antagonistically to execute the most efficient defense responses (Pieterse et al., 2012). Primary metabolites are the basic building blocks of nutrients that are required for normal growth and development of plants. On the flip side, the carbon skeletons and the stored energy of primary metabolites can also be utilized for defense purposes. An example of the alteration of primary metabolism in plants under a pathogen attack involves the post-translational derepression of invertase activity that led to an increased hydrolysis of sucrose into monosaccharides (Bonfig et al., 2010). Meanwhile, amino acids are the precursors of defensive proteins and defense-related secondary metabolites (Coruzzi and Last, 2000).

Secondary metabolites are also involved in plant defense. For example, glucosinolates, which are sulfur and nitrogen-containing plant secondary metabolites found in Brassicaceae. In *Arabidopsis thaliana*, glucosinolates are found in the sulfur-rich cells (Wittstock and Halkier, 2002). Myrosinases (thioglucosidase; EC3.2.1.147), which are present in myrosin cells in neighboring to sulfur-rich cells, will hydrolyze glucosinolates upon pathogen attack or upon mechanical damage that causes the disruption of plant tissue (Bones and Rossiter, 1996). Several glucosinolate hydrolysis products (GHPs), such as isothiocyanate, nitrile, epithionitrile and thiocyanate, can be generated depending on the side chain of their precursor glucosinolates and the presence of specifier proteins (Wittstock and Burow, 2010). Among the known GHPs, isothiocyanates are most studied. Isothiocyanates have been reported to be highly toxic to a broad range of natural enemies of plants including insects, fungi, bacteria and weeds (Halkier and Gershenzon, 2006; Gimsing and Kirkegaard, 2009; Stotz et al., 2011). Isothiocyanates are two edges swords. Not only they are toxic to susceptible pests and diseases, they are also found to be toxic to Arabidopsis at high dosage (Hara et al., 2010). Isothiocyanates also cause other negative effects on plants, such as triggering stomatal closure (Khokon et al., 2011), inducing cell death (Andersson et al., 2015), disrupting microtubules (Øverby et al., 2015a), depleting glutathione (Øverby et al., 2015b), and inhibiting root growth (Urbancsok et al., 2017).

The biological roles of other GHPs, such as nitriles, are not well understood. Nitriles are synthesized from glucosinolates by nitrile-specifier proteins or epithiospecifier proteins, in the presence of myrosinase (Lambrix et al., 2001; Kissen and Bones, 2009). Nitriles are less toxic compared to their corresponding isothiocyanates (Wittstock et al., 2003). It has been demonstrated that an epithiospecifier proteins overexpressing transgenic Arabidopsis, which can produce more nitriles, showed increased resistance to the bacterial pathogen *Pseudomonas syringae pv. tomato* DC3000 and the fungal pathogen *Alternaria brassicicola* (Miao and Zentgraf, 2007). This research indicates that the biological role of glucosinolate-derived nitriles in plants may be involved in disease resistance. Hossain and colleagues previously showed that 3-butenenitrile (3BN) could induce stomatal closure, ROS accumulation and NO production in guard cells of *A. thaliana* (Hossain et al., 2013), which are characteristic processes of DTI. However, to date, there is no study that elucidates the function of 3BN in enhancing the disease tolerance of Brassicaceae plants against pathogens. Therefore, in the present study we chose to investigate the effects of 3BN which is the nitrile-counterpart of the much studied sinigrin-derived allyl-isothiocyanate (Hara et al., 2010; Urbancsok et al., 2017). Among the different Brassicaceae species, *A. thaliana* was used in this study because it is the dicotyledonous model plant. The availability of a wide range of mutant lines and its complete genomic sequence provide extraordinary resources for functional biology studies (Reichelt et al., 2002).

To test the proposed function of 3BN, there were three objectives set out to be achieved in this study, i.e., (i) to evaluate the physiological and biochemical effects of 3BN treatment on Arabidopsis, (ii) to investigate the metabolites triggered by 3BN treatment in Arabidopsis, and (iii) to assess the enhanced disease tolerance of Arabidopsis conferred by 3BN treatment against necrotrophic pathogens.

MATERIALS AND METHODS

Plant Material and Growth Conditions

Arabidopsis thaliana wild-type Columbia (Col-0) and nitrate reductase (*nia1nia2*) mutant line were grown in soil in a growth chamber with 16 h light (100 μmol m^{-2} s^{-1})/8 h dark photoperiod at 22°C. The *nia1nia2* mutant line has been described previously (Wilkinson and Crawford, 1993) and the plants were watered with 2.5 mM ammonium nitrate.

Exposure to 3-Butenenitrile

3-butenenitrile (3BN, CAS 109-75-1) was purchased from Sigma-Aldrich (122793; 98%). 3BN was freshly diluted in 20 mL of commercial rapeseed oil to different concentrations (2.0, 2.5, 5.0, and 7.5 mM). Three weeks old *A. thaliana* plants were exposed to vapors of the different 3BN concentrations (20 mL in a 9-cm dish, with lid removed) for 24 h in a closed chamber (28.5 cm × 28.5 cm × 19.5 cm) (**Figure 1A**). The concentration of 3BN vapor emitted from a 2.5 mM 3BN solution into the chamber can be calculated to 1.578 nmol/cm^3. Plants of different genetic backgrounds were treated together in the same chamber. The setup for control (mock) treatment was identical with plants exposed only to 20 mL rapeseed oil. The effect of the 3BN treatment was compared between the wild-type and *nia1nia2* mutant line. Photographs were taken 2 days post-3BN treatment.

Analysis of Lesion Formation in 3BN Treated-Plants

Formation of lesion was visualized on rosette leaves 2 days post-3BN vapors treatment by trypan blue staining as described by Koch and Slusarenko (1990) with modifications. Detached leaves were subjected to 2.5 mg/mL of trypan blue and heated in boiling water bath for 1 min. The staining solution was then replaced with chloral hydrate solution (2.5 g/mL) and destained overnight.

Lesion formation was further validated by the electrolyte leakage method using a conductivity meter (Eutech CON 700, Singapore), essentially as described by Dionisio-Sese and Tobita (1998). This experiment was carried out 2 days post-3BN treatment. Electrolyte leakage was calculated using the following formula:

$$\text{Electrolyte leakage}(\%) = [\text{Conductivity (unboiled sample)}/\text{Conductivity (boiled sample)}] \times 100 \quad (1)$$

Microarray and Statistical Analysis

The rosette tissue of *A. thaliana* plants (Col-0 and *nia1nia2*) from the mock and 2.5 mM 3BN treatment were harvested after 24 h and immediately flash-frozen in liquid nitrogen and stored at −80°C until further processing. Total RNA was isolated from four biological replicates of each treatment and microarray analysis was performed using the Arabidopsis (V4) Gene Expression Microarray 4 × 44K (Agilent Technology, United States). The details of the procedures were described previously (Kissen et al., 2016).

For the statistical analysis of microarray data, data were preprocessed using the Limma package (version 3.2.3) as implemented in R (Smyth, 2005). Further data normalization and processing were following Kissen et al. (2016). Raw data have been deposited in Gene Expression Omnibus (accession GSE139089).

Gene Ontology Enrichment and Network Analysis

The identification of differentially expressed genes (DEGs) was set at a cut-off of $|\log_2\text{fold change}| \geq 1$ and adjusted $p < 0.01$. The identified DEGs from Col-0 and *nia1nia2* were analyzed for Gene Ontology (GO) enrichment analysis using PANTHER classification system[1] (Mi et al., 2019). Furthermore, the same set of DEGs was selected for network analysis by PATHWAY STUDIO software (Ariadne Genomics, Rockville, MD, United States) and for pathway mapping analysis by MAPMAN (Thimm et al., 2004).

Metabolite Extraction and Gas Chromatography-Mass Spectrometry (GC-MS) Analysis

Metabolites were extracted from shoot tissue of *A. thaliana* plants (Col-0 and *nia1nia2*) exposed to mock and 2.5 mM 3BN for 24 h (four biological replicates each) and derivatized with MSTFA [N-Methyl-N-(trimethylsilyl)trifluoroacetamide] (Sigma-Aldrich, 69479), followed by GC-MS as described previously (Alipanah et al., 2015). MetAlign software (PRI-Rikilt, Wageningen, The Netherlands) was used for the data integration, normalization, and alignment. Principal component analysis (PCA) was performed using SIMCA software (Umetrics, Sweden). The main goal was to identify metabolites that are produced at different levels (i) between mock and 3BN-treated conditions in each genotype or (ii) between Col-0 and *nia1nia2* plants under the same experimental conditions.

Phytohormone Analysis

SA, JA, and abscisic acid (ABA) were extracted and analyzed as described by Pan et al. (2010). The liquid chromatography system used for analysis was an ultra-performance liquid chromatography (UPLC) system (ACQUITY UPLC, Waters, Millford, MA, United States). The UPLC system was coupled to a Waters Xevo TQ-S triple quadrupole mass spectrometer (Waters,

[1] http://www.pantherdb.org/

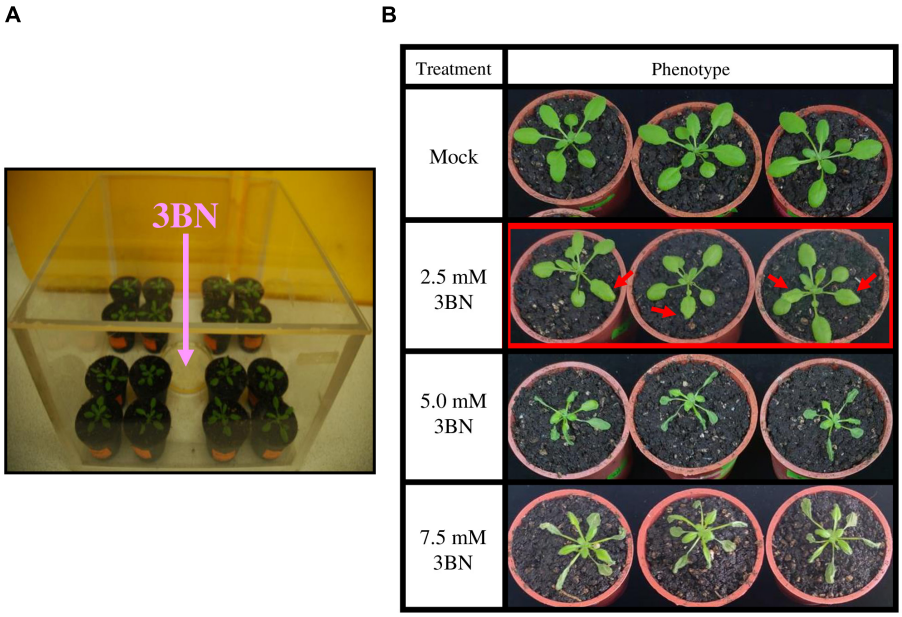

FIGURE 1 | 3BN treatment setup and response in Arabidopsis col-0 (wild-type). **(A)** Three weeks old Arabidopsis (wild-type) plants were separately treated with different concentrations of 3BN in closed containers for 24 h. **(B)** The lesion phenotype was observed for 2.5 mM 3BN treatment (red arrows) and severe necrosis was observed for 3BN concentrations ≥ 5.0 mM. Photographs were taken 2 days post-3BN treatment.

Milford, MA, United States). Chromatographic separations were performed on an ACQUITY UPLC HSS T3 Column (2.1 × 100 mm, 1.8 μm, Waters, Millford, MA, United States). 13C6- salicylic acid (13C6-SA), d5-jasmonic acid (D5-JA) and d6- abscisic acid (D6-ABA) were used as internal standards. Characteristic mass spectrometry transitions were monitored using negative multiple reaction monitoring (MRM) mode for SA (m/z, 137 > 93), 13C6-SA (m/z, 143 > 99), JA (m/z, 209 > 59), D5-JA (m/z, 214 > 62), ABA (m/z, 263 > 153), and D6-ABA (m/z, 269 > 159). Data acquisition and processing were performed using MassLynx version 4.1 and TargetLynx software (Waters Corp.).

Plant Pathogen Inoculation and Disease Response Assay

Prior to infection assay, 3BN-treated plants were placed in ventilated fume hood for 30 min to get rid of the 3BN vapor. The infection assay with *Pectobacterium carotovorum* ssp. *carotovorum* (Pcc) was done as described previously (Hsiao et al., 2017) with some modifications. Four rosette leaves from each 3 weeks old plant from the 24 h mock or 2.0 mM 3BN treatment were punctured with a 10 μL tip and inoculated with 10 μL liquid culture of 1×10^6cfu ml^{-1} of Pcc or water (control). The disease symptoms and lesion sizes on leaves were recorded at 16 h post-infection (hpi) and analyzed with Image J. *In planta* bacterial growth assays were performed by counting the bacterial colony-forming unit (CFU) after tissue homogenization and proper dilutions as described by Ishiga et al. (2017).

Botrytis cinerea (Bc) infection assay was performed as described previously (Huang et al., 2014) with modifications. Droplets of 10 μL of Bc spore suspension (10^6 spores ml^{-1}) were deposited on each side of the leaf midvein on four rosette leaves from each 3 weeks old plant after the 24 h mock or 2.0 mM 3BN treatment. The infected plants were kept at 100% relative humidity throughout the assay. The disease symptoms and lesion sizes on leaves were recorded at 48 hpi and analyzed with Image J. *In planta* fungal growth assays were performed by analyzing the relative transcript level of *B. cinerea Actin* (*BcActin*) and Arabidopsis *Actin* (*AtActin*) by qRT-PCR. The primers used for qRT-PCR are as described by Nie et al. (2017).

RESULTS

Arabidopsis Response to 3BN Treatment

The wild-type plants exhibited a dose-dependent necrosis compared to the mock condition (**Figure 1B**). Lesions began to appear on rosette leaves upon 2.5 mM 3BN treatment, while more severe necrosis was observed at higher concentrations of 3BN treatments, i.e., ≥ 5.0 mM.

On the contrary, leaves of the NO-deficient mutant *nia1nia2* did not show any sign of lesions upon the 2.5 mM 3BN treatment (**Figure 2A**). Consistently, trypan blue staining showed dark-blue staining in the wild-type leaves under the 2.5 mM 3BN treatment but this was not observed in the *nia1nia2* leaves (**Figure 2B**). The dark-blue staining on the wild-type leaves indicated that 3BN had caused lesion formation.

This finding was further validated by electrolyte leakage analysis (**Figure 3**). Notably, 2.5 mM 3BN treatment resulted in significant electrolyte leakage in the wild-type plants compared to mock condition but this was not observed in the *nia1nia2*

mutant plants. Significant electrolyte leakage only began to happen in the *nia1nia2* mutant plants upon exposure to 5.0 mM 3BN treatment.

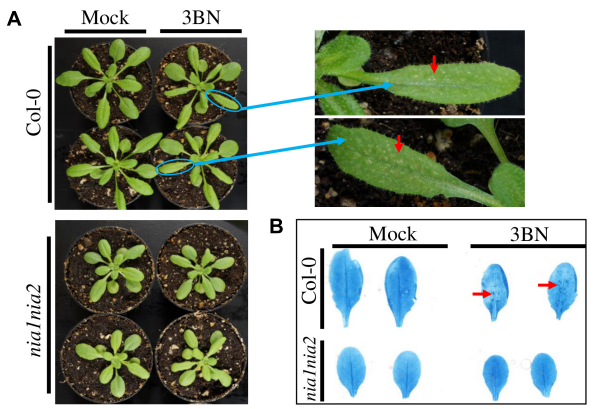

FIGURE 2 | Comparison of physiological and biochemical effects of 2.5 mM 3BN treatment between Arabidopsis Col-0 wild-type and *nia1nia2* mutant. **(A)** Signs of lesion formation (red arrows) were spotted on the wild-type leaves upon 3BN treatment. Photographs were taken 2 days post-3BN treatment. **(B)** Trypan blue staining revealed the presence of dark-blue stained spots, indicating lesion formation in Col-0 wild-type but not *nia1nia2* leaves upon 3BN treatment. Lesion was visualized on rosette leaves 2 days post-3BN vapors treatment.

Transcriptomic Responses in Arabidopsis Col-0 and *nia1nia2* Upon 2.5 mM 3BN Treatment

A total of 3939 DEGs was identified in Col-0 plants in response to 2.5 mM 3BN treatment of which 2173 genes were upregulated and 1766 genes were downregulated (**Figure 4A** and **Supplementary Table S1**). Relatively few DEGs, 2262, were identified in *nia1nia2* plants in response to 2.5 mM 3BN treatment of which 1509 genes were upregulated and 753 genes were downregulated (**Figure 4A** and **Supplementary Table S1**). A total of 1262 genes were upregulated in both Col-0 and *nia1nia2* plants, while 624 genes were downregulated in both the wild-type and mutant plants (**Figure 4A**). In other words, 911 and 247 genes were uniquely upregulated in Col-0 and *nia1nia2* plants, respectively. For downregulated genes, 1142 and 129 genes were unique to the wild-type and mutant plants, respectively (**Figure 4A**).

GO enrichment analysis of DEGs showed that monosaccharide metabolic process and fatty acid beta-oxidation were enriched by the upregulated genes in the Col-0 plants in response to the 3BN treatment while the enrichment was not detected in the *nia1nia2* plants (**Figure 4B**). On the other hands, carbohydrate metabolic process and sulfur compound metabolic process were enriched by the upregulated genes in the *nia1nia2* plants in response to the 3BN treatment (**Figure 4B**).

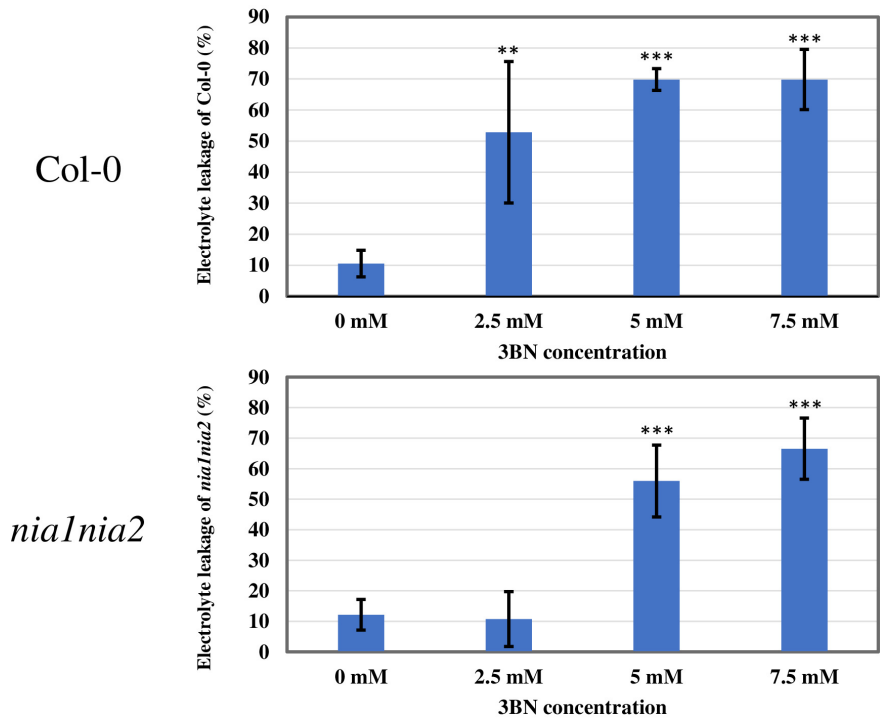

FIGURE 3 | Electrolyte leakage analysis of Arabidopsis Col-0 wild-type and *nia1nia2* mutant when subjected to different concentrations of 3BN treatments. This analysis was carried out 2 days post-3BN treatment. 2.5 mM 3BN treatment caused significant electrolyte leakage in wild-type but not in *nia1nia2* mutant. Values for electrolyte leakage are the average (error bars indicate SD) of six plants. Stars indicate a statistically significant difference (One-way ANOVA, $^{**}P < 0.01$, $^{***}P < 0.001$) to the control treatment.

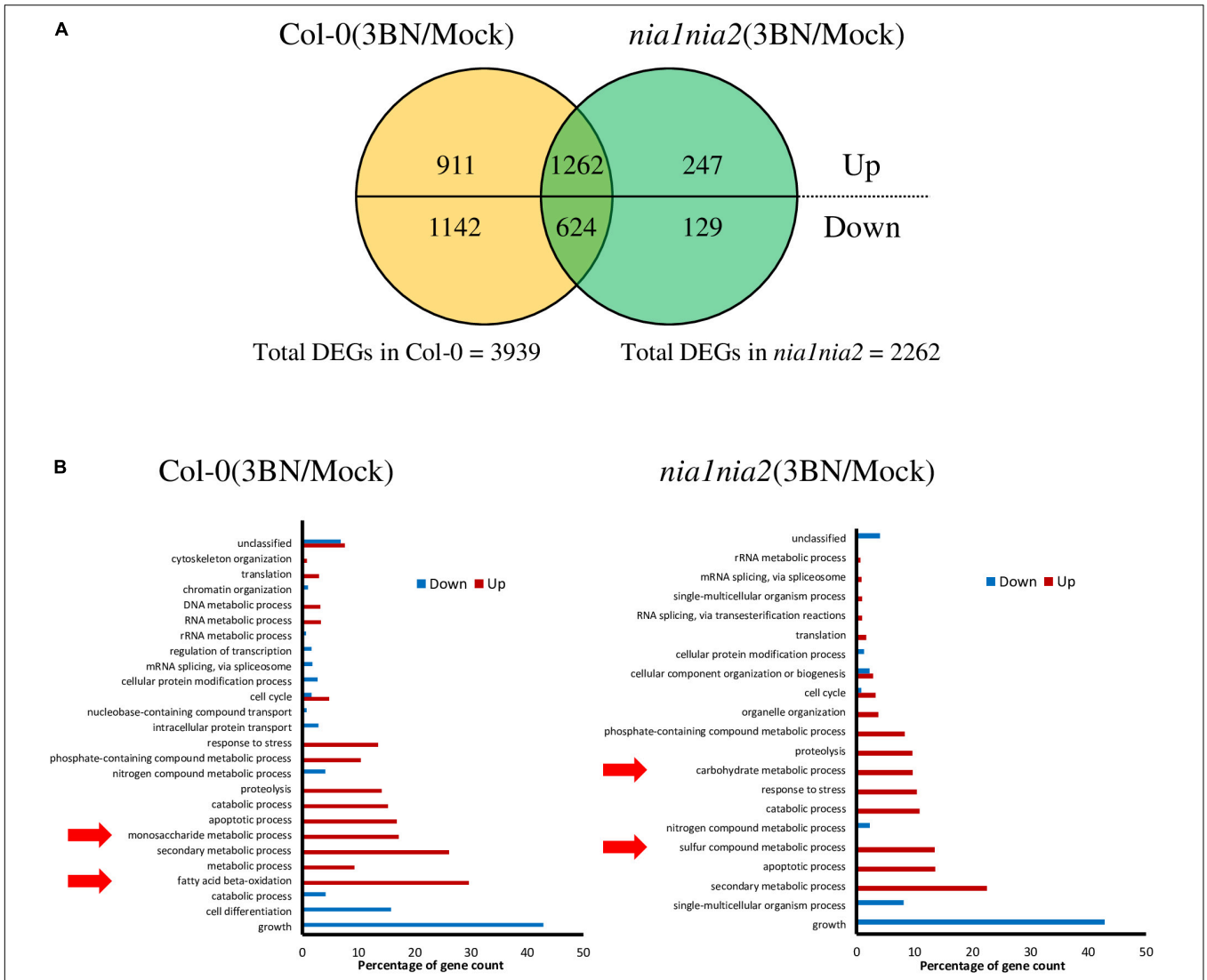

FIGURE 4 | An overview of microarray analysis results for Arabidopsis Col-0 wild-type and *nia1nia2* mutant upon 2.5 mM 3BN treatment for 24 h. **(A)** The comparison of the number of differentially expressed genes (DEGs) under the 3BN treatment between Col-0 and *nia1nia2*. **(B)** GO enrichment analysis of DEGs in Arabidopsis Col-0 wild-type and *nia1nia2* mutant upon 2.5 mM 3BN treatment. Enrichment of monosaccharide metabolic process and fatty acid beta-oxidation was uniquely found in the upregulated genes of the wild-type plants, while enrichment of carbohydrate metabolic process and sulfur compound metabolic process was uniquely found in the upregulated genes of the mutant plants.

The network enrichment analysis of Pathway Studio showed that a group of 159 genes was enriched in the plant defense term (*p*-value: 2.08838 E-4) in Col-0 plants (**Supplementary Table S2**). Among them, a total of 134 (84.3%) defense-related and phytohormone-associated genes were upregulated in the Col-0 plants upon 3BN treatment (**Supplementary Table S2**). Notably, the expression of SA-biosynthetic genes, *ICS1* (isochorismate synthase 1; At1g74710), *PAD4* (phytoalexin deficient 4; At3g52430), and *EDS1* (enhanced disease susceptibility 1 protein; At3g48090); and that of SA signaling genes, *NPR3*, *NPR4* (non-expressor of pathogenesis-related proteins 3, 4; At5g45110, At4g19660), *TGA3* (TGACG-binding transcription factor 3; At1g22070), *WRKY70* (WRKY DNA-binding protein 70; At3g56400), and *PR5* (pathogenesis-related gene 5; At1g75040), were induced by the 3BN treatment (**Supplementary Table S2**). In addition, the expression of JA-biosynthetic genes, *LOX1* and *LOX5* (lipoxygenase 1, 5; At1g55020, At3g22400) were also induced by the 3BN treatment (**Supplementary Table S2**).

Metabolite Profiling of Arabidopsis Col-0 and *nia1nia2* Upon 2.5 mM 3BN Treatment

As GO enrichment of the DEGs revealed an enrichment of primary metabolic process (**Figure 4B**), metabolite profiling was carried out (**Figure 5**). PCA plot of samples shows that the four biological replicates of the four samples (i.e.,

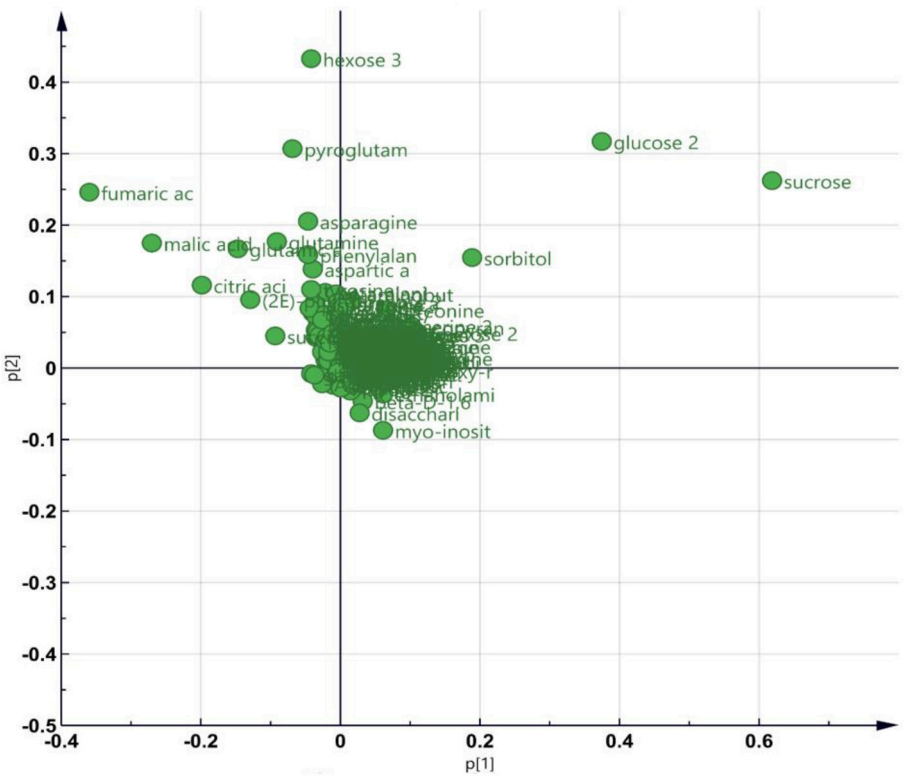

FIGURE 5 | An overview of metabolite profiling data for Arabidopsis Col-0 wild-type and *nia1nia2* mutant upon 2.5 mM 3BN treatment for 24 h. PCA plot depicting the metabolites with variable contents between any combination of paired samples.

Col-0_mock, Col-0_3BN, *nia1nia2*_mock, *nia1nia2*_3BN) were clustered according to their own groupings, indicating that the samples were of good quality for metabolite profiling (**Supplementary Figure S1** and **Supplementary Table S3**). The PCA plot of metabolites depicts that the four samples can be differentiated mainly based on the content of various types of sugars, carboxylic acids and amino acids (**Figure 5**).

The content of the metabolites in all four samples showed three important trends. Firstly, soluble sugars, such as sucrose, glucose and fructose, as well as sorbitol (sugar alcohol) were produced at lower levels in the Col-0 leaves than in the *nia1nia2* leaves under mock condition (**Figure 6**). The 3BN treatment generally increased the production of these soluble sugars and sorbitol in wild-type and mutant plants. Particularly, sucrose content was increased by the 3BN treatment in the *nia1nia2* leaves, while glucose and sorbitol were increased by the same treatment in the Col-0 leaves (**Figure 6**). Next, four carboxylic acids that are intermediate compounds in the Krebs cycle, namely fumaric acid, malic acid, citric acid and succinic acid were produced at higher levels in the Col-0 leaves than in the *nia1nia2* leaves under mock condition (**Figure 7**). The 3BN treatment generally increased the production of these carboxylic acids in Col-0 plants with significant difference for malic acid and citric acid (**Figure 7**). The third observation was that the 3BN treatment increased the production of six amino acids in Col-0 to a greater extent than in *nia1nia2* plants (**Figure 8**).

Changes of Phytohormone Production in Arabidopsis Col-0 and *nia1nia2* Upon 2.0 and 2.5 mM 3BN Treatments

Based on the microarray data, the expression of genes associated with phytohormone biosynthesis and signaling were upregulated in Arabidopsis Col-0 wild-type in response to 2.5 mM 3BN treatment (**Supplementary Table S2**). This finding suggests the involvement of phytohormone signaling in the 3BN-induced innate immune responses. Meanwhile, electrolyte leakage analysis was repeated with the inclusion of 2.0 mM 3BN treatment in the second trial (**Supplementary Figure S2**). Both trials showed consistent results where 2.5 mM 3BN treatment only caused significant electrolyte leakage in the Col-0 plants compared to mock condition but not in the *nia1nia2* mutant plants (**Figure 3** and **Supplementary Figure S2**). Interestingly, 2.0 mM 3BN treatment did not cause electrolyte leakage in both the wild-type and mutant plants (**Supplementary Figure S2**). Therefore, phytohormone production was measured for Col-0 and *nia1nia2* plants treated with 2.0 and 2.5 mM 3BN treatments in comparison with mock condition (**Figure 9**).

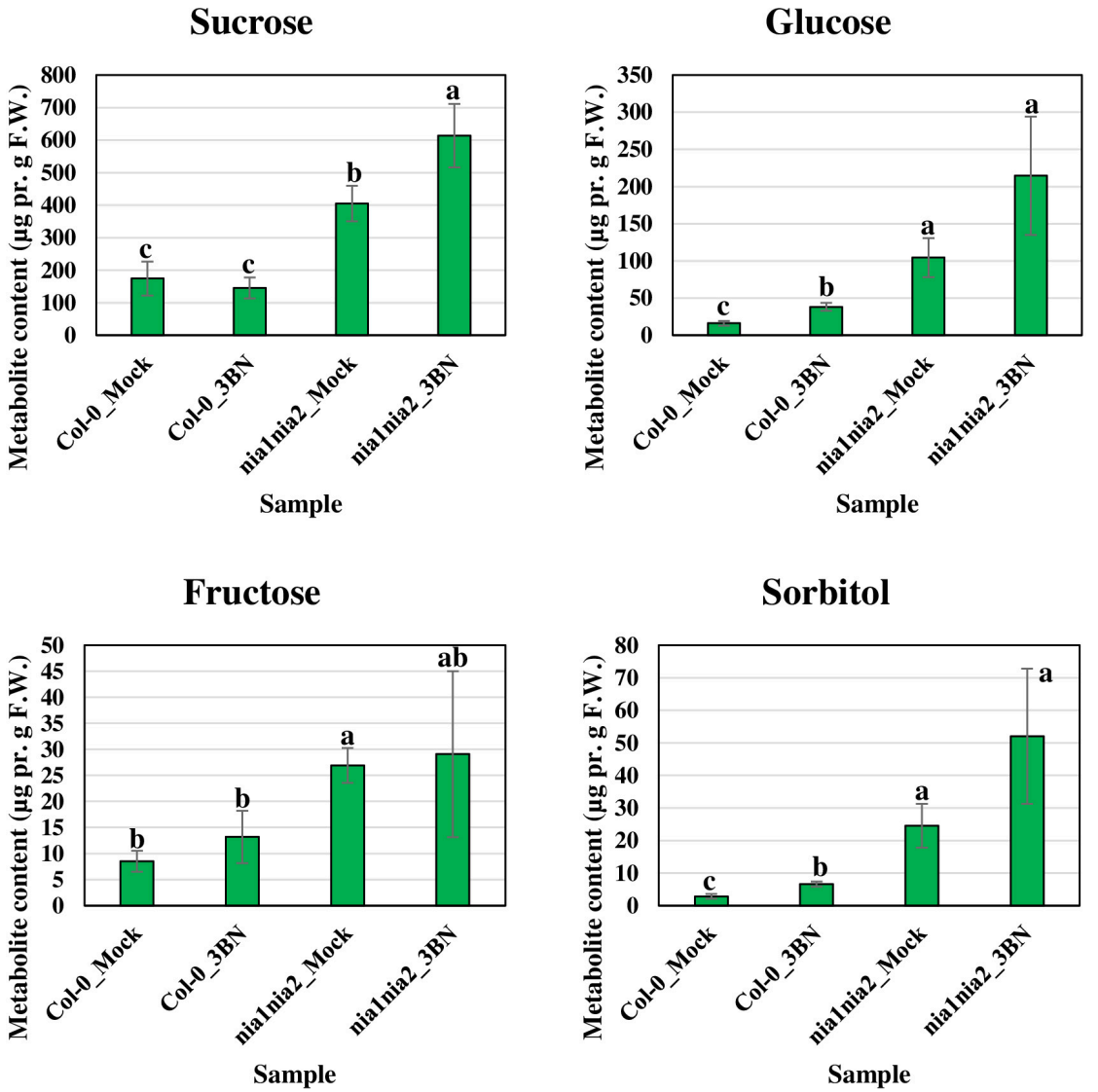

FIGURE 6 | Metabolite profiling of soluble sugars (including sorbitol, a sugar alcohol) for Arabidopsis Col-0 wild-type and *nia1nia2* mutant upon 2.5 mM 3BN treatment for 24 h. For sucrose, One-way ANOVA and Tukey *post hoc* test were used with different letters denoting a significant difference ($P < 0.05$). For glucose, fructose and sorbitol, where the homogeneity of variance assumption could not be fulfilled, Welch one-way test and pairwise *t*-test were used with different letters denoting a significant difference ($P < 0.05$).

Ultra-performance liquid chromatography (UPLC) analysis demonstrated that at 2.0 mM 3BN treatment, Arabidopsis Col-0 wild-type had an increase in the production of SA (2.2-fold) and JA (4.1-fold) while 2.5 mM 3BN treatment led to an increased production of SA (2.7-fold), JA (4.4-fold), and ABA (2.4-fold) in comparison with the mock condition (**Figure 9**). On the other hand, for *nia1nia2* mutant, the 2.0 mM 3BN treatment induced the production of SA (2.2-fold) and JA (20.3-fold) in consonance with the 2.5 mM 3BN treatment that increased the production of SA (3.2-fold) and JA (15.4-fold) (**Figure 9**). Although 3BN treatments increased the production of SA in both Arabidopsis Col-0 and *nia1nia2* plants, SA concentration in Col-0 was higher than in *nia1nia2* plants under mock, 2.0 and 2.5 mM 3BN treatment conditions (**Figure 9A**). Nevertheless, significant difference of SA concentration between Col-0 and *nia1nia2* plants was detected only under 2.5 mM 3BN treatment condition (*t*-test, $^{**}P < 0.01$, $n = 3$ per sample). On the other hand, although 3BN treatments increased the production of JA in both Arabidopsis Col-0 and *nia1nia2* plants, JA in *nia1nia2* was induced more by 3BN treatments than in Col-0 (**Figure 9B**). However, the difference of JA concentration between Col-0_2.0 mM 3BN and *nia1nia2*_2.0 mM 3BN and between Col-0_2.5 mM 3BN and *nia1nia2*_2.5 mM 3BN was not statistically significant, presumably due to large within-group variation.

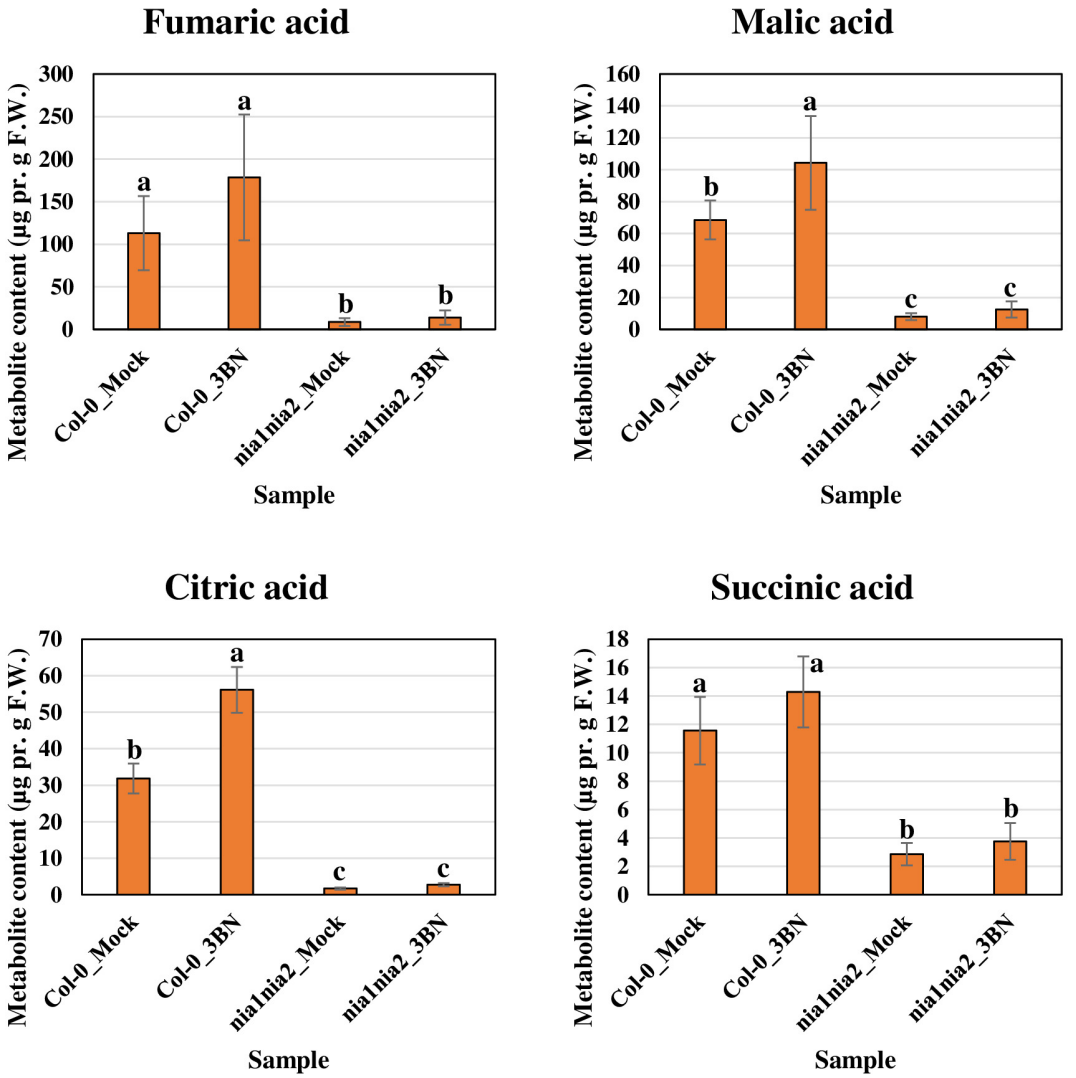

FIGURE 7 | Metabolite profiling of Krebs cycle-associated carboxylic acids for Arabidopsis Col-0 wild-type and *nia1nia2* mutant upon 2.5 mM 3BN treatment for 24 h. One-way ANOVA and Tukey *post hoc* test with different letters denoting a significant difference ($P < 0.05$).

Exposure to 2.0 mM 3BN Enhanced Arabidopsis Tolerance to Necrotrophic Pathogens

To examine whether 3BN-induced innate immune responses can enhance the disease tolerance of Arabidopsis, 2.0 mM 3BN treatment was selected mainly for three reasons, (i) 2.0 mM 3BN treatment did not cause electrolyte leakage on the leaves of Arabidopsis (**Supplementary Figure S2**), (ii) yellow chlorosis and lesion began to appear on the Col-0 leaves upon 2.5 mM 3BN treatment (**Figures 1–3**), and (iii) the production of phytohormones such as SA and JA began to be induced in Col-0 leaves upon 2.0 mM 3BN treatment (**Figure 9**). Three weeks old Arabidopsis Col-0 plants were first exposed to the mock and 2.0 mM 3BN treatments and then subjected to infection assays of *Pectobacterium carotovorum* ssp. *carotovorum* or *Botrytis cinerea*. Interestingly, compared with mock condition, exogenous application of 2.0 mM 3BN was effective in reducing the lesion size and pathogen growth on the leaves of Arabidopsis Col-0 in both of the bacterial (**Figure 10**) and fungal (**Figure 11**) infection assays.

DISCUSSION

The Involvement of NO in Lesion Formation of Arabidopsis Upon 3BN Recognition

One of the earlier responses of PTI and ETI in plants involves the rapid accumulation of oxygen-derived free radicals such as ROS and NO (Torres et al., 2006). It has been well known that ROS and NO are important signal molecules in plant defense against pathogens, implicated in (i) cross-linking of cell wall proteins,

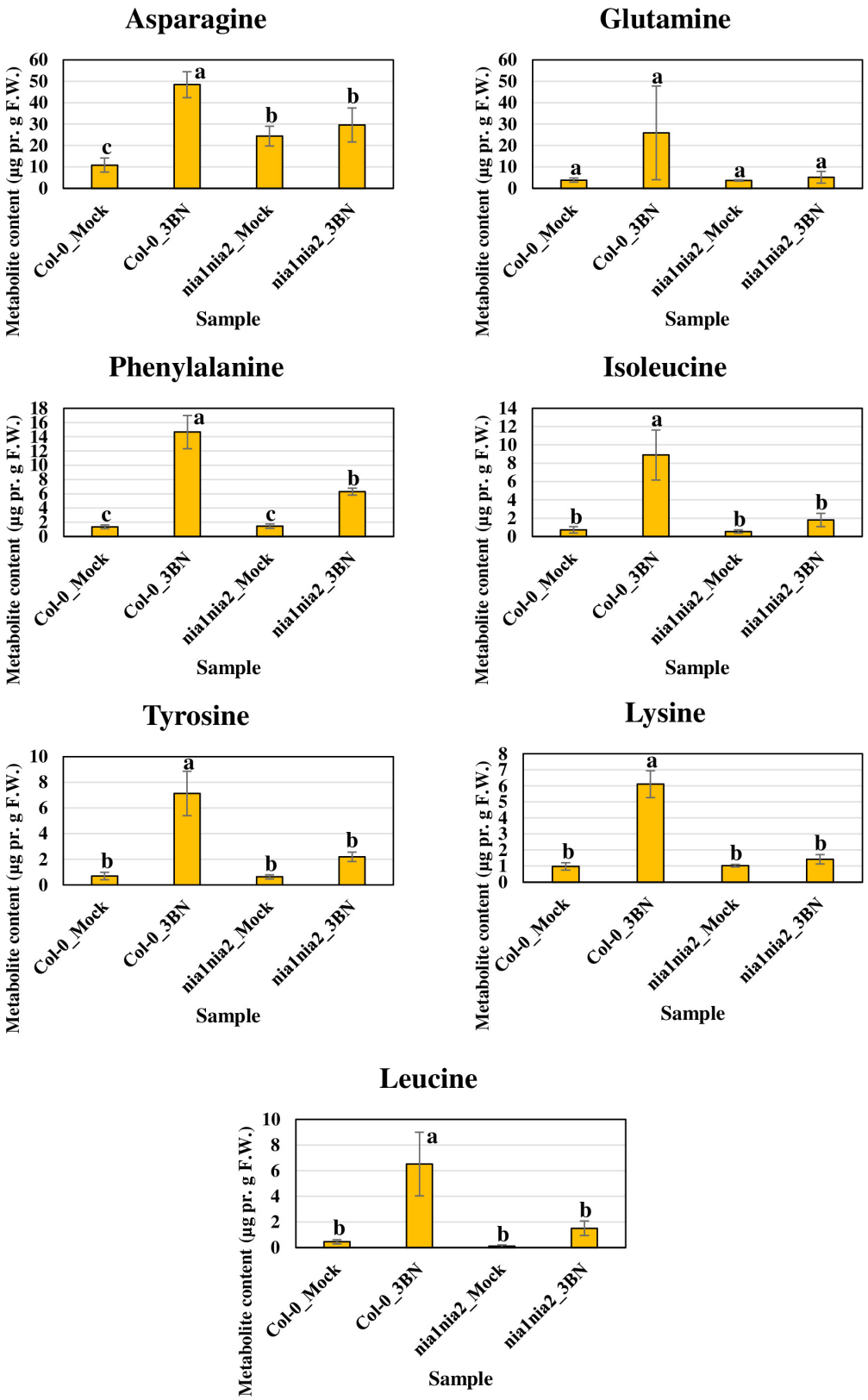

FIGURE 8 | Metabolite profiling of amino acids for Arabidopsis Col-0 wild-type and *nia1nia2* mutant upon 2.5 mM 3BN treatment for 24 h. One-way ANOVA and Tukey *post hoc* test with different letters denoting a significant difference ($P < 0.05$).

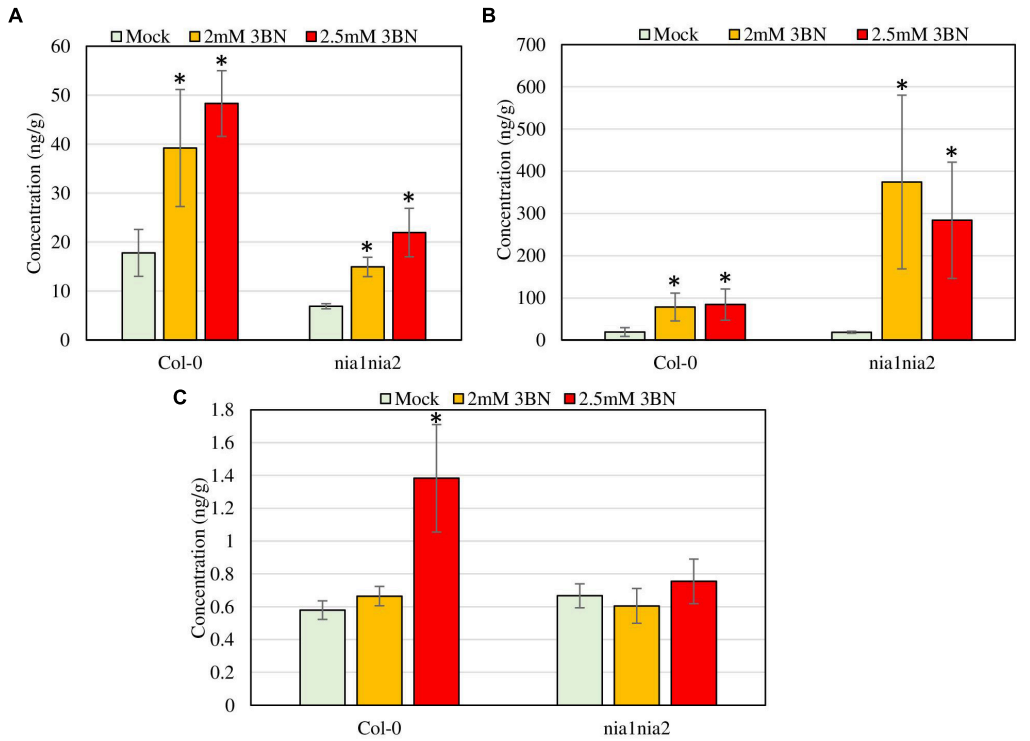

FIGURE 9 | Phytohormone profiling of Arabidopsis Col-0 wild-type and *nia1nia2* mutant upon 2.0 and 2.5 mM 3BN treatments for 24 h. **(A)** SA, **(B)** JA, and **(C)** ABA (*t*-test, $^*P < 0.05$, $n = 3$ per sample).

(ii) alteration of membrane permeability and ion fluxes, (iii) hypersensitive response, (iv) systemic acquired resistance, and (v) the production of phytoalexins (Wojtaszek, 1997; Romero-Puertas et al., 2004). The GHPs of interest in this study, 3BN, may play a role in the oxidative burst phenomenon.

In this study, 2.5 mM 3BN treatment caused lesion formation on the leaves of 3 weeks old Arabidopsis Col-0 wild-type while the same treatment did not cause any symptom on the leaves of NO-deficient *nia1nia2* mutant plants (**Figures 2**, **3**). To interpret this result, it is important to understand the various NO production mechanisms in plants. Generally, NO can be produced via enzymatic and non-enzymatic pathways (Gupta et al., 2011). Nitrate reductase and NO synthase-like (NOS-like) activities are the main sources of NO production in plants under normal physiological conditions (Mur et al., 2013). The nitrate reductase-defective double mutant, *nia1nia2*, accumulates a lower endogenous NO level than the Col-0 wild-type (Zhao et al., 2009, 2016). Therefore, it can be deduced that the relatively low endogenous NO level in *nia1nia2* plants was not sufficient to cause lesion formation upon exposure to the 2.5 mM 3BN treatment. This result demonstrates that NO plays a fundamental role in triggering lesion formation upon 3BN recognition.

NO was initially reported in mammals as a key redox-active signal molecule responsible for inflammatory and innate immune responses (Schmidt and Walter, 1994; Stamler, 1994). Since then, a growing body of evidence showed that NO is also playing a pivotal role in plant defense signaling as the NOS-like activity (NOS is a NO biosynthetic enzyme in metazoans) and the secondary messenger molecules in NO-mediated signaling pathways of mammalian cells, such as cyclic guanosine monophosphate (cGMP) and cyclic adenine dinucleotide phosphate ribose (cADPR), are also present in plants (Klessig et al., 2000; Neill et al., 2003; Astier et al., 2018). During pathogen attack, NO is known to regulate hypersensitive response in plants via S-nitrosylation of thiol-containing proteins (post-translational protein modification). For example, NO-mediated S-nitrosylation inhibited the activity of aconitase enzyme in the Krebs cycle (Gardner et al., 1997). The inhibition action resulted in an increased level of cellular iron which together in the presence of NO might contribute to cell death (Navarre et al., 2000). The targets of NO-mediated S-nitrosylation also include antioxidative enzymes such as peroxiredoxin II E (Romero-Puertas et al., 2007), catalase (Lin et al., 2012), and ascorbate peroxidase (de Pinto et al., 2013). Inhibition of these enzymes leads to increased ROS levels presumably responsible for plant cell death. In agreement, the expression of genes encoding two NADPH oxidases, also known as respiratory burst oxidase homologs (RBOHs), i.e., RBOH C (At5g51060), and RBOH F (At1g64060), which produce ROS, was induced by the 2.5 mM 3BN treatment in both Col-0 and *nia1nia2* plants (**Supplementary Table S1**). Conversely, the accumulation of NO during pathogen attacks was reported to be involved in a negative feedback loop by negatively regulating ROS production, via S-nitrosylation of NADPH oxidase, in order to prevent excessive cell death (Yun et al., 2011).

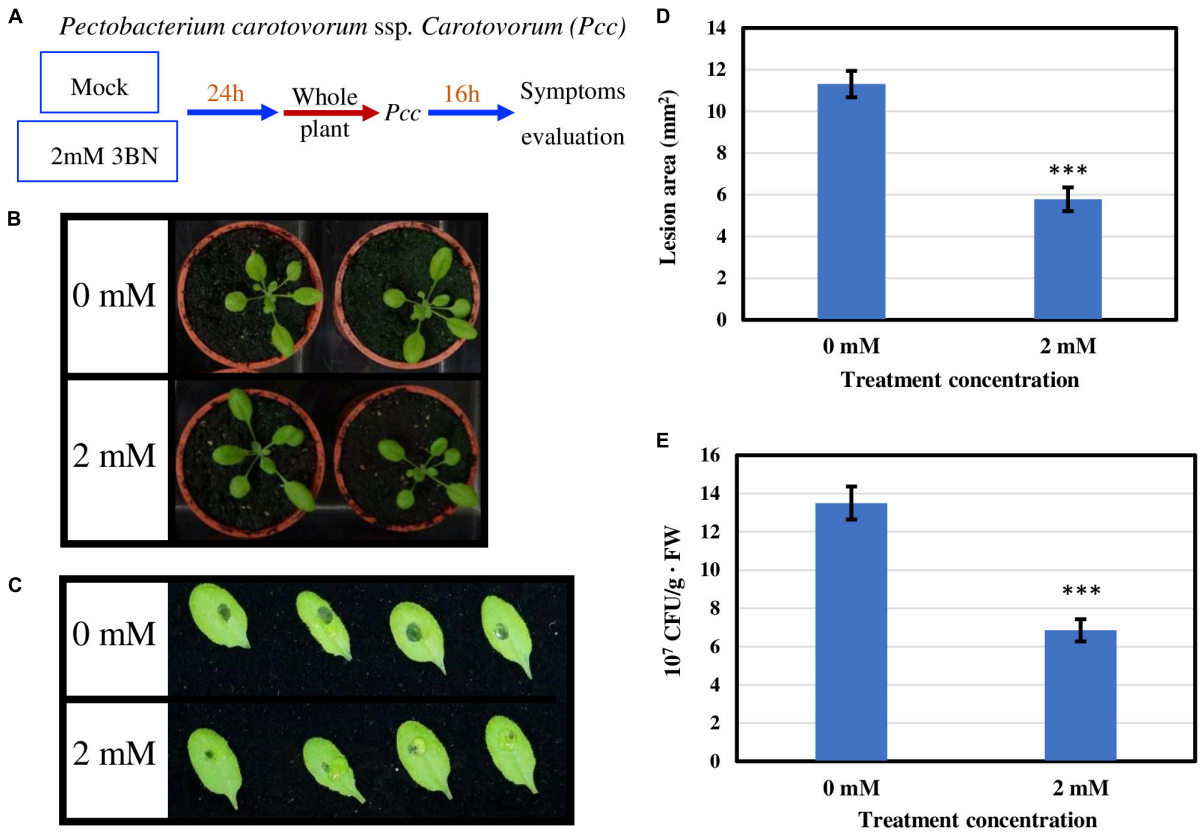

FIGURE 10 | Pathogen assays of Arabidopsis Col-0 with the necrotrophic bacterium *Pectobacterium carotovorum* ssp. *Carotovorum* (Pcc). **(A)** Arabidopsis Col-0 was challenged with the bacterium after having been exposed to a mock or 2.0 mM 3BN treatment for 24 h. **(B)** Representative pictures of plants exposed to a mock or 2.0 mM 3BN treatment for 24 h before pathogen inoculation. **(C)** Representative pictures of rosette leaves showing lesions post 16 h of inoculation with Pcc. **(D)** The lesion area at 16 h post-infection (*t*-test, $^{***}P < 0.001$, $n = 32$ leaves per treatment, with four batch data). **(E)** The bacterial population estimated by CFU at 16 h post-infection (*t*-test, $^{***}P < 0.001$, $n = 32$ leaves per treatment, with three batch data).

On the other hand, the electrolyte leakage analysis revealed lesion formation in the *nia1nia2* mutant at a 3BN treatment of ≥5.0 mM (**Figure 3**). As the NO-deficient phenotype of *nia1nia2* plants is accounted for by the mutation of nitrate reductase 1 and 2 (Zhao et al., 2016), the observed lesion formation of *nia1nia2* when exposed to higher 3BN concentrations could be due to ROS accumulation and/or the eventual build-up of NO catalyzed by other NO biosynthetic enzymes such as NOS-like activity in the mutant plants. It has been reported that NO can cooperate with H_2O_2 in triggering hypersensitive response cell death during incompatible plant-pathogen interactions (Yoshioka et al., 2011). Whether NO allies with ROS to activate the programmed cell death of Arabidopsis upon 3BN treatment still remains to be elucidated.

The Production of Soluble Sugars, Krebs Cycle-Associated Carboxylic Acids, and Amino Acids Is Induced in Arabidopsis by 2.5 mM 3BN Treatment

To optimize fitness under the changing environmental conditions, plants utilize a plethora of signal molecules and the associated-signaling pathways to plastically adjust their metabolism so that priority is given for development under favorable condition while defense responses are activated under unfavorable conditions (Malinovsky et al., 2017). Simple sugars and amino acids are primary metabolites that are indispensable for normal growth, development and reproduction of plants. By the same token, both of these primary metabolites have also been linked to plant stress responses. For instance, sugars were reported to interact with ROS signaling pathways where elevated levels of sugars can either stimulate or repress ROS production (Couée et al., 2006). The amino acid phenylalanine is the first precursor in phenylpropanoid pathway which gives rise to the formation of many important defense-related secondary metabolites (Fraser and Chapple, 2011).

Our metabolite profiling showed that the production of monosaccharide (glucose) and its derivative (sorbitol) in Arabidopsis Col-0 plants was increased by the 2.5 mM 3BN treatment, while the production of disaccharide (sucrose) in *nia1nia2* plants was increased by the same treatment (**Figure 6**). This observation indicates that sugar metabolism is differentially regulated between the Col-0 and *nia1nia2* plants under the 3BN treatment. By mapping the DEGs from Col-0 and *nia1nia2*

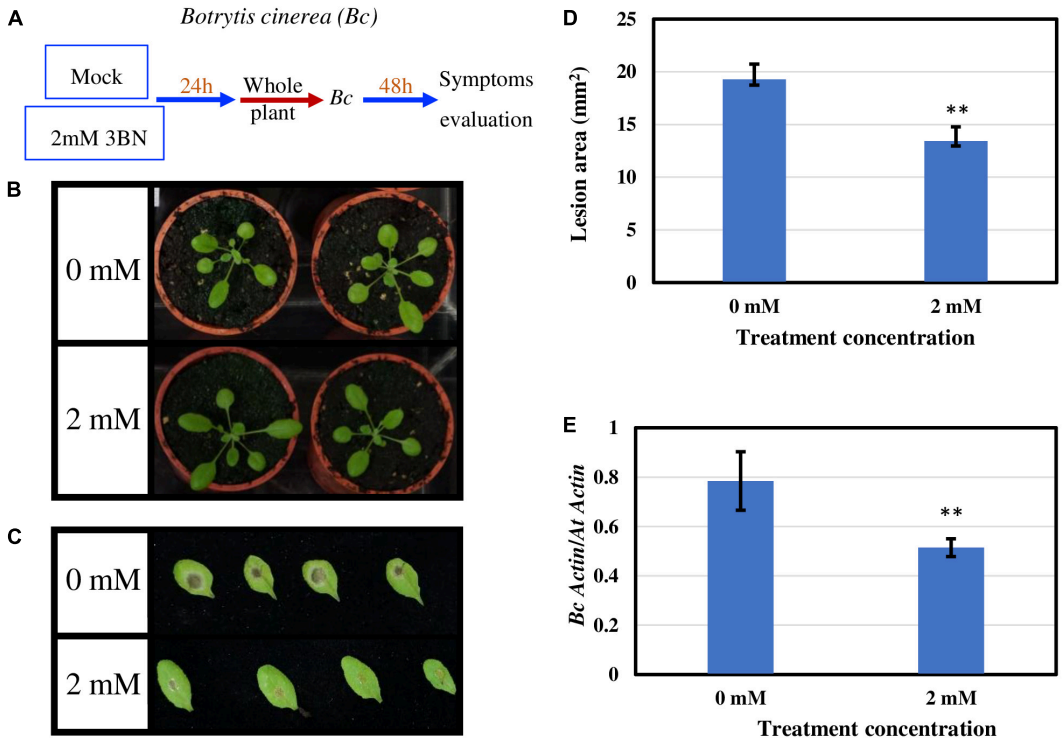

FIGURE 11 | Pathogen assays of Arabidopsis Col-0 with the necrotrophic fungus *Botrytis cinerea* (Bc). **(A)** Arabidopsis Col-0 was challenged with the fungus after having been exposed to a mock or 2.0 mM 3BN treatment for 24 h. **(B)** Representative pictures of plants exposed to a mock or 2.0 mM 3BN treatment for 24 h before pathogen inoculation. **(C)** Representative pictures of rosette leaves showing lesions post 48 h of inoculation with Bc. **(D)** The lesion area at 48 h post-infection (*t*-test, $^{**}P < 0.01$, $n = 48$ leaves per treatment). **(E)** Quantification of Bc growth at 48 h post-infection estimated by relative transcript levels of *BcActin* and *AtActin* using qRT-PCR (*t*-test, $^{**}P < 0.01$, $n = 5$ plants per treatment).

plants to the metabolic pathways in MAPMAN, we noticed that a higher number of genes associated with (i) starch and sucrose metabolism and (ii) glycolysis was up-regulated by 3BN treatment in the Col-0 in comparison with the *nia1nia2* plants (**Supplementary Figure S3** and **Supplementary Table S4**). Based on this finding, it can be inferred that sucrose degradation and glycolysis were concomitantly activated by the 2.5 mM 3BN treatment in the Col-0 plants. This could justify the metabolite results where 2.5 mM 3BN treatment did not increase the sucrose level but increased the levels of glucose and sorbitol in the Col-0 plants (**Figure 6**). Conversely, as sucrose degradation and glycolysis were not activated in the *nia1nia2* plants by the same 3BN treatment, an increase in the sucrose level was observed instead for the levels of monosaccharides and sorbitol (**Figure 6**). A previous study of comparative metabolomic analysis reported an increased endogenous content of soluble sugars upon melatonin treatment and *Pseudomonas syringae pv. tomato* (*Pst*) DC3000 infection in Arabidopsis Col-0 (Qian et al., 2015). The study also demonstrated that exogenous pre-treatment of soluble sugars could reduce the bacterial spread in Arabidopsis Col-0 but not in SA- and NO-deficient mutants (Qian et al., 2015).

The production of Krebs cycle-associated carboxylic acids, namely malic and citric acids was induced by the 3BN treatment only in the Arabidopsis Col-0 plants (**Figure 7**). Interestingly, apart from the observed induction of sucrose degradation and glycolysis, genes related to the carboxylic acid-producing processes in the Krebs cycle were also up-regulated by the 2.5 mM 3BN treatment in the Col-0 plants (**Supplementary Figure S3** and **Supplementary Table S4**). Meanwhile, no induction of Krebs cycle-associated genes was observed in the *nia1nia2* plants treated with 2.5 mM 3BN (**Supplementary Figure S3**). As mounting defense response is an energy-consuming process, it is not surprising that the Krebs cycle, the cellular energy production pipeline, is involved. Furthermore, the cycle also functions in producing the precursors of certain amino acids. In line with this notion, six amino acids, including asparagine, phenylalanine, isoleucine, tyrosine, lysine and leucine exhibited increased production in Arabidopsis Col-0 under 3BN treatment (**Figure 8**). This increased supply of amino acids could be channeled for the production of defensive proteins or defense-related secondary metabolites (Coruzzi and Last, 2000). It is noteworthy that the increased production of amino acids seen in Arabidopsis Col-0 plants upon 3BN treatment was compromised incompletely in *nia1nia2* plants (**Figure 8**). This finding can be partly attributed to the two mutated nitrate reductases in *nia1nia2* plants that negatively affect the nitrate reduction/assimilation, which is critical for the production of amino acids (Zhao et al., 2016).

Interestingly, a recent study reported that an acute dose of exogenous NO gas caused momentary metabolic changes in Arabidopsis at 6 h after treatment. The metabolic changes included elevated content of sugars, Krebs cycle carboxylic acids and amino acids along with accumulation of polyamines, fatty acids, phospholipids and nucleic acids (León et al., 2016). The transient effect with a metabolic change at 6 h, but not 24 h as reported in our study, might be due to the fact that NO was treated directly in the study while it may take some time for 3BN to act and generate NO in our study. Nevertheless, based on León et al. (2016), the 3BN-induced NO production is very likely to result in the observed concomitant activation of sucrose degradation, glycolysis and Krebs cycle in the Col-0 plants (**Supplementary Figure S3**). Besides that, the reported effects of NO on metabolic changes can also be depicted in our metabolite profiling results under mock condition. For example, the higher endogenous NO level in Col-0 plants compared with *nia1nia2* plants could account for the lower levels of soluble sugars but higher carboxylic acid levels in Col-0 plants compared with *nia1nia2* plants under the mock condition (**Figures 6**, **7**). This finding suggests that, to a certain degree, the concomitant activation of sucrose degradation, glycolysis and Krebs cycle has happened in the Col-0 plants under the mock condition. Given the co-induction of these processes under the mock condition, the amino acid levels in the Col-0 plants were still comparable with those measured in the *nia1nia2* plants (**Figure 8**). A possible explanation is that the efficiency of conserving metabolic resources, such as carbon, nitrogen and energy, is lower if Arabidopsis Col-0 plants accumulate higher amount of amino acids under the mock condition. Conserving metabolic resources for amino acid synthesis is critical because amino acids are the building blocks for various important molecules, including proteins, vitamins, nucleotides and secondary metabolites (Arnold et al., 2015). Thus, increased amino acid biosynthesis, presumably mediated by NO, was only detected when Col-0 plants were treated with 2.5 mM 3BN treatment (**Figure 8**).

The Production of SA and JA Is Induced in Arabidopsis by 2.0 mM 3BN Treatment in the Absence of Lesion Formation

Phytohormones are small endogenous, low-molecular-weight regulators of diverse growth, development and physiological processes (Checker et al., 2018). Besides that, they have also been attributed to the modulation of biotic and abiotic stress responses whereby crosstalks exist between the two networks (Ku et al., 2018). Under a stressful condition, antagonistic or synergistic crosstalks also happen between different phytohormones in plants (Ohri et al., 2015). Though complex, the crosstalks between phytohormone signaling cascades are deemed fundamental in fine-tuning the allocation of resources to the most appropriate defense mechanisms (Pieterse et al., 2012).

JA signaling is well known in triggering defense responses against necrotrophic pathogens (Mei et al., 2006), while SA signaling is effective against biotrophs/hemibiotrophs (Sticher et al., 1997). The finding that 2.0 mM 3BN treatment could increase the production of SA and JA is promising because it might enhance the broad-spectrum disease tolerance of Arabidopsis. As the fold-change was higher for JA than SA it remains to be elucidated whether the 3BN-induced defense responses are more effective against the necrotrophic pathogens. In addition, the 2.0 mM 3BN concentration did not cause lesion formation in the Col-0 plants as opposed to 2.5 mM 3BN treatment (**Figures 10B, 11B** and **Supplementary Figure S2**). As NO is responsible for the 2.5 mM 3BN-induced lesion formation in the Col-0 plants (as discussed in section The Involvement of NO in Lesion Formation of Arabidopsis Upon 3BN Recognition), it is very likely that the endogenous NO level accumulated in the Col-0 leaves under the 2.0 mM 3BN treatment condition is not sufficient for lesion formation. Therefore, we can infer that the 2.0 mM 3BN treatment establishes a primed state in Arabidopsis Col-0 plants by inducing the production of the phytohormones SA and JA in the absence of lesion formation.

The 2.5 mM 3BN treatment led to NO-mediated lesion formation and induced ABA levels only in Arabidopsis Col-0 plants, while *nia1nia2* plants have compromized NO levels and ABA induction. This observation could indicate a positive regulation between NO and ABA production in leaves. The physiological responses promoted by ABA have been well characterized in which ABA is known to induce callose accumulation and stomatal closure to prevent pathogens from entering into the plants (Oide et al., 2013; Eisenach et al., 2017). Nitrate reductase-catalyzed NO production is crucial for ABA-induced stomatal closure because the expression of key positive regulators in guard cell ABA signaling cascade was down-regulated in *nia1nia2* plants (Zhao et al., 2016). In agreement with our finding, GHPs, including 3BN, were reported to stimulate stomatal closure in Arabidopsis, a process accompanied by ROS and NO production as well as cytosolic Ca^{2+} fluctuation in the guard cells (Hossain et al., 2013).

The SA concentration in *nia1nia2* plants was relatively lower than in Col-0 plants under mock condition (**Figure 9A**), which suggests that SA production is stimulated by endogenous NO levels. Meanwhile, the increased production of SA in *nia1nia2* plants following the 3BN treatments, hints that NO and other secondary messengers, such as ROS, might act alone or synergistically to activate the 3BN-mediated SA signaling. The coordinated interplay between NO and SA has been characterized in detail (Freschi, 2013). For instance, sequence analysis on the promoters of NO-responsive genes in Arabidopsis revealed association with SA-responsive cis-regulatory elements (Palmieri et al., 2008). Moreover, NO has been reported to positively impact SA production and positively regulate SA signaling via two ways, i.e., (i) S-nitrosylation of non-expressor of pathogenesis-related proteins-1 (NPR1) to facilitate its oligomerization and interaction with SA receptors in cytosol, and (ii) S-nitrosylation of TGACG-Binding Factor-1 (TGA1) to stabilize the binding of the transcription factor to its downstream promoters (Mur et al., 2013). At the later bacterial infection stage, S-nitrosylation of SA-binding protein 3 (SABP3) inhibits its binding to SA, hence functioning as a negative feedback loop to suppress the activated SA signaling (Wang et al., 2009). Generation of ROS has also

been associated with the activation of different phytohormone signaling pathways, including SA, that eventually lead to stress responses (Mohanta et al., 2018).

The greater induction of JA production in the *nia1nia2* plants is probably due to its lower endogenous SA level as compared to Col-0 plants (**Figure 9A**). This could be explained by the antagonistic interactions between JA and SA signaling (Takahashi et al., 2004). The fact that the different concentrations of 3BN treatments increased JA production by a greater fold change than SA production in both the Arabidopsis genotypes, warrants us to have a closer look at the interplay between NO and JA production/signaling. Consistent with our microarray data (**Supplementary Tables S1, S2**), NO has been reported to positively impact JA production by inducing the expression of its biosynthetic genes, such as lipoxygenase 3 (*LOX3*) and 12-oxophytodienoate reductase 1, 2, and 3 (*OPR1*, *2* and *3*) (Mur et al., 2012). On the other hand, JA signaling can be suppressed by NO via a number of ways, i.e., (i) S-nitrosylation of NPR1 in the cytosol, (ii) the induction of WRKY70 by monomeric NPR1 in the nucleus, and (iii) the binding between TGA factors and octadecanoid-responsive Arabidopsis59 (ORA59) promoter (Mur et al., 2012; Freschi, 2013). This delicate, coordinated and reversible interactions between NO and JA/SA signaling enable Arabidopsis to mount effective defense responses to pathogens with different modes of infection.

The Disease Tolerance of Arabidopsis Against Necrotrophic Pathogens Is Enhanced by 2.0 mM 3BN Treatment

Exogenous application of 2.0 mM 3BN enhanced the disease tolerance of Arabidopsis Col-0 toward two types of necrotrophic pathogens, *Pectobacterium carotovorum* ssp. *carotovorum* (agent of bacterial root rot of sweet potato) (**Figure 10**) and *Botrytis cinerea* (agent of gray mold) (**Figure 11**). The infection assays of necrotrophic pathogens were carried out because 2.0 mM 3BN treatment increased the production of JA more than SA in Arabidopsis Col-0 plants (**Figure 9**). It is worth noting that the direct effect of 3BN on the pathogens could not be totally excluded even though precaution step had been taken by placing 3BN-treated plants in ventilated fume hood for 30 min to get rid of the 3BN vapor.

Based on the findings of this study, the proposed model of 3BN-induced plant defense responses in Arabidopsis involves potential key signaling compounds, NO, ROS, JA, and SA. NO is required for lesion formation (**Figures 2**, **3** and **Supplementary Figure S2**) and readjustment of metabolic processes involving the co-activation of sucrose degradation, glycolysis, Krebs cycle and amino acid synthesis (**Figures 6–8** and **Supplementary Figure S3**) in Col-0 plants treated with 2.5 mM 3BN. This gaseous molecule is also involved in mediating the 3BN-induced SA and JA production in Col-0 plants at lower concentration of 3BN treatment (2.0 mM) (**Figure 9A**). SA and JA are well known as an important signaling molecule responsible for local hypersensitive response and activation of systemic acquired resistance (Ponce de León and Montesano, 2013; Gao et al., 2015). The activation of SA and JA signaling pathway might also be involved in transcriptional reprogramming that alters the primary metabolite profiles in Arabidopsis as part of the defense mechanisms against pathogens (**Figures 6–8**). Apart from the induction of broad defense responses in Arabidopsis reported in this study, it is crucial to identify the membrane-bound PRR that might bind 3BN in order to propose 3BN as DAMP (Li et al., 2020). As a promising first step in this endeavor, our transcriptomic data showed that the expression of 16 genes encoding protein kinases was induced by 2.5 mM 3BN treatment in Col-0 plants (**Supplementary Table S2**). They include lectin-receptor kinases (At1g69270, At2g37710, At3g59700), cell wall-associated kinase (WAK1; At1g21250), FLG22-induced receptor-like kinase 1 (FRK1; At2g19190); BAK1-interacting receptor-like kinase 1 (BIR1; At5g48380) and chitin elicitor receptor kinase 1 (CERK1; At3g21630).

CONCLUSION

This study has demonstrated that exogenous application of 3BN, that belongs to the nitrile group of GHPs, can initiate an innate immune response by eliciting a broad range of signal molecules and pathways in Arabidopsis. At the concentration of 2.5 mM, 3BN treatment started to trigger a NO-mediated lesion formation in Arabidopsis. The same 3BN treatment also resulted in an elevated production of soluble sugars, Krebs cycle associated carboxylic acids and amino acids in Arabidopsis whose roles are closely related to the different stages of a plant immune response. Increased production of defense-related phytohormones such as SA, JA and ABA was observed in plants exposed to two different concentrations of 3BN treatments. As 3BN treatments of 2.5 mM and $\geq$ 5.0 mM caused lesion and severe necrosis respectively, a lower concentration of 3BN (2.0 mM) was used to test its feasibility in activating defense response of Arabidopsis without causing lesion formation. Intriguingly, this 3BN treatment also triggered an elevated synthesis of SA and JA. In the infection assay, 2.0 mM 3BN treatment was capable of enhancing the disease tolerance of Arabidopsis against necrotrophic pathogens such as *Pectobacterium carotovorum* ssp. *carotovorum* and *Botrytis cinerea*. In conclusion, this study proposes the potential of 3BN to function as DAMP in Brassicaceae.

DATA AVAILABILITY STATEMENT

The datasets generated for this study can be found in the GEO (accession GSE139089).

AUTHOR CONTRIBUTIONS

H-MT, AB, and RK conceived and designed the research project. H-MT, Y-CC, P-MY, AV, and RK conducted

the experiments. H-MT, BC, C-PC, FY, AB, and RK contributed to data interpretation and manuscript preparation. JR contributed to metabolite analysis. PW contributed to microarray analysis. All authors have read and approved the final version of the manuscript.

FUNDING

This work was supported by the Research Council of Norway (Projects 214329 and 230757) and Ministry of Science and Technology of Taiwan (MOST-107-2311-B-002-003-MY2 and MOST-108-2311-B-002-005).

ACKNOWLEDGMENTS

We thank Torfinn Sparstad for the microarray assistance. We thank Dr. Chih-Yu Lin and Ms. Ting-Hsiang Chang for UPLC-MS/MS parameter optimization and Metabolomics Core Facility, Agricultural Biotechnology Research Center at Academia Sinica, for technical support.

SUPPLEMENTARY MATERIAL

The Supplementary Material for this article can be found online at: https://www.frontiersin.org/articles/10.3389/fpls.2020.00257/full#supplementary-material

REFERENCES

Alipanah, L., Rohloff, J., Winge, P., Bones, A. M., and Brembu, T. (2015). Whole-cell response to nitrogen deprivation in the diatom *Phaeodactylum tricornutum*. *J. Exp. Bot.* 66, 6281–6296. doi: 10.1093/jxb/erv340

Andersson, M. X., Nilsson, A. K., Johansson, O. N., Boztş, G., Adolfsson, L. E., Pinosa, F., et al. (2015). Involvement of the electrophilic isothiocyanate sulforaphane in *Arabidopsis* local defense responses. *Plant Physiol.* 167, 251–261. doi: 10.1104/pp.114.251892

Arnold, A., Sajitz-Hermstein, M., and Nikoloski, Z. (2015). Effects of varying nitrogen sources on amino acid synthesis costs in *Arabidopsis thaliana* under different light and carbon-source conditions. *PLoS One* 10:e0116536. doi: 10.1371/journal.pone.0116536

Astier, J., Gross, I., and Durner, J. (2018). Nitric oxide production in plants: an update. *J. Exp. Bot.* 69, 3401–3411. doi: 10.1093/jxb/erx420

Bedini, A., Mercy, L., Schneider, C., Franken, P., and Lucic-Mercy, E. (2018). Unraveling the initial plant hormone signaling, metabolic mechanisms and plant defense triggering the endomycorrhizal symbiosis behavior. *Front. Plant Sci.* 9:1800. doi: 10.3389/fpls.2018.01800

Bones, A. M., and Rossiter, J. T. (1996). The myrosinase-glucosinolate system, its organisation and biochemistry. *Physiol. Plant.* 97, 194–208. doi: 10.1111/j.1399-3054.1996.tb00497.x

Bonfig, K. B., Gabler, A., Simon, U. K., Luschin-Ebengreuth, N., Hatz, M., Berger, S., et al. (2010). Post-translational derepression of invertase activity in source leaves via down-regulation of invertase inhibitor expression is part of the plant defense response. *Mol. Plant.* 3, 1037–1048. doi: 10.1093/mp/ssq053

Checker, V. G., Kushwaha, H. R., Kumari, P., and Yadav, S. (2018). "Role of phytohormones in plant defense: signaling and cross talk," in *Molecular Aspects of Plant-Pathogen Interaction*, ed. A. I. Singh (Singapore: Springer), 159–184. doi: 10.1007/978-981-10-7371-7_7

Chisholm, S. T., Coaker, G., Day, B., and Staskawicz, B. J. (2006). Host-microbe interactions: shaping the evolution of the plant immune response. *Cell* 124, 803–814. doi: 10.1016/j.cell.2006.02.008

Coruzzi, G., and Last, R. (2000). "Amino acids," in *Biochemistry and Molecular Biology of Plants*, eds B. B. Buchanan, W. Gruissem, and R. L. Jones (Rockville: American Society of Plant Physiologists), 358–410.

Couée, I., Sulmon, C., Gouesbet, G., and El Amrani, A. (2006). Involvement of soluble sugars in reactive oxygen species balance and responses to oxidative stress in plants. *J. Exp. Bot.* 57, 449–459. doi: 10.1093/jxb/erj027

Couto, D., and Zipfel, C. (2016). Regulation of pattern recognition receptor signaling in plants. *Nat. Rev. Immunol.* 16, 537–552. doi: 10.1038/nri.2016.77

de Pinto, M. C., Locato, V., Sgobba, A., Romero-Puertas, M. C., Gadaleta, C., Delledonne, M., et al. (2013). S-nitrosylation of ascorbate peroxidase is part of programmed cell death signaling in tobacco bright yellow-2 cells. *Plant Physiol.* 163, 1766–1775. doi: 10.1104/pp.113.222703

Dionisio-Sese, M. L., and Tobita, S. (1998). Antioxidant responses of rice seedlings to salinity stress. *Plant Sci.* 135, 1–9. doi: 10.1016/S0168-9452(98)00025-9

Eisenach, C., Baetz, U., Huck, N. V., Zhang, J., De, Angeli A, Beckers, G. J. M., et al. (2017). ABA-induced stomatal closure involves ALMT4, a phosphorylation-dependent vacuolar anion channel of *Arabidopsis*. *Plant Cell* 29, 2552–2569. doi: 10.1105/tpc.17.00452

Fraser, C. M., and Chapple, C. (2011). The phenylpropanoid pathway in *Arabidopsis*. *Arabidopsis Book* 9:e0152. doi: 10.1199/tab.0152

Freschi, L. (2013). Nitric oxide and phytohormone interactions: current status and perspectives. *Front. Plant Sci.* 4:398. doi: 10.3389/fpls.2013.00398

Fu, Z. Q., and Dong, X. (2013). Systemic acquired resistance: turning local infection into global defense. *Annu. Rev. Plant Biol.* 64, 839–863. doi: 10.1146/annurev-arplant-042811-105606

Gao, Q. M., Zhu, S., Kachroo, P., and Kachroo, A. (2015). Signal regulators of systemic acquired resistance. *Front. Plant Sci.* 6:228. doi: 10.3389/fpls.2015.00228

Gardner, P. R., Costantino, G., Szabó, C., and Salzman, A. L. (1997). Nitric oxide sensitivity of the aconitases. *J. Biol. Chem.* 272, 25071–25076. doi: 10.1074/jbc.272.40.25071

Gimsing, A. L., and Kirkegaard, J. A. (2009). Glucosinolates and biofumigation: fate of glucosinolates and their hydrolysis products in soil. *Phytochem. Rev.* 8, 299–310. doi: 10.1007/s11101-008-9105-5

Gupta, K. J., Fernie, A. R., Kaiser, W. M., and van Dongen, J. T. (2011). On the origins of nitric oxide. *Trends Plant Sci.* 16, 160–168. doi: 10.1016/j.tplants.2010.11.007

Halkier, B. A., and Gershenzon, J. (2006). Biology and biochemistry of glucosinolate. *Annu. Rev. Plant Biol.* 57, 303–333. doi: 10.1146/annurev.arplant.57.032905.105228

Hara, M., Yatsuzuka, Y., Tabata, K., and Kuboi, T. (2010). Exogenously applied isothiocyanates enhance glutathione S-transferase expression in *Arabidopsis* but act as herbicides at higher concentrations. *J. Plant Physiol.* 167, 643–649. doi: 10.1016/j.jplph.2009.11.006

Heil, M., and Land, W. G. (2014). Danger signals – damaged-self recognition across the tree of life. *Front. Plant Sci.* 5:578. doi: 10.3389/fpls.2014.00578

Hossain, M. S., Ye, W., Hossain, M. A., Okuma, E., Uraji, M., Nakamura, Y., et al. (2013). Glucosinolate degradation products, isothiocyanates, nitriles, and thiocyanates, induce stomatal closure accompanied by peroxidase-mediated reactive oxygen species production in *Arabidopsis thaliana*. *Biosci. Biotechnol. Biochem.* 77, 977–983. doi: 10.1271/bbb.120928

Hsiao, P. Y., Cheng, C. P., Koh, K. W., and Chan, M. T. (2017). The *Arabidopsis defensin* gene, AtPDF1.1, mediates defence against *Pectobacterium carotovorum* subsp. carotovorum via an iron-withholding defence system. *Sci. Rep.* 7:9175. doi: 10.1038/s41598-017-08497-7

Huang, P. Y., Yeh, Y. H., Liu, A. C., Cheng, C. P., and Zimmerli, L. (2014). The *Arabidopsis* LecRK-VI.2 associates with the pattern-recognition receptor *FLS2* and primes *Nicotiana benthamiana* pattern-triggered immunity. *Plant J.* 79, 243–255. doi: 10.1111/tpj.12557

Ishiga, Y., Watanabe, M., Ishiga, T., Tohge, T., Matsuura, T., Ikeda, Y., et al. (2017). The SAL-PAP chloroplast retrograde pathway contributes to plant immunity by regulating glucosinolate pathway and phytohormone signaling. *Mol. Plant Microbe Interact.* 30, 829–841. doi: 10.1094/MPMI-03-17-0055-R

Jones, J. D., and Dangl, J. L. (2006). The plant immune system. *Nature* 444, 323–329. doi: 10.1038/nature05286

Khokon, M. A., Jahan, M. S., Rahman, T., Hossain, M. A., Muroyama, D., Minami, I., et al. (2011). Allyl isothiocyanate (AITC) induces stomatal closure in *Arabidopsis*. *Plant Cell Environ.* 34, 1900–1906. doi: 10.1111/j.1365-3040.2011.02385.x

Kissen, R., and Bones, A. M. (2009). Nitrile-specifier proteins involved in glucosinolate hydrolysis in *Arabidopsis thaliana*. *J. Biol. Chem.* 284, 12057–12070. doi: 10.1074/jbc.M807500200

Kissen, R., Øverby, A., Winge, P., and Bone, A. M. (2016). Allyl-isothiocyanate treatment induces a complex transcriptional reprogramming including heat stress, oxidative stress and plant defence responses in *Arabidopsis thaliana*. *BMC Genomic* 17:740. doi: 10.1186/s12864-016-3039-x

Klessig, D. F., Durner, J., Noad, R., Navarre, D. A., Wendehenne, D., Kumar, D., et al. (2000). Nitric oxide and salicylic acid signaling in plant defense. *Proc. Natl. Acad. Sci. U.S.A.* 97, 8849–8855. doi: 10.1073/pnas.97.16.8849

Koch, E., and Slusarenko, A. (1990). *Arabidopsis* is susceptible to infection by a downy mildew fungus. *Plant Cell* 2, 437–445. doi: 10.1105/tpc.2.5.437

Ku, Y. S., Sintaha, M., Cheung, M. Y., and Lam, H. M. (2018). Plant hormone signaling crosstalks between biotic and abiotic stress responses. *Int. J. Mol. Sci.* 19:E3206. doi: 10.3390/ijms19103206

Kushalappa, A. C., Yogendra, K. N., and Karre, S. (2016). Plant innate immune response: qualitative and quantitative resistance. *Crit. Rev. Plant Sci.* 35, 38–55. doi: 10.1080/07352689.2016.1148980

Lambrix, V., Reichelt, M., Mitchell-Olds, T., Kliebenstein, D. J., and Gershenzon, J. (2001). The *Arabidopsis epithiospecifier* protein promotes the hydrolysis of glucosinolates to nitriles and influences *Trichoplusia ni herbivory*. *Plant Cell* 13, 2793–2807. doi: 10.1105/tpc.010261

León, J., Costa, Á, and Castillo, M. C. (2016). Nitric oxide triggers a transient metabolic reprogramming in *Arabidopsis*. *Sci. Rep.* 6:37945. doi: 10.1038/srep37945

Li, Q., Wang, C., and Mou, Z. (2020). Perception of damaged self in plants. *Plant Physiol.* doi: 10.1104/pp.19.01242 [Epub ahead of print].

Lin, A., Wang, Y., Tang, J., Xue, P., Li, C., Liu, L., et al. (2012). Nitric oxide and protein S-nitrosylation are integral to hydrogen peroxide-induced leaf cell death in rice. *Plant Physiol.* 158, 451–464. doi: 10.1104/pp.111.184531

Malinovsky, F. G., Thomsen, M. F., Nintemann, S. J., Jagd, L. M., Bourgine, B., Burow, M., et al. (2017). An evolutionarily young defense metabolite influences the root growth of plants via the ancient TOR signaling pathway. *eLife* 6:e29353. doi: 10.7554/eLife.29353

Mei, C., Qi, M., Sheng, G., and Yang, Y. (2006). Inducible overexpression of a rice allene oxide synthase gene increases the endogenous jasmonic acid level, PR gene expression, and host resistance to fungal infection. *Mol. Plant Microbe Interact.* 19, 1127–1137. doi: 10.1094/MPMI-19-1127

Mi, H., Muruganujan, A., Huang, X., Ebert, D., Mills, C., Guo, X., et al. (2019). Protocol update for large-scale genome and gene function analysis with the PANTHER classification system (v.14.0). *Nat. Protoc.* 14, 703–721. doi: 10.1038/s41596-019-0128-8

Miao, Y., and Zentgraf, U. (2007). The antagonist function of *Arabidopsis* WRKY53 and ESR/ESP in leaf senescence is modulated by the jasmonic and salicylic acid equilibrium. *Plant Cell* 19, 819–830. doi: 10.1105/tpc.106.042705

Mine, A., Seyfferth, C., Kracher, B., Berens, M. L., Becker, D., and Tsuda, K. (2018). The defense phytohormone signaling network enables rapid, high-amplitude transcriptional reprogramming during effector-triggered immunity. *Plant Cell* 30, 1199–1219. doi: 10.1105/tpc.17.00970

Mohanta, T. K., Bashir, T., Hashem, A., Abd-Allah, E. F., Khan, A. L., and Al-Harrasi, A. S. (2018). Early events in plant abiotic stress signaling: interplay between calcium, reactive oxygen species and phytohormones. *J. Plant Growth Regul.* 37, 1033–1049. doi: 10.1007/s00344-018-9833-8

Mur, L. A., Mandon, J., Persijn, S., Cristescu, S. M., Moshkov, I. E., Novikova, G. V., et al. (2013). Nitric oxide in plants: an assessment of the current state of knowledge. *AoB Plants* 5:ls052. doi: 10.1093/aobpla/pls052

Mur, L. A., Sivakumaran, A., Mandon, J., Cristescu, S. M., Harren, F. J., and Hebelstrup, K. H. (2012). Haemoglobin modulates salicylate and jasmonate/ethylene-mediated resistance mechanisms against pathogens. *J. Exp. Bot.* 63, 4375–4387. doi: 10.1093/jxb/ers116

Navarre, D. A., Wendehenne, D., Durner, J., Noad, R., and Klessig, D. F. (2000). Nitric oxide modulates the activity of tobacco aconitase. *Plant Physiol.* 122, 573–582. doi: 10.1104/pp.122.2.573

Neill, S. J., Desikan, R., and Hancock, J. T. (2003). Nitric oxide signalling in plants. *New Phytol.* 159, 11–35. doi: 10.1046/j.1469-8137.2003.00804.x

Nie, P., Li, X., Wang, S., Guo, J., Zhao, H., and Niu, D. (2017). Induced systemic resistance against *Botrytis cinerea* by *Bacillus cereus* AR156 through a JA/ET- and NPR1-dependent signaling pathway and activates PAMP-triggered immunity in *Arabidopsis*. *Front. Plant Sci.* 8:238. doi: 10.3389/fpls.2017.00238

Ohri, P., Bhardwaj, R., Bali, S., Kaur, R., Jasrotia, S., Khajuria, A., et al. (2015). The common molecular players in plant hormone crosstalk and signaling. *Curr. Protein Pept. Sci.* 16, 369–388. doi: 10.2174/1389203716666150330141922

Oide, S., Bejai, S., Staal, J., Guan, N., Kaliff, M., and Dixelius, C. (2013). A novel role of PR2 in abscisic acid (ABA) mediated, pathogen-induced callose deposition in *Arabidopsis thaliana*. *New Phytol.* 200, 1187–1199. doi: 10.1111/nph.12436

Øverby, A., Bævre, M. S., Thangstad, O. P., and Bones, A. M. (2015a). Disintegration of microtubules in *Arabidopsis thaliana* and bladder cancer cells by isothiocyanates. *Front. Plant Sci.* 6:6. doi: 10.3389/fpls.2015.00006

Øverby, A., Stokland, R. A., Åsberg, S. E., Sporsheim, B., and Bones, A. M. (2015b). Allyl isothiocyanate depletes glutathione and upregulates expression of glutathione S-transferases in *Arabidopsis thaliana*. *Front. Plant Sci.* 6:277. doi: 10.3389/fpls.2015.00277

Palmieri, M. C., Sell, S., Huang, X., Scherf, M., Werner, T., Durner, J., et al. (2008). Nitric oxide-responsive genes and promoters in *Arabidopsis thaliana*: a bioinformatics approach. *J. Exp. Bot.* 59, 177–186. doi: 10.1093/jxb/erm345

Pan, X., Welti, R., and Wang, X. (2010). Quantitative analysis of major plant hormones in crude plant extracts by high-performance liquid chromatography-mass spectrometry. *Nat. Protoc.* 5, 986–992. doi: 10.1038/nprot.2010.37

Pieterse, C. M., Van der Does, D., Zamioudis, C., Leon-Reyes, A., and Van Wees, S. C. (2012). Hormonal modulation of plant immunity. *Annu. Rev. Cell Dev. Biol.* 28, 489–521. doi: 10.1146/annurev-cellbio-092910-154055

Ponce de León, I., and Montesano, M. (2013). Activation of defense mechanisms against pathogens in mosses and flowering plants. *Int. J. Mol. Sci.* 14, 3178–3200. doi: 10.3390/ijms14023178

Qian, Y., Tan, D. X., Reiter, R. J., and Shi, H. (2015). Comparative metabolomic analysis highlights the involvement of sugars and glycerol in melatonin-mediated innate immunity against bacterial pathogen in *Arabidopsis*. *Sci. Rep.* 5:15815. doi: 10.1038/srep15815

Rajamuthiah, R., and Mylonakis, E. (2014). Effector triggered immunity. *Virulence* 5, 697–702. doi: 10.4161/viru.29091

Reichelt, M., Brown, P. D., Schneider, B., Oldham, N. J., Stauber, E. J., Tokuhisa, J. G., et al. (2002). Benzoic acid glucosinolate esters and other glucosinolates from *Arabidopsis thaliana*. *Phytochemistry* 59, 663–671. doi: 10.1016/S0031-9422(02)00014-6

Roh, J. S., and Sohn, D. H. (2018). Damage-associated molecular patterns in inflammatory diseases. *Immune Netw.* 18:e27. doi: 10.4110/in.2018.18.e27

Romero-Puertas, M. C., Laxa, M., Mattè, A., Zaninotto, F., Finkemeier, I., Jones, A. M., et al. (2007). S-nitrosylation of peroxiredoxin II E promotes peroxynitrite-mediated tyrosine nitration. *Plant Cell* 19, 4120–4130. doi: 10.1105/tpc.107.055061

Romero-Puertas, M. C., Perazzolli, M., Zago, E. D., and Delledonne, M. (2004). Nitric oxide signalling functions in plant-pathogen interactions. *Cell Microbiol.* 6, 795–803. doi: 10.1111/j.1462-5822.2004.00428.x

Schmidt, H. H., and Walter, U. (1994). NO at work. *Cell* 78, 919–925. doi: 10.1016/0092-8674(94)90267-4

Smyth, G. K. (2005). "limma: linear models for microarray data," in *Bioinformatics and Computational Biology Solutions Using R and Bioconductor*, eds R. Gentleman, V. J. Carey, W. Huber, R. A. Irizarry, and S. Dudoit (New York, NY: Springer), 397–420. doi: 10.1007/0-387-29362-0_23

Stamler, J. S. (1994). Redox signaling: nitrosylation and related target interactions of nitric oxide. *Cell* 78, 931–936. doi: 10.1016/0092-8674(94)90269-0

Sticher, L., Mauch-Mani, B., and Métraux, J. P. (1997). Systemic acquired resistance. *Annu. Rev. Phytopathol.* 35, 235–270. doi: 10.1146/annurev.phyto.35.1.235

Stotz, H. U., Sawada, Y., Shimada, Y., Hirai, M. Y., Sasaki, E., Krischke, M., et al. (2011). Role of camalexin, indole glucosinolates, and side chain modification of glucosinolate-derived isothiocyanates in defense of *Arabidopsis* against

Sclerotinia sclerotiorum. *Plant J.* 67, 81–93. doi: 10.1111/j.1365-313X.2011.04578.x

Takahashi, H., Kanayama, Y., Zheng, M. S., Kusano, T., Hase, S., Ikegami, M., et al. (2004). Antagonistic interactions between the SA and JA signaling pathways in *Arabidopsis* modulate expression of defense genes and gene-for-gene resistance to cucumber mosaic virus. *Plant Cell Physiol.* 45, 803–809. doi: 10.1093/pcp/pch085

Thimm, O., Bläsing, O., Gibon, Y., Nagel, A., Meyer, S., Krüger, P., et al. (2004). MAPMAN: a user-driven tool to display genomics data sets onto diagrams of metabolic pathways and other biological processes. *Plant J.* 37, 914–939. doi: 10.1111/j.1365-313x.2004.02016.x

Torres, M. A., Jones, J. D., and Dangl, J. L. (2006). Reactive oxygen species signaling in response to pathogens. *Plant Physiol.* 141, 373–378. doi: 10.1104/pp.106.079467

Urbancsok, K., Bones, A. M., and Kissen, R. (2017). Glucosinolate-derived isothiocyanates inhibit *Arabidopsis* growth and the potency depends on their side chain structure. *Int. J. Mol. Sci.* 18:E2372. doi: 10.3390/ijms18112372

Vlot, A. C., Pabst, E., and Riedlmeier, M. (2017). *Systemic Signaling in Plant Defense*. Chichester: John Wiley & Sons, Ltd.

Wang, Y. Q., Feechan, A., Yun, B. W., Shafiei, R., Hofmann, A., Taylor, P., et al. (2009). S-nitrosylation of AtSABP3 antagonizes the expression of plant immunity. *J. Biol. Chem.* 284, 2131–2137. doi: 10.1074/jbc.M806782200

Wilkinson, J. Q., and Crawford, N. M. (1993). Identification and characterization of a chlorate-resistant mutant of *Arabidopsis thaliana* with mutations in both nitrate reductase structural genes NIA1 and NIA2. *Mol. Gen. Genet.* 239, 289–297. doi: 10.1007/BF00281630

Wittstock, U., and Burow, M. (2010). Glucosinolate breakdown in *Arabidopsis*: mechanism, regulation and biological significance. *Arabidopsis Book* 8, e0134. doi: 10.1199/tab.0134

Wittstock, U., and Halkier, B. A. (2002). Glucosinolate research in the *Arabidopsis* era. *Trends Plant Sci.* 7, 263–270. doi: 10.1016/S1360-1385(02)02273-2

Wittstock, U., Kliebenstein, D. J., Lambrix, V., Reichelt, M., and Gershenzon, J. (2003). "Glucosinolate hydrolysis and its impact on generalist and specialist insect herbivores," in *Recent Advances in Phytochemistry*, ed. J. T. Romeo (Amsterdam: Elsevier), 101–125. doi: 10.1016/s0079-9920(03)80020-5

Wojtaszek, P. (1997). Oxidative burst: an early plant response to pathogen infection. *Biochem. J.* 322, 681–692. doi: 10.1042/bj3220681

Yoshioka, H., Mase, K., Yoshioka, M., Kobayashi, M., and Asai, S. (2011). Regulatory mechanisms of nitric oxide and reactive oxygen species generation and their role in plant immunity. *Nitric Oxide* 25, 216–221. doi: 10.1016/j.niox.2010.12.008

Yun, B. W., Feechan, A., Yin, M., Saidi, N. B., Le Bihan, T., Yu, M., et al. (2011). S-nitrosylation of NADPH oxidase regulates cell death in plant immunity. *Nature* 478, 264–268. doi: 10.1038/nature10427

Zhao, C., Cai, S., Wang, Y., and Chen, Z. H. (2016). Loss of nitrate reductases NIA1 and NIA2 impairs stomatal closure by altering genes of core ABA signaling components in *Arabidopsis*. *Plant Signal. Behav.* 11:e1183088. doi: 10.1080/15592324.2016.1183088

Zhao, M. G., Chen, L., Zhang, L. L., and Zhang, W. H. (2009). Nitric reductase-dependent nitric oxide production is involved in cold acclimation and freezing tolerance in *Arabidopsis*. *Plant Physiol.* 151, 755–767. doi: 10.1104/pp.109.140996

Zipfel, C. (2014). Plant pattern-recognition receptors. *Trends Immunol.* 35, 345–351. doi: 10.1016/j.it.2014.05.004

Conflict of Interest: The authors declare that the research was conducted in the absence of any commercial or financial relationships that could be construed as a potential conflict of interest.

frontiers in Plant Science

ORIGINAL RESEARCH
published: 04 June 2020
doi: 10.3389/fpls.2020.00711

Genomic Origin and Diversification of the Glucosinolate MAM Locus

*R. Shawn Abrahams[1,2], J. Chris Pires[1] and M. Eric Schranz[2]**

[1] Division of Biological Sciences, University of Missouri, Columbia, MO, United States, [2] Biosystematics Group, Wageningen University, Wageningen, Netherlands

Glucosinolates are a diverse group of plant metabolites that characterize the order Brassicales. The *MAM* locus is one of the most significant QTLs for glucosinolate diversity. However, most of what we understand about evolution at the locus is focused on only a few species and not within a phylogenetic context. In this study, we utilize a micro-synteny network and phylogenetic inference to investigate the origin and diversification of the *MAM*/IPMS gene family. We uncover unique *MAM*-like genes found at the orthologous locus in the Cleomaceae that shed light on the transition from *IPMS* to *MAM*. In the Brassicaceae, we identify six distinct *MAM* clades across Lineages I, II, and III. We characterize the evolutionary impact and consequences of local duplications, transpositions, whole genome duplications, and gene fusion events, generating several new hypothesizes on the function and diversity of the *MAM* locus.

Keywords: glucosinolates, brassicaceae, gene family, polyploidy, gene duplication, gene fusion

OPEN ACCESS

Edited by:
Ralph Kissen, Norwegian University of Science and Technology, Norway

Reviewed by:
Priyakshee Borpatragohain, Southern Cross University, Australia
Joshua Trujillo, Purdue University, United States

***Correspondence:**
M. Eric Schranz
eric.schranz@wur.nl

Specialty section:
This article was submitted to Plant Metabolism and Chemodiversity, a section of the journal Frontiers in Plant Science

Received: *15 October 2019*
Accepted: *05 May 2020*
Published: *04 June 2020*

Citation:
Abrahams RS, Pires JC and Schranz ME (2020) Genomic Origin and Diversification of the Glucosinolate MAM Locus. Front. Plant Sci. 11:711. doi: 10.3389/fpls.2020.00711

INTRODUCTION

Glucosinolates (GSL) are a diverse class of amino-acid derived sulfur containing metabolites characteristic of plants of the order Brassicales (Rodman et al., 1998; Borpatragohain et al., 2016; Kliebenstein and Cacho, 2016; Olsen et al., 2016; Chhajed et al., 2019; Blazevic et al., 2020). When the plant experiences physical damage, such as chewing by herbivores, compartments of the cell rupture and release myrosinase enzymes that hydrolyze the GSLs to create an isothiocyanate anion, damaging the attacker (Rodman et al., 1998). Besides their roles in direct defense, GSLs have also been shown to play important roles such as nutrient transport and physiological signaling (del Carmen et al., 2013). They are considered a key innovation of the Brassicales, as adaptations in the biosynthesis pathway have been shown to correlate with increased rates of speciation (Edger et al., 2015). The GSL pathway is a model for investigating processes underlying natural variation within and among species; including the roles of genome and gene duplication (Kliebenstein, 2008; Bekaert et al., 2012; Hofberger et al., 2013; Edger et al., 2015; van den Bergh et al., 2016; Wisecaver et al., 2017). Aliphatic GSLs, the largest sub-group of compounds, are especially implicated in this rate of speciation as they are only found in the most species-rich groups such as the family Brassicaceae.

The often multi-gene *methylthioalkylmalate* (*MAM*) locus, also called the Elong locus, accounts for much of the natural variation observed in aliphatic GSLs (Kliebenstein et al., 2001a,b; Textor et al., 2004, 2007; Kroymann and Mitchell-Olds, 2005; Benderoth et al., 2006, 2009; Keurentjes et al., 2006; de Kraker et al., 2007; Wentzell et al., 2007; de Kraker and Gershenzon, 2011; Zhang et al., 2015; Kliebenstein and Cacho, 2016; Kumar et al., 2019; Petersen et al., 2019). *MAM* enzymes catalyze the condensation reaction that extends the carbon chain in amino acid derived GSL precursors (Benderoth et al., 2006). The extended amino acid expands the types

(Kliebenstein and Cacho, 2016). Most of what we understand about the evolution of *MAM* has been learned from studying just a handful of species, without a broad phylogenetic context (Kliebenstein and Cacho, 2016). MAM diversification in the Brassicaceae is thought to have occurred independently in separate lineages. Specifically, *MAM* diversity has been largely examined in Lineage I of the family (*Arabidopsis* and relatives) and to a lesser extent in Lineage II (*Brassica* and relatives). This work has been supported by large gene datasets, though with differing gene tree topologies (Zhang et al., 2015; **Supplementary Figure S1**).

In *Arabidopsis thaliana*, phenotypic variation of the *MAM* locus is characterized by the accumulation of different majority carbon chain-length GSL profiles (Kliebenstein and Cacho, 2016). The most common profiles have majority three carbon (3C) or four carbon (4C) molecules, but can extend up to 8C majority profiles, with variability at the population level (Benderoth et al., 2009; Kliebenstein and Cacho, 2016). Copy number variation and allelic diversity/presence-absence drive these differences, as one *MAM* gene may mask the phenotype of another at the same locus (Benderoth et al., 2006, 2009). This plays out in the interactions between *MAM1* and *MAM2* in *A. thaliana* populations, where variation is well understood. The 4C majority phenotype is seen in populations where *MAM1* and *MAM2* are both present and intact or when *MAM2* is absent. In populations lacking a *MAM1* gene, the GSL profile exhibits a 3C majority phenotype. In some cases, *MAM1* and *MAM2* genes have been fused (e.g., gene chimerism) wherein they are reformed into a *MAM1-like* functional gene with partial *MAM2* sequences, or vice versa (Benderoth et al., 2006). Crop Brassicas most commonly accumulate 3C, 4C, or a mix of 3C and 4C majority profiles, the latter displaying a seemingly unmasked phenotype, unlike what we see in *A. thaliana* (Benderoth et al., 2009; Kliebenstein and Cacho, 2016).

Naming conventions for *MAM* orthologs are either directly based on *A. thaliana* (*MAM1*, *MAM2*, and *MAM3*) or based on *A. lyrata MAM* (*MAMa, MAMb*, and *MAMc*) (Benderoth et al., 2009). The *Arabidopsis* centered model of *MAM* diversity is vulnerable to miss-characterization as *Arabidopsis* genes may be highly derived, and thus not generalizable. We also see that the number of genes at the *MAM* locus can vary between populations as well as species, potentially misleading ancestral state estimations with poor sampling. To accurately understand *MAM* diversification, it is necessary for gene selection across a broader species phylogeny with comparisons to their primary metabolic ancestor, isopropylmalate synthase (*IPMS*).

Though diverged, *IPMS* and *MAM* share a high sequence similarity and similar enzymatic function (Moghe and Last, 2015). I*PMS* contains two conserved protein domains: a pyruvate carboxylase (HMGL-like), that is involved in the carbon condensation reaction, and a leucine allosteric domain (LeuA), that commits the protein to the leucine biosynthesis pathway forming a homodimer (Koon et al., 2004). *MAM* genes only retain the HMGL-like domain, the loss of LeuA being considered a key step in the transition of *MAM* from an *IPMS-like* gene (de Kraker et al., 2007). To our knowledge, no previous work has investigated when the loss of this domain occurred in the evolution of the locus.

In this study, we examine the evolutionary history and diversity of the *MAM/IPMS* gene family, uncovering critical steps in the origin of *MAM* and identifying patterns of domain-specific diversity across the Brassicaceae and its sister-family the Cleomaceae. We utilize a genomic networking methodology to analyze the wealth of newly available genome sequences (Zhao et al., 2017; Zhao and Schranz, 2019). The method analyses the conserved physical location of gene family members across queried genomes, known as synteny, to characterize the impact of different gene duplication types in the expansion of the *MAM/IPMS* gene family (Zhao et al., 2017; Zhao and Schranz, 2019). Ultimately we show that a mix of gene duplication types and domain changes played important roles in the evolution and innovation of the *MAM* locus.

MATERIALS AND METHODS

Genomic Network Construction

The genomic network analysis included 40 complete plant genomes representing 38 different species. This included 34 Brassicaceae species from Lineages I, II, III, and *Aethionema arabicum* as sister to the rest of the family, three genomes from the sister-family Cleomaceae, and three outgroup species (*Theobroma cacao, Citrus sinensis, and Vitis vinifera*) (**Supplementary Table S1**). For each genome, we utilized protein sequences in FASTA format and a BED/GFF file. One of two *Capsella rubella* genomes was excluded from downstream analysis due to insufficient quality. The *Thellungiella halophila* and *Thellungiella salsuginea* are two different sequencing efforts of the same species, now under the name *Eutrema salsugineum*. The genome sequenced as *Alyssum linifolium* has since been identified as *Descurainia pinnata*. Network analyses were performed as described in Zhao et al. (2017). Reciprocal all-against-all whole genome protein sequence comparison were made using RAPSeach2 (Zhao et al., 2012). MCScanX (Tang et al., 2008; Wang et al., 2012) was used to calculate generic collinearity between genomes and all comparisons were saved to generate the full genomic network.

Gene Family Network

We identified candidate *IPMS/MAM* genes using HMMER (Finn et al., 2011), cross-referencing the Pfam, PDBe, and GO databases with domain signature HMGL-like PF00682, and filtered by an inclusion threshold e-value of 0.007. Selected genes were later filtered by relative branch lengths as compared to known *IPMS* and *MAM* genes and then queried against the overall syntenic network with a 25 gene window to extract the gene family network. We visualized the resulting network in Cytoscape version 3.3.0 (Shannon et al., 2003). We then pruned the network of gene nodes that did not contain an HMGL-like domain but were dragged in by potential domain fusions. Clique percolation, as implemented in CFindier (Derényi et al., 2005; Palla et al., 2005; Fortunato, 2010), was used to locate all K-clique comments to identify communities or clusters of gene nodes.

Phylogenetic Inference

Full amino acid sequences for all gene family members were aligned using MAFFT (Kuraku et al., 2013; Katoh et al., 2017) and cleaned using Phyutility at a 50% occupancy threshold (Smith and Dunn, 2008). We used RAxML (Stamatakis, 2014) for phylogenetic inference with the GTRCAT model (Boostrap = 1000). The same procedure was repeated for the HMGL-like domain region of each gene FASTA file as estimated by HMMER. Supplemental sequence comparisons were made using MView (Madeira et al., 2019) and analyzed using R.

RESULTS

Synteny and Domain Analysis

Micro-synteny network analysis identified three major syntenic clusters (**Figure 1**), two of which encompass many genes of the known *MAM* gene clade (orange and green clusters) and one encompassing the known *IPMS* gene clade (blue cluster). Of the syntenic clusters found in the *MAM* clade, the green cluster identifies the ancestral *MAM* position, what we will call the *MAM*-Ancestral locus, and is equivalent to the Elong locus. The orange cluster represents a transposed and retained *MAM* locus-specific to Lineage II of the Brassicaceae, which we will call the *MAM*-Transposed locus. The analysis also recovered the 4th cluster of an unnamed lineage of genes that have retained only a single HMGL-like domain and are found in both our outgroup and in-group genomes. The *A. thaliana* representative gene of this clade (AT2G26800) has been shown to play a role in seed amino acid concentration (Peng et al., 2015). Relative branch lengths showed this gene clade as highly diverged from both MAM and IPMS sequences. Because of this, all genes of this clade were filtered from downstream analyses.

95.7% of IPMS genes identified by sequence were also found in the IPMS syntenic cluster. 39.6% of MAM genes, not associated with the conserved Lineage II transposition, were found in the MAM-Ancestral syntenic cluster. 51.6% of genes found in the Lineage II transposed sub-clade were found in the syntenic cluster. Differences in percent synteny are tied to increased rates of tandem duplications, as the local duplicate syntenic signal was often masked, and transposed duplication events, which remove syntenic context. It is expected that many new transposed duplicates are in the process of pseudogenization and are not active MAM genes.

All genes at the Cleomaceae *MAM*-Ancestral locus have retained their LeuA domain from their time as *IPMS* duplicates, with some showing syntenic connections to both the *MAM*-Ancestral and *IPMS* syntenic cluster (**Figure 1**). For example, Th2v2405 from *Tarenaya hassleriana* has more syntenic connections with *IPMS* cluster members than with genes of the *MAM*-Ancestral locus, despite belonging to the direct orthologous chromosomal region of the MAM-Ancestral locus in the Brassicaceae (**Figures 1**, **2**). Genes of the Cleomaceae *MAM*-Ancestral locus and the IPMS locus also appear to have a shared pattern of gene dosage. A duplication of the IPMS locus following WGD, brings the total *IPMS* gene number to two, followed by a compensatory reduction in MAM gene number at the *MAM*-Ancestral locus (**Figure 2C**). An exception to this is found in the *Tarenaya hassleriana* genome, where a novel transposed *MAM*-like gene has lost the LeuA domain. This allows for three *MAM*-like genes to co-occur with two *IPMS* genes (**Supplementary Figure S3**).

Gene Family Relationships

The HMGL-like domain and full protein sequence gene trees identified distinct IPMS and MAM clades (**Figure 1**). In both cases, Cleomaceae genes are sister to a larger Brassicaceae clade, and *Aethionema arabicum* is sister to the rest of the Brassicaceae, which agrees with the species tree topology. Within the core Brassicaceae, the domain and full sequence trees display topological incongruence to each other (**Figure 3**) and neither perfectly match the species tree.

The domain tree divides MAM into six supported clades (**Figure 3**). Though the branching order could not be determined, the supported clades were assigned *MAMa-f*. These domain clade designations are based on the *Arabidopsis lyrata* MAM gene-tree clades. Given the branch length, a measure of sequence divergence, of the genes found at the MAM-Transposed locus (**Figure 3**), the sub-clade of *MAMe* was designated *MAMet*. The closest non-*MAMet* domain sequence to the group was a *MAMe* sequence from the *Lunaria annua* genome.

Summary amino acid comparison at 80% similarity threshold shows *MAMa* is the most conserved domain, *MAMe* is the most variable domain, and *MAMet* and *MAMc* are the most diverged (**Supplementary Figure S5**). Exon/Intron comparisons of full *MAMet* genes show the expected number of domains for a functional MAM gene but with differences in exon size. When plotted on the species tree, *MAMa-b* and *MAMe* are ancestral to Lineage I, *MAMa-b* and *MAMd-f* are ancestral to Lineage II, and *MAMb* and *MAMd* are ancestral to Lineage III (**Figure 4** and **Supplementary Figure S3**).

The MAM full-sequence tree shows bootstrap support between clades, but also a breakdown of some domain clades as well as clade nesting (**Figure 3**). *MAMa* and *MAMb* separate by species lineage, while MAMc is unique to a small subset of Lineage I species and appears closely related to *MAMb* and *MAMe*. MAMd, and MAMe are primarily the same as in the domain tree, but with other domains nested within. MAMf is consistent with the domain tree and sister to Lineage II *MAMa*.

To test for potential gene fusion events, full sequences of *MAMa* and *MAMb* Lineage I genes were broken up into "before the domain," "domain," and "after domain" sequences (**Supplementary Figure S4**). Pairwise sequence comparisons were made between the Lineage I gene segments and corresponding segments of Lineage I *MAMe* genes, and Lineage II genes for *MAMa* or Lineage III genes for *MAMb*. In both cases, the domain portion best matches the corresponding domain regardless of Lineage. For Lineage I *MAMb*, the region before the domain is more similar to Lineage I MAMe than it is to Lineage II *MAMb*. For Lineage I *MAMa*, the region before the domain is more similar on average to Lineage I MAMe but was not significantly different from Lineage II *MAMa*.

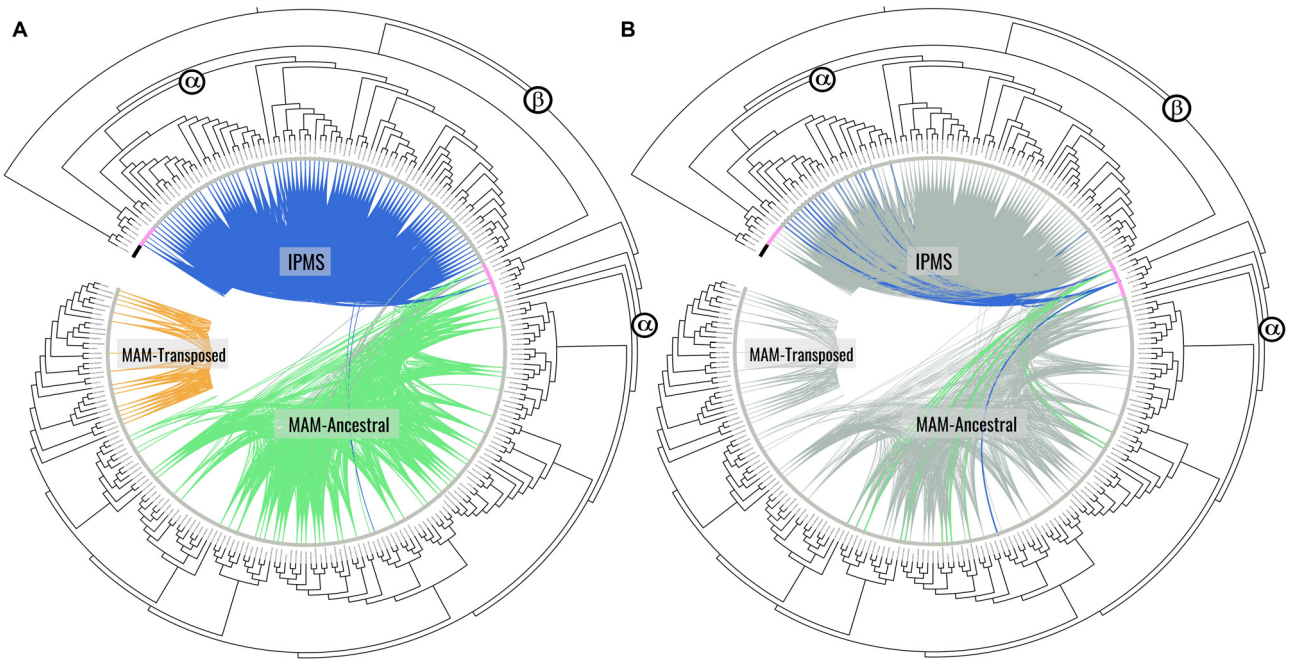

FIGURE 1 | Synteny clusters and gene tree phylogeny of identified *IPMS* and *MAM* genes consisting of 262 total. For **(A,B)** the bar along the tips represent species lineage where black bars indicate genes from out group genomes, the pink bar indicates genes from Cleomaceae genomes, and the gray bar indicates genes from Brassicaceae genomes. **(A)** Syntenic cluster analysis identified three distinct gene clusters, each representing a different conserved genomic location. The IPMS cluster in blue, the MAM-Ancestral cluster in green, and the novel lineage specific MAM-Transposed cluster in orange. Gray lines here indicate connections between the IPMS and MAM clusters. **(B)** Emphasizes those connections between MAM-like genes in the Cleomaceae that exhibit both *IPMS* & *MAM* cluster membership (Clevi.0004s0713 and tha_Th2v24105) despite being physically located at the MAM-Ancestral locus in their respective genomes. [For Bootstrap scores: **Supplementary Figure S6**; Online interactive trees: **(A)** http://bit.ly/2tHVgYK; **(B)** http://bit.ly/2Svu8Vf].

DISCUSSION

The origin of all specialized metabolic pathways is primary metabolic genes, often with similar enzymatic chemistry (Moghe and Last, 2015). This transition is mediated by the process of gene duplication and subsequent drift and neo/subfunctionalization (Conant and Wolfe, 2008; Moghe and Last, 2015). For the MAM locus of the glucosinolate (GSL) biosynthesis pathway, the role of tandem duplication events in the evolution of the locus has been well characterized at the population level. The majority of work has only looked at Arabidopsis and its close relatives, and to a lesser extent, in the crop Brassicas (Kliebenstein and Cacho, 2016). Much of what we understand about the MAM locus function has not been understood in the context of phylogeny, except to say that based on gene tree relationships, Lineage II and Lineage II have independently diversified from some initial gene substrate (Benderoth et al., 2009; Zhang et al., 2015). In this study, we utilized a micro-synteny network of genomes and phylogenetic inference to elucidate the evolutionary history of the MAM locus.

MAM in the Cleomaceae

The inclusion of Cleomaceae genomes in our analysis has provided novel insight into the origin of the *MAM* locus, following the whole genome duplication (WGD) event β, the hypothesized origin of *MAM* from *IPMS* (van den Bergh et al., 2016). We estimate through micro-synteny and gene tree information that the Ancestral-*MAM* locus at the formation of the Cleomaceae was characterized by multiple MAM-like gene duplicates, the result of tandem duplications or local transposition (**Figure 2**). These genes are different from what has been characterized in the Brassicaceae orthologous Ancestral-*MAM* locus, the Elong locus. They have retained their LeuA domain, the loss of which has been considered a critical step in the evolution of Brassicaceae MAM (de Kraker et al., 2007). Within the Cleomaceae, some genes of the Ancestral-*MAM* locus exhibit both Ancestral-*MAM* and *IPMS* syntenic cluster identity (**Figure 1**). The syntenic window for these intermediates is shifted in comparison to other analyzed neighboring MAM-like genes. This allows for the inclusion of neighboring non-MAM genes that are more characteristic of the IPMS genomic context. This evidence supports the hypothesis that the Ancestral-MAM locus was once a full context duplicate of the IPMS locus, and in the process of specialization over millions of years, degraded in collinearity.

How these MAM-like genes interact with GSL biosynthesis is unknown, but they have shown levels of expression in the leaf, seed, and roots in *Tarenaya hassleriana* (van den Bergh et al., 2016). The retention of the LeuA domain suggests that MAM-like proteins may have some continued interaction with IPMS or leucine biosynthesis. The ways in which genes respond to duplication events are constrained by their biochemical

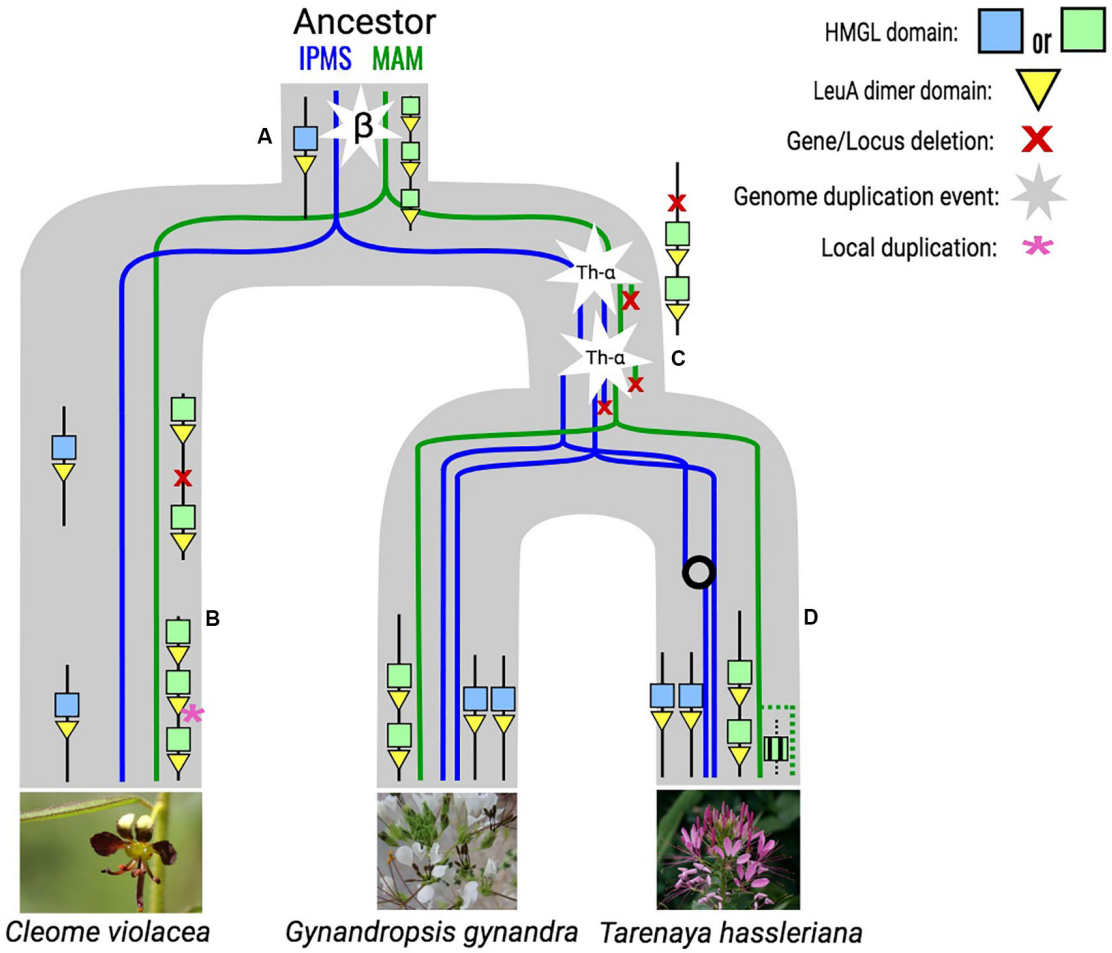

FIGURE 2 | Inferred evolutionary trajectory of *MAM* and *IPMS* loci in the cleomaceae based on genomic synteny and phylogenetic information. **(A)** The MAM-Ancestral locus originated from the β whole genome duplication event and is characterized by *MAM*–like genes that experience local duplication and have retained their LeuA domain. **(B)** In the genome of *Cleome violacea* there is a gene deletion followed by a novel tandem duplication at the MAM locus. **(C)** Following the Th-α whole genome triplication the *IPMS* locus is duplicated and the *MAM* locus experiences compensatory gene loss and is reflected in the *Gynandropsis gynandra* genome. **(D)** In the *Tarenaya hassleriana* genome, the IPMS locus experiences a gene conversion event that maintains sequence similarity between the two copies. There is also a novel transposition of the MAM-like gene from the MAM-Ancestral locus that does not maintain the LeuA domain. As the placement of the Th-α whole genome duplication event is not confirmed to be fully shared by both lineages, an alternative reconstruction is also possible.

interactions, and therefore may shed insight into enzyme behavior (Bekaert et al., 2012; Birchler and Veitia, 2012; Conant et al., 2014; McLysaght et al., 2014). For example, given that IPMS experiences purifying selection of local gene duplicates and that *MAM-like* Cleomaceae genes found at the *MAM*-Ancestral locus do exhibit some local duplication, it is likely that these MAM-like genes have significantly sub- or neofunctionalized from their IPMS ancestor in terms of biochemical role. With that said, the dosage effects of *IPMS* are broader than only limiting local duplication, and through stoichiometric effects constrain most duplication types. Only after the β WGD event, is IPMS able to be retained and reduced in multiples of two. A pattern we see recapitulated after subsequent WGD events, with a few potential exceptions (**Supplementary Figure S2**). Following Th-α, the Cleomaceae whole-genome triplication (WGT) or hexaploidy, there is an expected full context duplication of the IPMS locus, but with no context duplication of the Ancestral-*MAM* locus (**Figure 2C**). In fact, we see a compensatory loss of a *MAM-like* gene following the increase in IPMS copy number. The presence of stoichiometric conflict between IPMS and these *MAM*-like genes would support the hypothesis that they have retained some IPMS role and constraint. Further sampling across the Cleomaceae will be necessary to see if these patterns hold.

In the *Tarenaya hassleriana* genome, there is a novel a transposition of *MAM* (**Figure 2D**). This transposed gene does not have a LeuA domain, bringing the overall *MAM/IPMS* gene number beyond what would be expected under an IPMS dosage constraint (**Supplementary Figure S2**). This transposed locus has been shown to express in several tissues and to a greater extent in the leaf when compared to *MAM*-like counterparts at the Ancestral-*MAM* locus (van den Bergh et al., 2016). Increased species sampling, as well as an understanding of population-level

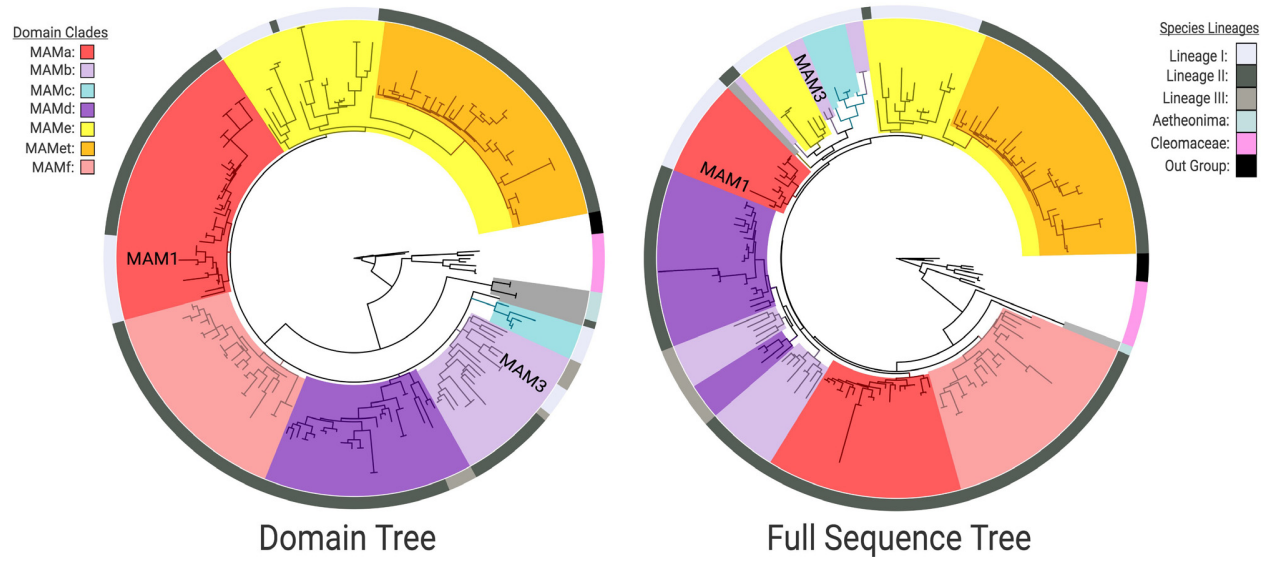

FIGURE 3 | Clade comparison between Brassicaceae MAM domain and full sequence gene trees highlighting incongruence. HMGL-like sequences were used for the domain tree and resolved six clades of MAM (MAMa-f) but could not infer branching order. In the full sequence tree there is a breakdown of MAMa and MAMb that is correlated with species lineage. In both trees, the placement of MAM1 and MAM3 from the *Arabidopsis thaliana* Col genome are indicated. [For Bootstrap scores: **Supplementary Figure S7** – Domain Tree; **Supplementary Figure S8** – Full Sequence; Online interactive trees: Domain – http://bit.ly/2Hb5jlS; Full Sequence – http://bit.ly/37btHEZ].

variation in Cleomaceae *MAM*, is necessary for any conclusions on the dosage to be explored further using these methods. Direct biochemical assays of these *MAM*-like proteins will also be critical for characterizing any role they may play in glucosinolate biosynthesis and how that may differ from what is seen in the Brassicaceae. The Cleomaceae, and potentially the Capparaceae, which also shares the β duplication event (Edger et al., 2015), could serve as a powerful window into the evolution of early Brassicaceae *MAM* and a model for how gene families transition from primary to specialized metabolism.

MAM in the Brassicaceae

Between Lineages I, II, and III of the Brassicaceae, we have identified six distinct clades of *MAM*, *MAMa-f*, based on conserved HMGL-like domain sequences (**Figure 3** and **Supplementary Figure S3**). Based on occurrence patterns across the family, we can say that *MAMb* and *MAMd* clades are ancestral to all three lineages, and *MAMa* and *MAMe* may be ancestral to only Linages I and Lineage II. The latter conclusion could not be confirmed by gene tree information and may be vulnerable to sampling bias. The dispute between the chloroplast and nuclear species tree topologies could also affect the evolutionary relationships between the MAM clades and hamper our ability to predict (Nikolov et al., 2019). Improved sampling across the Brassicaceae is necessary before a robust estimation of the ancestral type can be made. That said, we are confident that *MAMc, MAMet,* and *MAMf* domain types are more recent innovations occurring in Lineage I and Lineage II, with specific branch placements (**Figure 4** and **Supplementary Figure S3**).

Given the functional role this domain plays in MAM biochemistry, we expect amino acid differences between domain types to be associated with generalizable patterns in *MAM* function. *MAMa* is the most conserved of the domains (**Supplementary Figure S5B**), suggesting that *MAMa* genes may contribute a necessary function to GSL biosynthesis, as compared to other MAM types. *MAMc* and *MAMet* are the most diverged, each having several unique amino acid substitutions when compared to other domain types (**Supplementary Figure S5B**). Across all the domains, some sites were characterized by amino acid variability within and between domain types. Based on the characterization of *MAM* proteins in *Brassica juncea* (Kumar et al., 2019), we identified that oxo-acid binding sites were most often found at flexible amino acid positions followed by COA binding sites (**Supplementary Figure S5A**). A better understanding of these patterns can give us insight into the forces driving the adaptation of *MAM*.

The domain and full-sequence gene trees conflict most significantly within the core Brassicaceae (**Figure 3**). In the full-sequence tree Lineage I *MAMa* and *MAMb* genes appear more closely related to *MAMe* genes than to other genes of their shared domain. Sequence comparison reveals split-sequence similarities in both *MAMa* and *MAMb* domain clade groups. This pattern suggests two possibilities: (1) *MAM* genes experienced convergent evolution of their amino acid sequences, or (2) a gene fusion event of separate *MAM* types occurred sometime during the divergence of Lineage I MAM. The latter scenario is both the more parsimonious conclusion, and it is supported by the previous characterization of population-level gene fusion events at the Ancestral-*MAM* locus (Benderoth et al., 2009). Given that Lineage I *MAMa* and *MAMb* genes show a close phylogenetic relationship to Lineage I *MAMe*, in conflict with the domain tree, it is the most likely donor gene. Both fusion events would

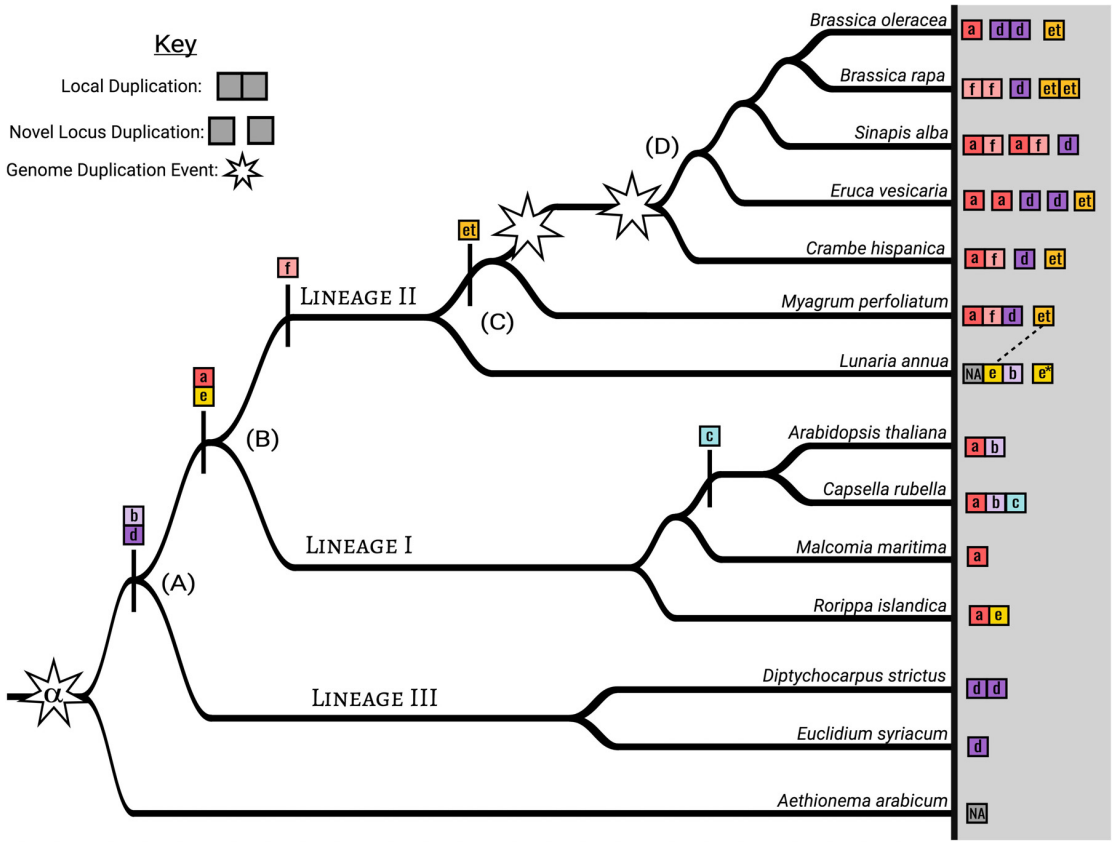

FIGURE 4 | MAM clade and genomic context diversity within the Brassicaceae based on a subsample of analyzed genomes. Each square represents a MAM gene with an indicated HMGL-like domain type. Connected squares are found at the same physical location in the genome and not connected squares represent separate MAM loci (i.e., the MAM-Ancestral locus, a syntenic duplicate of the of the MAM-Ancestral locus, or MAM-Transposed). Non-syntenic gene transpositions were not included. **(A)** We estimate that the shared ancestor of Lineages I, II, and III maintained both MAMb and MAMd domain types. In the Lineage III genomes sampled MAMb genes were not located at the MAM-Ancestral locus, but at transposed loci. **(B)** At the ancestor of Lineage I and II, MAMa and MAMe appear, while the MAMc innovation occurs within a sub clade of Lineage I. **(C)** MAMf originates at the ancestor of Lineage II. The MAMet transposition that creates the MAM-Transposed locus occurs following the split from Lunaria annua, with all MAMet genes being closely related to a MAMe gene at the MAM-Ancestral locus. Lunaria annua also contains a context duplication of the MAM-Ancestral locus* that does not appear to be associated with whole genome duplication. **(D)** The unnamed whole genome duplication found in the tribe Brassiceae of Lineage II has resulted in multiple context duplications of the MAM-Ancestral locus. Full comparison is found in **Supplementary Figure S3**.

have occurred at separate nodes of the Lineage I species tree, *MAMa/MAMe* fusion happening earlier than the *MAMb/MAMe* event. Improved sampling of Lineage I is necessary to identify the specific species branch points at which the events occurred. The fusion of MAM genes at the MAM-Ancestral locus, though largely studied from only a population level, may have been a critical driver of MAM diversity and innovation within Lineage I in the Brassicaceae.

Most of the genes in each domain clade exist at the *MAM*-Ancestral locus. This is true for genes of the *MAMe* group except for a nested clade of transposed genes, *MAMet*, that form the unique syntenic cluster MAM-Transposed (**Figures 1**, **4**). There are subsequent transpositions from the MAM-Transposed locus, many of which show signs of degradation. The initial transposition occurred sometime following the split from the ancestor of *Lunaria annua* to the common ancestor of *Thellungiella (Eutrema)* and the rest of Lineage II (**Supplementary Figure S3**). Following the transposition event, there is a loss of all *MAMe* domain type genes. Of our dataset, *L. annua* is the only member of Lineage II to retain any copies of *MAMe*. Of those *MAMe* genes, most appear closely related to Lineage I *MAMe* genes, while one copy is most closely related to *MAMet* in both the domain and full sequence trees (**Figure 3**). This transposition event is the earliest conserved instance of a novel *MAM* context, which allows for an escape from cis-regulatory effects that may be experienced at the *MAM*-Ancestral locus (Chen and Ni, 2006; Conant and Wolfe, 2008). The possibilities exist that these genes are performing some yet to be characterized function or potentially may represent the GSL-PRO locus characterized in Brassica species. With this current analysis, we cannot further speculate on the role *MAMet* genes may be playing in GSL biosynthesis, except to say that experimental analysis of these genes will be necessary to understand their place in metabolic innovation.

Polyploidy offers another mechanism for *MAM diversification, by escaping* potential cis-regulatory effects of other *MAM* genes or sub- and neofunctionalization of resulting duplicates. In the Cleomaceae, the *MAM*-Ancestral locus duplicates are not retained following genome doubling, putatively due to the presence of their LeuA domain and restrictions under gene dosage. Without such dosage constraints in Brassicaceae *MAM*, most genomes sampled show retention of a duplicated *MAM*-Ancestral locus following known WGD events. For example, the WGT event in the tribe Brassiceae of Lineage II resulted in three homoeologous *MAM*-Ancestral loci in subsequently diploidized genomes (**Figure 4** and **Supplementary Figure S2**). In *Brassica rapa*, *Brassica oleracea, and Eruca vesicaria*, the *MAM*-Ancestral loci maintain a single MAM domain type (*MAMa, MAMd, or MAMf*) at each. Whereas in other genomes, like Sinapis alba, *MAMa* and *MAMf* genes remain paired although duplicated at separate loci. We propose that phenotypic differences between Brassica and Arabidopsis, such as the ability to co-synthesize different carbon chain majority phenotypes, are facilitated by the physical separation of MAM genes within the genome. By influencing the rate of diversification for MAM genes at the different MAM-Ancestral loci and allowing for novel genomic interactions, the WGT may have been a critical step in driving the specialized metabolic innovation we see in this dynamic crop lineage.

CONCLUSION

The *MAM*/IPMS gene family serves as an excellent example of how a primary metabolic gene can, over millions of years and leveraging any source of novelty, give rise to a diverse lineage of highly adaptive specialized metabolic genes. Utilizing micro-synteny gene networks and broad phylogenetic sampling, we find that multiple modes of gene duplication have significantly influenced the evolutionary trajectory of the *MAM* locus and thereby diversity of aliphatic GSL profiles. By exploring some of the evolutionary consequences of whole-genome duplication, gene transposition, local duplication, and gene fusion, we have generated several new testable hypotheses as to the nature of MAM and GSL diversity. In the future, new experimental approaches and broad phylogenetically informed sampling will be critical to continue developing a robust understanding of this important gene family.

DATA AVAILABILITY STATEMENT

The datasets generated for this study can be found in the information provided in **Supplementary Material**.

AUTHOR CONTRIBUTIONS

RSA performed research and wrote the manuscript. JCP helped design the study and edited the manuscript. MES designed the study and helped write and edit the manuscript.

FUNDING

RSA was supported by a NSF GROW fellowship which allowed him to travel and work in Netherlands.

ACKNOWLEDGMENTS

We thank J. Wiscaver, D. Kleibenstein, and the two reviewers for insights and critical feedback. We also thank Tao Zhao with help with the synteny network analysis pipeline.

SUPPLEMENTARY MATERIAL

The Supplementary Material for this article can be found online at: https://www.frontiersin.org/articles/10.3389/fpls.2020.00711/full#supplementary-material

FIGURE S1 | (A) Benderoth et al., 2009 describes the MAM lineage in terms of orthology to *Arabidopsis lyrata* gene tree clades. While the topology generally agrees with our tree, the emphasis on Arabidopsis and close relatives gives a limited picture of MAM diversity. This tree also supported the hypothesis that MAM has evolved separately in the Lineage I and II. **(B)** Zhang et al., 2015 generally agrees with this hypothesis though they do show shared clades not solely informed by the species tree. Some of their topology conflicts with our full sequence tree and yet agrees with the domain specific tree. This may be due to how their alignment was cleaned and their species sampling.

FIGURE S2 | The overall gene counts per genome for the *MAM/IPMS* gene family. Gene numbers, especially in *IPMS*, are correlated with recent polyploidy. Three genomes conflict with the expected IPMS dosage expectation of multiples of two. The *Raphanus raphanistrum* and *Stanleya pinnata* IPMS deviations may be an artifact of lower quality genomes, but the Eruca vesicaria retention appears to be a newly sub-functionalized *IPMS* copy, exhibiting an intermediate syntenic relationships to that of some MAM-Ancestral genes in the Cleomaceae. For MAM, the number of Loci indicates whether *MAM*-Ancestral or MAM-Transposed has experienced a context duplication. The number of genes at that locus is the overall total of genes across all syntenic loci of that type.

FIGURE S3 | Here we show the full domain clade distribution of MAM genes across the genomes, regardless of synteny or genomic position. This data was used ultimately to place the points of innovation for different MAM types in **Figure 4**.

FIGURE S4 | MAM protein sequences were divided into before domain, domain, and after domain segments and each significantly different section of the MAMa or MAMb genes from lineage I were compared to corresponding MAMe sections.

FIGURE S5 | Amino acid sequence comparisons at 80% sequence similarity. **(A)** Colored rectangles indicate specific biochemical functions as described by Kumar et al. (2019) in Brassica juncea. Green - metal binding sites; Yellow - catalytic sites; Red - 2- oxo acid binding sites; Blue - CoA binding sites. **(B)** Summarizes all sites with a uniquely divergent amino acid to quantify the significance of domain divergence.

FIGURE S6 | Full gene family phylogeny with bootstrap scores at 1000 bootstraps with syntenic clusters mapped. Used in **Figure 1**. May also be accessed via: http://bit.ly/2tHVgYK.

FIGURE S7 | Domain tree phylogeny with clades colored and bootstrap scores at 1000 bootstraps. Used in **Figure 3**. May also be accessed via: http://bit.ly/2Hb5jlS.

FIGURE S8 | Full gene family phylogeny with bootstrap scores at 1000 bootstraps with clades colored. Used in **Figure 3**. May also be accessed via: http://bit.ly/37btHEZ.

REFERENCES

Bekaert, M., Edger, P. P., Hudson, C. M., Pires, J. C., and Conant, G. C. (2012). Metabolic and evolutionary costs of herbivory defense: systems biology of glucosinolate synthesis. *New Phytol.* 196, 596–605. doi: 10.1111/j.1469-8137.2012.04302.x

Benderoth, M., Pfalz, M., and Kroymann, J. (2009). Methylthioalkylmalate synthases: genetics, ecology and evolution. *Phytochem. Rev.* 8, 255–268. doi: 10.1007/s11101-008-9097-1

Benderoth, M., Textor, S., Windsor, A. J., Mitchell-Olds, T., Gershenzon, J., and Kroymann, J. (2006). Positive selection driving diversification in plant secondary metabolism. *Proc. Natl. Acad. Sci. U.S.A.* 103, 9118–9123. doi: 10.1073/pnas.0601738103

Birchler, J. A., and Veitia, R. A. (2012). Gene balance hypothesis: connecting issues of dosage sensitivity across biological disciplines. *Proc. Natl. Acad. Sci. U.S.A.* 109, 14746–14753. doi: 10.1073/pnas.1207726109

Blazevic, I., Montaut, S., Burcul, F., Olsen, C. E., Burow, M., Rollin, P., et al. (2020). Glucosinolate structural diversity, identification, chemical synthesis and metabolism in plants. *Phytochemistry* 169:112100. doi: 10.1016/j.phytochem.2019.112100

Borpatragohain, P., Rose, T. J., and King, G. J. (2016). Fire and Brimstone: Molecular interactions between sulfur and glucosinolate biosynthesis in model and crop Brassicaceae. *Front. Plant Sci.* 7:1735. doi: 10.3389/fpls.2016.01735

Chen, Z. J., and Ni, Z. (2006). Mechanisms of genomic rearrangements and gene expression changes in plant polyploids. *BioEssays* 28, 240–252. doi: 10.1002/bies.20374

Chhajed, S., Misra, B. B., Tello, N., and Chen, X. (2019). Chemodiveristy of the glucosinolate-myrosinate system at the single cell type resolution. *Front. Plant Sci.* 10:618.

Conant, G. C., and Wolfe, K. H. (2008). Probabilistic cross-species inference of orthologous genomic regions created by whole-genome duplication in yeast. *Genetics* 179, 1681–1692. doi: 10.1534/genetics.107.074450

Conant, G. C., Birchler, J. A., and Pires, J. C. (2014). Dosage, duplication, and diploidization: clarifying the interplay of multiple models for duplicate gene evolution over time. *Curr. Opin. Plant Biol.* 19, 91–98. doi: 10.1016/j.pbi.2014.05.008

de Kraker, J.-W., and Gershenzon, J. (2011). From amino acid to glucosinolate biosynthesis: protein sequence changes in the evolution of methylthioalkylmalate synthase in *Arabidopsis*. *Plant Cell* 23, 38–53. doi: 10.1105/tpc.110.079269

de Kraker, J. W., Luck, K., Textor, S., Tokuhisa, J. G., and Gershenzon, J. (2007). Two *Arabidopsis* genes (IPMS1 and IPMS2) encode isopropylmalate synthase, the branchpoint step in the biosynthesis of leucine. *Plant Physiol.* 143, 970–986. doi: 10.1104/pp.106.085555

del Carmen, M., Moreno, D. A., and Carvajal, M. (2013). The physiological importance of glucosinolates on plant response to abiotic stress in Brassica. *Int. J. Mol. Sci.* 14, 11607–11625. doi: 10.3390/ijms140611607

Derényi, I., Palla, G., and Vicsek, T. (2005). Clique percolation in random networks. *Phys. Rev. Lett.* 94:160202.

Edger, P. P., Heidel-Fischer, H. M., Bekaert, M., Rota, J., Glockner, G., Platts, A. E., et al. (2015). The butterfly plant arms-race escalated by gene and genome duplications. *Proc. Natl. Acad. Sci. U.S.A.* 112, 8362–8366. doi: 10.1073/pnas.1503926112

Finn, R. D., Clements, J., and Eddy, S. R. (2011). HMMER web server: interactive sequence similarity searching. *Nucleic Acids Res.* 39, W29–W37. doi: 10.1093/nar/gkr367

Fortunato, S. (2010). Community detection in graphs. *Phy. Rep.* 486, 75–174. doi: 10.1016/j.physrep.2009.11.002

Hofberger, J. A., Lyons, E., Edger, P. P., Pires, J. C., and Schranz, M. E. (2013). Whole genome and tandem duplicate retention facilitated glucosinolate pathway diversification in the mustard family. *Genome Biol. Evol.* 5, 2155–2173. doi: 10.1093/gbe/evt162

Katoh, K., Rozewicki, J., and Yamada, K. D. (2017). MAFFT online service: multiple sequence alignment, interactive sequence choice and visualization. *Brief. Bioinform.* 20, 1160–1166. doi: 10.1093/bib/bbx108

Keurentjes, J. J., Fu, J., de Vos, C. H., Lommen, A., Hall, R. D., Bino, R. J., et al. (2006). The genetics of plant metabolism. *Nat. Genet.* 38, 842–849. doi: 10.1038/ng1815

Kliebenstein, D. J. (2008). A role for gene duplication and natural variation of gene expression in the evolution of metabolism. *PLoS One* 3:e1838. doi: 10.1371/journal.pone.0001838

Kliebenstein, D. J., and Cacho, N. I. (2016). Nonlinear selection and a blend of convergent, divergent and parallel evolution shapes natural variation in glucosinolates. *Adv. Bot. Res.* 80, 31–55. doi: 10.1016/bs.abr.2016.06.002

Kliebenstein, D. J., Gershenzon, J., and Mitchell-Olds, T. (2001a). Comparative quantitative trait loci mapping of aliphatic, indolic and benzylic glucosinolate production in *Arabidopsis thaliana* leaves and seeds. *Genetics* 159, 359–370.

Kliebenstein, D. J., Lambrix, V. M., Reichelt, M., Gershenzon, J., and Mitchell-Olds, T. (2001b). Gene duplication in the diversification of secondary metabolism: tandem 2-oxoglutarate-dependent dioxygenases control glucosinolate biosynthesis in *Arabidopsis*. *Plant Cell* 13, 681–693. doi: 10.1105/tpc.13.3.681

Koon, N., Squire, C. J., and Baker, E. N. (2004). Crystal structure of LeuA from Mycobacterium tuberculosis, a key enzyme in leucine biosynthesis. *Proc. Natl. Acad. Sci. U.S.A.* 101, 8295–8300. doi: 10.1073/pnas.0400820101

Kroymann, J., and Mitchell-Olds, T. (2005). Epistasis and balanced polymorphism influencing complex trait variation. *Nature* 435, 95–98. doi: 10.1038/nature03480

Kumar, R., Lee, S. G., Augustine, R., Reichelt, M., Vassao, D. G., Palavalli, M. H., et al. (2019). Molecular basis of the evolution of methylthioalkylmalate synthase and the diversity of methionine-derived glucosinolates. *Plant Cell* 31, 1633–1647. doi: 10.1105/tpc.19.00046

Kuraku, S., Zmasek, C. M., Nishimura, O., and Katoh, K. (2013). aLeaves facilitates on-demand exploration of metazoan gene family trees on MAFFT sequence alignment server with enhanced interactivity. *Nucleic Acids Res.* 41, W22–W28. doi: 10.1093/nar/gkt389

Madeira, F., Park, Y. M., Lee, J., Buso, N., Gur, T., Madhusoodanan, N., et al. (2019). The EMBL-EBI search and sequence analysis tools APIs in 2019. *Nucleic Acids Res.* 47, W636–W641. doi: 10.1093/nar/gkz268

McLysaght, A., Makino, T., Grayton, H. M., Tropeano, M., Mitchell, K. J., Vassos, E., et al. (2014). Ohnologs are overrepresented in pathogenic copy number mutations. *Proc. Natl. Acad. Sci. U.S.A.* 111, 361–366. doi: 10.1073/pnas.1309324111

Moghe, G. D., and Last, R. L. (2015). Something old, something new: conserved enzymes and the evolution of novelty in plant specialized metabolism. *Plant Physiol.* 169, 1512–1523. doi: 10.1104/pp.15.00994

Nikolov, L. A., Shushkov, P., Nevado, B., Gan, X., Al-Shehbaz, I. A., Filatov, D., et al. (2019). Resolving the backbone of the Brassicaceae phylogeny for investigating trait diversity. *New Phytol.* 222, 1638–1651. doi: 10.1111/nph.15732

Olsen, C. E., Huang, X. C., Hansen, C. I. C., Cipollini, D., Orgaard, M., Mathes, A., et al. (2016). Glucosinolate diversity within a phylogenetic framework of the tribe Cardamineae (Brassicaceae) unraveled with HPLC-MS/MS and NMR-based analytical distinction of 70 desulfoglucosinolates. *Phytochemistry* 132, 33–56. doi: 10.1016/j.phytochem.2016.09.013

Palla, G., Derényi, I., Farkas, I., and Vicsek, T. (2005). Uncovering the overlapping community structure of complex networks in nature and society. *Nature* 435, 814–818. doi: 10.1038/nature03607

Peng, C., Uygun, S., Shiu, S.-H., and Last, R. L. (2015). The Impact of the Branched-Chain Ketoacid Dehydrogenase Complex on Amino Acid Homeostasis in Arabidopsis. *Plant Physiol.* 169, 1807–1820. doi: 10.1104/pp.15.00461

Petersen, A., Hansen, L. G., Mirza, N., Crocoli, C., Mirza, O., and Halkier, B. A. (2019). Changing substrate specificity and iteration of amino acid chain elongation in glucosinolate biosynthesis through targeted mutagenesis of *Arabidopsis* methylthioalkylmalate synthase 1. *Biosci. Rep.* 39:BSR20190446.

Rodman, J. E., Soltis, P. S., Soltis, D. E., Sytsma, K. J., and Karol, K. G. (1998). Parallel evolution of glucosinolate biosynthesis inferred from congruent nuclear and plastid gene phylogenies. *Am. J. Bot.* 85, 997–1006. doi: 10.2307/2446366

Shannon, P., Markiel, A., Ozier, O., Baliga, N. S., Wang, J. T., Ramage, D., et al. (2003). Cytoscape: a software environment for integrated models of biomolecular interaction networks. *Genome Res.* 13, 2498–2504. doi: 10.1101/gr.1239303

Smith, S. A., and Dunn, C. W. (2008). Phyutility: a phyloinformatics tool for trees, alignments, and molecular data. *Bioinformatics* 24, 715–716. doi: 10.1093/bioinformatics/btm619

Stamatakis, A. (2014). RAxML version 8: a tool for phylogenetic analysis and post-analysis of large phylogenies. *Bioinformatics* 30, 1312–1313. doi: 10.1093/bioinformatics/btu033

Tang, H., Bowers, J. E., Wang, X., Ming, R., Alam, M., and Paterson, A. H. (2008). Synteny and collinearity in plant genomes. *Science* 320, 486–488. doi: 10.1126/science.1153917

Textor, S., Bartram, S., Kroymann, J., Falk, K. L., Hick, A., Pickett, J. A., et al. (2004). Biosynthesis of methionine-derived glucosinolates in *Arabidopsis thaliana*: recom- binant expression and characterization of methylthioalkylmalate synthase, the condensing enzyme of the chain-elongation cycle. *Planta* 218, 1026–1035. doi: 10.1007/s00425-003-1184-3

Textor, S., de Kraker, J. W., Hause, B., Gershenzon, J., and Tokuhisa, J. G. (2007). MAM3 catalyzes the formation of all aliphatic glucosinolate chain lengths in *Arabidopsis*. *Plant Physiol.* 144, 60–71. doi: 10.1104/pp.106.091579

van den Bergh, E., Hofberger, J. A., and Schranz, M. E. (2016). Flower power and the mustard bomb: comparative analysis of gene and genome duplications in glucosinolate biosynthetic pathway evolution in Cleomaceae and Brassicaceae. *Am. J. Bot.* 103, 1212–1222. doi: 10.3732/ajb.1500445

Wang, Y., Tang, H., Debarry, J. D., Tan, X., Li, J., Wang, X., et al. (2012). MCScanX: a toolkit for detection and evolutionary analysis of gene synteny and collinearity. *Nucleic Acids Res.* 40:e49. doi: 10.1093/nar/gkr1293

Wentzell, A. M., Rowe, H. C., Hansen, B. G., Ticconi, C., Halkier, B. A., and Kliebenstein, D. J. (2007). Linking metabolic QTLs with network and cis-eQTLs controlling biosynthetic pathways. *PLoS Genet.* 3, 1687–1701. doi: 10.1371/journal.pgen.0030162

Wisecaver, J. H., Borowsky, A. T., Tzin, V., Jander, G., Kliebenstein, D. J., and Rokas, A. (2017). A global co-expression network approach for connecting genes to specialized metabolic pathways in plants. *Plant Cell* 29, 944–959. doi: 10.1105/tpc.17.00009

Zhang, J., Wang, X., Cheng, F., Wu, J., Liang, J., Yang, W., et al. (2015). Lineage-specific evolution of Methylthioalkylmalate synthases (MAMs) involved in glucosinolates biosynthesis. *Front. Plant Sci.* 6:18. doi: 10.3389/fpls.2015.00018

Zhao, T., Holmer, R., de Bruijn, S., Angenent, G. C., van den Burg, H. A., and Schranz, M. E. (2017). Phylogenomic synteny network analysis of MADS-box transcription factor genes reveals lineage-specific transpositions, ancient tandem duplications, and deep positional conservation. *Plant Cell* 29, 1278–1292. doi: 10.1105/tpc.17.00312

Zhao, T., and Schranz, M. E. (2019). Network-based microsynteny analysis identifies major differences and genomic outliers in mammalian and angiosperm genomes. *Proc. Natl. Acad. Sci. U.S.A.* 116, 2165–2174. doi: 10.1073/pnas.1801757116

Zhao, Y., Tang, H., and Ye, Y. (2012). RAPSearch2: a fast, and memory-efficient protein similarity search tool for next generation sequencing data. *Bioinformatics* 28, 125–126. doi: 10.1093/bioinformatics/btr595

Conflict of Interest: The authors declare that the research was conducted in the absence of any commercial or financial relationships that could be construed as a potential conflict of interest.

Advantages of publishing in Frontiers

OPEN ACCESS
Articles are free to read for greatest visibility and readership

FAST PUBLICATION
Around 90 days from submission to decision

HIGH QUALITY PEER-REVIEW
Rigorous, collaborative, and constructive peer-review

TRANSPARENT PEER-REVIEW
Editors and reviewers acknowledged by name on published articles

Frontiers
Avenue du Tribunal-Fédéral 34
1005 Lausanne | Switzerland

Visit us: www.frontiersin.org
Contact us: info@frontiersin.org | +41 21 510 17 00

REPRODUCIBILITY OF RESEARCH
Support open data and methods to enhance research reproducibility

DIGITAL PUBLISHING
Articles designed for optimal readership across devices

FOLLOW US
@frontiersin

IMPACT METRICS
Advanced article metrics track visibility across digital media

EXTENSIVE PROMOTION
Marketing and promotion of impactful research

LOOP RESEARCH NETWORK
Our network increases your article's readership